Synergism of Reciprocating Sliding Wear and Electrochemistry (Tribocorrosion) of NiTiNOL60 Alloy in Corrosive Media

by

Anthony Onyebuchi OKOANI

A thesis

Submitted in fulfilment of the requirements for the degree of
Doctor of Philosophy (PhD)

Department of Mechanical Engineering

School of Engineering, Computer and Mathematical Sciences

Auckland University of Technology (AUT) New Zealand

2024

Abstract

A fundamental quest of modern tribo-electrochemistry is to unravel the prevailing failure mechanisms on the surface interactions of materials and tools when operated in tribological and corrosive environments. This follows their global economic impacts and the associated costs of remediating the corrosion-tribological-related failures in load-bearing applications, primarily where NiTiNOL60 alloy is widely utilised. Thereby making it imperative to investigate the tribocorrosion behaviour of this alloy. Although previous studies have explored the performance of this alloy in corrosive environments, particularly in artificial seawater, limited information exists regarding the tribocorrosion behaviour in a broader range of hydrogen (H^+) and hydroxyl (OH^-) ion groups. Hence, this study discusses the sliding wear, electrochemical activities and the synergistic tribo-corrosion interactions of NiTiNOL60 alloy in various corrosive media (H_2SO_4, NaOH, and saline solution) prepared in accordance with the standards for analytical grades.

In this work, the investigation of NiTiNOL60 alloy under various electrochemical and sliding wear test conditions employed experimental procedures compliant with the ASTM standards. The setup configuration involves coupling a linear reciprocating tribometer to a 3-electrode cell potentiostat. This allowed the sliding of Al_2O_3 against the flat surface of the specimens in dry and wet conditions. The simultaneous reciprocating sliding and the potentiodynamic polarisation measurements were initiated after the system stabilised in an open circuit potential (OCP). The material preparations and characterisations confirmed the compositions of the Ni-rich alloy featuring a dense network of B2-NiTi + Ni_4Ti_3 cubic and rhombohedral crystal matrix structures. Our findings revealed that the recorded surface and microstructural deformations emanated from the combined effects of electrochemical reactions and sliding wear. While the reciprocating sliding promoted delamination, abrasion, and adhesion, the electrochemical activities accelerated oxidational and corrosive wear mechanisms in both cathodic and anodic regimes. This validated the significant role of pH in the tribocorosion process, where the depassivation rate depends on factors like contact pressure, sliding velocity, and passive film properties. These factors triggered plastic deformations along the wear tracks, particularly in the severe and mild wear regimes. This resulted in material losses, and the maximum wear volume recorded in the saline environment was accelerated by mechanical wear, corrosion, and third-body abrasion. Due to shear forces, grain deformations and elongation were predominant in the alkaline environment. Delamination and micro-cracks were prominent under higher applied loads due to surface tensile stress and contact pressure, which initiated and propagated cracks perpendicular to the sliding direction.

This research has demonstrated that, as opposed to an independent electrochemical test, direct measurement utilising electrochemical impedance spectroscopy can yield a substantially better estimate of the ohmic resistance in a tribocorrosion system. The measurements with the linear reciprocating sliding wear indicated that surface damages recorded on the sample in load-bearing actions were promoted by the tribocorrosion synergy. The findings and deductions provide insight into wear mechanisms and localised corrosion and highlight the influence of pH on corrosive wear and crack propagation. These have practical implications for optimising the performance and durability of NiTiNOL60 alloy in the investigated corrosive environments, offering valuable insights for load-bearing engineering applications.

Keywords: *NiTiNOL60 alloy; Al_2O_3 ball; Electrolytes; Tribocorrosion; Sliding wear; Electrochemical potential; Oxidation; Thermal effect; Wear mechanisms.*

Statement of Authentication

Attestation of authorship

I declare that this doctoral thesis submission is my work, containing the original primary data obtained experimentally, analysed and disseminated in journal publications and conferences by my co-authors and me. To the best of my knowledge and belief, it contains no material previously published or, to a substantial extent, has been submitted for the award of any degree from a university or other academic institution of higher learning.

Signature _____

Anthony Onyebuchi Okoani

Declaration of collaboration and co-authored works

The manuscripts co-authored in the following chapters originated from the work initiated and completed during the research degree enrolment and supervision of A.O Okoani at AUT. The authors' contributions are outlined below, and the co-authors agreed that the information presented is representative of their actual contributions and consent for the research outputs to be presented as part of this PhD thesis.

STUDENT AND SUPERVISOR APPROVALS					
By signing, you are confirming that the co-author contributions stated in the table(s) below are accurate.					
Student Name	Anthony Okoani	**Signature**		**Date**	24-09-2024
Supervisor Name	Professor M. Ramezani	**Signature**		**Date**	25/09/2024

Co-authored publications

Journal articles

Chapter Number:	**6**
Manuscript Title:	**Corrosion and wear interplay: Tribo-electrochemical evaluation of NiTiNOL60 alloy in sulfuric acid**
Publication Status:	**Published**
Reference, if published:	**https://doi.org/10.1016/j.rinma.2023.100523**
AUTHOR(S) NAME:	**CONTRIBUTION**
Anthony Okoani	Conception and design of the project or output; Data curation; Formal analysis; Investigation; Methodology; Writing – original draft, review & editing; Visualisation.
Ashveen Nand	Methodology; Supervision; Writing – review & editing.
Maziar Ramezani	Conceptualisation; Methodology; Resources; Supervision; Writing – review & editing.

Chapter Number:	7
Manuscript Title:	Tribo-electrochemical investigation of 60NiTi alloy in saline solution
Publication Status:	Published
Reference, if published:	https://doi.org/10.1016/j.jalmes.2024.100074
AUTHOR(S) NAME:	CONTRIBUTION
Anthony Okoani	Conception and design of the project or output; Data curation; Formal analysis; Investigation; Methodology; Writing – original draft, review & editing; Visualisation.
Ashveen Nand	Methodology; Supervision; Writing – review & editing.
Maziar Ramezani	Conceptualisation; Methodology; Resources; Supervision; Writing – review & editing.

Chapter Number:	8
Manuscript Title:	Tribocorrosion behaviour of NiTiNOL60 alloy in an alkaline environment
Publication Status:	Published
Reference, if published:	https://doi.org/10.1016/j.rineng.2023.101305
AUTHOR(S) NAME:	CONTRIBUTION
Anthony Okoani	Conception and design of the project or output; Data curation; Formal analysis; Investigation; Methodology; Writing – original draft, review & editing; Visualisation.
Ashveen Nand	Methodology; Supervision; Writing – review & editing.
Maziar Ramezani	Conceptualisation; Methodology; Resources; Supervision; Writing – review & editing.

Chapter Number:	9
Manuscript Title:	Comparative study of the tribocorrosion performance of NiTiNOL60 in acidic, alkaline, and saline environments
Publication Status:	Published
Reference, if published:	https://doi.org/10.1007/s11665-024-09646-6
AUTHOR(S) NAME:	CONTRIBUTION
Anthony Okoani	Conception and design of the project or output; Data curation; Formal analysis; Investigation; Methodology; Writing – original draft, review & editing; Visualisation.
Ashveen Nand	Methodology; Supervision; Writing – review & editing.
Maziar Ramezani	Conceptualisation; Methodology; Resources; Supervision; Writing – review & editing.

Chapter Number:	2
Manuscript Title:	Investigating the tribocorrosion behaviour of NiTiNOL60 alloy in engineering and biomedical applications – An overview
Publication Status:	Submitted for Publication
Reference, if published:	
AUTHOR(S) NAME:	CONTRIBUTION
Anthony Okoani	Conceptualisation; Review; Writing – original draft, review & editing; Visualisation.

Ashveen Nand	Supervision; Writing – review & editing.
Cho-Pei Jiang	Writing – review & editing; Validation.
Maziar Ramezani	Conceptualisation; Supervision; Writing – review & editing; validation.

Chapter Number:	**4**
Manuscript Title:	**Tribological Performance of 60NiTi Alloy Under Varying Contact Conditions and Elevated Temperatures in Linear Reciprocating Sliding**
Publication Status:	**Unpublished/Ready for submission for Publication**
Reference, if published:	
AUTHOR(S) NAME:	**CONTRIBUTION**
Anthony Okoani	Conception and design of the project or output; Data curation; Formal analysis; Investigation; Methodology; Writing – original draft, review & editing; Visualisation.
Ashveen Nand	Methodology; Supervision; Writing – review & editing.
Miguel Angel Selles	Conceptualisation; Methodology; Resources; Writing – review & editing
Maziar Ramezani	Conceptualisation; Methodology; Resources; Supervision; Writing – review & editing.

Chapter Number:	**5**
Manuscript Title:	**Passive oxide film formation and the electrochemistry of NiTiNOL60 alloy immersed in corrosive mediums**
Publication Status:	**Unpublished/Ready for submission for Publication**
Reference, if published:	
AUTHOR(S) NAME:	**CONTRIBUTION**
Anthony Okoani	Conceptualisation; Review; Writing – original draft, review & editing; Visualisation.
Ashveen Nand	Supervision; Writing – review & editing.
Paul Kilmartin	Methodology; Resources - laboratory access; Writing – review & editing.
Maziar Ramezani	Conceptualisation; Supervision; Writing – review & editing; validation.

Conference paper:

A. Okoani, A. Nand, M. Ramezani (2024). Tribo-Corrosion Wear Mechanisms of NiTiNOL60 Alloy in Aqueous Sodium Hydroxide. Proceedings of the 10th International Conference on Tribology in Manufacturing Processes & Advanced Surface Engineering (ICTMP2024), June 26–28, Universitat Politècnica de València, Alcoi Spain, pp. 41. https://doi.org/10.4028/b-9sEuzV

Dedication

This work is dedicated to my entire family for their support and in the loving memory of my beloved papa, whose demise occurred prior to the completion of my pursuit overseas.

Acknowledgements

The last lap of this journey has been overwhelming, but as I reminisce about the 4+ years at AUT, I appreciate God almighty for his grace in attaining this milestone. This academic journey has brought me the pleasure of meeting Professor M. Ramezani (my mentor), who has helped shape my career path and introduced me to his impressive network.

I would like to thank all the people who, in many ways, contributed to accomplishing this goal; indeed, your invaluable contributions made this dream come true. To begin, my heartfelt thanks go to my supervisors, Prof. M. Ramezani and Dr A. Nand, for their unalloyed support, critiques, and timely/ constructive feedback that have made this journey a reality. In a special way, I would like to thank Prof. Christopher DellaCorte of NASA, USA, for graciously supplying the NiTiNOL60 alloy samples. I am also grateful to Professors Paul Kilmartin and Miguel Ángel Sellés Cantó of the School of Chemical Sciences, University of Auckland and Universitat Politècnica de València, Alcoi Spain, respectively, for granting access to their laboratories and resources.

I will always appreciate Josephine Prasad (ECMS PhD coordinator) and Emiliana Faapoi of GRS for their invaluable roles, without which this degree might not have been accomplished. Special thanks to Dr Valentina Kirova-Veljanovska of the AUT Medical Centre, who ensured the research did not overwhelm my well-being. To my well-deserved friends who have completed their PhD, Dr Emenike Okonkwo (JCU Australia), Dr Ramya Nagarajan (UoA), Dr Si Thu Paing (AUT), and Sahem Al-Adwan (AUT), thanks for all your immeasurable support throughout the PhD journey. I would also like to thank the management of the ECMS School AUT for their financial support, the technicians at the Mechanical Engineering workshop, Dr Timothy Christopher of the shared research equipment platform (ShaRE), UoA and my colleagues (Tingzhen, Joshua, Ravisrini) at the Tribology and Surface Engineering Laboratory for their support. To my Kiwi families and friends, I would like to say thank you all for accepting me as part of your cohort; be assured that the wonderful moments we shared will remain evergreen. I will not forget to acknowledge my colleagues at the University of Nigeria, particularly Engr. Professors C.A. Mgbemene, J.I. Ume, and O.V. Ekechukwu for their fatherly advice and relentless efforts in writing all my recommendation letters during the PhD application.

My sincere appreciation goes to my cherished family members for their financial and emotional support, especially my mom, whose relentless prayers kept me going. Undoubtedly, the journey is over, and the goal has been actualised with overwhelming joy. Lastly, to all my friends, who are too numerous to mention here, thank you all for standing by me, especially during the toughest moments of my PhD journey. 😊

Contents

List of Figures

List of Tables

CHAPTER 1: INTRODUCTION

1.1. Motivation

The mechanical and electrochemical interactions between moving surfaces are concepts at the heart of innumerable natural phenomena [1]. Whether in the joints of a human skeleton [2], in rolling elements of a jet turbine [3, 4], or crucial components on a space station [5]. In some situations, neither natural events nor human-designed devices are exempt from friction, wear and corrosion attack. The applications of some engineering materials have been restricted to primarily non-tribological applications following severe galling and significant wear rates often encountered in sliding contacts, especially in load-bearing. The exposure of such material results in a corrosive environment, thereby leading to corrosive wear, which is another concern in many applications. NiTiNOL60 alloy has gained vast use in engineering and biomedical applications where the combined actions of mechanical wear and corrosion, also known as tribocorrosion, pose a significant challenge to its optimal performance. Hence, this study will investigate the tribocorrosion of this alloy in corrosive mediums under various loading conditions.

Tribocorrosion has long been the subject of investigations in both engineering and medical fields following the intrinsic interactions of the phenomena (tribology and corrosion) that have aroused the interest of humankind since ancient times. This has regained great attention due to its significant role in the premature failure of components in many systems [6-8]. The interaction between wear and corrosion in an aqueous environment can produce a synergistic effect that degrades materials faster than wear or corrosion alone. Wear can occur due to two-body or three-body interactions between the sliding pairs. The primary wear mechanism is oxidative wear, in which the passive oxide film is mechanically removed. Wear-accelerated corrosion or corrosion-accelerated wear results from a synergistic deterioration process that starts when corrosion occurs concurrently with wear [9]. This is common where increasing engineering activities such as seawater hydraulic drive, submarine oil production systems, etc., require high-performance frictional pair material [10]. These, therefore, necessitate the need for the wear performance of materials in their various load-bearing applications [11] to clearly understand the impact of tribocorrosion on the functioning of the tribo-system.

1.2. Background of the Study

The concept of tribology regarding scientific discipline and economic implications originated in the second half of the twentieth century. According to Siddaiah, et al. [9], tribological contacts account for a global economic wear loss of about US$300 billion annually, where losses from friction and wear amount to 73% and 27%, respectively [9]. Du, et al. [12], in their study, confirmed that over 80 % of machine failures are caused by abrasion on the surface of the components.

Corrosion, which results in the degradation of material surfaces, is not only an engineering issue but also an economic problem. Accordingly, this area of study has been investigated over the past decades with significant studies in various parts of the world on the cost of corrosion and how it affects a country's economy. A report supported by NACE International estimated the global impact of corrosion cost to be US$ 2.5 trillion in 2013, equivalent to approximately 3.4 % of the global Gross Domestic Product (GDP) [13]. The Australasian Corrosion Association presented that the effect of corrosion contributes between 3.5% to 5.2% (average of 4.35%) of the global gross domestic product. Extrapolating the figures for Australia's GDP, it amounts to a high estimate of AU$ 78 billion per annum spent on remediating corrosion-related assets. Applying the same estimated impact for New Zealand, which has a smaller economy, the cost of corrosion is approximately NZ$ 16 billion. Another study by Shekari, et al. [14] concluded that adopting corrosion control practices could yield savings of about 15 – 35% between $ 375 and $ 875 billion. According to their report, these costs typically do not include corrosion safety or environmental impacts, which can have significant financial, regulatory, and legal consequences for an establishment.

The unusually high activity of tribological surfaces in chemical interactions between solids and ambient liquids and gases is well recognised, and the phenomenon is termed tribochemistry or tribocorrosion [15]. This research field has attracted attention to preventing tribological components from corrosive degradation by the surrounding media/ environment [16]. According to published research, tribocorrosion has been thoroughly studied for biomedical applications, including dental and bone implants, micro-electro-mechanical systems (MEMS), and marine applications where tribosystems are subjected to electrochemically active conditions [9]. However, understanding the mechanism of tribocorrosion in these systems has gotten more difficult with the introduction of new functional surfaces, materials, and lubricants for multifunctional mechanical applications. Consequently, extensive research on the tribocorrosion of passive materials, such as stainless steels and titanium alloys, has been conducted in recent decades, following their various applications in corrosive environments [6, 17, 18].

In most engineering applications, conventional materials such as high-strength steels (HSS) are often utilised due to their high resistance-to-weight ratio and yield strength values ranging from 460 to 960 MPa [19-21]. However, these low-alloyed steels do not produce a protective oxide layer on the surface due to their low content in alloying materials progenitors of passive film formation (Cr, Ni, Mo, etc.) [22, 23]. Pepper, et al. [24] reported that traditional steel-based bearing materials like M50, 440C, etc., despite being highly magnetic and electrically conductive, are employed due to their high hardness, ease of fabrication, and good tribological qualities. Yet, they suffer wear and corrosion attacks if left unprotected. Consequently, specific properties and characteristics, as presented in Table 1.1, are required for high-performance bearings, gears and other mechanical components, such as high strength and hardness, high thermal conductivity, and the ability to be manufactured to very high levels of precision with regard to final dimensions and surface finish [24].

Table 1.1: Comparing the thermophysical and mechanical properties of NiTiNOL60 with other conventional bearing alloys [25, 26].

Property	**NiTiNOL60**	**440C**	**M-50**
Density (g/cc)	6.7	7.7	8.0
Hardness (HRC)	52 – 62	58 – 62	60 – 65
Thermal conductivity (W/m-^{o}K)	~9 - 14	24	~36
Tensile/ (Flexural strength) (MPa)	~1000 (1500)	1900	2500
Young's Modulus (GPa)	~95	200	210
Poisson's ratio	~0.34	0.3	0.3
Fracture toughness (MPa/$\sqrt{m}$)	~20	22	20 – 23
Electrical resistivity (Ω-m)	~1.04x10^{-6}	~0.60x10^{-6}	~0.18x10^{-6}
Max. Temp. use (℃)	~400	~400	~400
Magnetic	Non	Magnetic	Magnetic
Corrosion resistance	Excellent (Aqueous media)	Marginal	Poor

In addition, spacecraft systems require bearings that can withstand both environmental corrosion and transient stresses from vibrations associated with launches, such as corrosive ambient maritime conditions [26, 27]. Several surface treatments, such as boronising, nitriding, thermal oxidation, carburising, and laser surface treatments, have been investigated to improve these alloys' tribological characteristics [28-30]. Notwithstanding the surface treatments and the high resistance properties to wear and corrosion, many engineering materials still fail in tribological applications and are also

prone to corrosion-related failures [19, 31]. These challenges have gradually prompted the need for biocompatible materials. This extraordinary need to create engineering systems that are more durable and long-lasting presents new and emerging issues for tribological systems.

In that quest, Arne Ölander discovered the first smart alloy in 1932, referred to as the shape memory alloy (SMA), suitable for different industrial fields [32]. In 1962, William J. Buehler and Fredrick Wang discovered NiTiNOL, and it has since become the most well-recognised alloy system regarding the shape memory effect, even though it was not the first discovered alloy that possessed the shape memory effect [33]. The term "NiTiNOL" is derived from the alloy's constituent elements (Ni and Ti), as well as the abbreviation for the Naval Ordinance Laboratory (NOL), where the phenomenon was discovered [5, 34, 35]. Buehler and colleagues acknowledged and defined the material's "shape-memory effect" and noted its ability to undergo a reversible change in its crystal structure when heated and cooled over a temperature gradient [36], as shown in Fig. 1.1. At temperature below the M_f, the austenite structure returns to martensite, with no macroscopic shape change; in contrast $T>M_f$ results in martensite deformation [37, 38]. Thus, there is an increasing interest in NiTi alloys as solid-state actuators in the aerospace industry despite the tremendous success in biomedical applications.

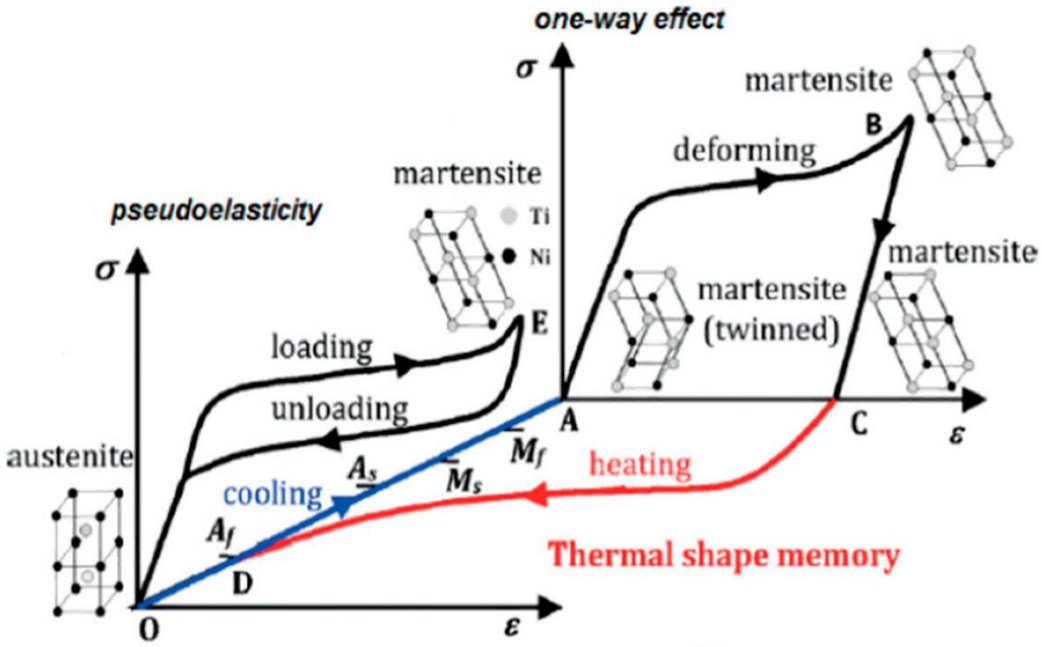

Fig. 1.1: Representation of stress-strain-temperature diagram for NiTiNOL alloy [38].

Although the Ni-rich NiTiNOL60 alloy was developed to replace bearings that experience corrosion and wear issues in the water recovery system of the International Space Station [39]. However, it is crucial to address this alloy's low transformation temperature

(≥100 ℃) and poor dimensional stability during cyclic loading before using it as an actuator. Miller et al., in their report, also noted that the loadbearing, tribological, and time-temperature-transition (TTT) behaviour of binary and ternary Ni-rich NiTiNOL60 compounds play vital roles in such systems [40]. It is established that the transformation temperatures of Ni-rich binary compositions are significantly lower than room temperature and the Ti-rich compositions. Thus, the equiatomic NiTi has a higher transformation temperature for SMAs and a higher recoverable strain. On the other hand, NiTi alloys having Ni 50–55 at% or 55–60 wt% have specific properties like lower density, high hardness, high corrosion resistance, and non-magnetic nature, making them very useful in various industries [36]. Despite the limitations of Ni-rich alloys for shape-memory applications, 55Ni–45Ti (at.%) alloy discovered by Buehler et al. possessed high hardness, stably non-magnetic, and excellent corrosion resistance, which makes this alloy particularly suitable for roll-bearing applications [35]. Recent research has demonstrated that macro-alloyed Ni-rich compositions containing Pt, Pd, Zr, and Hf precipitate out secondary phases, increasing transition temperatures to approximately 100 ℃ and satisfying the first important criteria [33, 39, 41]. Thereby exhibiting high resistance to wear. As a result, the tribological behaviour of NiTi alloys has been investigated and compared to many conventional engineering materials such as steels, Ni-based, and Stellite alloys [42, 43]. These investigations have shown NiTi's higher wear resistance than many tribological materials [44].

Following the scientific attention drawn by nickel-titanium alloys, Kosec, et al. [45] categorised the related research conducted at the time of their study into the following fields: basic corrosion and electrochemical studies, mechanical and material property studies, and surface treatment studies [45]. Although the wear resistance of conventional tribo-materials strongly depends on their mechanical properties, such as hardness, toughness, and work-hardening [46]. However, these properties are not the primary factors responsible for the high wear resistance of these alloys. The numerous applications of NiTi-based alloy, which exposes the material to wear and harsh corrosive environments [45, 47], warrant a thorough investigation of their tribocorrosion phenomena in different corrosive media. However, many researchers have investigated tribochemistry and/or tribocorrosion on many engineering and biomedical materials to clarify the synergistic interactions. Yet, little is known about the underlying mechanisms of NiTiNOL60 alloy in this intriguing field of study [10]. In light of the above, further research is required to reveal the tribo-electrochemical synergistic interactions and the wear rates of NiTiNOL60 alloy under different experimental conditions, hence the knowledge gap that this research attempts to address. This will be investigated through

an experimental approach using three different electrolyte solutions (NaCl, H_2SO_4 and NaOH) and a setup configuration of a linear reciprocating ball-on-plate tribometer coupled to a three-electrode cell potentiostat. This experimental setup has the advantage of reproducing a generic sliding contact in a simpler and more controlled way.

1.3. Problem Statement and Research Questions

Tribocorrosion is a complex mechanism that affects the performance of mechanical systems through wear-corrosion synergism, which occurs either in the form of wear-accelerated corrosion or corrosion-accelerated wear. These degradation processes can have serious consequences that might result in physical injury or death, such as when biomedical implants fail, the release of metals into food products, contamination of the environment, or financial losses arising from the need to replace affected equipment/ components. These deductions and the existing literature have revealed that while the sliding wear mechanism for NiTiNOL60 has been established, more attention needs to be devoted to elucidating relevant deformation mechanism(s) for the combined actions of corrosion and sliding wear. Additionally, many researchers have focused their testing of this alloy in the simulated artificial seawater solution. Still, studies have yet to present a comparative evaluation of this alloy through its investigation in various corrosive mediums. These necessitates the following research questions:

1. How does the NiTiNOL60 alloy surface interact in dissimilar corrosive mediums?
2. How would the testing parameters (temperature, pH, applied load, sliding speed, etc.) impact the surface deterioration of this alloy?
3. How does the thermal effect influence the phase stability within the alloy?
4. What could be the wear mechanisms and/or the passivation kinetics of NiTiNOL60 alloy under the synergistic tribo-electrochemical testing conditions?

1.4. Significance

Following the rising concern on the tribological performance of NiTiNOL60 alloy in corrosive environments, it is evident that corrosion and wear play vital roles in material deterioration in engineering and medical applications. This study will offer a mechanical viewpoint on the multidisciplinary aspects of tribocorrosion, thereby promoting the use of NiTiNOL60 alloy in its vast application areas. The results presented herein apply to various industries, such as the automotive, aerospace, marine, mining, petrochemical, food, and biomedical sectors. Therefore, the findings from the research will offer valuable insights into the tribocorrosion of NiTiNOL60 for designers of loading-bearing structures, particularly in chemically active environments.

1.5. Aim and Objectives

This research aims to unravel the tribocorrosion and its influencing factors in the accelerated degradation of NiTiNOL60 alloy in an electrochemically active environment. The specific objectives to actualise this goal are to:

i. Evaluate the sliding wear and electrochemistry of the alloy to establish the optimal parameters for tribocorrosion measurements.
ii. Examine the alloy in various electrolytes using tribocorrosion configurations.
iii. Investigate the influence of testing parameters (temperature, applied load, pH, etc.), sample surface and electrolyte ions on the material's behaviour.
iv. Analyse the resulting wear tracks to ascertain the surface transformation caused by the combined effects of the two processes.
v. Study the effect of applied potential and third body wear on the tribocorrosion.
vi. Identify the wear mechanisms and wear rates and quantify the material loss due to the synergistic sliding wear and electrochemical activities.
vii. Present a comparative evaluation of NiTiNOL60 alloy performance and its wear mechanisms/ rates in the various electrolyte solutions.

1.6. Outline and Thesis Structure

This thesis is structured following the AUT requirements for PhD thesis submission. It contains ten (10) chapters, which are schematically presented in Fig. 1.2 and summarised as follows:

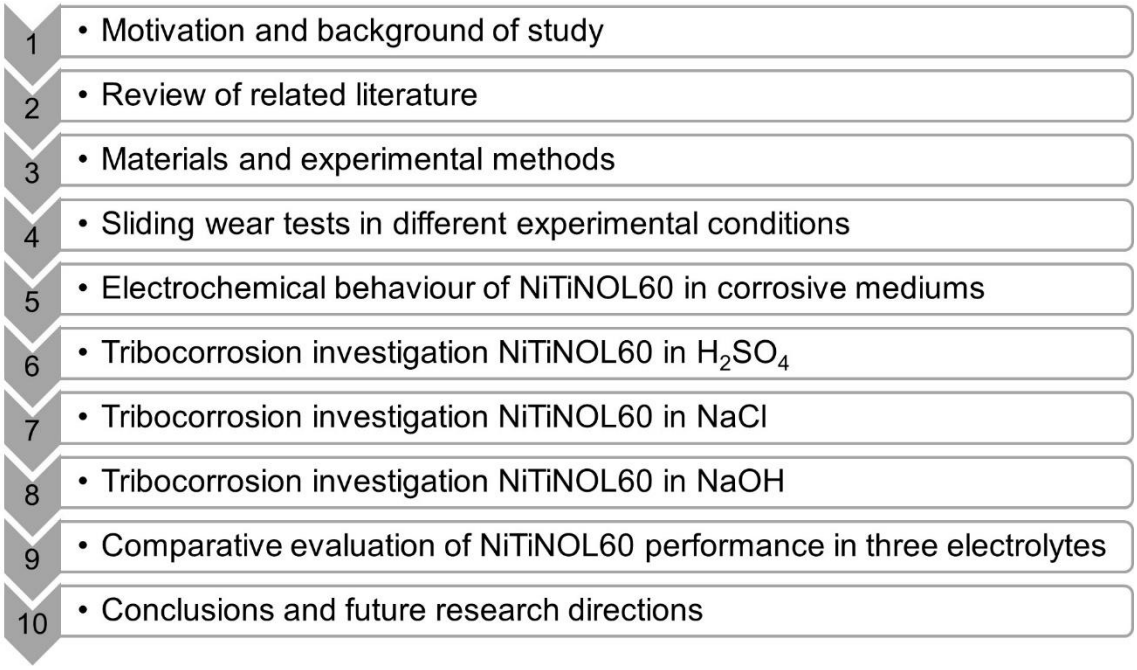

Fig. 1.2: Schematic flow outline for this study.

Chapter 1 highlights this research's motivation, background, and overview. It further presents the aim, objectives, and significance of the study.

Chapter 2 presents an extensive literature review that covers some fundamental theories of tribology and electrochemistry while focusing on the tribological and electrochemical interactions of NiTiNOL60 alloy. This section also summarised some related literature on tribocorrosion of engineering materials and some methods currently employed for surface-engineered materials.

Chapter 3 outlines the experimental approach(s) employed for this investigation. It further presents the preparation of the material and reagents and detailed experimental procedures.

Chapter 4 presents the sliding wear behaviour of NiTiNOL60 alloy in wet, dry and elevated temperature conditions. It also describes the material characterisation and wear rates.

Chapter 5 covers the electrochemistry of NiTiNOL60 alloy exposed to different electrolytes. The investigation includes electrochemical impedance spectroscopy (EIS), open circuit potential (OCP), potentiodynamic (PD) polarisation, and cyclic voltammetry measurements.

The subsequent Chapters (6–9) will illustrate an integrated tribocorrosion configuration to investigate the synergistic sliding wear and electrochemical activities of NiTiNOL60 alloy in corrosive environments. A comparative report will be presented on the material's performance in the three electrolyte solutions used for this study.

Chapter 6 illustrates the investigation of tribocorrosion of an alumina ball (Al_2O_3) sliding against a NiTiNOL60 alloy surface in a sulfuric acid environment.

Chapter 7 presents the tribocorrosion behaviour of NiTiNOL60 alloy in saline solution.

Chapter 8 presents the tribocorrosion behaviour of NiTiNOL60 alloy in alkaline medium.

Chapter 9 compares the tribocorrosion behaviour of NiTiNOL60 alloy in the three corrosive environments.

Chapter 10 highlights the main conclusions drawn from this study, its contribution to knowledge, and possible prospects for future research directions for prospective researchers in the field of tribocorrosion.

References – the IEEE referencing style has been adopted for this thesis's in-text citation and reference listing.

CHAPTER 2: LITERATURE SURVEY

2.1. Preface

This review aims to summarise the current state of research in the tribocorrosion of NiTi-based alloys, highlighting the key findings, methodologies, and future research directions. Its focus is on the interactions between mechanical wear, corrosion, and the associated tribocorrosion mechanisms in different corrosive mediums, including simulated physiological solutions that mimic the practical environments in engineering and biomedical applications of NiTiNOL60 alloy. The study will begin by examining the fundamental aspects of NiTi alloy, including its composition, microstructure, and surface properties, and their influence on tribocorrosion behaviour. It will then delve into the experimental techniques employed to study tribocorrosion, such as ball-on-plate reciprocating sliding and electrochemical testing, providing insights into wear and corrosion mechanisms, surface characterisation, and material degradation. Furthermore, the review will discuss the influence of various parameters, including pH, temperature, applied load, sliding velocity, and electrolyte composition, on the tribocorrosion behaviour of NiTi alloy. In addition, it will explore the role of passive oxide films, tribo-films, and material transfer processes in tribocorrosion, along with the effects of surface modifications, coatings, and alloy composition on corrosion resistance and wear performance. The study will conclude by highlighting the existing challenges and knowledge gaps in the field and suggesting future research directions to enhance the understanding and scope of prospective tribocorrosion researchers. It will provide researchers and engineers with a comprehensive overview of the current knowledge of NiTiNOL60 alloy tribocorrosion and inspire further investigations to address the complex tribocorrosion challenges associated with NiTi alloys. The review manuscript draft in section 2.2 has been submitted to a journal for peer review and publication.

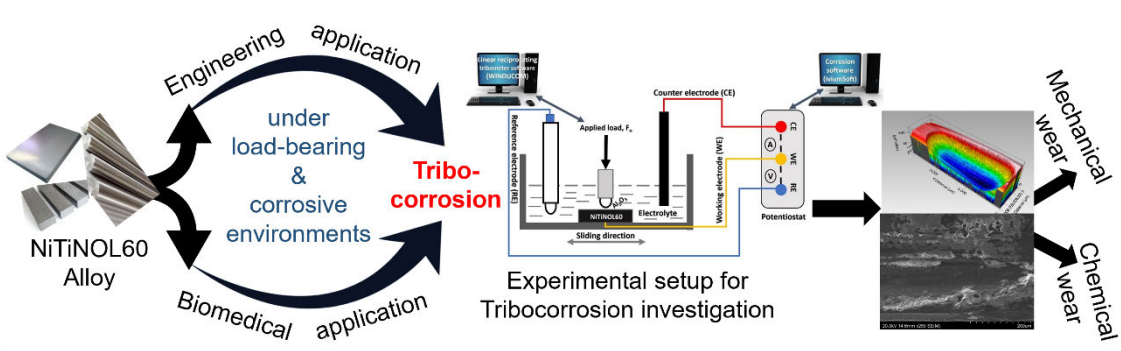

Graphical abstract for the tribocorrosion of NiTiNOL60 alloy.

2.2. Investigating the tribocorrosion behaviour of NiTiNOL60 alloy in engineering and biomedical applications – An overview

2.2.1. Introduction

The demands for a better understanding of surface degradation processes, mainly when tribological components are operating in corrosive environments, have arisen because of the need to choose or design new surfaces for future equipment, minimise operating costs, and extend the life of existing machinery [48, 49]. This has led to the current study field of tribocorrosion, which aims to address the aforementioned issues and understand the mechanisms of surface deterioration when mechanical wear and chemical/ electrochemical processes combine [50-52]. Tribocorrosion is a multifaceted degradation phenomenon that occurs when metals are subjected to mechanical wear and corrosion simultaneously [1, 7, 53].

The interaction between moving surfaces in a tribological loading situation/contact is a concept that exists in many phenomena in nature, be it in the components of spacecraft [40], human joints [54], rolling elements of a jet turbine [5], etc. Literature information states that tribological contacts result in a global economic loss of approximately US$ 300 billion annually, with friction contributing to 73% of the total loss and wear contributing to 27% [9]. Corrosion is also reported to have a global estimated cost of about US$ 2.5 trillion, equivalent to 3.4 % of the 2013 Gross Domestic Product of the United States [13]. Tribological applications in a corrosive environment often result in a surface alteration [55-57], and understanding this complex phenomenon and its complexity arises from the interactions involved in moving surfaces as influenced by several parameters (mechanical, material, electrochemical reaction, and environment) [7, 52, 53]. The interaction is a significant mechanism of degradation that has a big impact on the effectiveness and dependability of metallic materials. As such, superalloys are preferred over conventional materials in high service temperatures (650 ℃) and other tribological operations [58-60] where the structural component may fail due to creep and/or fatigue.

This phenomenon, characterised by its synergy from the combined action of mechanical loading and corrosion attack influenced by the environment [45, 61], is known as tribocorrosion. Its occurrence still prevails as the primary mechanism governing the deterioration of material through the interaction of wear and corrosion in numerous applications such as marine engineering [62, 63], biomedical implants [2, 64], aerospace [40, 58], and chemical mechanical polishing [22]. In these applications, several phenomena, including abrasive wear, adhesive wear, corrosive wear, fretting corrosion,

galvanic corrosion, and pitting corrosion, take place simultaneously, which can shorten the useful life of equipment/components, leading to unpredicted failures [52, 65, 66]. Different materials have been considered to remedy the situation; thus, steels are the most highly utilised engineering alloys due to their desirable properties of high tensile strength and good machinability [67]. For manufacturing implants, stainless steels are considered following their remarkably high-temperature resistance and performance against corrosive media. Still, their high wear resistance makes them unsuitable in high-temperature and load-bearing applications [64]. Low-carbon steels are also unsuitable because they are susceptible to aqueous corrosion [68]. López-Ortega, et al. [69] reported that the tribocorrosion of passive materials like stainless steel and titanium alloys has been widely studied for different applications and corrosive environments in recent decades. They highlighted that wear locally destroys and removes the protective oxide layer formed on the surface of passive materials, which exposes the underlying fresh material to the electrolyte [69]. Another study by Shabalovskaya, et al. [70] highlights the potential threat of metallic release from implant devices and the subsequent research focus on surface modifications and coatings [71-73]. This has been a significant area of research due to the potential health risks associated with metallic exposure [74, 75].

Another area of interest is the application of graphene and graphene oxide additives as barrier coatings in tribological applications due to their remarkable thermal conductivity, excellent mechanical strength, high surface area as well as weak van der Waals interaction between adjacent atomic-thick lamellae [76]. It is reported that graphene-based materials used as additives to water and lubricating oils have significantly improved friction reduction, protection of contact interfaces against wear and corrosion mitigation through thin film formation [76, 77]. Kumar, et al. [77] highlighted the relevance of graphene barrier coatings and categorised the commonly used graphene-based anti-corrosion into pure graphene and graphene composite coatings. However, the dispersion stability, structural features, and dosage of graphene-based dispersoids, along with contact geometry, play important roles in governing tribological properties [76]. Accordingly, Zuo, et al. [78] investigated the effect of various concentrations and tribocorrosion behaviour of graphene oxide (GO) particles in micro-arc oxidation (MAO) coating on the Ti6AL4V alloy. Their study confirmed that the GO additive effectively enhanced the corrosion/tribocorrosion resistance of MAO coatings and further reported that the best tribocorrosion resistance was achieved by combining MAO coating and 10 mL/L of GO [78]. Another study by Acar, et al. [79] investigated boron-doped and graphene oxide-doped TiO_2 nanotubes (TNT). Their study reported that the graphene

oxide doped TNT sample had the highest corrosion resistance and surface hardness, showing the best tribocorrosion resistance.

Since the lifespan of most engineering and biomedical materials is often affected by corrosion and sliding wear properties [16, 18, 52, 74, 80-82], it has prompted the growing interest and investigation for a suitable material that can withstand the synergistic impact of wear and corrosion [73, 83]. Accordingly, researchers have explored Nickel and Titanium as significant elements mostly used in high-temperature applications [58-60, 84-86]. These elements have superior oxidation and corrosion resistance with excellent stable mechanical properties at higher service temperatures [36]. NiTiNOL60 alloy has been widely adopted in tribological applications due to its unique properties, such as high hardness, high corrosion resistance, low elastic modulus, and non-magnetic properties [87, 88]. This alloy's high mechanical and corrosion resistance properties promote its application in harsh/aggressive environments, including marine [63] and biomedical implants [89]. Despite the excellent corrosion resistance property of NiTiNOL60 alloy, tribocorrosion still prevails as the primary mechanism governing the deterioration of material through the interaction of wear and corrosion in many engineering applications such as marine engineering [62, 63, 90], biomedical implants [2], aerospace [3, 40, 58], and chemical mechanical polishing [22]. Aside from the aerospace, marine, and biomedical applications, Mathew, et al. [91] listed the automotive, food and textile, chemical, and oil industries, mining and metallurgy, thin films, micro and nanotechnology coating, and the transportation industry as additional sectors where tribocorrosion synergy occurs.

Although NiTi alloys produced by traditional methods such as casting, wrought, etc., were the focus of many studies on tribocorrosion, the tribocorrosion characterisation of NiTi alloys produced by additive manufacturing processes is a relatively new and less explored topic in the literature [92, 93]. As a result, Buciumeanu, et al. [94] investigated the synergistic effects of corrosion and wear in phosphate-buffered saline on as-printed NiTi shape memory alloy processed by additive manufacturing laser beam-directed energy deposition (LB-DED) techniques such as laser-engineered net shaping (LENS). They further compared the tribocorrosion behaviour of NiTi alloy with Ti-6Al-4V, the most commonly used titanium alloy in biomedical applications, produced using the same processing technology (LB-DED, LENS). Their study found that when compared to the Ti-6Al-4V alloy [95], the NiTi alloy is less vulnerable to the discharge of metallic ions [75] during its service life as an implant [94, 96]. NiTi shape memory alloys possess several multifunctional properties resulting from a reversible martensitic transformation. Further studies showed that understanding the effects of specific parameters such as

transformation temperatures, matrix strength, hysteresis, and transformation strain of NiTi alloys, which are functions of composition, thermomechanical treatment, and crystallographic orientation, is crucial for practical purposes [87, 97, 98]. This study has shown the need for a more recent review of the tribocorrosion of NiTi alloy. Accordingly, Mischler and Munoz [7] summarised the aspects of tribocorrosion studied at the time of their report. The information revealed that some areas have received little attention, and the fact that the combined actions of tribology and electrochemical reactions impact various activities makes this review relevant. Therefore, this paper provides a comprehensive review of the tribocorrosion behaviour of NiTiNOL60 alloy in corrosive environments, focusing on understanding the interactions between mechanical wear, corrosion, and the associated degradation mechanisms. Examining the experimental findings and research advancements will help unravel the performance of NiTi alloy under simultaneous mechanical and electrochemical stresses in tribological and corrosive conditions. Further, it tends to critically analyse the recent status of NiTi alloy tribocorrosion and highlight the future areas to be investigated to aid in the selection and application of NiTiNOL60 alloy.

2.2.2. Ni-Ti-based alloys and the fundamental concepts in tribology and corrosion

2.2.2.1. Ni-Ti alloys

The need to create engineering systems that are more durable and long-lasting presents new and emerging issues for tribological interfaces. In that quest, Arne Ölander, in 1932, discovered the first smart alloy, referred to as the shape memory alloy (SMA), suitable for different industrial fields [32]. It was acknowledged that the material's "shape-memory effect" showed improved recovery after a significant degree of strain and could replicate their memorised shapes [36]. In 1962, William J. Buehler and Fredrick Wang discovered Ni-Ti alloy at the Naval Ordnance Laboratory (NOL), Ohio, USA, thus, the name NiTiNOL [5, 34, 35]. Other thermo-mechanical characteristics of NiTiNOL, such as pseudoelasticity or high damping, were discovered later [32]. Since then, several metallic alloys with intrinsic physical, mechanical, and electrical properties, including shape memory behaviour, have been utilised in various industrial applications.

Figure 2.1 presents a nearly stoichiometric Ni–Ti alloy phase equilibrium diagram; the transformation from B2 → B19' occurs in a single step. In austenite, big grains (~ 6.6 to 21.7 μm) undergo the same transformation but with a relatively small Ni advantage. Grain development is the direct outcome of heating to a relatively high temperature of > 800 °C, which also causes uneven release of the metastable Ni_4Ti_3 phase [99]. As the diagram illustrates, Ni_3Ti is the cuboid-shaped γ′ phase (hard-ordered phase)

responsible for increasing the operating temperature of the SMA. At high and low temperatures, the stress-induced superelasticity and thermally-induced shape memory effect aid SMAs' recovery of their original shapes [100]. Patel and Bahera examined the triangular region of the NiTi phase diagram in their work, and they emphasised the combined influence of SMA and superalloy qualities based on the phases that occurred [36]. In another study, Dobrzański, et al. [99] investigated the effect of mass concentration of nickel in the range of 48 – 51% on the martensite start (M_s) temperature value. They deduced that the M_s temperature for the stoichiometric chemical composition of Ni50 – Ti50 is around 65 ℃. This temperature also slightly increases with increasing titanium content. Conversely, when the nickel concentration is increased above equilibrium, the M_s temperature is drastically lowered to around 140 ℃ [99]. Therefore, it is possible to express the series of precipitation processes in austenite with structure B2 systematically depleted in alloying elements under such circumstances as B2 → Ti_3Ni_4 → Ti_2Ni_3 → $TiNi_3$ [99, 100].

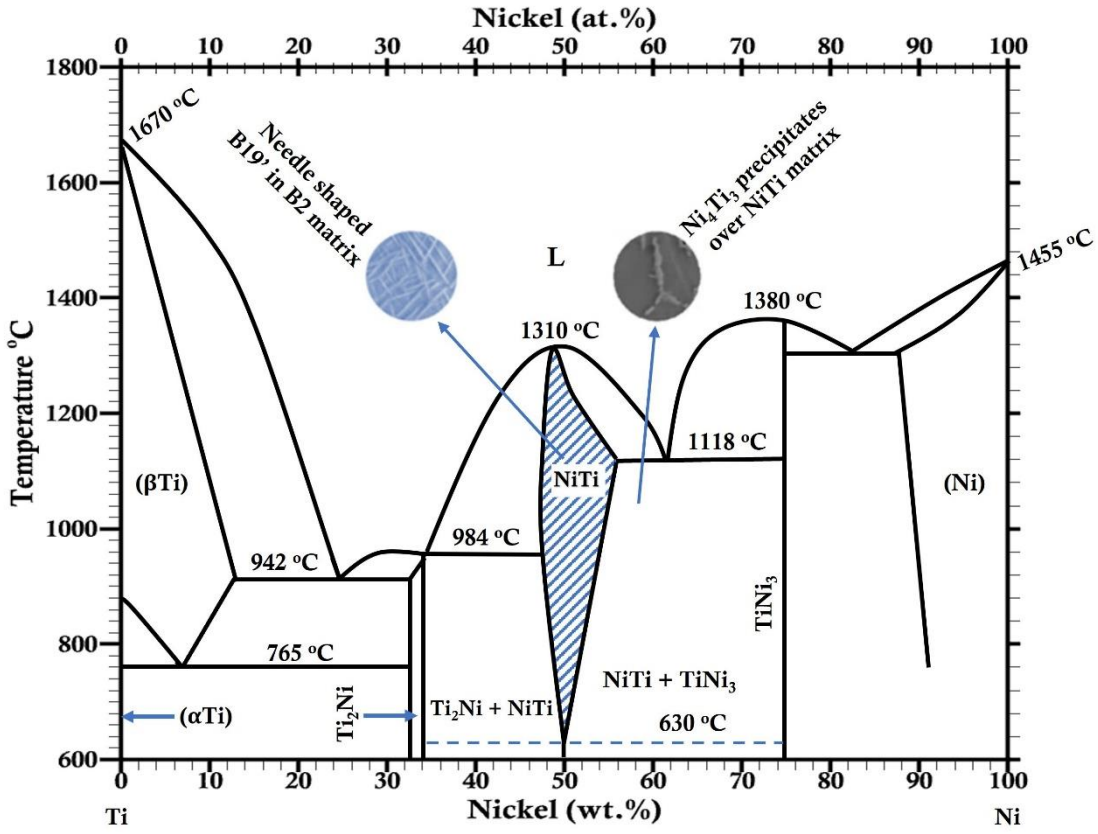

Fig. 2.1: Binary phase equilibrium diagram of Ni-Ti alloy.

Equiatomic NiTi has a higher transformation temperature for SMAs and a higher recoverable strain. On the other hand, NiTi with Ni 50 – 55 at. % or 55 – 60 wt. % has specific properties like lower density, high hardness, high corrosion resistance, and non-

magnetic nature, making it very useful in various industries [36]. 55NiTi (55 wt.% Ni (50 at. % Ni)) with near equal atomic ratio has shape memory effect and superelasticity. It is a typical shape memory alloy and has attracted extensive attention from researchers [100, 101]. Nickel-titanium alloy with composition 60 wt.% Ni and 40 wt.% Ti (i.e., 55 at. % Ni and 45 at. % Ti) is referred to as NiTiNOL60 alloy. NiTiNOL60 alloy is a Ni-rich intermetallic nickel-titanium alloy that contains a broad combination of physical and mechanical properties such as high hardness, low elastic modulus, resistance to aqueous corrosion, and good biocompatibility [5, 34, 35]. These unique combinations make this alloy an attractive candidate for medical components such as implants and prostheses, where hard and biocompatible materials with low stiffness are typically employed. NiTi-based shape memory alloys have been shown to exhibit the shape memory effect (thermally induced transformation) and superelasticity (mechanically induced transformation) depending on composition, processing methods, and other factors [100]. However, the production technology for NiTiNOL is crucial considering the great affinity of titanium for carbon and oxygen, as well as the requirement to reduce the creation of non-metallic impurities in the elements' involvement. Aside from minimising the formation of non-metallic inclusions, it is essential to achieve an alloy with a precise, stable chemical composition [99]. As a result, high-quality raw materials, those having 99.99 wt.% Ni and 99.8 wt.% Ti is required for the fabrication of NiTiNOL. According to Stanford [102], the Hot Isostatic Pressing (HIP) method commonly used for the processing and fabrication of 60NiTi alloy is described in NASA's technical report [102, 103]. Another study by Khanlari, et al. [104] presented Ni-rich 58NiTi and 60NiTi fabricated from elementally blended Ni and Ti powders using a laser powder bed fusion technique.

Nickel and titanium are the two significant elements mostly used in high-temperature applications [60, 84]. Superalloys are preferred over conventional materials for such high service temperatures (650 ℃), particularly where the structural component may fail due to creep and/or fatigue [69, 105, 106]. NiTiNOL60 has superior oxidation and corrosion resistance with excellent stable mechanical properties at higher service temperatures [36], leading to its wide medical and engineering applications. Notwithstanding, the previous study by Okoani, et al. [107] presented that Ni-Ti-based alloys face significant concern in tribological applications, such as automotive, spacecraft [24], marine [62, 63], food and beverage processing [108-110], pharmaceutical [111], biomaterial [112], actuators [113] and biomedical sectors such as orthopaedic [114], endodontic [99] and orthodontic [99].

2.2.2.2. Medical applications of Ni-Ti alloys

The advancement in medicine and material engineering has promoted the utilisation of implant materials, including stainless steel, cobalt-chromium alloy, organic polymer, magnesium matrix composite, nickel-titanium shape memory alloy, and titanium alloy [115, 116]. While biomaterials like ceramics (alumina), polymers (UHMWPE), and metals (titanium and cobalt-chromium alloys) show outstanding biocompatibility, they have their drawbacks, including the potential for hazardous substances in the alloying elements [64, 89, 91, 117]. Titanium alloys are among the metallic materials most commonly employed in biomedical applications [94, 118]. They are appropriate as implant materials due to their unique combination of corrosive and mechanical qualities [119]. It is well known that when exposed to bodily fluids such as saliva, phosphate-buffered saline, etc., all titanium alloys have the ability to form a protective coating that can prevent corrosion [120]. Under these circumstances, the protective layer can delay or stop the dissolution of the metallic ions (without involving any mechanical action) [121]. Still, mechanical loading can damage this layer, thereby releasing metallic ions. Figure 2.2 illustrates the artificial implant in a hip joint depicting tribocorrosion and fretting corrosion due to tribological interfaces around the hip joints [80, 119, 122]. As a result, CoCr alloys are frequently combined with Ti alloys to considerably reduce micro-motions and fretting corrosion [16, 119]; however, metallic materials alloyed with chromium release carcinogenic elements, which can cause serious health issues. Although cobalt-chromium alloy possesses good corrosion resistance and tolerates large loads, both metals possess cytotoxicity [123]. The widely used titanium alloy Ti–6Al–4V is an αβ–type alloy that is associated with toxic alloying elements: Vanadium (V) and Aluminium (Al). That may result in issues related to the development of Alzheimer's disease and inflammatory cell reactions [119, 124]. To combat the problem, NiTi shape memory alloys and magnesium-based alloys were introduced to satisfy more specialised needs, like non-conventional reconstructive surgery involving hard tissues or organs (NiTi as vascular stents) and bone tissue engineering and regeneration (magnesium-based alloys). Although magnesium matrix composites and alloys have quick biodegradation rates, they have low mechanical qualities and are not corrosion-resistant [80, 112, 115]. These have promoted the need to develop biomaterials with a lower modulus of elasticity, increased corrosion resistance, and more acceptable biocompatibility [64, 125].

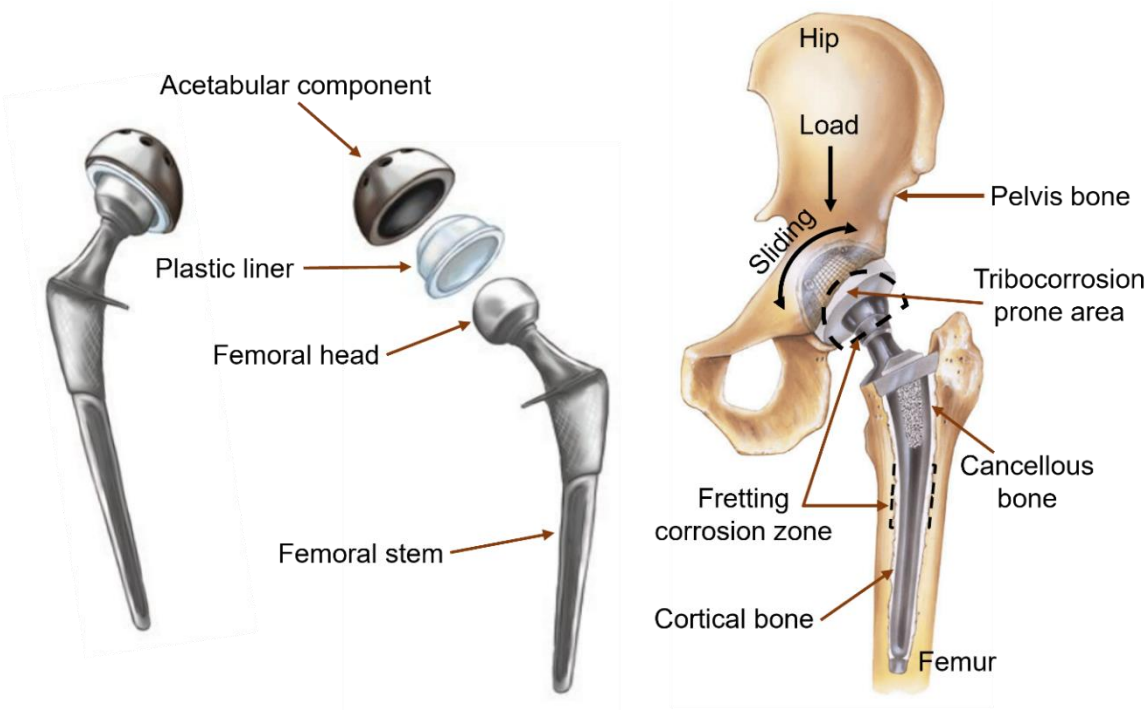

Fig. 2.2: Schematic representation of tribocorrosion effect in a hip joint implant.

Consequently, Ni-Ti alloys are emerging as the optimum choice as numerous researchers have examined and compared the corrosion and/or tribological properties of these biomaterials to those of other materials, including Ti and its alloys, CoCr alloys, 316L stainless steel, etc. [65, 67, 126-129]. Buciumeanu, et al. [94] investigated the viability of substituting NiTi alloy for Ti-6Al-4V alloy in some medical applications, such as implants. This is because metallic implants designed for medical bone replacement should have characteristics similar to the organic tissue that must be replaced [64, 94]. It has excellent biocompatibility, high corrosion resistance, suitable mechanical properties (high strength, sufficient ductility, low Young's modulus, high hardness, etc.), high wear resistance, and osseointegration. Table 2.1 compares the mechanical properties of cortical bone and some selected metals often used as biomaterials. Given that bone's ultimate compressive strength is less than 340 MPa, implants intended for general bone replacement applications should, as shown in Table 2.1, have a strength of 340 MPa or above [80, 130]. This is because porous structures promote bone in-growth, lower the implant's Young's modulus, and help to lessen the stress shielding phenomenon. Thus, NiTi-based alloy demonstrates the acceptable characteristics that make it a suitable biomaterial for bone replacement and implant.

Table 2.1: Comparing the mechanical properties of common implant biomaterials and cortical bone [80, 130].

Material	Young's modulus (GPa)	Ultimate tensile strength (MPa)	Fracture toughness (MPa)
Cortical bone	10–30	130–150	2–12
Trabecular bone	0.01–3	2–70	–
NiTi alloy	30–50	1355	30–60
Mg alloy	40–50	100–250	15–40
Ti alloy	105–125	900	~80
316L stainless steel	200	540–1000	~100
CoCrMo alloy	240	900–1540	~100

In orthodontics, following the intricate tribo-electrochemical process in the oral environment, Kassab and Gomes [131] examined the fracture of NiTi wires in artificial oral environments. It is established that there is a considerable risk of corrosion-induced fracture when using super-elastically strained NiTi implants in fluoride-containing oral environments [131, 132]. Figure 2.3 depicts a dental implant using a biomaterial, and in the complex oral environment, ingesting food particles and fluid substances in the presence of saliva results in temperature and pH variations that promote corrosion (fretting) activities. Further actions from chewing food products trigger the micro-movements between the implant abutment, the gum tissues and the jawbone, contributing to the enamel/ crown wear and distorting the periodontal ligament. The combined wear and corrosion interactions lead to the tribocorrosion phenomenon.

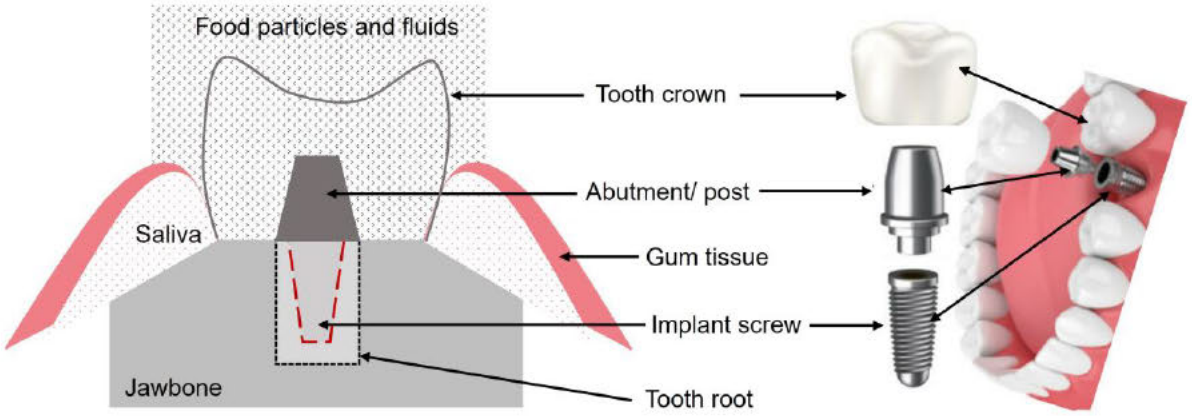

Fig. 2.3: Schematic representation of tribo-corrosion affected area in an oral environment.

The invention of NiTi instruments has since proven beneficial to endodontic treatment [133] because of the easier and more effective root canal preparation made possible by their higher taper. Tools manufactured of NiTi alloys have advantages over those made of stainless steel alloys in terms of mechanical qualities, including increased fatigue resistance, high flexibility, and resistance to fracture from twisting in either a clockwise or anticlockwise direction [70, 134]. Brantley, et al. [119] stated that stainless steel, cobalt chromium, nickel-titanium, and beta-titanium are the four main orthodontic alloys that are currently widely used for orthodontic wires, brackets, and devices. Despite the benefits, each alloy has some associated drawbacks regarding clinical application [119, 135, 136]. Table 2.2 summarises the general compositions and mechanical properties of these alloys.

Table 2. 2: Mechanical properties of four major orthodontic alloys [119].

Alloy	General composition	Elastic modulus (GPa)	0.1% yield strength (MPa)
Stainless steel	Fe–Cr–Ni	160–180	960–1500
Cobalt–chromium	Co–Cr–Fe–Ni	150–180	830–1200
Nickel–titanium	Ni–Ti	32–36	200–550
Beta–titanium	Ti–Mo–Sn–Zr	60–68	620–690

2.2.2.3. Engineering applications of Ni-Ti alloys

Ni-Ti alloys have gained vast engineering applications due to their outstanding corrosion resistance and good mechanical qualities [107]. Ni-based superalloys are used in the aerospace industry for nuclear power plant boilers, turbine blades, and aero-engine casings [36]. Variable geometry chevrons, variable camber fan blades, actuators, bearings, general flow control, adaptive intake nozzles, flaps, and other hinged components are just a few of the aerospace applications for NiTi alloys [27, 100, 137]. Although they are less common, alloys with higher nickel contents (e.g., 52 to 57 at. % Ni) have several beneficial properties for structural applications, including high hardness, resistance to corrosion, and low density, thereby making these alloys beneficial in tribological and tool manufacturing [47]. Accordingly, Buehler and Wang [35] suggested using these alloys in non-magnetic hand tools, hardened penetrators, and bearings for water-flooded rotating components. The exceptionally high hardness and low effective modulus ensure this alloy can withstand extreme strains without permanently deforming, which lowers the possibility of structural damage at contact areas during shock loading. Because of these qualities and its superior corrosion resistance, NASA considered using

this alloy in the International Space Station's water recycling system in place of bearings [27, 33, 138].

DellaCorte [4] studied the mechanical components representing severe bearing or gear applications that have long challenged the bearing community. The field of applications was categorised into low, moderate, and critical needs. The study highlighted considerations needed in shock/ high loads as critical for aircraft landing gears, space gyros and mining vehicle bearings. Critical considerations are required for corrosion design requirements in aircraft control surface bearings, landing gears, marine machinery, food processing, and water treatment plants. While X-ray tube bearing requires critical consideration in high temperature and electrical conduction applications, their study revealed that materials used for X-ray tubes should be compatible with solid film lubricant, tolerate radiation and be able to operate in a vacuum (little or no outgassing tendency) [4].

Near-equiatomic and Ti-rich compositions have typically been used for solid-state actuation in appliances, including those found in spacecraft, automobiles, and marine equipment [24, 47]. Moreover, unlike Ti alloys, the combined Ni and Ti materials have been shown to possess hardness comparable to tool steels and the ability to be comparably lubricated [33, 35].

Protection mechanisms against tribocorrosion

Different measures, such as surface modifications and coatings, have been employed in the protection of metallic components against surface deterioration, which is often aggravated by tribocorrosion [50, 139-141]. The benefit of this protective layer is to promote the longevity of the components and decrease manufacturing costs [142]. According to Fotovvati, et al. [140], the different coating methods, materials and applications all tend to a common purpose of protecting a part or exposed structure from mechanical or chemical damage (i.e., tribocorrosion). Dong, et al. [143] investigated the erosion wear behaviour of NiTi alloy coating fabricated via high-frequency induction heating technology. Shen, et al. [144] studied the enhanced anti-tribocorrosion performance of Ti-DLC coatings deposited on steel substrate using a filtered cathodic vacuum arc (FCVA). According to their report, the Ti-DLC coatings at –200 V presented the best anti-tribocorrosion performance with the least values of friction coefficient and wear rates, thereby suggesting that Ti-DLC coating is a potential protective material for marine equipment. In another study, López-Ortega, et al. [145] investigated the performance of a thermally sprayed aluminium (TSA) coating modified by plasma electrolytic oxidation (PEO) technique for offshore submerged components protection.

The results showed that the TSA coating modified by PEO showed a significant improvement in the corrosion, wear and tribocorrosion resistance leading to smaller material losses and lower coefficient of friction (COF) [145]. Dong, et al. [121] presented the surface modified techniques and emerging functional coating of dental implants. They attributed the major reasons for implant failure to poor osseointegration and bacterial infection. Some researchers have investigated the effects of graphene on tribocorrosion behaviour [77, 78]. For improved surface protection, further research into the development of more advanced coating techniques is required.

2.2.2.4. Tribology and tribological concepts

Figure 2.4 presents a summarised representation of tribological concepts during reciprocating sliding. As is known, tribology encompasses the wear, friction, and lubrication of a material, while friction is an underlying force that impacts almost all interface-related applications. The interface-related applications could be categorised from solid-solid and solid-liquid to liquid-liquid interfaces [146]. Friction is often associated with mechanical wear; hence, controlling its level between the contact surfaces of two moving bodies is necessary. The coefficient of friction is used to measure friction, and it can be calculated using Eq. (2.1) as follows:

$$\mu = \frac{F_t}{F_n} \tag{2.1}$$

where μ = coefficient of friction, F_t = tangential force and F_n is the normal load applied on the moving body.

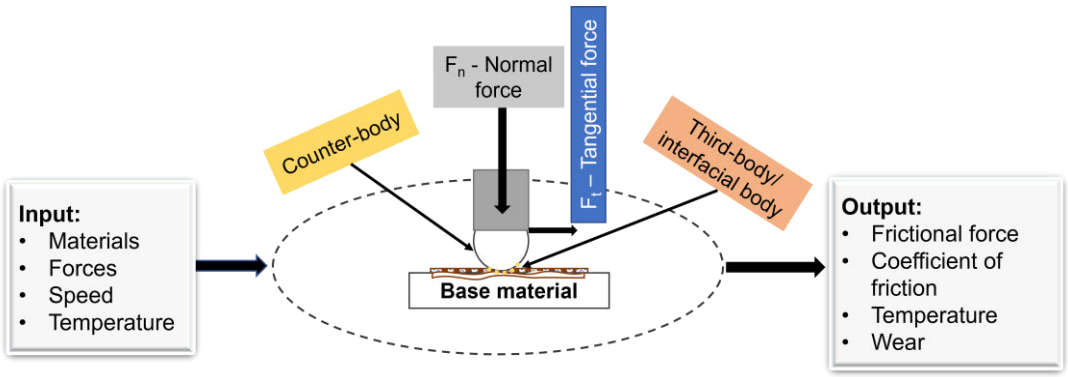

Fig. 2.4: Schematic representation of a tribological system.

Leonardo da Vinci first introduced the fundamental understanding of interfacial friction through the distinction between motion resistance in sliding and rolling motions, as reported by Yi, et al. [146]. Recent investigations on macroscopic interaction evaluate the impact of load, contact area, and sliding speed on macroscopic solid motions. Figure 2.5 depicts the combined effect of load and sliding speed on the sliding wear process in

metals [147]. The image shows increased temperature at the contact interface, heavy mechanical damage at higher load, and increased sliding speed, resulting in plastic deformation and wear loss.

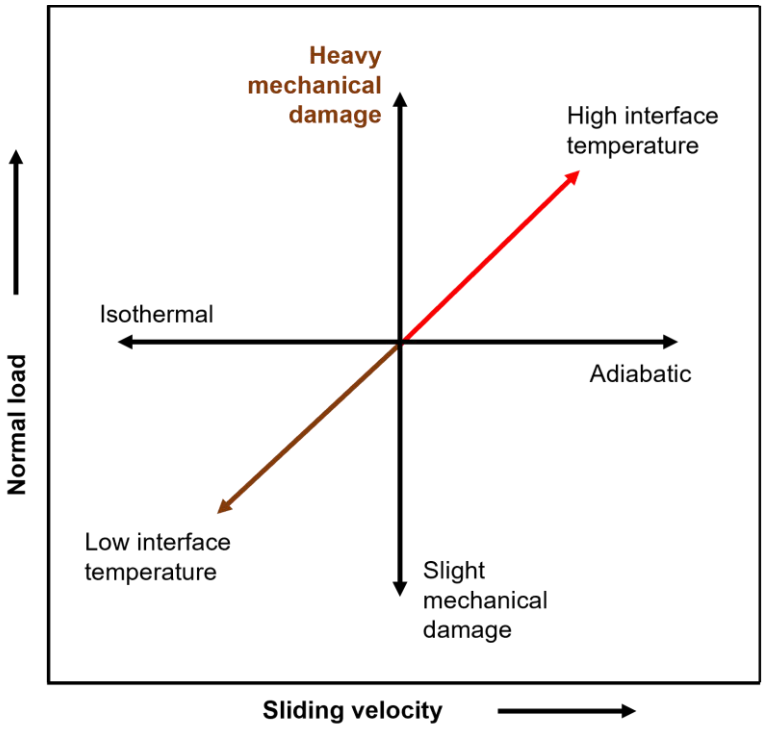

Fig. 2.5: Effect of load and sliding speed on the sliding wear process in materials.

Since wear occurs due to relative motion between two surfaces, surface damage during wear is mainly related to the surface of the two contact materials and environmental conditions under lubricated and/or unlubricated systems. Several wear equations in the literature can be used to quantify wear and theoretically determine the amount of material loss. This includes Archard's law, a simple equation (Eq. 2.2) used in wear analysis to compute material loss (wear volume).

$$\frac{V}{L} = K\frac{F_n}{H} \tag{2.2}$$

where V = wear volume loss (mm^3), L = total sliding distance (m), F_n = applied normal load (N), H = hardness of the material (MPa), and K = wear coefficient (non-dimensional).

However, there are some drawbacks because the equation does not consider the effect of sliding speed, contact area, interface temperature, lubrication, etc. Measuring the wear rate of a material in the absence of corrosion is required to determine the pure mechanical wear. This can be accomplished with a sliding wear test that solely utilises tribological factors. Profilometry is a technique for quantifying material loss through experimentation. By measuring the height and width of profiles across the wear track, this technique aids in identifying materials removed or displaced in sliding contact.

2.2.2.5. Sliding wear mechanisms of Ni-Ti-based alloys

Different wear mechanisms can be identified depending on the relationship between the interactions between a material's mechanical properties, applied load, and contact pressure. Wear can generally be classified into adhesive wear (this occurs based on the micro-joints between the two surfaces during relative motion), surface fatigue wear (occurs during cyclic loading), corrosion wear (usually accelerated by oxidation in a corrosive environment), and abrasive wear (occurs as ploughing, or cracking when hard surface slides against a softer surface) [53, 148]. Since the elastic or reversible deformation occurs when the average contact pressure is lower than the yield strength of the contacting material, repeated rolling/sliding results in crack initiation and propagation, leading to fatigue wear. Plastic or irreversible deformation occurs when the average contact pressure exceeds the yield strength of a material. A different wear mechanism known as cutting or micro-cutting happens when the high strain created at the indenter edges causes the sharp edges of sliding bodies to cut through areas of the softer sliding material. When there are blunt asperities, the moving indenter uses a process known as ploughing to drive the materials in the contact zone apart [53, 147, 148]. The wear rate estimations can quantify the material loss or removal per unit time. As represented in Figure 2.6, Hutchings [147] described the relationship between wear rate and contact resistance on a logarithmic scale, i.e., the wear behaviour of a material sliding against a smooth, hard surface, as a function of the normal load [147].

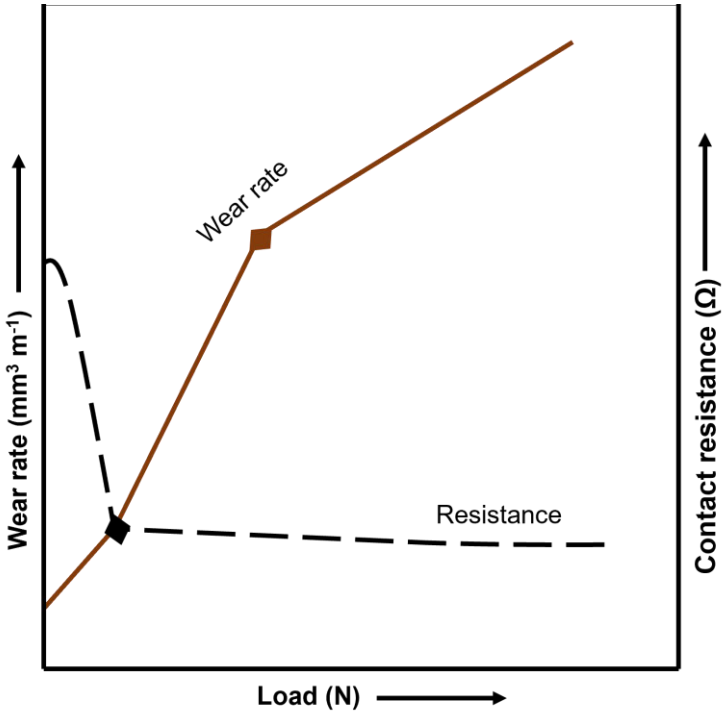

Fig. 2.6: The relationship between wear rate and electrochemical contact resistance.

As depicted in Figure 2.6, it is evident that Archard's equation (Eq. 2.2) is obeyed, whereby at higher loads (depending on the contact geometry) leading to significantly higher contact pressures, the wear rate increases significantly. Higher contact resistance is often recorded at low loads because the local contact pressure at asperities contacts is inadequate to penetrate the passive oxide film. Hence, insufficient contact pressure significantly increases the wear rate by approximately 100. This wear transition is attributed to the presence of a thin oxide film at the contact surfaces [53].

2.2.2.6. The fundamentals of corrosion

Corrosion is the reaction (chemical, electrochemical, physical or combination) of a material and its environment with a consequent deterioration in its properties. While the corrosion phenomenon is related to the material, the environment, and the interface between both, this study focuses on the electrochemical reaction of materials under tribological contacts. The interaction of a metal and a corrosive environment reveals that the oxidising agent oxidises metal. Various electrochemical interactions show that factors influencing corrosion include the position of the metal in the electrochemical series, pH, electrolyte concentration, impurities in the metal, concentration of oxygen, and temperature difference [69, 149]. Two common surface reactions in aqueous electrolytes or a specific corrosive environment are the cathodic (oxidising agent-induced electron consumption) and anodic (metal atom electron removal) reactions [7, 61]. The following chemical reactions represent the anodic and cathodic half-cell reactions during the electrochemical process (Eqs. 3–5).

$$\mathrm{M} \rightarrow \mathrm{M}^{+z} + \mathrm{ze}^{-} \quad (\mathrm{Oxidation} \equiv \mathrm{Anodic}) \tag{2.3}$$

$$\mathrm{zH}^{+} + \mathrm{ze}^{-} \rightarrow \mathrm{H}_{z} \uparrow \quad (\mathrm{Reduction} \equiv \mathrm{Cathodic}) \tag{2.4}$$

$$\mathrm{M} + \mathrm{zH}^{+} \rightarrow \mathrm{M}^{+z} + \mathrm{H}_{z} \uparrow \quad (\mathrm{Redox} \equiv \mathrm{Overall}) \tag{2.5}$$

The material undergoes various electrochemical responses through the immune state (where the metal is not corroded), active state (corrosion leading to metal loss or dissolution of one of the constituents of the corrosive environment into the metal) and the passive state (metal generates a protective oxide passive film on its surface which reduces corrosion rate). Corrosion damage in the form of general or localised corrosion can be used to determine the corrosion mechanism. Metals with low corrosion potential will undergo anodic polarisation, increasing the anodic dissolution rate. The metal with a high corrosion potential will undergo cathodic polarisation, slowing the dissolution rate down [150]. Pitting, the conventional corrosion form, exists in different stages even though pitting is self-initiating and self-propagating, making it difficult to determine the

borders for every stage, including the nucleation, metastable pit formation, and stable pitting [151].

2.2.2.7. Corrosive wear mechanisms of Ni-Ti-based alloys

Most metals and alloys face surface deterioration when in contact with water-based corrosive environments. According to Eq. (2.6), the reaction between metal and water generates a surface metal oxide and releases hydrogen [152, 153].

$$\mathrm{Me} + \mathrm{H_2O} \rightarrow \mathrm{MeO_x} + \mathrm{xH_2} \tag{2.6}$$

As reported by Vilhena, et al. [81], the electrochemical behaviour (reduction reactions) that take place at the cathodic branch are dependent on the nature of the corrosive environment and are summarised as follows in equations (2.7 – 2.10):

$$\mathrm{O_2} + 4\mathrm{H^+} + 4\mathrm{e^-} \rightarrow 2\mathrm{H_2O} \quad (\text{Oxygen reduction in acidic medium}) \tag{2.7}$$

$$\mathrm{O_2} + 2\mathrm{H_2O} + 4\mathrm{e^-} \rightarrow 4\mathrm{OH^-} \quad (\text{Oxygen reduction in alkaline environment}) \tag{2.8}$$

$$2\mathrm{H_2O} + 2\mathrm{e^-} \rightarrow 2\mathrm{OH^-} + \mathrm{H_2} \quad (\text{Water reduction in neutral/alkaline medium}) \tag{2.9}$$

$$2\mathrm{H^+} + 2\mathrm{e^-} \rightarrow \mathrm{H_2} \quad (\text{Proton reduction in an acidic environment}) \tag{2.10}$$

During electrochemical activities on metal surfaces, corrosion can be uniform or localised. Other common forms of corrosion include:

- Stress corrosion cracking: Occurs when a metal under stress cracks in a corrosive environment.
- Galvanic corrosion (two-metal corrosion): Occurs when two dissimilar metals in electrical contact are exposed to an electrolyte.
- Pitting: Formed by small anodes on a metal surface, creating holes or pits.
- Intergranular corrosion: Occurs at or near grain boundaries in a metal.
- Crevice corrosion: Localised corrosion that occurs in crevices, shielded areas where stagnant solution can form.
- Erosion corrosion: Occurs due to the combined effects of corrosion and relative motion of a corrosive fluid on a metal surface.
- Selective leaching or dealloying: Preferential removal of one element from a solid alloy by corrosion.

2.2.2.8. Tribocorrosion: historical background and concept

The history of tribocorrosion (tribo-electrochemistry) dates back to 1875 when Edison observed a variation in friction coefficient at various applied potentials [91]. Tribocorrosion can be described as a degradation phenomenon of material surfaces

(wear, cracking, corrosion, etc.) subjected to the combined action of mechanical loading (friction, abrasion, erosion, etc.) and corrosion attack caused by the environment (chemical and/or electrochemical interaction), as highlighted in Fig. 2.7.

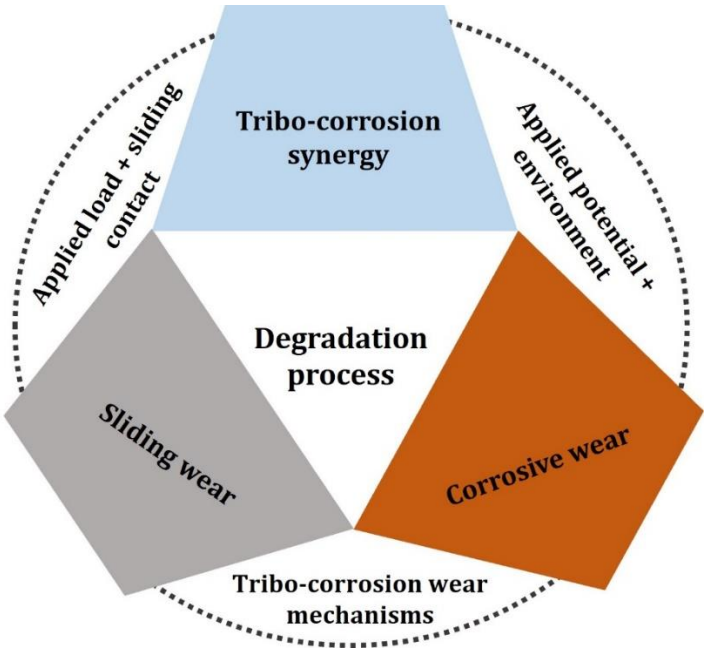

Fig. 2.7: Schematic illustration of tribocorrosion concept.

Material degradation due to simultaneous chemical and mechanical effects may occur under various conditions and contact modes, as shown in Figure 2.7. According to Siddaiah, et al. [9], tribocorrosion is a surface alteration that involves the joint action of relatively moving mechanical contact with electrochemical reactions [9]. It measures the tribological quantities, such as friction and wear, in a controlled and reproducible manner, as well as the electrochemical interactions of the system. Two-body or three-body contacts between sliding surfaces are a common cause of tribocorrosion. The relative motion of the surfaces can be unidirectional, as in the case of a pin-on-disk wear test apparatus or reciprocating. Fretting involving reciprocating motion of small magnitude is a particular type of tribological contact. Rolling contact occurring in ball bearings also experiences tribocorrosion. Particle impingement happens in erosion-corrosion as a combination of mechanical and chemical attacks on materials in pumps and pipes carrying slurries. The distinctive features of the tribocorrosion mechanism, tribology, and corrosion actions are influenced by environmental factors [7], as presented in Fig. 2.8.

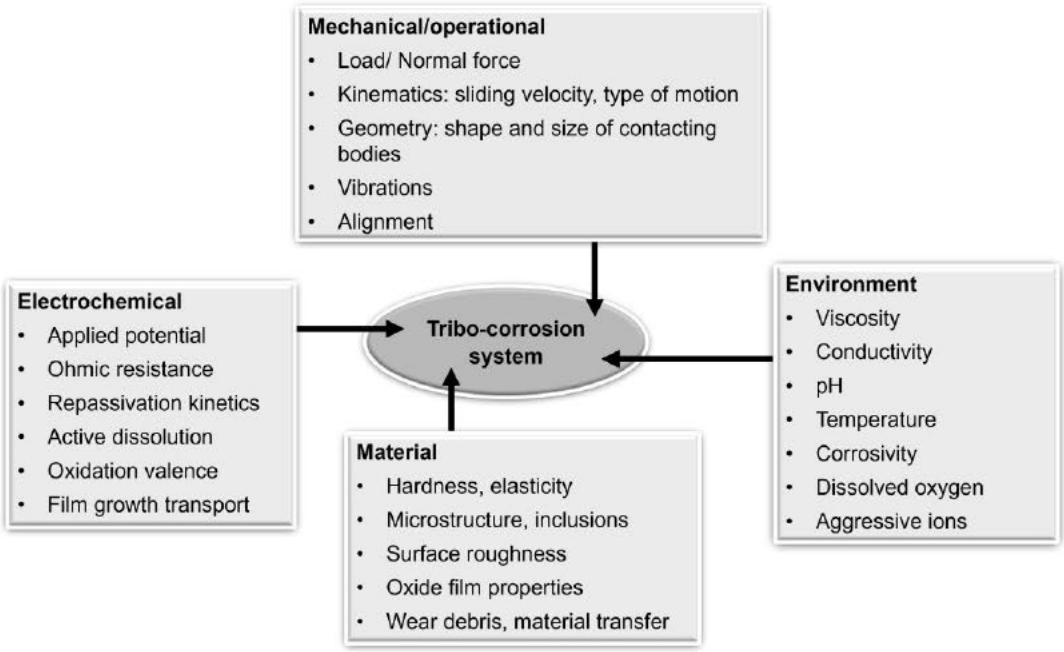

Fig. 2.8: Factors influencing tribocorrosion.

Considering the impact of the relative motion in erosion-corrosion issues, Wellman [154] highlighted the relationship between sliding velocity and temperature presented in the following Table 2.3.

Table 2.3: Examples of industrial erosion-corrosion issues as a function of the sliding velocity and temperature [154].

	Low temperature	**High temperature**
Low velocity	Offshore and marine structures	Fluidised bed
	Slurry transportation of solids	Combustors
	Chemical processing	Coal-fired boilers
	Exhaust valves	Chemical processing
High velocity	Oil and gas industry	Aero engines
	Mining	Oil and gas industry
	Fuel injection systems	Steam turbines
		Gas turbines
		Turbochargers

2.2.2.9. Tribo-electrochemical test procedures for sliding contacts

To investigate the tribocorrosion behaviour of a material, mechanical and corrosion responses must be collected and monitored during tribocorrosion testing [6, 155-159]. Figure 2.10 shows the schematic representation of a tribocorrosion system.

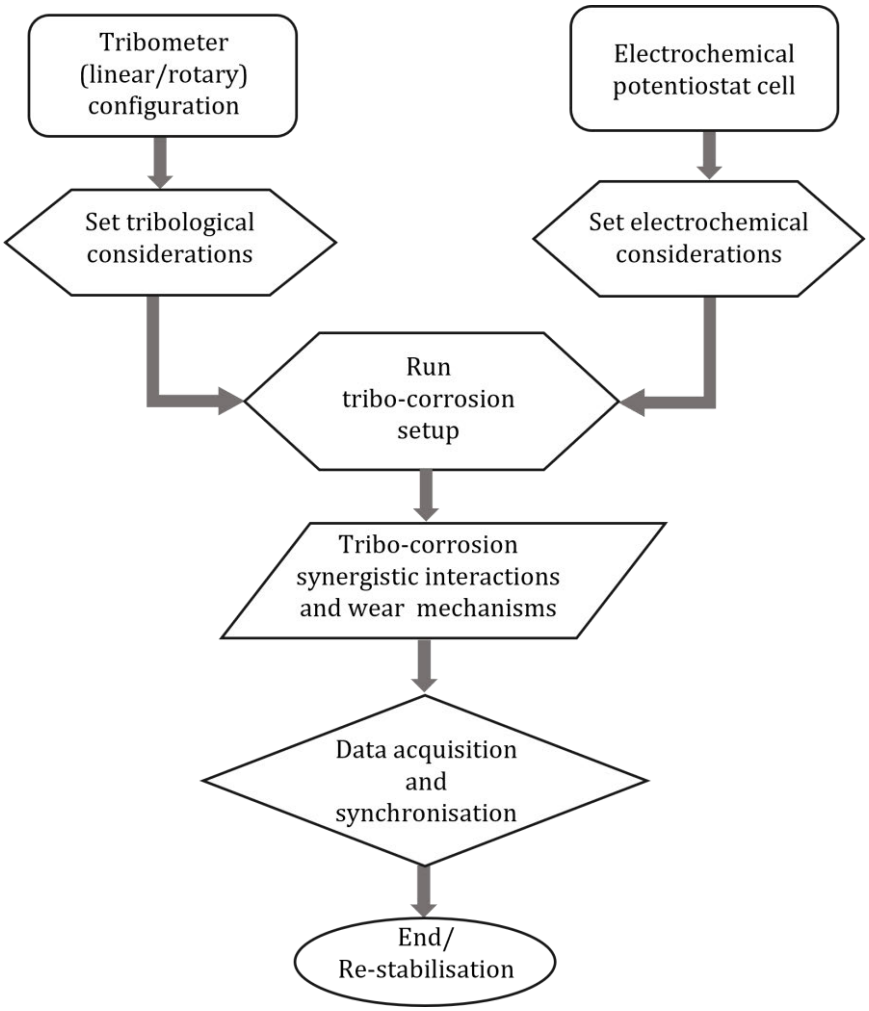

Fig. 2.9: Schematic flowchart for tribo-corrosion experimental setup.

As shown in Figure 2.9, the tribometer measures the evolution of frictional forces and other tribological properties as it creates relative motion in either unidirectional (rotatory) or bidirectional (reciprocating) sliding of two surfaces against each other. On the other hand, an electrochemical technique/ potentiostat cell is employed to monitor the corrosion response from the test system [6, 91]. Hence, typical electrochemical interfacing consists of three electrode configurations, including (1) a reference electrode (RE) (saturated calomel electrodes (SCE) or silver/silver chloride electrodes (Ag/AgCl)) with a stable-well-defined potential, (2) a counter electrode (CE) made of inert material (graphite rod or platinum wire), and (3) a working electrode (WE) often the specimen under investigation. The electrode configurations are coupled to a potentiostat to register the potential between the reference electrode and the working electrode or the current between the counter electrode and the working electrode. Okoani, et al. [107] presented a schematic representation of a typical tribocorrosion test setup for a linear reciprocating ball-on-plate configuration in their study.

2.2.2.10. Tribocorrosion wear mechanisms

Numerous studies have examined the tribocorrosion behaviour of NiTi alloy in various corrosive media and test conditions [52, 114, 160]. These studies report that the degradation caused by the combined effects of mechanical and electrochemical processes is generally distinct from these failure mechanisms operating independently [94]. For example, a 2014 study by Kosec et al. showed that while artificial saliva increased the wear of NiTi, mechanical loading caused corrosion to accelerate [45, 161]. At the onset of sliding during the tribocorrosion process, titanium alloys and other passive metals undergo a sudden drop in the initial corrosion resistance, E_{oc} [6, 162]. This is explained by destroying a thin passive layer along the wear track and exposing the electrolyte to new metal surfaces [149]. Passive metals are particularly susceptible to tribocorrosion because sliding can easily remove the passive film's protective properties, causing a rapid corrosion rate before the surface repassivates [6, 126, 163]. The metal in the worn track experiences the following oxidation processes, which result in the formation of soluble ions and/or solid corrosion products [155, 164]:

$$\mathrm{M} \rightarrow \mathrm{M^{n+}} + \mathrm{ne^-} \tag{2.11}$$

$$\mathrm{M} + \mathrm{n/2H_2O} \rightarrow \mathrm{MO_{n/2}} + \mathrm{nH^+} + \mathrm{ne^-} \tag{2.12}$$

To account for wear after the electrochemical measurements, the wear track is considered to consist of two distinct zones: the active area A_{act}, where the initial passive film has been removed, and the passive area A_{repass}, where the film was either not removed, or it had enough time to be restored. The surface area of the wear track, A_{tr}, is considered the surface area measured at the end of the sliding test, with $A_{tr} = A_{act} + A_{repass}$. The material loss in the wear track, W_{tr}, is decomposed into components connected to the different wear track zones in the wear track, as mathematically shown by Azzi and Klemberg-Sapieha [155].

$$\mathrm{W_{tr}} = \mathrm{W_{act}^{c}} + \mathrm{W_{act}^{m}} + \mathrm{W_{repass}^{c}} + \mathrm{W_{repass}^{m}} \tag{2.13}$$

where: $\mathrm{W_{tr}}$ = material loss along the wear track, $\mathrm{W_{act}^{c}}$ = material loss due to corrosion of active material, $\mathrm{W_{act}^{m}}$ = material loss due to mechanical wear of active material, $\mathrm{W_{repass}^{c}}$ = material loss due to corrosion of repassivated material, $\mathrm{W_{repass}^{m}}$ = material loss due to mechanical wear of repassivated material.

Further, the mechanistic interpretation [165] of the tribocorrosion phenomenon [1], i.e., the total wear volume (V_t) as the sum of the material loss due to sliding wear (V_{mech}) and the loss of material due to corrosion or electrochemical oxidation (V_{chem}) is shown in Eq. 2.14 [166].

$$V_t = V_{mech} + V_{Chem} \tag{2.14}$$

Using the wear volume, the specific wear rate can be estimated from Archard's wear law, Equation 2.2.

$$\text{Specific wear rate} = \frac{\text{wear volume}}{\text{normal load} \times \text{sliding distance}} \tag{2.15}$$

From a physical point of view, tribocorrosion includes a variety of mechanical and chemical degradation phenomena, namely, corrosive wear, erosive wear, wear accelerated corrosion, erosion corrosion, oxidative wear, fretting corrosion, stress corrosion cracking, and corrosion fatigue. The simultaneous wear and corrosion actions lead to an irreversible transformation of the material occurring at a tribological contact [167]. The continual sliding between the interacting bodies results in wear, i.e., particle detachment and particles trapped at the interfaces, which are referred to as third bodies as shown in Figure 2.10. These third-body particles can oxidise and/or spread to cover one or both surfaces (forming a transfer film). The film or accumulation of third bodies alters the contact conditions of the initial bodies, and the resulting wear can be explained as a mass flow between the interacting bodies and the third bodies [53]. The mechanical abrasion of passive film usually leads to wear-accelerated corrosion due to the high chemical reactivity of the bare metal surface exposed to the corrosive environment. On the other hand, the passive films seem to decisively influence the surface mechanical response of metals and the third body behaviour. Under tribocorrosion conditions, two main mechanisms contribute to material removal from the surface: wear-accelerated corrosion and mechanical removal from the sliding contact [6, 61, 164].

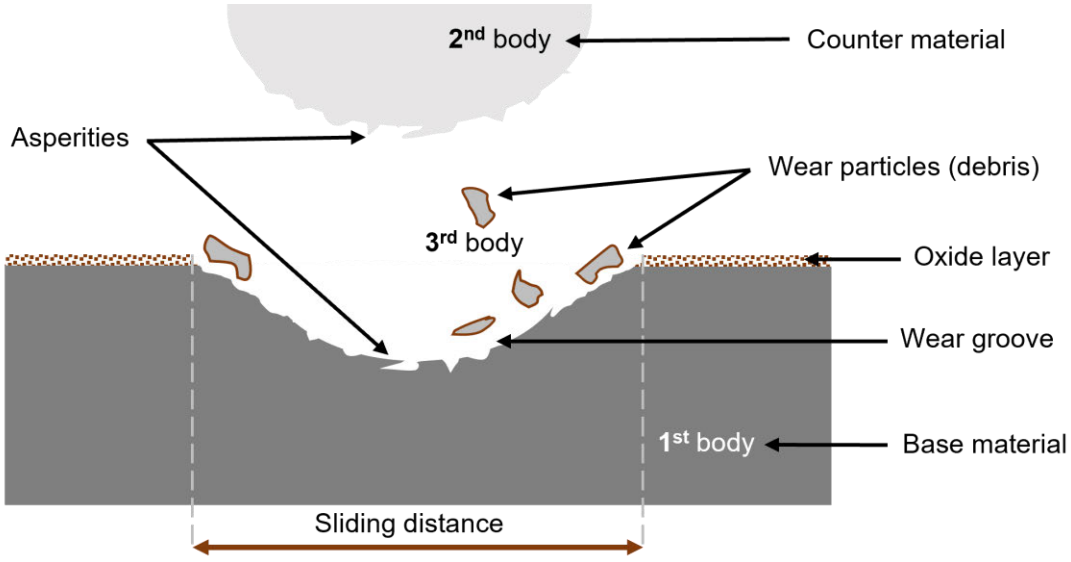

Fig. 2.10: Representation of a third body wear phenomenon during tribocorrosion.

2.2.2.11. Tribocorrosion: current status, challenges, and future prospects

2.2.2.12. Current status and challenges

Fundamentally, tribocorrosion studies deal with an irreversible transformation of materials or their function due to simultaneous mechanical and chemical/ electrochemical interaction between surfaces in relative motion [51, 168]. As stated earlier, tribocorrosion is a complex phenomenon due to simultaneous actions that adversely affect each other. Recently, research in tribocorrosion has received significant attention because the process occurs in almost all engineering and some medical applications. Thus, tribocorrosion has become a subject of intense study, attracting researchers from different fields based on the multidisciplinary approach of the systems involved. Table 2.4 presents a summarised update on the recent tribocorrosion reviews. Notably, research on tribocorrosion in medical applications has up-to-date information compared to engineering applications, where the last review was in 2018.

Table 2.4: Summary of review papers on tribocorrosion and NiTi in the past decade.

Title and reference	Remark/ recommendation
A review on wear, corrosion, and wear-corrosion synergy of high entropy alloys **[19]**	Their study comprehensively evaluated the critical developments in wear, corrosion, and wear-corrosion resistance made by high entropy alloys (HEAs) over the previous 20 years. According to their study, scientists interested in studying the tribocorrosion of recently designed and manufactured HEAs have several difficulties due to the need for more pertinent papers on wear-corrosion synergy. Thus, the conclusion is that this relatively uncharted area awaits exploration by more researchers to understand the wear-corrosion synergy of HEAs fully.
Recent approaches to limit the tribocorrosion of biomaterials: A review **[16]**	Their analysis of the literature gave an overview of the research trend. The ability to create lifelong biomaterial apparatuses should be a key component of biomaterials research and development. Accordingly, a new wave of research was first essential to understand the intricacy of biomaterials' interactions with the human body and then attempt to produce the necessary devices to fulfil our needs.

(Bio)Tribocorrosion in dental implants: Principles and techniques of investigation **[51]**	In the domains of tribology and medicine, the highlighted problems in the review, such as the prevention or minimisation of tribocorrosion in biological tribopairs, etc., undoubtedly represent a scientific challenge for the upcoming years.
Nickel-titanium alloys as orthodontic archwires: A narrative review **[169]**	The study evaluated NiTi archwires from a clinical perspective, focusing on mechanical properties and the effects of tooth alignment, biofilm formation and Ni ion release. The authors anticipate that their findings will shape the future of the NiTi archwire field in terms of welding different types of archwires, computational methods, and improvement in coating technologies.
New thermomechanically treated NiTi alloys – A review **[127]**	The study examined various exclusive methods of manufacturing nickel-titanium (NiTi) alloy to enhance the mechanical characteristics of NiTi endodontic devices. As previously mentioned, thermomechanical treatment of NiTi alloy permits a shift in phase composition that, in clinical settings, manifests as martensite or R-phase. Compared to ordinary NiTi, thermomechanically treated NiTi alloys have been claimed to have a larger deflection angle at failure and to be more flexible with improved cyclic fatigue resistance.
60NiTi: A review of recent research findings, potential for structural and mechanical applications, and areas of continued investigations **[21]**	This article summarises and evaluates a wide range of previous and current research on 60NiTi to identify areas that need more investigation. Specifically, recent findings show that wear and friction behaviour are inherently contradictory. Their work indicated that more research is necessary to fully understand how alloying affects other characteristics, mainly wear. It is anticipated that as knowledge and development of this alloy improve, its use in various applications will rise.
Tribocorrosion of passive materials: A review of test	They reviewed the test protocols and electrochemical methods used to evaluate the tribocorrosion behaviour of passive materials over the last few decades. As

procedures and standards **[6]**	mentioned in their study, a test protocol suggested by several authors to remedy the drawbacks of the ASTMG119 standard served as the foundation for developing the UNE 112086 standard. They also shed light on the electrochemical methods and investigations made by tribocorrosion researchers.
Significance of tribocorrosion in biomedical applications: Overview and current status **[91]**	They focused on orthopaedic surgery and dentistry to highlight the complexity of tribocorrosion processes and provided an overview of bio-tribocorrosion.

A detailed study of the tribocorrosion mechanisms was recently initiated in different fields to clarify the extent of interacting material surfaces. As a result, many researchers have investigated several studies on tribocorrosion to explore the underlying mechanisms of this interlinked phenomenon. A significant area of focus is understanding the synergistic interactions of the testing parameters of the system. Therefore, this results in the need to develop a mechanistic model considering the interlinked actions of sliding wear, electrochemical corrosion, passivation and repassivation, and other surface/ morphological impacts. A clear understanding of the tribocorrosion synergistic interactions and mechanisms would allow accurate predictions to quantify the effects of various operating parameters through theoretical and/or empirical models. So, much more research must be required to reveal the drawbacks of tribocorrosion of 60NiTi alloy and its metallurgical relatives. Accordingly, researchers have investigated several studies on tribocorrosion of Ni-Ti alloys and other similar materials. Table 2.5 summarises the tribocorrosion studies conducted so far, but it is evident that the researchers mainly focused on biomedicals, lubrication, and sliding wear [22, 94, 170, 171] with little insight into the underlying mechanisms of wear-corrosion synergy.

The current status of tribocorrosion in some selected applications of NiTi-based alloys is outlined as follows; it is established that Ni-Ti alloys have gained attention in marine and offshore applications following the report of López-Ortega, et al. [172]. Lopez et al. stated that tribocorrosion is a crucial failure cause in offshore applications due to the synergistic effects of wear and the corrosiveness of seawater. In their work, they investigated the effect of temperature on the tribocorrosion behaviour of two steel grades [69]. Considering the aforementioned extreme conditions, another study conducted by Guadalupe, et al. [152] investigated tribocorrosion in pressurised water reactors (PWR)

at harsh environmental conditions (elevated temperature and high pressure). Their study focused on modelling tribocorrosion in PWR based on a mechanistic appraisal of mechanical and chemical loading [152]. To gain a better knowledge of the tribocorrosion performance of NiTi alloy in marine environments, Yan, et al. [166] examined the microstructure, phase, and tribocorrosion behaviour of 60NiTi alloy in a simulated seawater environment. According to their research, material loss under tribocorrosion circumstances is significantly influenced by the synergistic impact between wear and corrosion [166]. Moreover, the following order shows a decrease in the contribution to the overall material loss: corrosion-induced wear (ΔW_c) > pure wear (W_0) > wear-induced corrosion (ΔC_w) > pure corrosion (C_0). The corrosion and wear interplay in the tribo-electrochemical behaviour of the NiTiNOL60 alloy in sulfuric acid and alkaline media were examined in our previous study [107, 173]. The findings demonstrated that oxidative wear dominates in the electrochemical regime and causes a cathodic shift during potentiodynamic polarisation measurements, while abrasive wear is the primary mechanism under reciprocating sliding [107, 174]. In a different study, Kosec, et al. [45] examined the effects of various surface finishes and the microstructures of superelastic NiTi sheets and orthodontic archwires while examining their electrochemical and tribocorrosion capabilities. The results of their investigation demonstrated that the measured electrochemical and tribocorrosion parameters were significantly influenced by the microstructure of the alloys under investigation [45, 88, 161].

Table 2.5: Summary of selected works showcasing the tribocorrosion investigations, test parameters, and findings over the past 15 years.

Title and reference	Tribometer configuration	Counter body	Applied load & Temperature	Scan rate & Sliding speed	Electrolyte & Electrode	Findings and remark
Comparative study of the tribocorrosion performance of NiTiNOL60 in acidic, alkaline, and saline environments **[52]**	Bidirectional ball-on-flat configuration	Ø 10 mm Al_2O_3 ball	3, 5, & 8 N Room temp. (RT) 22 ℃	2 mV/s 4 Hz	H_2SO_4, NaOH, 3.5 % NaCl. Calomel, Graphite rod	The study revealed that the pH of the corrosive environments played a significant role in the tribocorrosion process). The highest wear volume was recorded in the saline medium. Shear forces caused grain deformations in the alkaline solution. While in an acidic medium, the electro-mechanically induced transformations promoted various wear patterns.
Microstructure, phase and tribocorrosion behaviour of 60NiTi alloy **[166]**	Unidirectional rotating (ball-on-disc)	Ø 5 mm Si_3N_4 ball	1, 5 & 10 N RT	2 mV/s	Artificial seawater. Calomel, Platinum	They employed a systematic tribocorrosion test to study the tribocorrosion performance of 60NiTi alloy thoroughly. Their findings show that the negative synergy between electrochemistry and tribology increases material loss.
The tribocorrosion behaviour of NiTi alloy **[45]**	Reciprocal/reciprocating (pin-on-disc)	Ø 6 mm Al_2O_3 ball	1 to 5 N RT	0.1 mV/s, 1 mV/s 5 mm/s	Artificial simulated saliva. Ag/AgCl, Platinum	The superelastic NiTi sheet and orthodontic archwire were studied considering their microstructures and the effect of different surface finishes. The study confirmed that the investigated alloys' microstructure significantly affected the measured electrochemical and tribocorrosion properties.
Corrosion and wear interplay: Tribo-electrochemical evaluation of NiTiNOL60 alloy in sulfuric acid **[107]**	Reciprocating ball-on-flat configuration	Ø 10 mm Al_2O_3 ball	3, 5, & 8 N RT	2 mV/s 4 Hz	Sulfuric acid. Calomel,Graphite rod	Their findings demonstrated that tribochemical wear influences several wear mechanisms, with delamination and microcracks notably prominent under higher applied loads.

Tribocorrosion behaviour of NiTiNOL60 alloy in an alkaline environment **[173]**	Reciprocating ball-on-plate configuration	Ø 10 mm Al_2O_3 ball	3, 5, & 8 N RT	2 mV/s 4 Hz	Alkaline solution Calomel, Graphite rod	The investigation shows that sliding action and wear mechanisms on the tribological wear track have distorted the microstructure grains, leading to the elongation of grains in the direction of sliding wear.
Tribo-electrochemical investigation of 60NiTi alloy in saline solution **[175]**	Linear reciprocating ball-on-flat configuration	Ø 10 mm Al_2O_3 ball	3, 5, & 8 N RT	2 mV/s 4 Hz	Saline solution Calomel (SCE), Graphite rod	The study highlighted the impact of mechanical forces and electrochemical activities on the surface of 60NiTi alloy. The continuous reciprocating sliding subjected the contact surfaces to fatigue wear, leading to surface deterioration and plastic deformation.
Tribocorrosion behaviour of NiTi alloy as orthopedic implants in Ringer's simulated body fluid **[114]**	Ball-on-disk rotary wear tester	Ø25.4mm ZrO_2 ball	0.2, 0.5, 1.0 & 2.0 N RT	7.5 mV/s 75 rpm	Ringer's simulated body fluid. Saturated calomel electrode (SCE), Platinum sheet	Particle concentration and applied load effects were taken into account. The wear component of the material loss was more significant than the corrosion component, indicating wear accountability for the material loss. The primary wear mechanism is two-body abrasive wear, with mechanical abrasion predominating in the corrosion-wear regime.
Tribocorrosion behaviour of NiTi biomedical alloy processed by an additive manufacturing laser beam-directed energy deposition technique **[94]**	Reciprocating ball-on-plate configuration	Ø 10 mm Al_2O_3 ball	1 N 37 ± 2 ℃	1 Hz	Phosphate buffered saline (PBS) solution SCE	The study demonstrated how additive manufacturing techniques, like LB-DED, can enhance NiTi alloy's wear and corrosion resistance. The improvement in LB-DED NiTi alloy's wear and corrosion behaviour in the presence of PBS solution suggests it is less susceptible to releasing metallic ions than the conventional Ti-6Al-4V alloy.
Tribocorrosive study of new and in vivo exposed nickel titanium and	Reciprocal tribometer	Ø 6 mm Al_2O_3 ball			Simulated saliva	The comparison revealed that the in vivo exposed archwires had a higher rate of mechanical wear and more corrosion wear.

stainless steel orthodontic archwires **[126]**			37 ℃ & RT	0.33 mm/s	Ag/AgCl, Platinum	Compared to the new archwires in simulated saliva, the in vivo exposed NiTi and SS archwires showed better electrochemical properties.
Microstructure and tribocorrosion properties of NiTi/AlNi2Ti ternary intermetallic alloy **[176]**	Ball-on-flat reciprocating sliding tribometer	Ø 6 mm Al_2O_3 ball	5 N RT	2 mV/s 1 Hz	0.5 mol/L H_2SO_4 (SCE), Platinum sheet	The study created a novel corrosion-resistant NiTi/AlNi2Ti alloy using an arc melting process. According to the tribocorrosion results, the OCP of the NiTi/AlNi2Ti alloy decreases as sliding begins and then gradually increases during passivation. The OCP value decreases in direct proportion to the increase in frictional force, suggesting a strong wear-corrosion synergistic effect.
Analysis of microstructure, mechanical properties, wear characteristics and corrosion behaviour of SLM-NiTi under different process parameters **[177]**	MFT-5000 multifunctional friction and wear testing machine	4 mm stainless steel quenched steel ball	10N 37 ± 0.5 ℃ and 25 ± 0.5 ℃ (RT)	5 mm/s	SBF and 3.5 wt% NaCl SCE, Ag/AgCl, Platinum	They investigated the effects of process variables (high P, high V and low P, low V). The results indicate that low P and low V are more favourable to creating the B19′ martensite phase, while high P and high V favour the formation of the B2 austenite phase. The samples have roughly the same coefficient of friction (0.6), but the LP sample is more resistant to corrosion, while the HP sample has superior stability and resistance to friction.
Tribological and tribocorrosion behaviour of nickel sliding against oxide ceramics **[12]**	Linear reciprocal tribometer	Ø 6 mm alumina & zirconia balls	2.74 N	2 mV/s 1 Hz, 20 mm/s	0.1M citrate buffer sol. Mercury sulphate electrode (MSE), Platinum wire	They discovered a linear correlation between nickel and alumina wear. Under passive conditions (no oxide film), alumina and zirconia were found to be worn, but not under cathodic conditions. Nickel rubbing against an alumina ball containing nickel, aluminium, and oxygen forms a tribolayer during sliding in dry conditions.

Tribocorrosion behaviours of Ti-6Al-4V and Monel K500 alloys sliding against 316 stainless steel in artificial seawater **[163]**	Ring-on-block test rig	49.22 mm × 13.06 mm was made of 316 stainless steel	100 N RT, 25 ± 1 ℃	10 mV/s 0.5 m/s	Artificial seawater and distilled water SCE, Platinum plate	In both distilled water and seawater, 316 stainless steel suffers more severe wear when sliding against Monel K500 alloy, more than when sliding against Ti-6Al-4V alloy. However, the wear loss of 316 stainless steel is greater in distilled water than in seawater when sliding against Ti-6Al-4V alloy, which could result from the protective effect of galvanic corrosion.
Mechanical and chemical mechanisms in the tribocorrosion of a Stellite type alloy **[42]**	Reciprocating (ball-on-plate)	Ø 6 mm Al_2O_3 ball	1.1, 5.8, 11.7, 17.5 N	2 mV/s 1 Hz, 20 mm/s	0.5 H_2SO_4 solution Mercury sulfate, Platinum coil	The findings indicate that the tribocorrosion behaviour of this alloy is significantly influenced by the current electrochemical circumstances (presence or absence of a passive film). Considering the influence of the passive film, Archard's wear law and existing models for wear-accelerated corrosion could adequately characterise the effect of electrode potential and normal load on the overall degradation by tribocorrosion.
Influence of temperature on the corrosion and tribocorrosion behaviour of high-strength, low-alloy steels used in offshore applications **[69]**	Reciprocating ball-on-disc tribometer	Ø 10 mm Al_2O_3 ball	49 N 23 ℃ & 2 ℃	1 mV/s 2.5 Hz	Synthetic seawater Ag/AgCl, Platinum wire	They employed two different electrolyte temperatures for tribocorrosion testing. At 23 ℃, the steels showed a greater COF during tribocorrosion tests. It was established that temperature significantly impacted the steel's tribocorrosion behaviour, as evidenced by the larger material losses attributable to corrosion at higher test temperatures.
Tribocorrosion behaviour of mooring high strength low alloy steels in synthetic seawater **[167]**	Ball-on-disc unidirectional tribometer	Ø 10 mm alumina ball	5 N RT	1 mV/s 100 rpm	Synthetic seawater Ag/AgCl, Platinum wire	The study revealed that the corrosion products and the applied potential significantly influence the friction coefficient of the steel. Under the selected testing conditions, the two steel grades exhibited a similar tribocorrosion behaviour in seawater.

Mechanical and electrochemical deterioration mechanisms in the tribocorrosion of Al alloys in NaCl and in $NaNO_3$ solutions **[178]**	Reciprocating ball-on-plate tribometer	Ø 6 mm alumina ball	1.3, 4 N 22 ℃	1 Hz, 11.4 mm/s	0.05 M NaCl & 0.1 $NaNO_3$ solutions SCE, Platinum wire	The investigation showed that wear rates in $NaNO_3$ solutions are somewhat lower than in NaCl. It was further discovered that wear-accelerated corrosion had a minimal contribution to the total degradation of the aluminium alloy, which was primarily controlled by mechanical wear.
Tribocorrosion and corrosion behaviour of quaternary Ti-24Nb-xZr-ySn alloys in SBF **[124]**	Ball-on-flat reciprocating sliding configuration	Ø 10 mm alumina ball	1 N 37 ℃	1 Hz	SBF + ion concentrations Calomel, Graphite bar	The study varied the composition of Zr. As a result, the alloy with a lower Zr composition showed better corrosion resistance, while those with a higher Zr composition depicted better resistance to mechanical contact. Further study on these properties is required to determine the suitability of the alloys as contact or static implant materials.
Bio-tribocorrosion resistance of CoB-Co2B and Co2B layers on CoCrMo alloy **[23]**	Linear reciprocating ball-on-flat tribometer	Ø 5 mm Al_2O_3 ball	20 N 15–30 ℃	1 mV/s	Calf serum Ag/AgCl, Platinum wire	Their findings demonstrate how the cobalt boride layer can enhance the CoCrMo alloy's functionality and prolong its service life in biomedical applications.
Synergistic interactions between wear and corrosion of Ti-16Mo orthopedic alloy **[80]**	Ball-on-plate-tribometer	Ø 10 mm ZrO_2 ball	1.5 N 37 ± 0.5 ℃	0.5 mV/s 1 Hz, 0.03 m/s	PBS SCE	Their findings show that the wear mechanism of Ti-16Mo alloy depends on the interplay between abrasion and adhesion. In their conclusion, Ti-16Mo alloy is a promising candidate for orthopaedic implant applications.
The effect of pH, fluoride and tribocorrosion on the surface properties of dental archwires **[132]**	reciprocal tribometer	Ø 6 mm Al_2O_3 ball	1 N 37 ℃	0.5 & 1 mV/s	Artificial saliva	Increased fluoride concentration in artificial saliva does not significantly affect the properties of NiTi alloy and stainless steel AISI 304. The positive hysteresis in the cyclic

					SCE	potentiodynamic curve showed susceptibility of NiTi to localised corrosion at the highest concentration studied. In contrast, the stainless steel dental archwire was found to be susceptible at smaller concentrations.
Tribo-corrosion and corrosion behaviour of titanium alloys with and without DLC films immersed in synthetic urine **[179]**	Reciprocating tribometer	Ø 4.76 mm Al_2O_3 ball	5 N	1 mV/s 1 Hz	Synthetic urine Ag/AgCl, Platinum wire	Their investigation, which compared 60NiTi, NiTi60T, and Ti–6Al–4V, found that 60NiTi alloy, without thermal treatment, is 70 times more susceptible to corrosion in the absence of DLC film. While the DLC coating enhanced the resistance to corrosion of the 60NiTi alloy and the Ti-6Al-4V alloy, the NiTi60T sample was significantly more susceptible to corrosion without DLC film.
Tribocorrosion of different biomaterials under reciprocating sliding conditions in artificial saliva **[81]**	Reciprocating sliding wear tester	Ø 10 mm ZrO_2 ball	3, 6, 10 N 21 ± 2 ℃	1 mV/s 3 & 6 Hz (0.012, 0.024 m/s)	Artificial saliva SCE, Platinum wire	The investigation focused on biomedical materials used in implants under different contact conditions. The data showed that the Co28Cr6Mo alloy had the lowest wear and friction, whereas the Nb specimen had poor tribological performance. Of the three specimens with the highest corrosion potential value, the cP-Ti specimen exhibited a more noble behaviour.
Tribocorrosion behaviour of additive manufactured Ti-6Al-4V biomedical alloy **[96]**	Reciprocating ball-on-plate tribometer	Ø 10 mm Al_2O_3 ball	1N 20 ± 2 ℃	1 Hz	PBS fluid	The findings demonstrated that the microstructure and manufacturing processes used for the cast, hot pressing (HP), and laser engineered net shaping (LENS) Ti-6Al-4V alloys affect the tribocorrosion performance. Compared to the cast and HP samples, the LENS Ti-6Al-4V samples showed superior wear and corrosion resistance.

2.2.2.13. Future perspectives

This review has shown that while the frictional behaviour and the interaction between wear and corrosion in corrosive environments have been studied extensively, the role of the 'third-body' (wear debris or contaminants trapped in the sliding contact) has received less attention. Compared to the well-studied areas of lubrication and sliding wear, there is a lack of information on how various parameters influence the tribocorrosion of Ni-Ti alloys [180-182]. To optimise the performance of Ni-Ti-based alloys, it is crucial to investigate the underlying tribocorrosion processes, including the kinetics of passivation and repassivation. This highlights the need for a mechanistic model that considers the interlinked actions of sliding wear, electrochemical corrosion, passivation and repassivation, and other surface/morphological changes [149].

Understanding these synergistic interactions and mechanisms would allow accurate predictions of material loss due to the combined effects of wear and corrosion. Theoretical and/or empirical models can be employed for this purpose [183, 184]. Incorporating theoretical modelling in this area has gained significant interest in recent decades. López-Ortega, et al. [6] suggested developing models to predict material loss due to the synergistic effect of wear and corrosion. Similarly, Stack [185] and Blau, et al. [10] emphasised the need to understand the performance and mechanisms of implants in medical applications. Guadalupe, et al. [152] combined a tribological third-body approach with a mechanical description to model tribocorrosion in a pressurised water reactor (PWR) environment. Their model provided a deeper understanding of the mechanisms involved and yielded quantitative predictions that agreed well with experimental observations.

Corrosion is a vital component of a tribo-electrochemical system [149]. Simulating the corrosive testing environment requires considering the potential determined by the material's electrochemical properties and the concentration of oxidising agents [186]. A corresponding corrosion potential can be imposed on the metal using an external current source to simulate the effect of oxidising agents [184, 187, 188]. Electrochemical techniques like open circuit potential (OCP), potentiodynamic polarisation (PD), potentiostatic polarisation (PS), and electrochemical impedance spectroscopy allow researchers to vary corrosion conditions by adjusting the applied potential [91, 162, 189].

Bio-tribocorrosion, the deterioration of materials due to the combined effects of wear, corrosion, and biological interactions, is another under-investigated area. While Delgado-Brito, et al. [23] and De Stefano, et al. [51] have explored bio-tribocorrosion in medical applications due to contact with body fluids, this aspect needs to be addressed

in engineering applications. Understanding bio-tribocorrosion is crucial, especially considering microbial interactions in marine and offshore environments.

2.2.2.14. Summary

This study provides an overview of current trends in NiTi alloy with regard to corrosion and wear synergy in engineering and medical applications. This follows the gradual surface deterioration of metals and biomaterials due to tribocorrosion, which has posed a significant challenge to the life span of materials and inadvertently affects the efficiency of various load-bearing operations/applications. Understanding the synergy between the sliding wear and electrochemical measurements provides a promising approach to investigating the mechanisms, passivation kinetics and parametric effects on the tribocorrosion process. In this study, the complexities of tribocorrosion, which often is influenced by several parameters (mechanical and corrosion) coupled with the lack of an integrated/ efficient test system, have been highlighted. Also, the behaviour of NiTiNOL60 alloy and its interactions in different corrosive media and the wear mechanisms under the synergistic tribo-electrochemical testing conditions, as well as the individual sliding wear and corrosion activities have been revealed.

Following the research gap mentioned in Chapter 1, which emphasised the necessity of identifying the pertinent deformation mechanism(s) for a combined action of sliding wear and corrosion. Over the course of this study, the research questions have been addressed, and the following points have been summarised based on the review and investigations.

- The complexities of tribocorrosion, often influenced by several parameters (mechanical and electrochemical) coupled with the lack of an integrated/efficient test system, have been highlighted.
- This study has revealed the behaviour of NiTiNOL60 alloy and its interactions in different corrosive media (acidic, alkaline and saline solution) covering a wide pH range.
- The sliding wear tests conducted at various testing parameters (temperature, pH, applied load, sliding speed, etc.) have demonstrated the surface deterioration of the tested alloy. Then, the surface characterisations revealed wear degradations from mild to severe wear regimes, which are often aggravated by certain combinations of test parameters.
- The tests at elevated temperatures and the XRD examination were used to ascertain the thermal effects and phase stability of the Ni-Ti-based alloy.

- The wear mechanisms of NiTiNOL60 alloy under the synergistic tribo-electrochemical testing conditions, as well as the individual sliding wear and corrosion activities have been revealed in this study.

Overall, this review has contributed to the limited knowledge gap in the literature and is expected to serve as a guide to researchers while designing tribocorrosion experiments and/or improving on an already existing study.

Chapters 4 & 5 embargoed until 5th September 2026

Chapters 4 & 5 embargoed until 5th September 2026

Chapters 4 & 5 embargoed until 5th September 2026

Chapters 4 & 5 embargoed until 5th September 2026

Chapters 4 & 5 embargoed until 5th September 2026

Chapters 4 & 5 embargoed until 5th September 2026

Chapters 4 & 5 embargoed until 5th September 2026

Chapters 4 & 5 embargoed until 5th September 2026

Chapters 4 & 5 embargoed until 5th September 2026

Chapters 4 & 5 embargoed until 5th September 2026

Chapters 4 & 5 embargoed until 5th September 2026

Chapters 4 & 5 embargoed until 5th September 2026

Chapters 4 & 5 embargoed until 5th September 2026

Chapters 4 & 5 embargoed until 5th September 2026

Chapters 4 & 5 embargoed until 5th September 2026

Chapters 4 & 5 embargoed until 5th September 2026

Chapters 4 & 5 embargoed until 5th September 2026

Chapters 4 & 5 embargoed until 5th September 2026

Chapters 4 & 5 embargoed until 5th September 2026

Chapters 4 & 5 embargoed until 5th September 2026

Chapters 4 & 5 embargoed until 5th September 2026

Chapters 4 & 5 embargoed until 5th September 2026

Chapters 4 & 5 embargoed until 5th September 2026

Chapters 4 & 5 embargoed until 5th September 2026

Chapters 4 & 5 embargoed until 5th September 2026

Chapters 4 & 5 embargoed until 5th September 2026

Chapters 4 & 5 embargoed until 5th September 2026

Chapters 4 & 5 embargoed until 5th September 2026

Chapters 4 & 5 embargoed until 5th September 2026

Chapters 4 & 5 embargoed until 5th September 2026

Chapters 4 & 5 embargoed until 5th September 2026

Chapters 4 & 5 embargoed until 5th September 2026

Chapters 4 & 5 embargoed until 5th September 2026

Chapters 4 & 5 embargoed until 5th September 2026

Chapters 4 & 5 embargoed until 5th September 2026

Chapters 4 & 5 embargoed until 5th September 2026

Chapters 4 & 5 embargoed until 5th September 2026

Chapters 4 & 5 embargoed until 5th September 2026

Chapters 4 & 5 embargoed until 5th September 2026

Chapters 4 & 5 embargoed until 5th September 2026

Chapters 4 & 5 embargoed until 5th September 2026

Chapters 4 & 5 embargoed until 5th September 2026

Chapters 4 & 5 embargoed until 5th September 2026

Chapters 4 & 5 embargoed until 5th September 2026

Chapters 4 & 5 embargoed until 5th September 2026

Chapters 4 & 5 embargoed until 5th September 2026

Chapters 4 & 5 embargoed until 5th September 2026

Chapters 4 & 5 embargoed until 5th September 2026

Chapters 4 & 5 embargoed until 5th September 2026

Chapters 4 & 5 embargoed until 5th September 2026

Chapters 4 & 5 embargoed until 5th September 2026

Chapters 4 & 5 embargoed until 5th September 2026

Chapters 4 & 5 embargoed until 5th September 2026

Chapters 4 & 5 embargoed until 5th September 2026

Chapters 4 & 5 embargoed until 5th September 2026

CHAPTER 6: TRIBOCORROSION TESTING IN ACIDIC ENVIRONMENT

6.1. Preface

This chapter presents the tribocorrosion behaviour of NiTiNOL60 alloy in sulfuric acid. This electrolyte was considered to reflect the acidic environments in the process industries and simulated body fluids where conventional engineering materials deteriorate due to mechanical wear and corrosion. The highlights for the journal article published https://doi.org/10.1016/j.rinma.2023.100523 in the Journal of Results in Materials are as follows:

Highlights:

- Novel tribocorrosion study on NiTiNOL60 alloy in a sulfuric acid medium.
- Synergistic effects of sliding wear and corrosion on material degradation.
- Identified multiple wear mechanisms, including delamination and micro-cracks.
- Abrasive wear is predominant under sliding wear conditions.
- Electrochemical activities influenced corrosive wear in anodic and cathodic regimes.

Graphical abstract

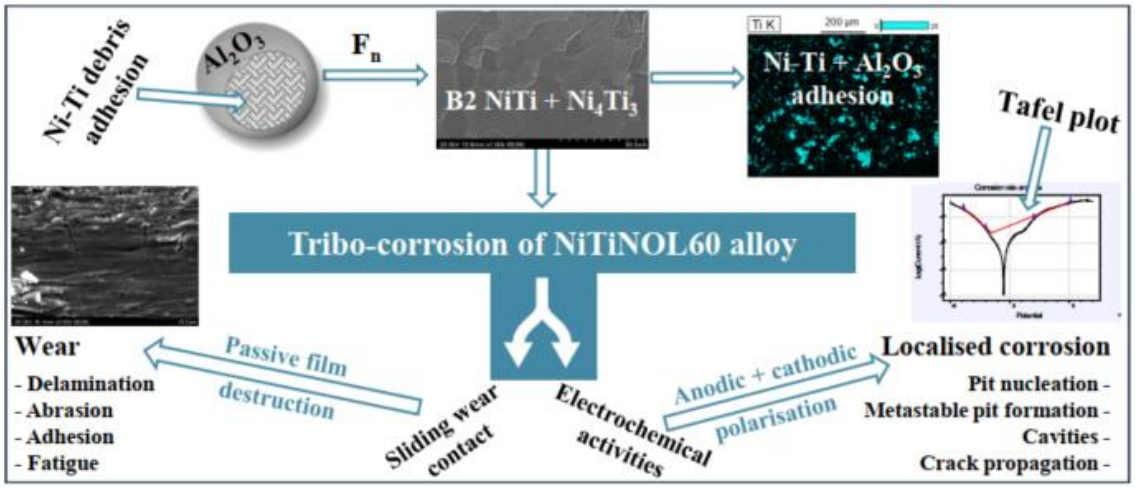

Graphical abstract showing the tribocorrosion interface for NiTiNOL60 alloy

6.2. Corrosion and wear interplay: Tribo–electrochemical evaluation of NiTiNOL60 alloy in sulfuric acid

6.2.1. Overview

Tribocorrosion, the synergistic interaction between mechanical wear and corrosion, is a critical concern in various applications, including engineering and biomedical, where metallic components are exposed to sliding or rolling contact in corrosive environments [1, 7]. It is a significant concern in various industrial applications, such as automotive, spacecraft [24], marine [62, 63], food and beverage processing [108-110], pharmaceutical [111], biomaterial [93, 112], actuators [113] and biomedical sectors such as orthopaedic [114], endodontic [99] and orthodontic [93, 99]. According to Salas, et al. [124], Ti-6Al-4V alloy (Ti64) gained vast application in the biomedical industry due to its outstanding corrosion resistance and good mechanical qualities. However, the toxicity of V (Vanadium) and Alzheimer's disease linked to Al have prompted researchers in the past decades to focus on developing new metallic materials free of harmful components [124]. In this regard, novel Ti-based alloys that only contain highly biocompatible elements like Ni, Nb, Zr, and Sn have been discovered. These alloys exhibit excellent biocompatibility, low elastic modulus, high specific strength, and adequate corrosion resistance for vast biomedical and engineering applications [93]. Notwithstanding the excellent properties, metallic components experience surface deformations during sliding or rolling contact under corrosive environments [127]. Among the different corrosive environments, acidic conditions pose unique challenges due to their aggressive nature, leading to accelerated material deterioration [11, 22, 173]. Considering the engineering materials used in the aforementioned sectors, NiTi alloys have shown superior wear resistance compared to other conventional materials such as steels, Ni-based, and Co-based tribo-alloys [251]. Accordingly, Nickel-titanium (Ni-Ti) alloy, such as NiTiNOL60, has been weighed as a suitable replacement for conventional metals and, as a result, has received considerable scientific attention due to their biocompatibility, unique shape memory and mechanical properties [198]. NiTiNOL was discovered by William J. Buehler and colleagues in the late 1950s at the Naval Ordinance Laboratory, USA, while working on shielding materials [25, 36, 251]; hence, the combined name of alloy with the laboratory, Nickel-Titanium Naval Ordinance Laboratory - NiTiNOL. NITINOL exhibits better recovery from significant amounts of strain and can replicate its original shape owing to the shape memory property. The superelastic property of NiTi-based alloys ensures substantial recoverable strain during deformation caused by stress-induced martensitic transformation. At relatively low temperatures and under external force, the initial parent phase (austenite) transforms into a martensite

phase accompanied by macroscopic deformation. The austenite phase undergoes a significant deformation during loading and subsequently transforms into detwinned martensite [87]. Martensite and austenite undergo a reversal transition upon unloading with significant recoverable strain [47, 211]. Understanding the impact of strain rate on the tensile characteristics of superelastic NiTi has been the focus of extensive research. According to Neupane and Farhat [251], the superelasticity of NiTi under tensile loading conditions has demonstrated that the tension at the austenite to martensite transition increases with increasing strain rate. These microstructural changes significantly affect the wear and deformation behaviours of superelastic NiTi. Miller, et al. [40] reported that Ni-rich NiTi alloys had gained interest as prospective materials for specialised bearing and gear applications in the last decade. Another study presented that NiTi alloy with a near-equal atomic ratio is often used in many applications, such as bearings and engine blocks, aerospace, communication, naval ships and medical devices due to its good shape memory effect or super-elasticity, high wear-resistant performance and superior corrosion resistance [174], yet NiTiNOL60 alloy may be subject to tribological conditions leading to wear [4].

When subjected to tribological conditions in acidic environments, the tribocorrosion behaviour of NiTi alloy becomes an essential consideration for its reliability and performance. Consequently, tribocorrosion has garnered significant research interest as scientists and engineers seek to unravel the underlying mechanisms and develop effective mitigation strategies. When contact bodies operate in a corrosive environment, surface chemical phenomena can significantly affect their deterioration. In this case, it is essential to ascertain the tribocorrosion behaviour of the material in a specific corrosive environment such as sulfuric acid. Thus, understanding the tribocorrosion behaviour of NiTiNOL60 alloy in acidic media is essential for optimising its performance and longevity. The aggressive nature of acidic environments can significantly influence NiTi alloys' degradation mechanisms, wear rates, and corrosion resistance. For example, under sliding or erosive conditions, the passive film can be removed by abrasion, thus exposing the underlying reactive material to more severe corrosion. On the other hand, surface films were found to modify the mechanical behaviour of the underlying metal and, thus, its wear response [178]. In another study, Muñoz and Espallargas [165] reported that mechanical parameters significantly affect the rate of electrochemical material removal, whereas the rate of mechanical material removal is dependent on the electrochemical conditions at the time. Furthermore, they defined the total wear volume (V_t), which is the sum of the material loss due to sliding wear (V_{mech}) and the material loss owing to corrosion or electrochemical oxidation (V_{chem}), as the mechanistic interpretation of the

tribocorrosion phenomena. As reported, numerous variables, including load, sliding speed, surface films, temperature, hardness, and work-hardening, affect the contact surfaces in tribocorrosion. Hence, this present study aims to investigate the tribo-electrochemical behaviour of NiTiNOL60 alloy in a sulphuric acid (H_2SO_4) medium, with a focus on understanding the synergy between the specific wear rate and the associated tribo-electrochemical degradation mechanisms.

6.2.2. Material preparation and characterisation

The material used for this investigation was prepared following the procedure outlined in subsection 3.3.2 of Chapter 3. Subsequently, the material characterisation prior to and after tribocorrosion was investigated. The experimental methodology and measurements for tribocorrosion as presented in subsection 3.5.3 in Chapter 3 of this thesis were adopted for the investigations in H_2SO_4 corrosive environments shown in this Chapter.

6.2.3. Results and discussions

6.2.3.1. Surface characterisation

The metallographic investigation was conducted using the optical microscope, SEM and EDS. Figure 6.1 shows the SEM-EDS and the quantitative composition analysis of the NiTiNOL60 sample. For the SEM, a 20 KV penetrating voltage was used to scan the sample surface at full scale to ensure adequate penetration of the X-rays through the subsurface regions. Using EDS to quantify the elemental compositions and characterise the polished sample, the spectral image and the accompanying Table present the quantitative compositions of the material investigated.

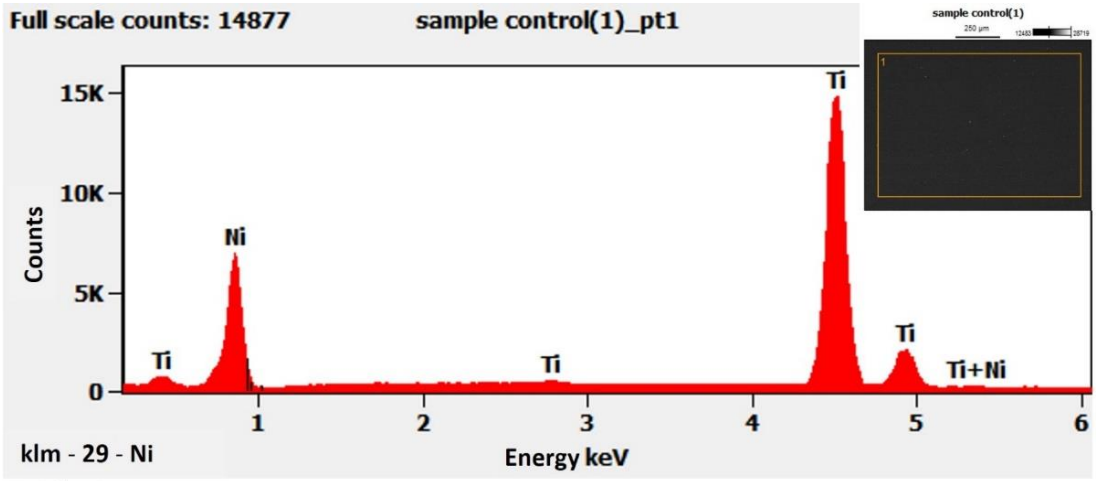

Weight %

	Ti	Ni
sample control(1)_pt1	40.14	59.86

Fig. 6.1: EDS spectral imaging of the polished NiTiNOL60.

The analysis confirmed that the specimen was a binary nickel-titanium alloy containing 60 wt.% Ni and 40 wt.% Ti (55 at.% Ni, 45 at.% Ti), i.e., a Ni-rich intermetallic NiTiNOL60 alloy [40, 252]. This was in good agreement with the compositions of NiTiNOL60 alloy previously reported in the literature [40].

To examine the subsurface of the sample on a microscopic scale, the cross-sectional part of the sample was obtained through wire cutting, abraded, polished, and etched using Kroll's reagent: 82.7 % H_2O, 14.1 % HNO_3, and 3.2 % HF for 30 seconds. This revealed the microstructural compositions of the sample presented in the microscopic image in Figure 6.2. The examination under the optical microscope reveals the microstructural arrangement of NiTiNOL60 alloy with distinct regions of consolidated and unconsolidated grain network clusters. The majority of the micrograph image is represented by the NiTi + Ni_4Ti_3 region composed of ordered cubic and rhombohedral crystal matrix structures [47, 249] and fine and coarse grain network structures [101]. The dense network of unconsolidated and consolidated grain clusters reveals the inhomogeneity in the microstructural grains [252, 253], thus supporting the non-equi-atomic elemental distribution shown in Figure 6.1, which tends to have Ni-rich or Ti-rich zones [41]. The dominance of the B2 NiTi and Ni_4Ti_3 matrix highlighted in the micrograph suggests globular and needle-like shaped precipitates B19' in the B2 matrix [36, 198].

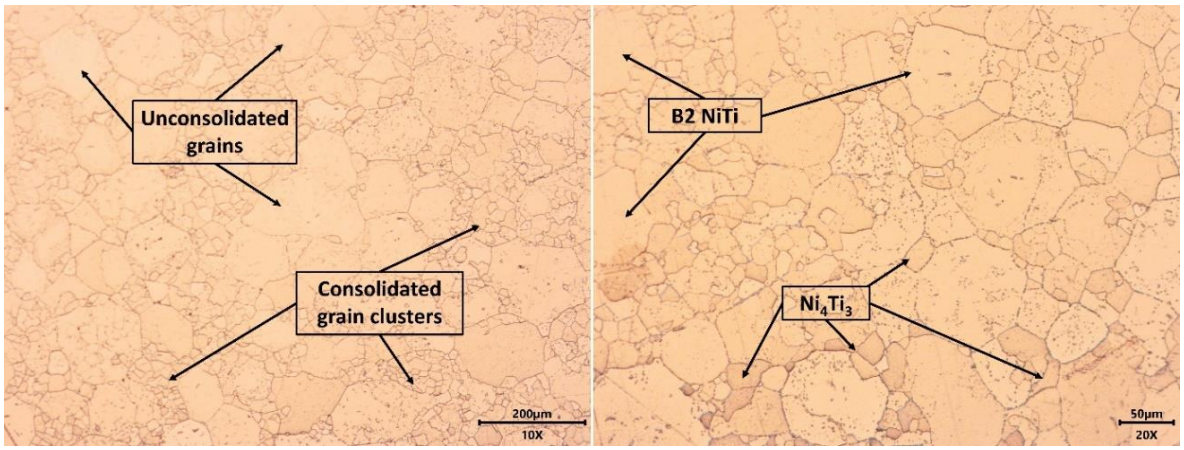

Fig. 6.2: Optical microscopic images of NiTiNOL60 at different magnifications.

6.2.3.2. Frictional behaviour during reciprocating sliding

During the reciprocating sliding wear tests, the frictional behaviours were monitored, and the measured parameters were recorded on the WINDUCOM software tool. The parameters were analysed to determine the material's coefficient of friction (CoF) characteristics over the course of the reciprocating sliding. As shown in Figure 6.3, the CoF is plotted as a function of sliding time for three applied loads. Clearly, at the initial sliding stage, the applied load had a reasonable running-in time characterised by the interfacial friction interactions leading to the breakdown of oxide layers [146, 229], localised heating of the contact surfaces and oxidation of asperities. The fluctuations recorded in the CoF plots could be attributed to the distortions caused by wear debris and formed layers (passivation) during tribocorrosion.

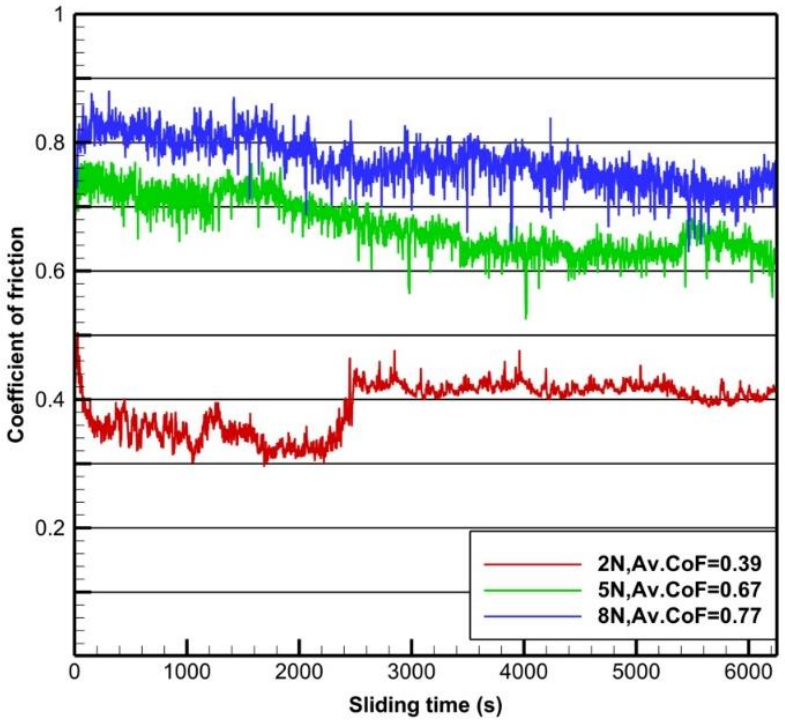

Fig. 6.3: Friction coefficient plot against sliding time for NiTiNOL60 in H_2SO_4.

Based on the CoF plots, the applied load of 2N required a longer running-in time to wear the passive layer, unlike the 5N and 8N loads. At higher loads (5N and 8N), it is evident that the contact surfaces overcame a running-in time during the continuous sliding by removing the passive layer, penetrating and wearing off the sample surface, and eventually exposing the material sub-surface. Whereas, for an applied load of 2N, the CoF increased after 30 minutes of break-in point, whereby the passive film on the sample surface was destroyed and maintained approximately 0.4 CoF throughout the sliding duration until a steady-state value was attained. As the contact pressure increases, the passive layers are easily destroyed through a continuous reciprocating sliding contact; this creates more surface roughness and widens the wear track, thereby increasing the surface area available for oxidation. The examined surfaces in Figure 5 micrographs show the least amount of chemical and mechanical wear mechanisms for the 2N load when compared with the other loads investigated. According to Zeng and Dong [181], friction is most severe at higher loads, and this is supported by the results obtained for the 8N load with the highest average CoF μ = 0.77, maximum wear volume alongside the increased chemical and mechanical mechanisms.

6.2.3.3. Surface examination

The sliding actions of the contact surfaces created a wear track within the sliding stroke length of 10 mm. Examining the wear scar reveals mild to severe wear mechanisms, with

delamination and adhesive wear being more predominant. The recorded wear mechanisms conform with the four main mechanisms of adhesive wear, abrasive wear, fatigue wear and tribochemical wear reported in the literature [165, 254]. Following the SEM images in Figure 6.4, the specimen investigated at 2N, 4Hz condition shows little detachment and adhesion of the wear debris. In contrast, the SEM micrographs at higher loads show extensive abrasion and delamination, which propagates when subjected to various loading conditions. The rate of abrasion and depassivation could be attributed to a number of variables, including the mechanical characteristics of the metal, the contact geometry, the applied force, and the effects of hydrodynamic lubrication [184]. From the results, micro-cracks were discovered to be more pronounced at 8N load, and it is believed to have developed from surface tensile stress and extended perpendicular to the direction of sliding. While corrosion pits progressed from the initial nucleation stage into metastable pit formation and stable pitting [151]. Our analysis shows that corrosion pit nucleation and micro-crack propagation were promoted by the contact pressure on the interacting surfaces and the third-body wear effects [214].

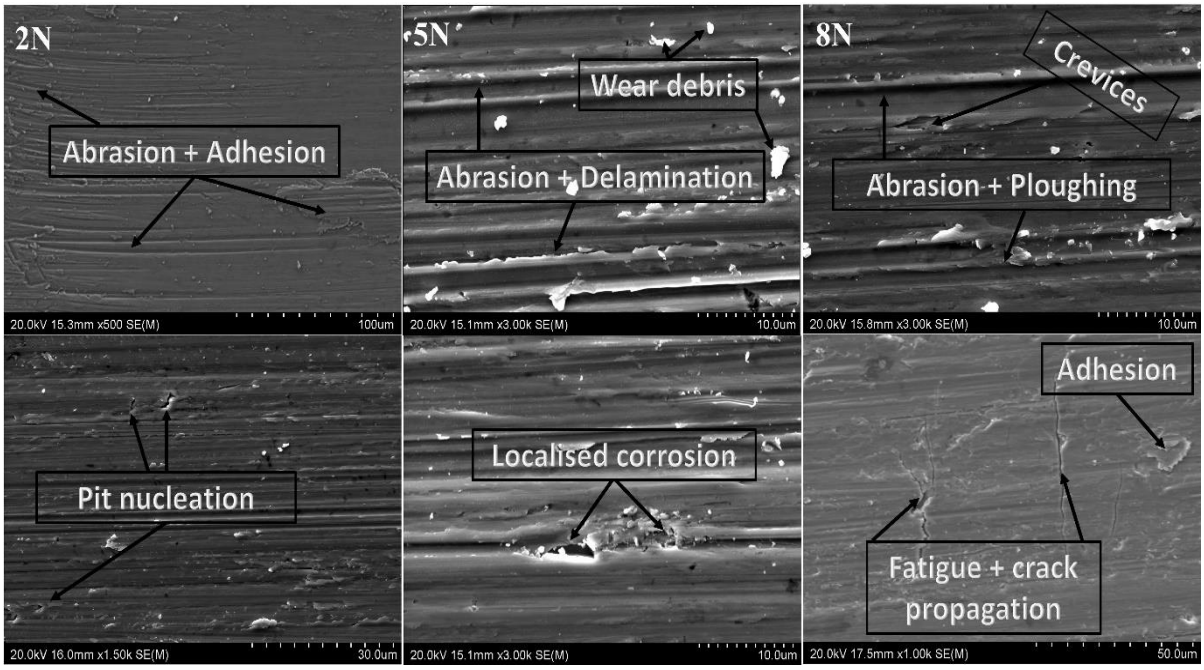

Fig. 6.4: SEM examination revealing the wear mechanisms during tribocorrosion in H_2SO_4.

Considering the high level of adhesion, it was imperative to further examine the wear tracks using the EDS characterisation technique to determine the makeup of the surface wear particles. Figure 6.5 presents the EDS results, which revealed oxidation and Al debris as the elemental compositions detected along the wear tracks. The overall scan of the surfaces represented by point 1 show that the oxide composition increases with

load increase while the adhesion of the Al debris decreases. The increased oxidation promoted electrochemical activities that subsequently led to an increased corrosion rate.

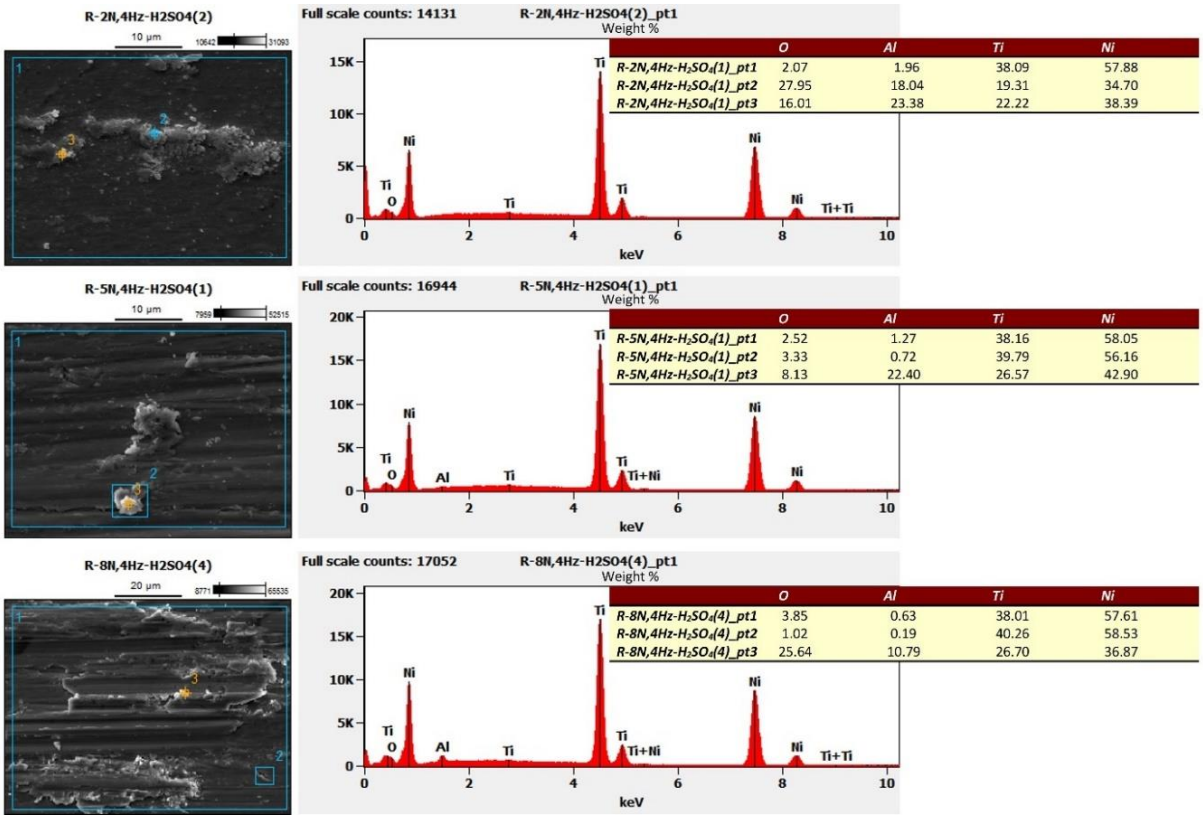

Fig. 6.5: EDS examination of wear debris adhesion along the wear track.

Since Al debris formed the greater composition of elements detected along the wear track of NiTiNOL60 samples, there was also a need to investigate the sliding surfaces of the counter material (Al_2O_3 ball) sliding against NiTiNOL60 alloy. From Figure 6.6, it can be established that the rate of material detachment and adhesion onto the contact surfaces occur simultaneously. As shown in the image, the ball surface revealed wear debris, and further examination of the surfaces at different applied loads presents the spectral images as well as their corresponding elemental compositions. The surfaces were clearly oxidised in the electrolyte mediums, and the oxide contents decreased with increasing load. Conversely, the deposition of the Ni-Ti wear debris increased as the contact pressure increased, thereby breaking down the oxidised layer and enhancing the material detachment and adhesion. As the contact pressure at 2N was not adequate to break in the material surface, this shows why the greater surface was oxidised, whereas the continuous reciprocating sliding at higher loads caused the breakdown of the oxide layers. Points 2 reveal Ni and Ti as the adhered material onto the ball surface, while point 3 confirms the alumina as the base material, with Al having the maximum percentage composition. In light of this, it is evident that the significant impact of contact

pressures at higher applied loads leads to the detachment of the interacting surfaces asperities, which then initiates abrasion and adhesion mechanisms.

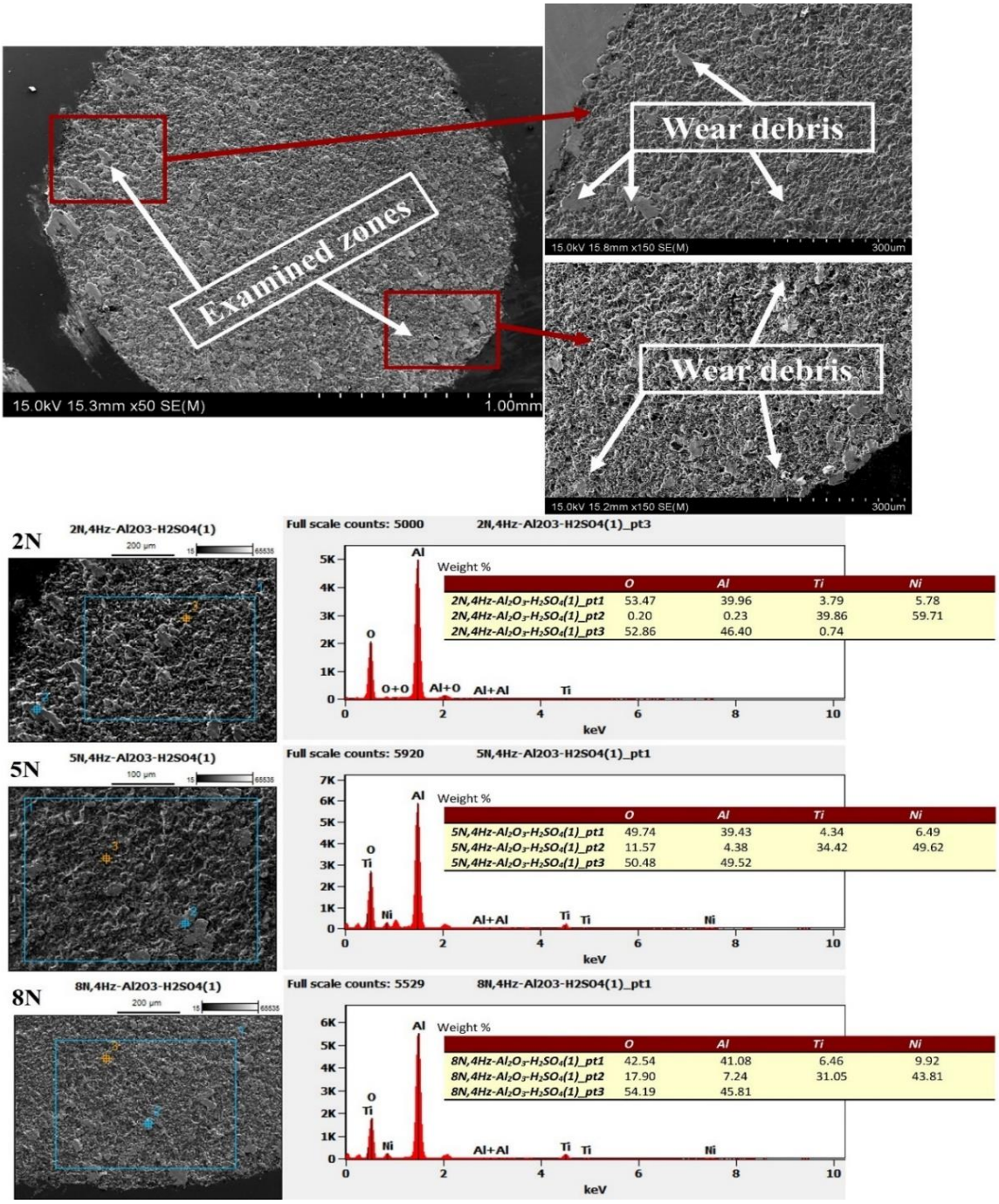

Fig. 6.6: SEM and EDS characterisation of the counter material (Al_2O_3 ball) sliding surface in sulphuric acid solution.

The EDS results in Figure 6.6 were further examined using the spectral imaging technique to analyse the alumina ball sliding surface at 8N load. The spectral imaging depicted in Figure 6.7 clearly identifies the oxidised points on the surfaces as the bright

patches shown in the purple tint. The yellow colour distribution across the micrograph determines the base material (alumina ball) with black patches of wear debris adhesion. While the blue and red colours highlight the Ti and Ni wear debris adhesion, which is attached to the ball surfaces during sliding contact.

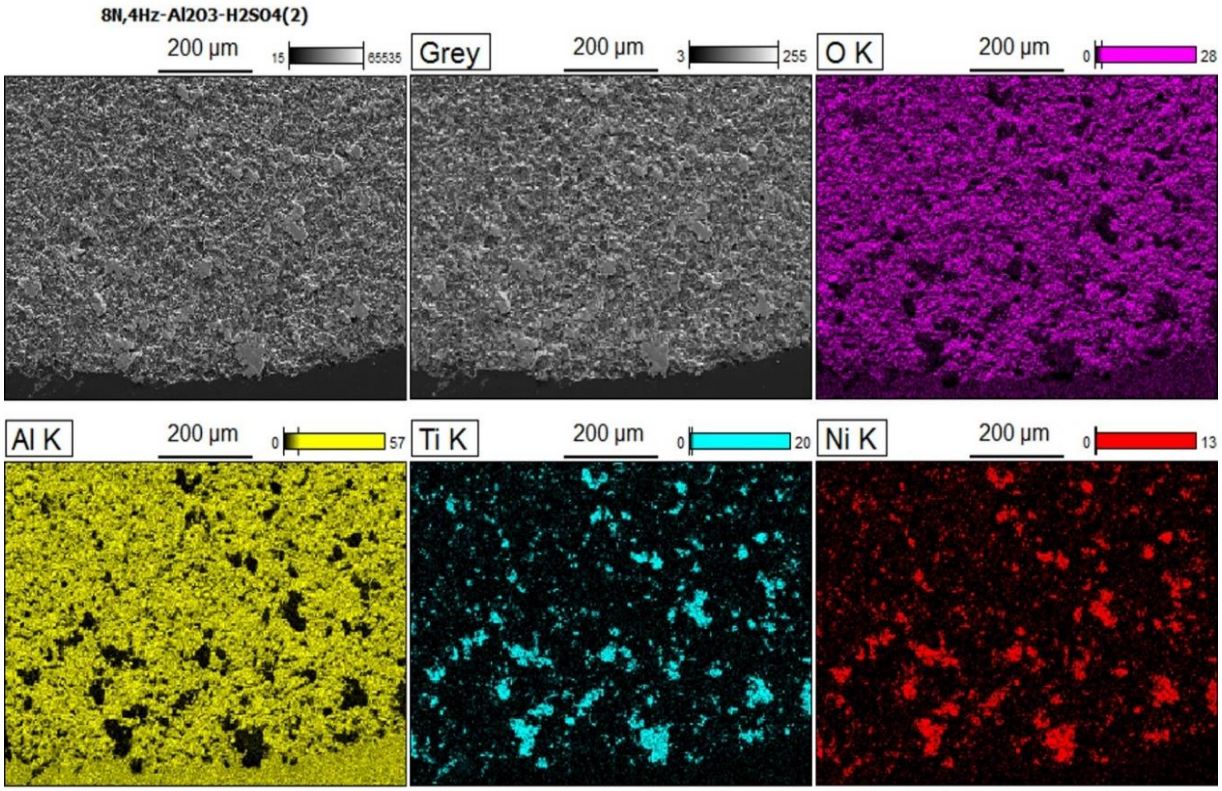

Fig. 6.7: EDS spectral imaging of the counter material (Al_2O_3 ball) surface at 8N applied load in H_2SO_4.

6.2.3.4. Potentiodynamic polarisation

The potentiodynamic polarisation was used to investigate the passivation behaviour of the NiTiNOL60 alloy under tribocorrosion conditions in an acidic solution, and the results are presented in Figure 6.8 and Table 6.1. From the Tafel plots, it is evident that the anodic domain of the polarisation curve is initiated with an active dissolution region, where metals are easily converted to ions and transported to electrolyte solutions and eventually enter a passive region following passivation [93, 166]. According to Ghali [151], the electrochemical breakdown of oxides of some metals is reduced cathodically to the metals or ions in aqueous solutions. The curves clearly show that corrosion occurred in the cathodic and anodic regimes with distinctive passivation regimes. The specimens investigated at 5N and 8N loading conditions exhibited similar passivation behaviours, while the E_{corr} values became more positive as the load increased. This deduction aligns with the findings presented in Salas, et al. [124].

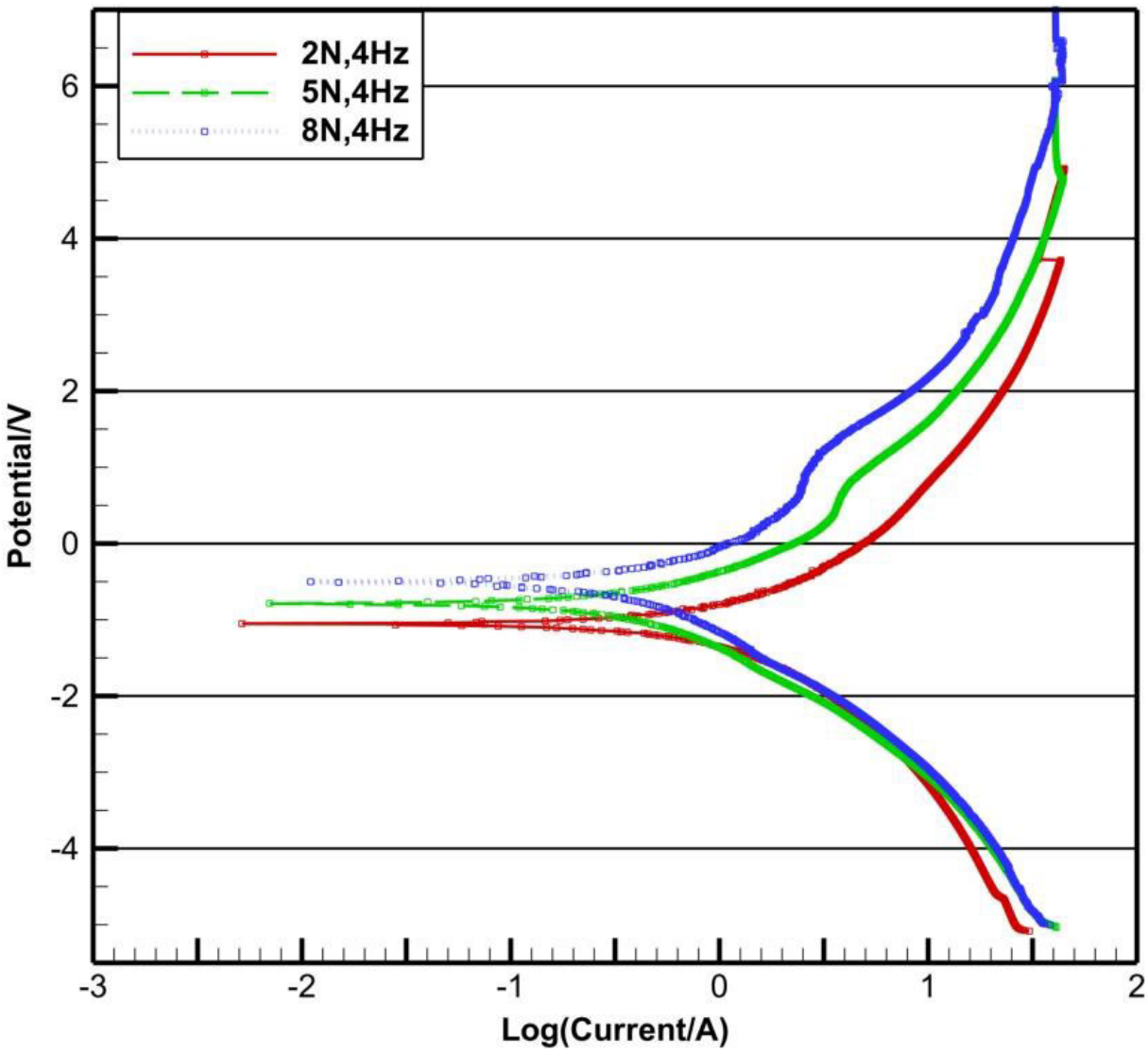

Fig. 6.8: Tafel plots at different applied loads after potentiodynamic polarisation measurements using a Calomel reference electrode in H_2SO_4.

Analysis of the Tafel plots gave rise to the following parameters presented in Table 6.1. The Table denotes the electrochemical activity of the material during tribocorrosion as well as the fitted parameters. Tafel analysis provided information on variables like corrosion potential, corrosion current density, passivation resistance, as well as corrosion rate; whereas the model data presents a good fit. According to our analysis, an increase in the applied load increased the corrosion current while the corrosion potential tends towards zero; this caused the polarisation resistance to continuously decrease and, in turn, increased the corrosion rate. The increase in i_{corr} values is correlated with the progression of the sample's corrosion rate (Cr); this is inversely connected to their polarisation resistance (Rp) values [124]. This demonstrates that the corrosion potential,

which controls the anodic or cathodic polarisation activity, governs the dissolution rate of metals [150, 173].

Table 6.1: Electrochemical parameters from the corrosion rate analysis of potentiodynamic polarisation measurements in H_2SO_4.

Corrosion rate analysis	Pol. Res.			Tafel data			Model data		
	2N	5N	8N	2N	5N	8N	2N	5N	8N
E_{corr} (V)	-0.167	-0.322	-0.506	-1.842	-1.257	-1.171	-0.226	-0.507	-0.699
$I_{corr.}$ (A)	2.988E-5	3.424E-5	4.182E-5	1.451E-3	1.795E-3	2.565E-3	1.181E-3	1.148E-3	1.425E-3
$I_{corr.}$ (A/cm^2)	7.312E-7	8.378E-7	1.023E-6	3.55E-5	4.392E-5	6.276E-5	2.889E-5	2.808E-5	3.487E-5
R_p (ohm)	726.700	634.100	519.200	743.400	436.900	295.400	616.300	397.400	309.600
b_a V/dec	-	-	-	5.748	4.843	5.623	3.024	2.186	2.359
b_c V/dec	-	-	-	4.372	2.878	2.530	3.756	2.021	1.784
C. Rate (mm/y)	0.023	0.027	0.033	1.143	1.411	2.017	0.928	0.902	1.120

Considering the wear mechanisms shown in Fig. 6.4 and the corrosion effect, an etched cross-section of the sample was examined to ascertain the propagation of corrosion pits and cracks beyond the contact surface. Figure 6.9 presents the SEM micrograph, EDS spectrum and the corresponding elemental distributions as shown in the table. The results show that localised corrosion, such as pit and crevice, occurred during tribocorrosion. The corrosion pit and cavities shown could be attributed to the corrosion-abrasion synergy, which impedes the reactivity between the anode surface and the electrolyte [255, 256]. Further examination of the pit using EDS reveals the maximum oxygen concentration for points 1 and 2 at the pit region. At point 3, a decline in the oxide composition was recorded, showing that oxidation promoted the pit nucleation. Point 4 confirms the exact composition of the material with no oxygen concentration.

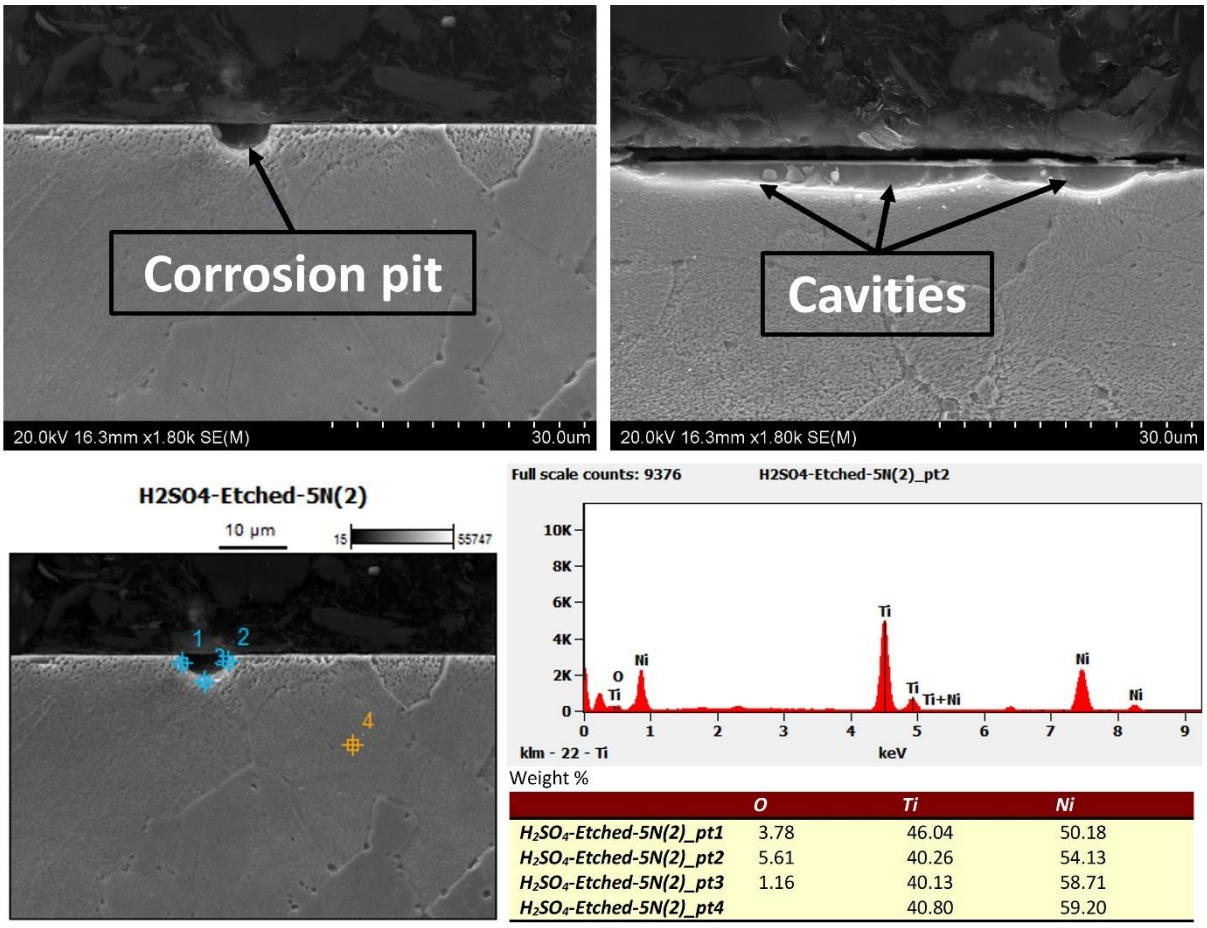

Weight %

	O	Ti	Ni
H_2SO_4-Etched-5N(2)_pt1	3.78	46.04	50.18
H_2SO_4-Etched-5N(2)_pt2	5.61	40.26	54.13
H_2SO_4-Etched-5N(2)_pt3	1.16	40.13	58.71
H_2SO_4-Etched-5N(2)_pt4		40.80	59.20

Fig. 6.9: SEM-EDS examination for localised corrosion in the material subsurface.

6.2.3.5. Hardness measurement

To ascertain the effect of tribocorrosion on the specimen, micro- and macro-indentation hardness measurements were carried out using the methods outlined in sub-section 6.2.2. Prior to the tribocorrosion testing, the sample's average Rockwell hardness of the specimen was measured, and it was found to be 62.5 HRC, which is consistent with the values reported in the literature [25, 170, 210]. Measurements after the testing reveal that the sample's average macro hardness, as determined by the Rockwell Hardness test, was 63.3 HRC. Whereas the micro-indentation Vicker's hardness along the wear track presents the average values of Hv (537.93/1.0kgf/10s, 547.77/1.0kgf/10s and 578.83/1.0kgf/10s) for 2N, 5N and 8N respectively. In contrast, the measurement outside the wear track had a relatively lower Vicker's hardness value of HV 537.83/1.0kgf/10s. As the applied load increased, the hardness values along the wear track increased, and the recorded high values could be attributed to work-hardening as a result of compressive forces and precipitation hardening through the rapid formation of nanoscale Ni_4Ti_3 precipitates during sliding [40, 130, 204]. Also, the non-uniform network structures

in Figure 6.2 could contribute to the variations in the microhardness values along the wear track [101].

6.2.3.6. Contact surface interactions and tribo-corrosion mechanisms

Considering the tribocorrosion synergistic interactions, the contributing mechanisms are investigated following the wear behaviours revealed in Figure 6.4 and computing the specific wear rate using Equation 1. The results are shown in Figure 6.10, which compares the specific wear rate and the polarisation resistance during electrochemical measurements. It is evident from the graphical trend that increased applied load reduces the polarisation resistance, which in turn amounts to an increased corrosion rate. This demonstrates that the material yield due to the synergy between wear and corrosion is larger than the effects of each factor acting alone [172]. The constant rubbing of the contact surfaces during reciprocating sliding results in the wear mechanisms caused by the high level of material detachment following the synergistic interplay between mechanical and electrochemical processes [257].

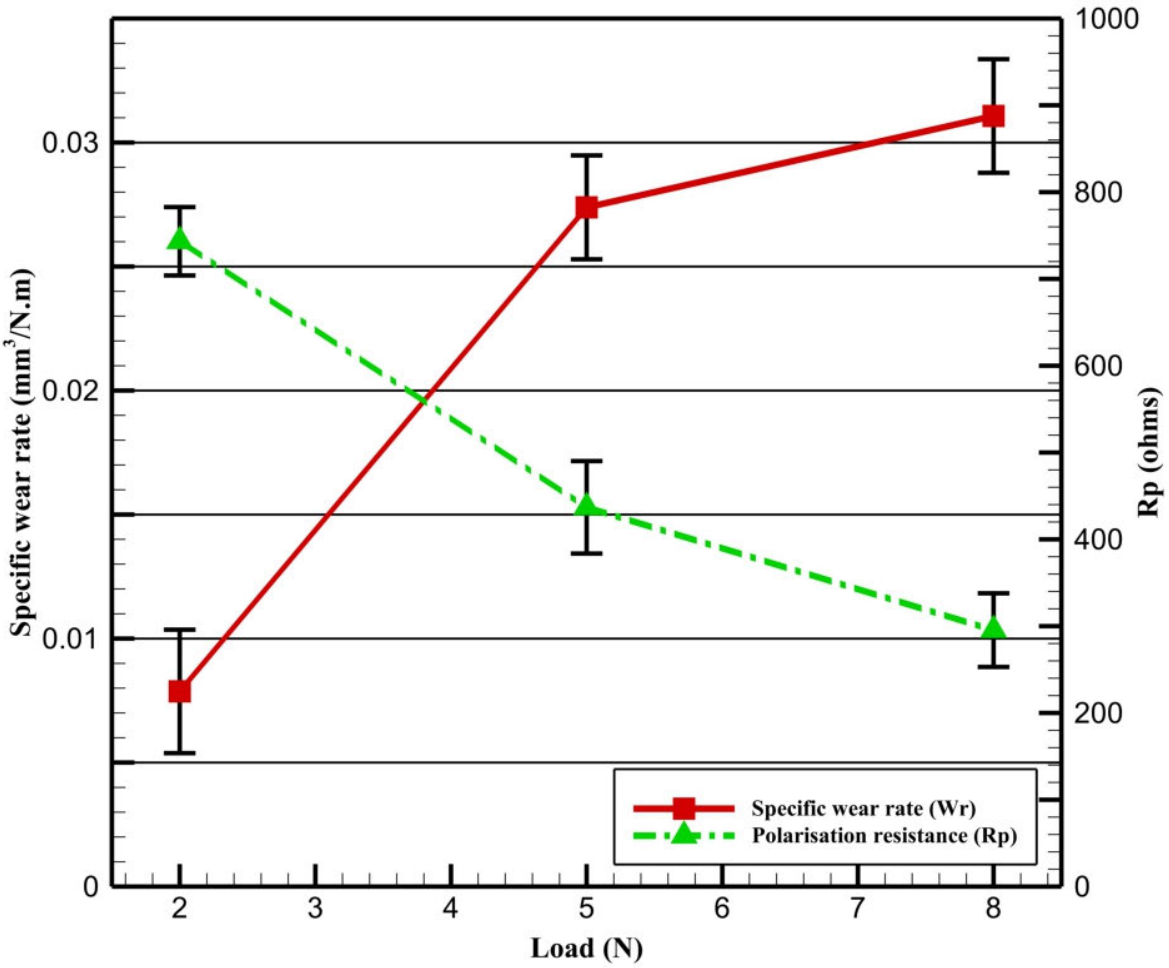

Fig. 6.10: Specific wear rate and polarisation resistance relationship in H_2SO_4.

During tribocorrosion, the simultaneous actions promoted an increase in the oxidation of the exposed surfaces. While sliding contacts initiated the breakdown of the passive films, which led to delamination, mild to severe abrasion, and adhesion, the oxidised surfaces promoted localised corrosion, as demonstrated by the SEM and EDS characterisations [166]. Liu, et al. [93] presented in their study that while surface defects promote passivation rates in the early stages of exposure, corrosion protection is best at a slowly formed passive film. It is established that the corrosion damage mechanism at the asperities of contact surfaces involves mechanical and chemical components, with the observable damage typically coming from both [165]. Hence, the synergistic interactions resulted in material losses and various wear mechanisms caused by the mechanistic approach, which involves the primary contributions of mechanical wear and wear-accelerated corrosion, i.e., anodic dissolution [17, 258].

6.2.4. Summary

The present study investigated the simultaneous interactions of wear and corrosion in a dilute sulfuric acid solution under varied applied loads. The experimental results provided insights into the tribocorrosion behaviour of NiTiNOL60 alloy in an acidic environment. The results show that material losses under tribocorrosion conditions are significantly influenced by the synergistic interaction between wear and corrosion. SEM/EDS metallographic investigation depicts that B2 NiTi and the stable Ni_4Ti_3 matrix structures dominate the NiTiNOL60 alloy microstructural network. As shown from our analyses, the mechanical action frequently results in the local removal of metal and oxide particles, thereby exposing the metal surface, which is subsequently followed by a repassivation process. The main mechanism under sliding investigation is abrasive wear, whereas oxidative wear predominates in the electrochemical regime, triggering a cathodic shift during potentiodynamic polarisation measurements. Additionally, the degree of this shift increases with the increase of applied normal load due to depassivation under sliding contact. It is established that the delamination and, subsequently, plastic deformation of the material surface during depassivation were influenced by the initiation and propagation of pits and micro cracks on the passive layer during repeated sliding. Thus, the contact pressure on the interacting surfaces promoted corrosion pit nucleation and micro-crack propagation.

CHAPTER 7: TRIBOCORROSION TESTING IN SALINE MEDIUM

7.1. Preface

This chapter illustrates the synergistic interactions between reciprocating sliding wear and the electrochemical activities, i.e., the tribo-corrosion behaviour of NiTiNOL60 alloy exposed to saline environments, which simulates the artificial seawater environment that mimics the environments where NiTiNOL60 alloy has its vast applications, especially in the marine and offshore environments. The highlights for the journal article published https://doi.org/10.1016/j.jalmes.2024.100074 in the Journal of Alloys and Metallurgical Systems are as follows:

Highlights:

- This study examined the behaviour of 60NiTi alloy in a saline environment.
- The research integrated tribological and electrochemical analyses.
- Potentiodynamic polarisation revealed localised corrosion in cathodic and anodic regions.
- Abrasive adhesive, oxidative, corrosive and fatigue wear mechanisms were unveiled.
- Equilibrium rate at passivation and repassivation plays a key role in tribocorrosion

7.2. Tribo–electrochemical investigation of 60NiTi alloy in saline solution

7.2.1. Overview

In recent years, there has been a growing interest in understanding the performance of Nickel-Titanium (NiTi) alloys in corrosive environments [7, 45]. This stems from the recognition that corrosion plays a vital role in tribocorrosion systems, impacting both engineering [224, 256] and medical applications [131, 133]. The significance of corrosion is particularly pronounced in marine environments, where materials often face surface damage and material loss due to the corrosive nature of the surroundings [62, 69]. Several factors influence corrosion in these environments, including the metal's position in the electrochemical series, pH levels, presence of electrolytes, metal impurities, oxygen concentration, and temperature variations [172]. Offshore applications subject materials to extreme environmental conditions, hastening their degradation. In such marine environments, multiple concurrent phenomena, including tribocorrosion, can reduce the lifespan of structural materials and lead to unexpected failures.

Traditional materials like high-strength steels are commonly used in offshore structural applications due to their favourable strength-to-weight ratios [69]. However, their low alloy content in elements that promote passive film formation, such as Chromium (Cr), Nickel (Ni), and Molybdenum (Mo), results in the formation of a porous and weakly adherent ferric oxyhydroxide (FeOOH) compound on the surface [255]. This porous rust film allows the electrolyte to penetrate and reach the bare steel, perpetuating corrosion and material loss. Consequently, low-alloyed steels are susceptible to corrosion even in their intended applications. For example, tribocorrosion plays a crucial factor in the premature failure of components within mooring systems [69], underscoring the complex interaction between wear and corrosion. While passive materials like stainless steels and titanium alloys are known for their resistance to tribocorrosion in various corrosive environments, their high cost limits their use in offshore applications compared to lower-alloyed steels that satisfy mechanical requirements at the expense of corrosion resistance. Alternative materials, such as conventional steel-based bearing materials (e.g., M50 and 52100), while electrically conductive and magnetically suitable, are prone to corrosion if not adequately protected [24, 259].

High-performance bearings, gears, and mechanical components require specific attributes, including high strength, hardness, thermal conductivity, precision manufacturing, and surface finish capabilities [24]. According to Meddah, et al. [260], Titanium alloys have gained traction for aerospace and other applications such as the

biomedical, automotive and energy industries. In spacecraft systems, bearings are expected to tolerate transient loads from launch-related vibration and environmental corrosion, such as from corrosive ambient marine conditions [26]. However, this alloy's low transformation temperature and poor dimensional stability must be addressed to employ it as structural and load-bearing components in aircraft applications.

Metallic alloys with a significant Titanium (Ti) content tend to be suboptimal tribological materials, struggling to respond effectively to lubrication and unable to withstand loads, making them unsuitable for moving mechanisms and tribological applications [24, 25, 34]. Highly alloyed stainless steel, such as superduplex grades, offers mechanical properties and high corrosion resistance but remains susceptible to localised corrosion types like pitting and crevice corrosion despite overall corrosion resistance [67]. In addition, the high density of materials leads to high centrifugal forces and limited fatigue life when used as bearing rolling elements. These factors have prompted the need for a more suitable material or metallic alloy that meets the aerospace requirements for excellent corrosion resistance and good tribological properties, especially for applications in extreme environments. Consequently, NiTi-based alloys have emerged as promising alternatives for bearings and potential offshore structural materials, boasting a unique combination of characteristics, including low density, high specific strength, low Young's modulus, superelasticity, biocompatibility, shape memory effects, and excellent corrosion resistance [34]. As shown in Table 1.1 which compares the thermophysical and mechanical properties of NiTiNOL60 alloy and the conventional engineering materials in which NiTiNOL60 alloy tends to replace in load-bearing and corrosive applications [25, 26]. The table shows that NiTiNOL60 has a lower Young's modulus than steel while maintaining a similar hardness.

Ni-rich NiTi alloys have gained increasing interest for specialised bearing and gear applications, especially in corrosive environments [40]. For instance, NiTiNOL60 alloy was developed to replace bearings experiencing corrosion and wear issues in the water recovery system of the International Space Station due to its superior mechanical and functional properties [40]. Research has shown that load bearing, tribological, and time-temperature-transition behaviours of Ni-rich compounds play critical roles in such systems [40, 210]. The Ni content in Ni-Ti-based alloys significantly influences phase transformation temperatures. It alters the specific temperatures where austenitic NiTi transforms to martensitic NiTi, affecting the key mechanical and thermal properties [253].

60NiTi, also referred to as NiTiNOL60, is an equi-atomic, ordered intermetallic alloy composed of 60 wt% Ni and 40 wt% Ti. Its distinctive combination of high hardness, low apparent elastic modulus, light weight and resistance to aqueous corrosion make it an

attractive candidate for aerospace and marine/offshore applications, particularly as a bearing material and in lubricated spacecraft triboelements [24, 26, 261]. The unique properties and shape-memory effect of Ni-Ti-based alloys have generated substantial scientific interest [25]. Accordingly, Meddah et al. [260] investigated the sliding wear performance of NiTi alloy annealed with different nickel contents. They found that the higher the Ni concentration, the more resistant the material was to adhesive and abrasive wear, which in turn decreased the wear rates that typically rose with applied load. Another study examined the microstructural evolution, mechanical properties, and oxidation performance of highly Ni-rich NiTi alloys with added V through vacuum arc melting. Their study revealed that while V content above 3 at% changed the morphology and distribution of the Ni_3Ti_2, increased the hardness of the alloy, the V content less than 3 at% improved the oxidation resistance of the binary 60NiTi alloy at 500 ℃ [200]. Given the considerable attention surrounding NiTi alloys, previous research can be categorised into several areas: basic corrosion and electrochemical studies, mechanical and material property investigations, and surface treatment studies [45]. However, the need for tribocorrosion investigations became apparent as tribological and electrochemical factors interact in complex ways [80]. Previous studies have shown that the electrochemical material removal rate depends on mechanical parameters, while prevailing electrochemical conditions influence the mechanical material removal rate. The synergistic interaction of wear and corrosion leads to more significant material loss compared to their individual effects [173]. As reported by Muñoz and Espallargas [165], the mechanism of fretting corrosion involves both mechanical and chemical components, with the observable damage typically coming from both. Further, Yan, et al. [166] highlighted that the mechanistic method separates the two primary contributions into mechanical wear and anodic dissolution (wear-accelerated corrosion).

Following the high level of surface damage and material loss due to tribocorrosion in corrosive environment often represented by a 3.5 wt% NaCl (artificial seawater) solution which depicts the environment where some engineering materials, including NiTi alloy, Ti-based alloys, stainless steels etc., commonly face deterioration, especially in load bearing applications. Various studies have investigated the tribocorrosion of these materials in artificial seawater environments, but there is still limited information on the tribocorrosion of NiTi in seawater environments. Ti-6Al-4V and Monel K500 alloys siding against 316 stainless steels were investigated. According to their results, the samples experienced larger wear losses in seawater compared with distilled water [163]. Ayyagari, et al. [90] studied high entropy alloys in dry and marine environments. According to their findings, at accelerated electrochemical corrosion, the sample

($Al_{0.1}$CoCrFeNi) displayed a higher degree of passivation, a higher pitting resistance, and a lower rate of corrosion. In their study, Yan, et al. [166] employed a unidirectional tribological technique to study the microstructure, phase and tribocorrosion behaviour of 60NiTi alloy. Their findings showed that the corrosion and tribocorrosion resistance of 60NiTi alloy were improved by solution treatment. Alkan and Gök, [262] examined the effect of sliding wear on AISI 316 stainless steel in seawater. Their results revealed the role of electrochemical potential (i.e., cathodic potential shift towards the anodic potential) in material loss. Based on the wear impact, another researcher investigated the behaviour of YSZ coating deposited on a stainless steel substrate in a saline solution. Their study revealed that despite the protective layer, an increase in potential significantly increased the material loss of 304 stainless steel as well as the YSZ coating [263]. Consequently, this study aims to address the existing research gap by employing a bidirectional tribocorrosion technique to investigate the synergistic behaviour of NiTiNOL60 alloy in a saline electrolyte, mimicking conditions relevant to offshore and spacecraft applications.

7.2.2. Materials and experimental methods

Material preparation, characterisation and tribocorrosion investigations in 3.5 wt.% NaCl corrosive environments were conducted using the methodological approaches outlined in Chapter 3 of this thesis.

7.2.3. Results and discussions

7.2.3.1. Metallographic investigations after tribocorrosion

The oxide-free (mirror finish) surface samples were examined using SEM and EDS surface characterisation techniques. The characterisation results of the polished sample confirmed the presence of a non-equiatomic sample composed of Ni and Ti elements of 59.26 and 40.74 wt.%, respectively, with little or no trace of any other element, thereby confirming the sample as a Ni-rich 60NiTi alloy. Hence, the EDS results confirm that the sample under investigation as 60NiTi alloy having approximately the same weight percentage compositions of 60 and 40 for Ni and Ti, respectively, which aligns with the literature information reported by previous researchers [47, 252].

Further examination of the surface on a microscopic scale reveals the microstructural composition of the sample. This was achieved through a cross-sectional part of the sample obtained using wire cutting, and the surface was ground, polished and equally etched for the subsurface examination. The micrograph shown in Figure 7.1 presents the microstructural arrangements of NiTiNOL60 before tribocorrosion investigation.

According to the micrograph, NiTiNOL60 is an ordered intermetallic material compound with cubic and rhombohedral crystal matrix structures, supporting earlier researchers' observations [252]. The closely packed grain network of unconsolidated and consolidated grain clusters could be referred to as the existence of inhomogeneity in the microstructural grains [253]. This may be explained by the non-equiatomic composition of NiTiNOL60, which has a propensity for Ni-rich or Ti-rich zones. This affirms the dominance of Ni_4Ti_3 and B2 NiTi matrix as presented in our previous report [173], while Khanlari, et al. [249, 252] referred to the phases as cubic and rhombohedral crystal structures. According to Du, et al. [101], the microstructure 60Ni-40Ti is alternately composed of fine and coarse network structures, which are relatively uneven on the microscopic scale, so its microhardness fluctuates more violently.

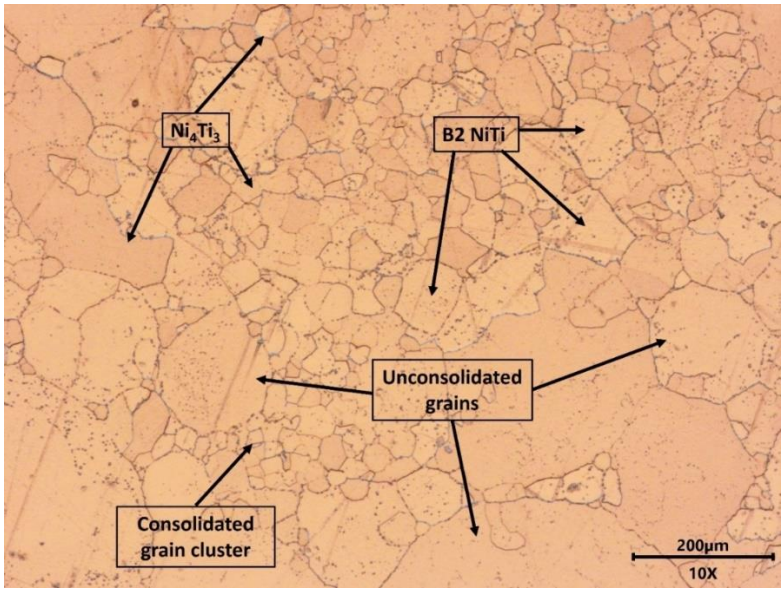

Fig. 7.1: Optical micrograph of NiTiNOL60 microstructural grain arrangement.

After the tribo-electrochemical tests in the corrosive environment, the reciprocating sliding between the contact surfaces created a wear track on the examined surface of NiTiNOL60. As a result, we examined the wear tracks using SEM and EDS characterisation at the same penetrating voltage of 20 KV used to examine the untested oxide-free sample to ensure adequate penetration of the rays into the subsurface layers. The surface morphologies of the corroded wear tracks are shown in Figure 7.2. The micrographs highlight mild to severe surface degradation caused by mechanical and chemical attacks in the electrolyte medium. The level of corrosion attack shown in Figure 7.2 depends on the impact of the applied load. Clearly, corrosion pits and crevices advanced from the nucleation stage to metastable pit formation and then to stable pitting, where the material deforms plastically. This aligns with the existing literature stating that pitting is self-initiating and self-propagating, thereby making it difficult to determine the

borders for every stage, such as nucleation, metastable pit formation and stable pitting [151]. From our analysis, the contact pressure on the interacting surfaces promoted corrosion pit nucleation and propagation. The average corrosion pits measured on the corroded surface of 60NiTi wear track generally ranged between 25 and 120 μm.

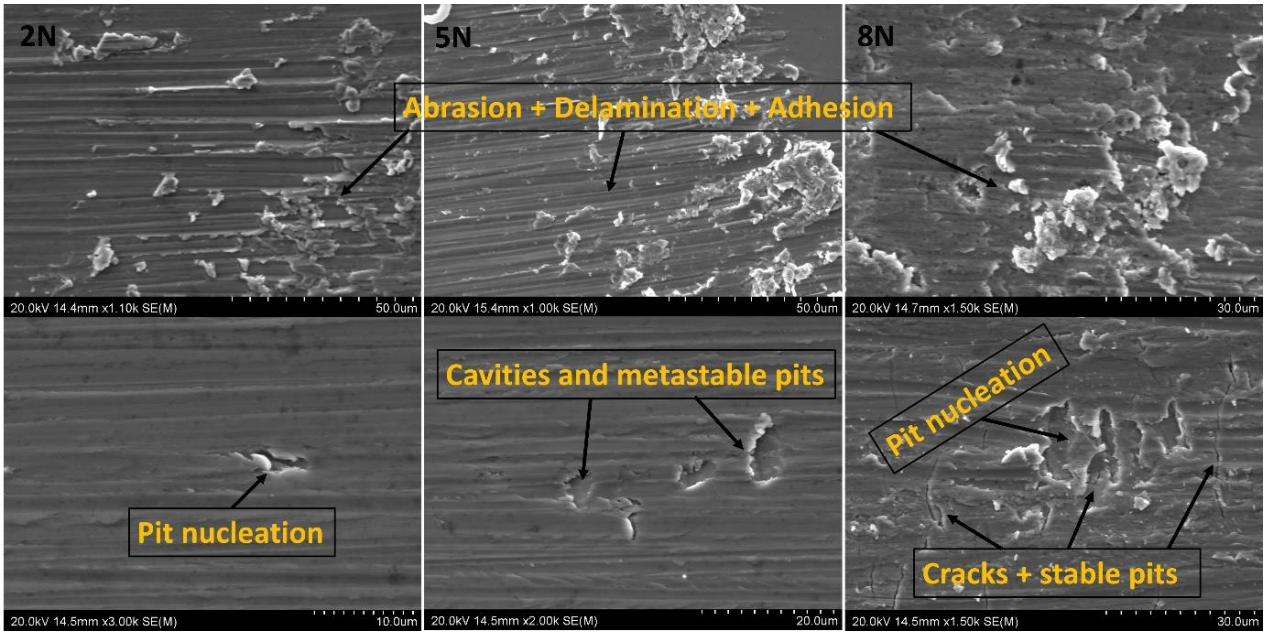

Fig. 7.2: SEM images showing the wear mechanisms along the wear track under different applied loads.

Following the high level of wear debris attachment, we further analysed the wear track surfaces using EDS to ascertain the composition of the attached wear particles on the surfaces. Figure 7.3 presents the EDS surface examination along the wear track using the point-and-shoot approach for a sample surface subjected to a 5N load. The quantitative elemental composition of examined points confirms the surface oxidation, which promoted the corrosive mechanism shown in Figure 7.2. The micrographs also show the adhesion of the wear debris caused by detachment and delamination.

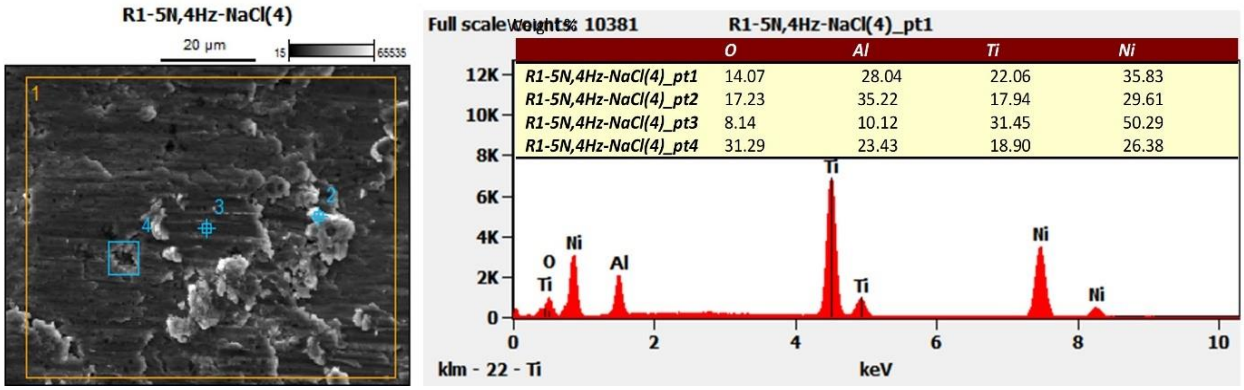

Fig. 7.3: EDS examination of wear track at an applied load of 5N in $NaCl_{aq}$.

Similarly, the high level of adhesion and distinctive attachment of wear particles observed at the sample surface at an applied load of 8N prompted further examination. Accordingly, we employed the spectral imaging technique for detailed and distinctive examination. Figure 7.4 shows the spectral imaging of the elemental distribution which clearly highlights the concentration of the oxidised areas. As depicted in the micrographs, the regions with higher concentration can easily be identified with the bright areas. The purple micrograph represents the oxidation distribution within the region, while the yellow colour distribution highlights the areas with high adhesion of the counter material debris and the elemental distribution of the contacting surfaces. The blue and red colours show the elemental distributions of the base material spread across the micrographs.

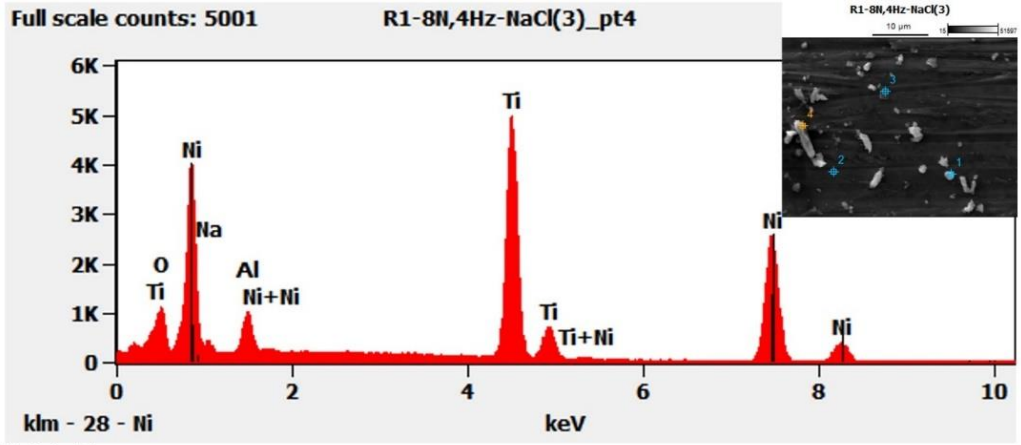

Weight %

	O	Na	Al	Ti	Ni
R1-8N,4Hz-NaCl(3)_pt1	13.66	2.84	5.11	32.02	46.37
R1-8N,4Hz-NaCl(3)_pt2				41.47	58.53
R1-8N,4Hz-NaCl(3)_pt3	28.55	1.12	12.43	24.74	33.16
R1-8N,4Hz-NaCl(3)_pt4	14.02	3.92	4.72	31.98	45.36

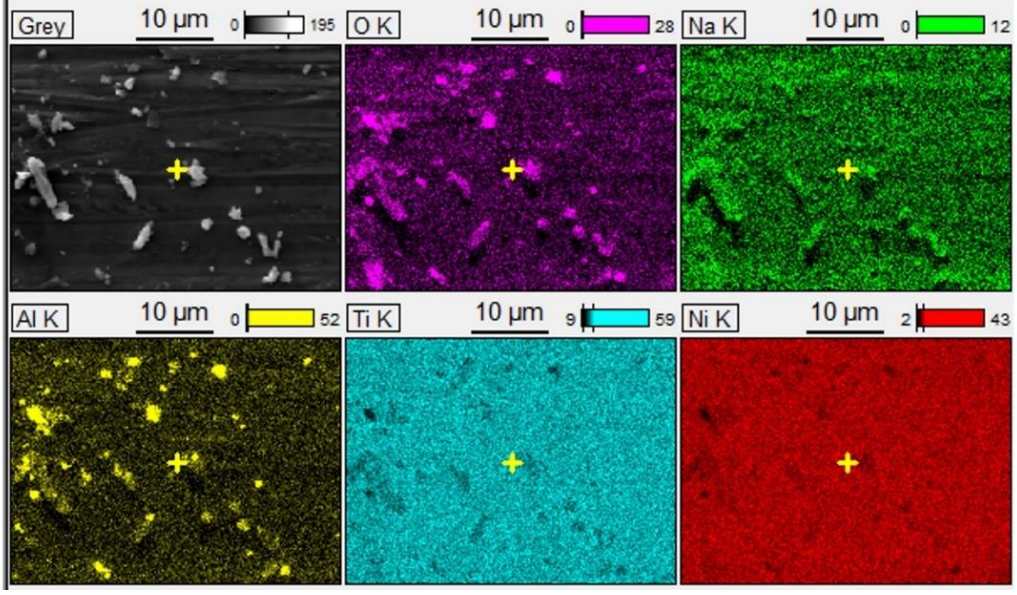

Fig. 7.4: EDS spectral imaging of adhered wear debris on the wear track NiTiNOL60.

7.2.3.2. Analysis of the reciprocating sliding friction and wear behaviours

The variations of the coefficient of friction (CoF) during the tests were analysed to measure the wear behaviour of the material throughout the sliding duration. Fig. 7.5 presents a similar frictional behaviour for the investigated three applied loads, except for the running-in time recorded at the 2N load. The initial stage of sliding was characterised by the interfacial friction interactions leading to the breakdown of oxide layers [146, 229], localised heating of the contact surfaces and oxidation of asperities. The continuous reciprocating sliding at higher contact pressure wears the passive layers as well as the subsurface of the material [148]. This indicates that any increase in the contact pressure increases the surface roughness and widens the wear track, which creates a larger surface area for oxidation. This is supported by the SEM micrographs in Figure 7.2, where the sample surface investigated at 2N showed the least chemical and mechanical wear mechanisms. It is evident that the highest average coefficient of friction (μ = 0.93) was recorded for the 8N wear track. This confirms the increased roughness/ wider wear track, the highest wear volume and various wear mechanisms that could possibly result in plastic deformation [198]. The mechanisms were promoted by the high level of detachment as the CoF levels also indicate that friction is most severe at higher loads [181], i.e., 8N and 5N (applicable to our study), unlike in the 2N load where the applied load at 4 Hz showed a gradual material loss (wear) at the interacting surfaces.

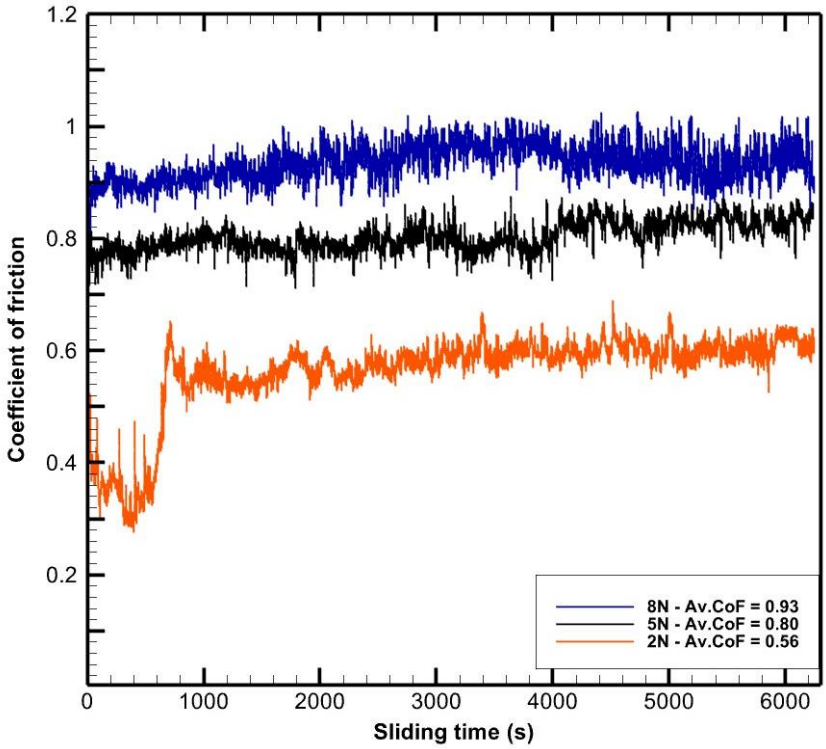

Fig. 7.5: Plot of friction coefficient against sliding time at different applied loads.

Considering the high level of material detachment and adhesion noted in Figs. 7.3 and 7.4 and supported by the high average CoF values in Fig. 7.5, we examined the surface of the counter body (Al_2O_3 ball) sliding against NiTiNOL60 alloy during the tribocorrosion tests using SEM and EDS techniques. Figure 7.6 presents the level of adhesion caused by the micro-joint formation [147] between the contact surfaces of the alumina ball and 60NiTi during sliding actions. For the examined surfaces at the three applied loads, an area scan reveals the elemental compositions deposited on the surfaces. The surfaces were oxidised in all the electrolyte mediums, with the oxide concentration decreasing with increased applied load. The highest oxygen concentration was recorded at the 2N load, while the 8N load showed the lowest oxygen concentration. This implies that the lower contact pressure at the applied load of 2N was inadequate for the breakdown/ wear of the oxide layer formed during tribocorrosion, supported by the delayed running-in time shown in the CoF plot in Figure 7.5. Hence, the validation that the significant impact from the contact pressures at higher applied loads causes detachment of the interacting surfaces, subsequently resulting in abrasion and adhesion mechanisms [148]. The adhered wear particles (debris) could be seen for the surfaces at 5N and 8N loads, with less pronounced deposits for the ball surface at the applied load of 2N. Thus, only one point (area scan) was examined for the surface at 2N, unlike the three to four points examined for the surfaces sliding at the applied loads of 5N and 8N following the pronounced adhesion of wear particles. While point 2 in the quantitative result confirms the actual composition of the attached materials to be NiTiNOL60 base materials - Ni and Ti, points 3 and 4 for 8N and 5N loads reveal the greater concentration of the alumina ball with little deposits of the specimen.

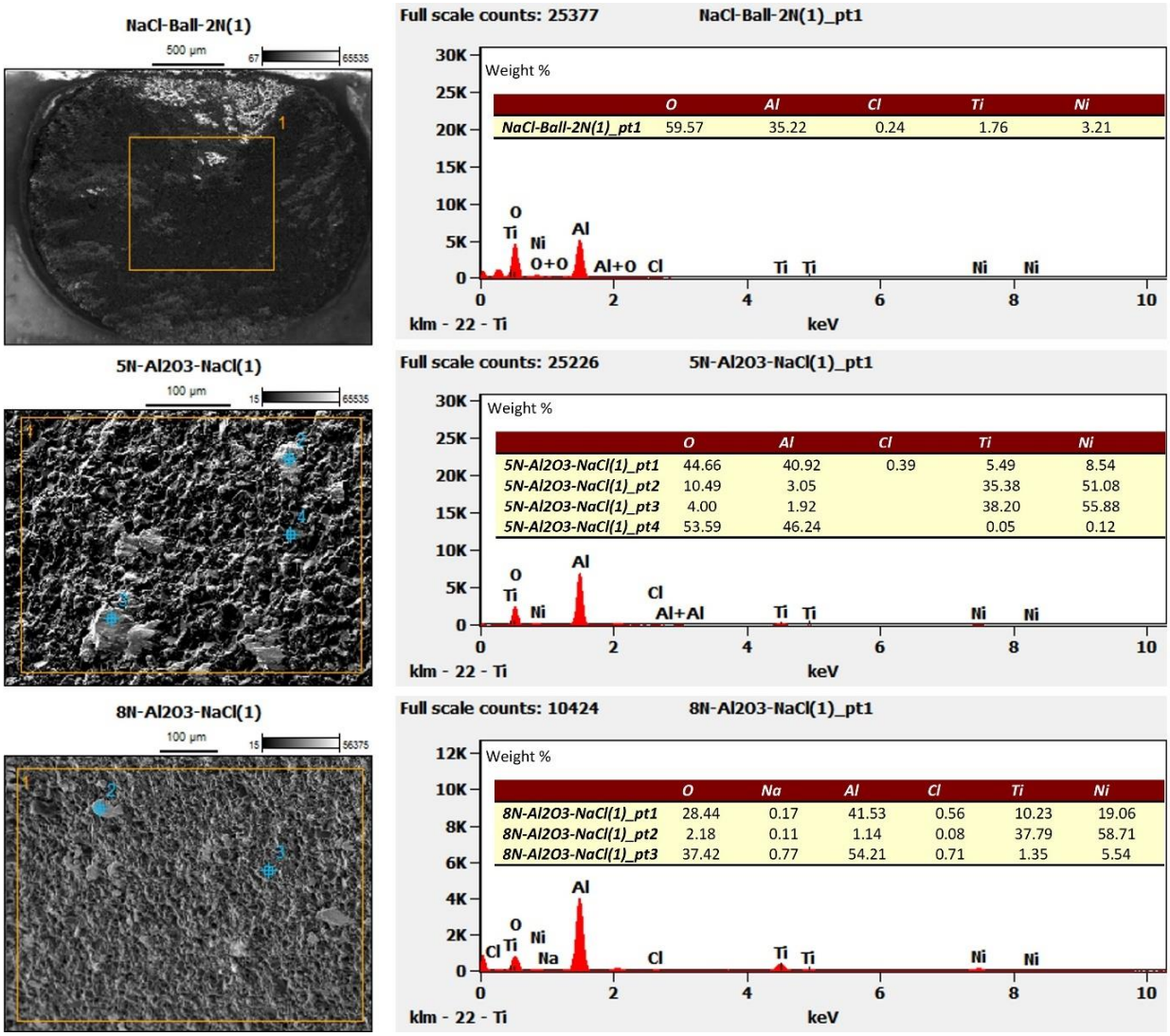

Fig. 7.6: EDS of Al_2O_3 surfaces sliding against NiTiNOL60 at 2N, 5N and 8N applied loads.

7.2.3.3. Electrochemical measurements of potentiodynamic polarisation

In electrochemical reactions involving metals and electrolytes, oxidation is prevalent, and this has been confirmed by the SEM and EDS results shown in Figs 7.4, 7.5 and 7.6. The electrochemical results obtained from this investigation are shown in both tabulated and graphical representations. Table 7.1 represents the summarised electrochemical parameters obtained through the IviumSoft data acquisition tool during the tribocorrosion measurements. The table denotes that at the open circuit system, which represents the electrochemical activity of the material, parameters such as the corrosion potential, corrosion current density, passivation resistance and corrosion rate estimated were obtained from Tafel analysis. From our study, it could be deduced that an increase in the applied load increased the corrosion current and pushed the corrosion potential towards zero, thereby leading to a continuous drop in the polarisation resistance, which in turn

increased the corrosion current. This confirms that a metal's dissolution rate depends on the corrosion potential, which likely determines the anodic or cathodic polarisation activity [150].

Table 7.1: Electrochemical parameters estimated from Tafel analysis in NaCl.

Sample	E_{corr} (V)	$I_{corr} \times 10^{-3}$ (A)	R_p (Ω)	Corrosion Rate (mm/y)
NiTiNOL60 @ 2N	–2.105	4.784	744.70	1.346
NiTiNOL60 @ 5N	–1.594	5.473	357.40	2.194
NiTiNOL60 @ 8N	–1.356	6.588	146.90	2.851

Following the results shown in Table 7.2, Figure 7.7 depicts the potentiodynamic polarisation curves of the sample after immersion in 3.5 wt.% NaCl solution and tribocorrosion investigation. The curves depict electrochemical activities that occurred in the cathodic and anodic regimes, resulting in pit nucleation and metastable pit formation, cavities, and cracks [81, 152]. Further, it shows a distinct passivation platform area, indicating that a stable passivation film forms on the material's surface within the corresponding self-corrosion voltage range, protecting the base material from corrosion. According to previous reports, the electrochemical breakdown of oxides of some metals is reduced cathodically to the metals or ions in aqueous solutions [151]. In aqueous solutions, solution anions, halides and nonhalide types can play a significant role in passive film growth and breakdown. Halide ions such as Cl^- can give rise to severe localised corrosion (e.g., pitting); this is evident in the SEM micrographs and the Tafel plots showing cavitation that increased significantly as the applied load increased. The surface damage could also be attributed to the continuous destruction of the passivation film, which exposed the material subsurface to more corrosion attacks and subsequently led to plastic deformation [217]. Evidently, the cavitation shown in Fig. 7.7, resulting from the adhesion and repassivation on the anode surface, could impede the reactivity between the anode surface and the electrolyte [11, 237, 255]. As the electrochemical activity proceeds and the passive film dissolves, the system overcomes the driving factors and attains equilibrium as the corrosion potential tends to be more stable [101]. Repassivation generates surface protective oxide film (TiO_2), which offers great resistance in static corrosion, unlike in the combined actions of corrosion and mechanical wear [264]. As oxidation progressed, oxygen atoms diffuse towards the NiTi substrate, while Ni atoms diffuse outward on the surface, hence the rich zones of Ni and Ti [217]. The localised corrosion and plastic deformation, which resulted due to the synergistic interactions, were promoted by the reactions in both regimes. According to Guadalupe

et al. [152], the chemical reaction between metal and water generates a surface metal oxide and releases hydrogen, as demonstrated in Eq. 5.

$$Me + H_2O \rightarrow MeO_x + xH_2 \quad (5)$$

Further, Vilhena et al. [81] reported that the electrochemical behaviour (reduction reactions) that take place at the cathodic branch are dependent on the nature of the corrosive environment, for instance, the oxygen reduction in the alkaline medium as represented in Eq. 6.

$$O_2 + 2H_2O + 4e^- \rightarrow 4OH^- \quad (6)$$

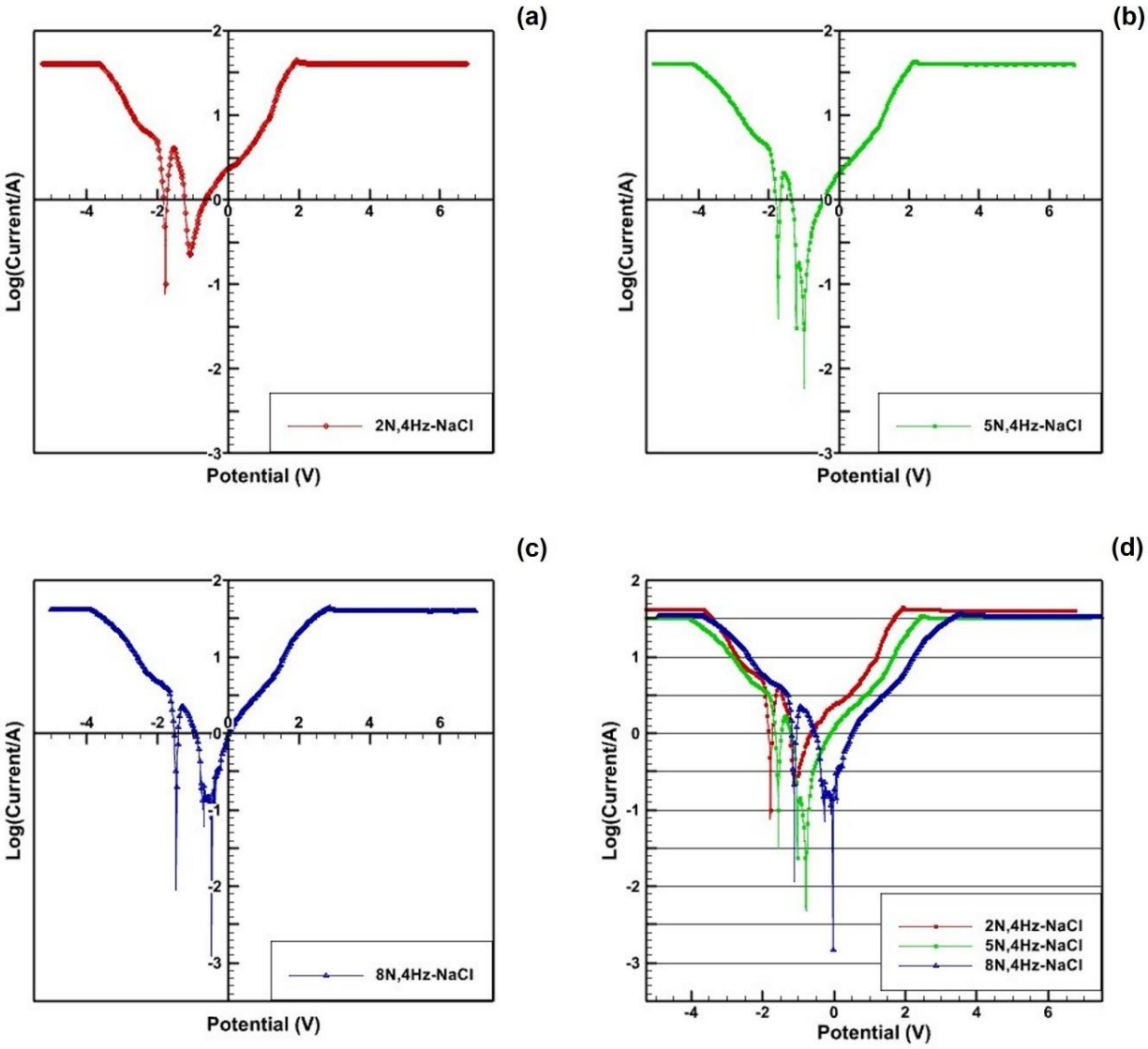

Fig. 7.7: Tafel plots showing the log current and corrosion potential relationships at different applied loads in $NaCl_{aq}$.

7.2.3.4. Wear mechanisms

The simultaneous reciprocating sliding and electrochemical potential activities promoted the various wear mechanisms [258, 262] recorded in this investigation. Based on the wear synergy, we quantified the results using the methods and equations outlined in section 2 to depict the wear volume, specific wear rate and corrosion rate, as presented in Figure 7.8. The mechanistic approach distinguishes between two critical contributions of mechanical wear and anodic dissolution, i.e., wear-accelerated corrosion [17, 173]. From the plots, it is evident that an increase in the applied normal load increased the wear volume, corrosion rate and specific wear rate due to the synergistic interaction. The tribocorrosion interaction promotes the shearing of asperities following sliding and frictional heating at the contact interfaces, which consequently results in large surface deformation [215]. During the tests, reciprocating sliding removes the passive film and promotes enhanced anodic metal oxidation on the bare metal until repassivation [217]. This results in a sudden cathodic shift of the potential towards the negative but stabilises with a drop in corrosion current as the system attains a steady state. The cathodic shift, however, is less noticeable at lower loads where less surface damage occurs. The formation of cavities is promoted by the presence of voids on the sample surface, which potentially elongate to the subsurface. The combined effects of void formation, as well as the intermetallic phase distortion, result in increased surface roughness and a more significant friction coefficient [12, 101]. These synergistic interactions supported by the third-body abrasion recorded at higher applied loads result in significant surface damage (localised corrosion and plastic deformation). Hence, the material loss occurring due to the synergism between wear and corrosion is more significant when compared to their individual impacts [80, 172]. The results clearly show that the localised corrosion of the material was controlled by oxidation of the alloy in the anodic regime, which subsequently resulted in the metallic dissolution. The graphical trends illustrating a continual increase in corrosion and wear rates validate that the halide ions in the electrolyte gave rise to wear-accelerated corrosion.

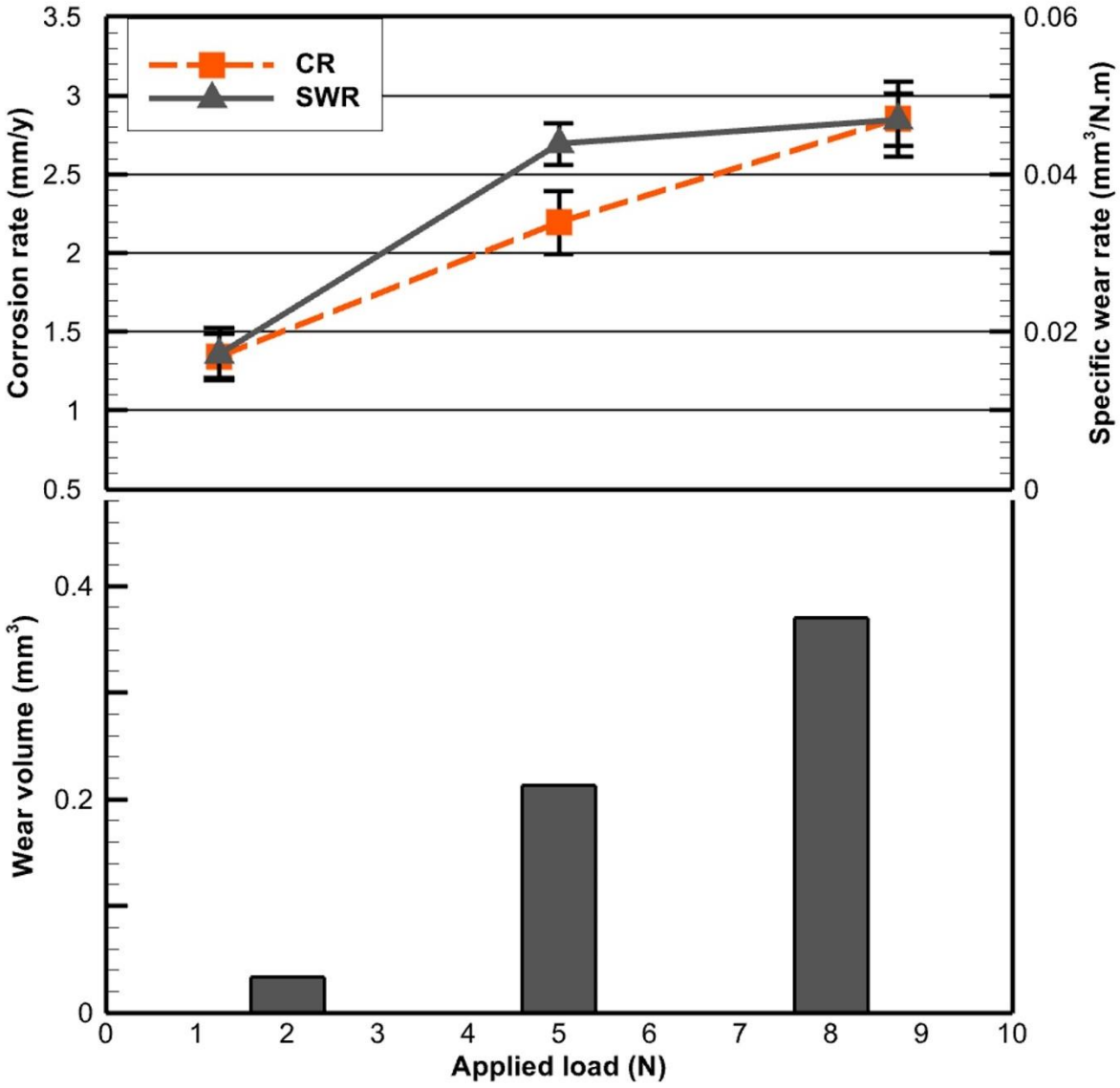

Fig. 7.8: Wear volume, specific wear rate and corrosion rate.

Figure 7.9 illustrates a summarised tribocorrosion wear mechanism of NiTiNOL60 alloy investigated in the saline environment. Our analysis deduced that all the sample surfaces examined under the different loads were oxidised. While the oxidised surfaces promoted localised corrosion as confirmed with the SEM and EDS examinations, the sliding contacts initiated the breakdown of oxide/ passive films [166], which led to delamination, followed by mild to severe abrasion, adhesion and subsequently to plastic deformation of the material. The contact pressure from the applied load evidently contributes to the gradual material detachments and grain refinements or elongations. The SEM results and the evolution of the coefficient of friction with sliding time shown in Figure 7.5 confirm that increased applied load increases the contact pressure and the effects of third-body wear, which advances fatigue and crack propagation as sliding contact continues [214].

As a result of the constant sliding of the contact surfaces during linear reciprocating wear tests, the material deforms plastically, which promotes the transfer of wear debris to the opposing body and lowers the rate of corrosive wear [265]. According to the CoF levels, the wear processes caused by the high material detachment occurred due to a synergistic interplay [164] between mechanical and electrochemical actions [165, 166, 257]. The different stages of pitting and crack propagation, as reported in subsection 7.2.3.1, highlight the susceptibility of the exposed surface of NiTiNOL60 in NaCl solution. This reveals the need for enhanced hydrophilicity of NiTiNOL60 alloy surfaces in its applications. The analyses have demonstrated that the Archard's wear law, which takes into account the effect of the passive film for wear-accelerated corrosion, could accurately represent the influence of electrode potential and normal load on the total degradation via tribocorrosion synergy [42].

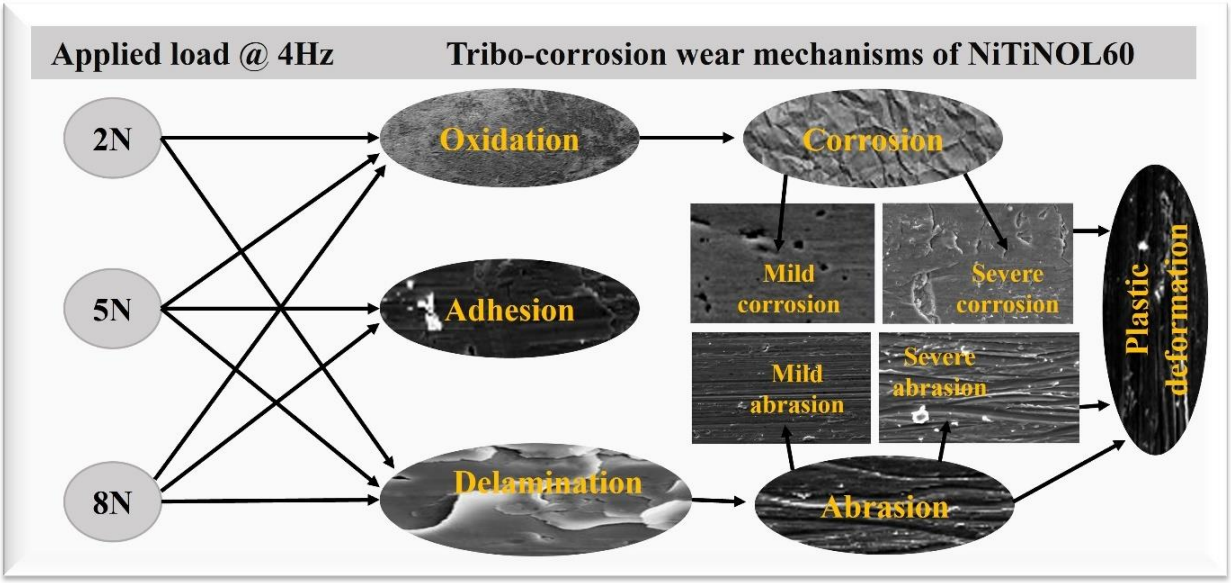

Fig. 7.9: Simplified representation of tribocorrosion wear mechanisms of NiTiNOL60 alloy in $NaCl_{aq}$.

7.2.3.5. Hardness measurements of NiTiNOL60 exposed to NaCl environment after tribocorrosion

A heterogeneous distribution of roughness was observed along the wear tracks, especially for higher applied loads, unlike in the wear tracks for surfaces subjected to lower loads. Du, et al. [101] reported that the microhardness of NiTiNOL60 fluctuates more violently because of uneven network structures. To validate this information, we evaluated the hardness of the wearing body (NiTiNOL60) before and after the tribocorrosion tests. Using the method described in section 3.6 of Chapter 3, we calculated the hardness by measuring the force applied and comparing it to the

geometrical aspects of the indentation, such as the surface area or depth of the indented shapes, diamond (Vicker's) and cone (Rockwell). Accordingly, we measured the Rockwell hardness of a polished sample before the tests and obtained an average value of 62.5 HRC, aligning with the value reported in the literature [25, 170, 210]. Figure 7.10 shows the average results obtained from the micro indentation hardness tests along the sample's wear tracks after each trial. We deduced from the results that the hardness values we measured outside the wear track (i.e., at zero load) show the lowest Vicker's hardness average value of HV 538.44/1.0 kgf/10 s. In contrast, the average Rockwell Hardness value measured for the sample after testing gave an average macro hardness value of 67 HRC. This implies that Rockwell hardness recorded less than a 10 % increase during tribocorrosion actions. This could be attributed to different factors, including compressive forces during sliding, friction-induced hardening, and work-hardening of Ni-Ti agglomeration, as well as the repassivation of oxide films, particularly at higher contact pressures [130, 266]. The work-hardening due to the reciprocating sliding results in an inhomogeneous distribution of hardness and wear imbalance between the different hardness zones, ultimately causing a deterioration in tribology performance [43]. Supported by the metallographic results, the EDS confirms the formation of oxide layers in the electrolyte medium, while the micrograph in Figure 7.1 presented fine eutectic network structures of consolidated and unconsolidated grain clusters. The non-uniformity of the microstructural grains is believed to have been attributed to the low hardness measured outside the wear track, unlike in uniform and fine eutectic network structures where hardness is expected to be higher due to the compact grains.

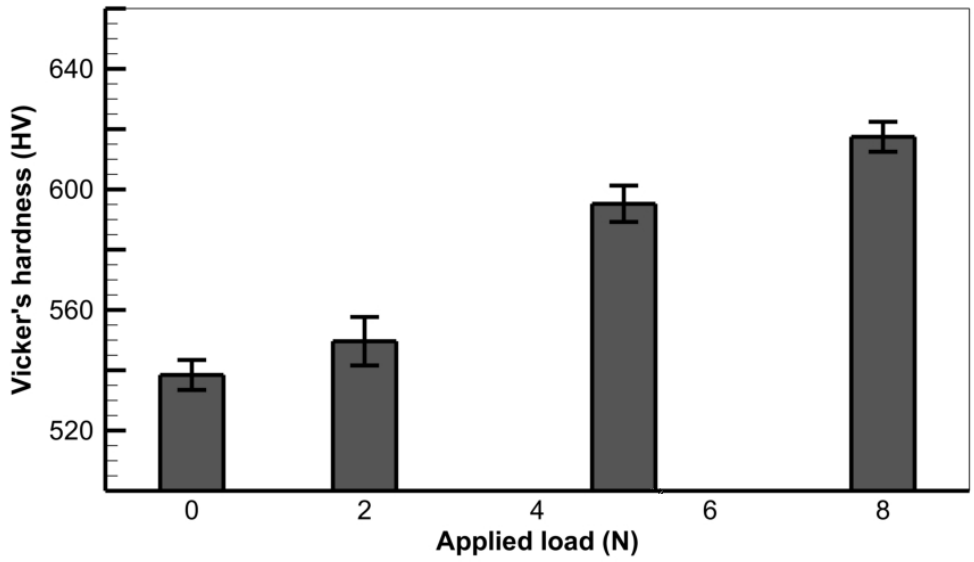

Fig. 7.10: Graphical representation of the microhardness tests of samples in $NaCl_{aq}$.

7.2.4. Summary

This study delving into the details of wear, corrosion, and their synergistic interactions has shed light on the multifaceted interplay between wear rates, coefficient of friction, applied potential, electrochemical reactions, and the wear-corrosion mechanisms governing the behaviour of NiTiNOL60 alloy. The findings presented in this research offer valuable insights into the complex processes that govern the material's surface and wear track. Our investigation underscores the critical role of equilibrium between passivation and repassivation rates in determining corrosion and wear rate mechanisms. We have confirmed that the progression of corrosion pits, cavities, and cracks is notably accelerated by the presence of sufficient contact pressure at the sliding interfaces, coupled with an increase in corrosion current density. Additionally, the mechanistic interactions promote frictional heating at the contact body interface and asperity shearing at high strain rates during sliding. The observations highlight the profound impact of mechanical forces and electrochemical reactions on the material's surface integrity. Abrasive wear emerged as the predominant wear mechanism, particularly under higher loads. The continuous reciprocating sliding action subjected the contact surfaces to fatigue damage and plastic deformation, resulting in surface degradation. In summary, this study elucidates the synergy between wear and corrosion, revealing their detrimental effects on the surfaces of 60NiTi alloy which will serve as a guide in material selection consideration and the incorporation of this alloy in engineering design. The insights gained from this research contribute to a deeper understanding of the wear-corrosion dynamics, with potential implications for improving the durability and performance of materials in various engineering and industrial applications. Further research in this direction holds the promise of enhancing the robustness and longevity of critical components subjected to wear and corrosion challenges.

CHAPTER 8: TRIBOCORROSION TESTING IN ALKALINE SOLUTION

8.1. Preface

This chapter presents the tribocorrosion behaviour of NiTiNOL60 alloy in an alkaline environment. The choice for this electrolyte is based on its use in the processing industries as a cleaning agent. This investigation is relevant to ensure that an appropriate grade material is selected to address both metal release and corrosion degradation of materials, especially in the food and beverage industries.

The findings from the study have been published in the Journal of Results in Engineering https://doi.org/10.1016/j.rineng.2023.101305

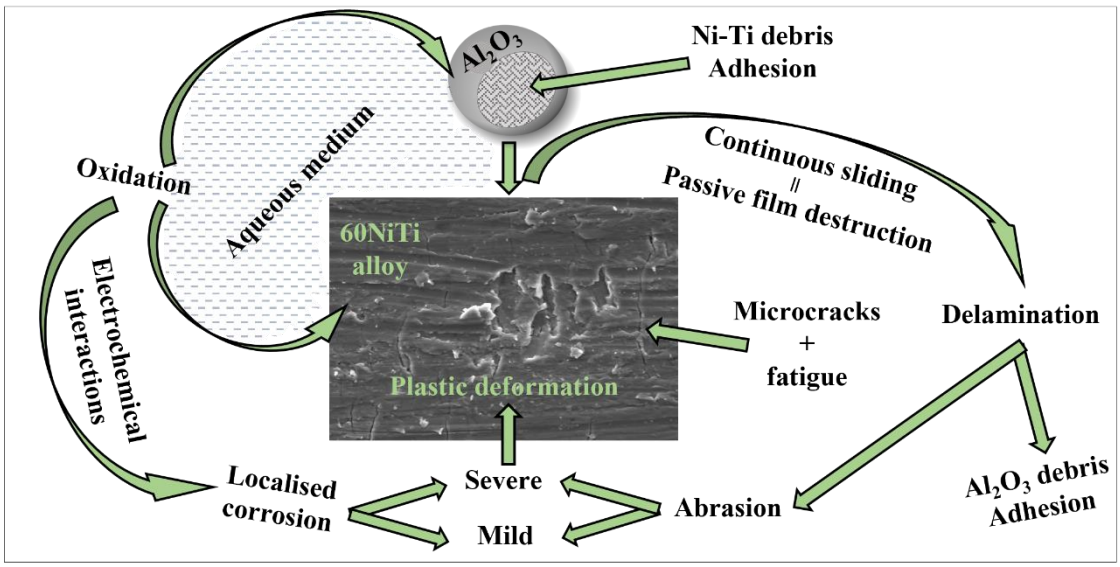

Graphical abstract

8.2. Tribocorrosion behaviour of NiTiNOL60 alloy in an alkaline environment

8.2.1. Overview

Tribocorrosion, a phenomenon where the combined effects of mechanical wear and chemical corrosion lead to material degradation [227, 259], has become a research hotspot in recent years due to its significant impact on the performance and longevity of metallic materials in various demanding environments. Understanding the tribocorrosion behaviour of different materials is crucial to enhancing the durability and efficiency of systems in which these materials are employed [267]. Traditionally, 316L stainless steel has been used in load-bearing applications in corrosive environments [109], such as liquid-handling systems and hydraulic machinery. This is attributed to its impressive mechanical properties, excellent formability, relatively low cost, and good corrosion resistance [10, 67, 101]. However, the low resistance of the steel-grade materials to localised corrosion, tribocorrosion wear, and cavitation erosion as a result of low hardness (around 200 HV) limits their use in aggressive environments. Du, et al. [101] highlighted that more than 80% of machine failures are caused by abrasion on the surface of the component. These support the concern around the increasing rate of product contamination and surface deterioration of equipment in the process industries (food and beverage, pharmaceutical, etc.) arising from mechanical loading and harsh corrosive conditions [108, 111]. Metals in various flow systems, such as chemical reactors, are prone to tribocorrosion. In such systems, the corrosion attack on the metal surface in the corrosive environment is accelerated by the fluid flow, while the wear occurs due to mechanical loading and/ or sliding contact [111, 227]. Thus, it is imperative that the synergistic interactions of sliding wear and electrochemical reactions in a corrosive environment be investigated [9, 22]. The tribocorrosion study ideally involves the integration of a tribometer and a potentiostat in a controlled system. The tribometer provides controlled mechanical loading and relative motion and measures the friction force, while the potentiostat determines open-circuit potential (OCP) and electrochemical measurements [268].

NiTiNOL60, also known as 60NiTi, is a binary nickel-titanium alloy containing 60 wt.% Ni and 40 wt.% Ti which has been shown to achieve the highest hardness amongst the binary compounds after heat treatment at 1050 ℃ [40]. It was first discovered by William J. Buehler and his colleagues in the late 1950s at the Naval Ordnance Laboratory, Maryland, USA; this gave rise to the name NiTiNOL (Nickel-Titanium Naval Ordnance Lab), commonly used for 60NiTi alloy [25, 35, 99, 101]. The non-equiatomic phase of the Ni-rich (NiTiNOL60) alloy differs from the equiatomic shape memory alloy. NiTiNOL60 is

an ordered intermetallic material compound consisting of a B2, cubic crystal structure matrix containing one or more secondary phases, including the metastable NiTi and Ni3Ti2 phases, and the equilibrium Ni3Ti phase, also referred to as globular Ni_3Ti precipitates [26, 47, 210]. In general, NiTiNOL60 alloy is a versatile material owing to its unique properties and wide range of applications from aerospace, automotive, turbine blades [234] and actuators [113, 269] in various engineering fields to medical devices and biomechanics [27, 89, 137, 205, 270, 271]. In addition, Nickel alloys have an excellent track record for providing corrosion resistance and high strength at high temperatures in various applications, making the material an enviro-metal [5, 270]. However, the cost of NiTi-based alloys limits their use in most desirable applications.

The material properties of NiTi alloys have been investigated by several researchers. DellaCorte [138] and Pepper, et al. [24] investigated the superelastic behaviour of NiTiNOL60 material for space bearing. Du, et al. [101] reported that NiTiNOL60 coating on 316L stainless steel substrate remarkably improves corrosion resistance. Zhang, et al. [272] showed that magnetron sputtering coating of NiTiNOL60 alloy improved the hardness and corrosion resistance when compared with 316 stainless steel substrates. Khanlari et al. [41], Khanlari, et al. [170] investigated the sliding wear behaviour of NiTi alloys under dry and lubricated contacts and determined their wear mechanisms under different working conditions.

Kosec, et al. [45] studied the effects of different microstructures on tribocorrosion behaviour of NiTi alloys in simulated saliva. Yan, et al. [166] studied the microstructure and tribocorrosion performance of NiTiNOL60 alloy in artificial seawater. They identified B2 TiNi and stable $TiNi_3$ phases in the as-cast NiTiNOL60. They reported that solution treatment could lead to the precipitation of metastable Ti_3Ni_4 phase in the matrix without dissolving the $TiNi_3$ phase completely. Meanwhile, Chen, et al. [176] demonstrated that B2-NiTi phase transformed into a martensite B19’ NiTi phase during tribocorrosion process. In addition, they highlighted that some tiny pits at the interface of the phases could contribute to the wear contact stresses accelerating the corrosion effect. Xu, et al. [80] investigated the synergistic interactions between wear and corrosion of Ti-16Mo orthopaedic alloy. They reported that the corrosion rate increases under sliding contact. Thus, they concluded that corrosion and wear accelerate each other significantly, with a reported corrosion rate and wear rate increase of about 100 times and 40%, respectively, under tribocorrosion in Ringer’s simulated body fluid.

While literature information reveals that most tribocorrosion studies conducted so far were focused on environments such as acidic, seawater and simulated body fluids, there needs to be more research on understanding the tribocorrosion performance of

NiTiNOL60 alloy in alkaline environments. Therefore, in this paper, we investigated the tribocorrosion behaviour of NiTiNOL60 alloy in a NaOH (caustic soda) environment, which is peculiar to a variety of manufacturing processes as a cleaning agent due to its effectiveness in dissolving greases, fats, and protein-based deposits. Understanding how an alkaline environment impacts the tribocorrosion of NiTiNOL60 alloy can provide valuable insights into enhancing the alloy's lifespan and effectiveness in various applications.

8.2.2. Materials and experimental methods

Material preparation, characterisation and tribocorrosion investigations in aqueous sodium hydroxide medium were conducted using the methodological approaches outlined in Chapter 3 of this thesis.

8.2.3. Results and discussions

8.2.3.1. Surface characterisation of the sample wear track after tribocorrosion

Examination of the wear track after the tribocorrosion tests under different loads and electrochemical conditions reveals abrasion, debris adhesion, pits, delamination, plough and cracks, as seen in Figure 8.1. Both mechanical and chemical wear, which occurred as a result of sliding contact and corrosion attacks, are clearly shown in the images. The localised corrosion (pits, cracks and crevices) observed on the surface occurred as a result of the oxidised layer on the exposed surface, supported by the electrochemical reactions during the open circuit potential and the potentiodynamic polarisation [226]. Microcracks (perpendicular to the sliding direction) and delamination were also observed along the wear tracks. According to He, et al. [273], corrosion pits can also promote the nucleation of fatigue crack by providing stress concentration.

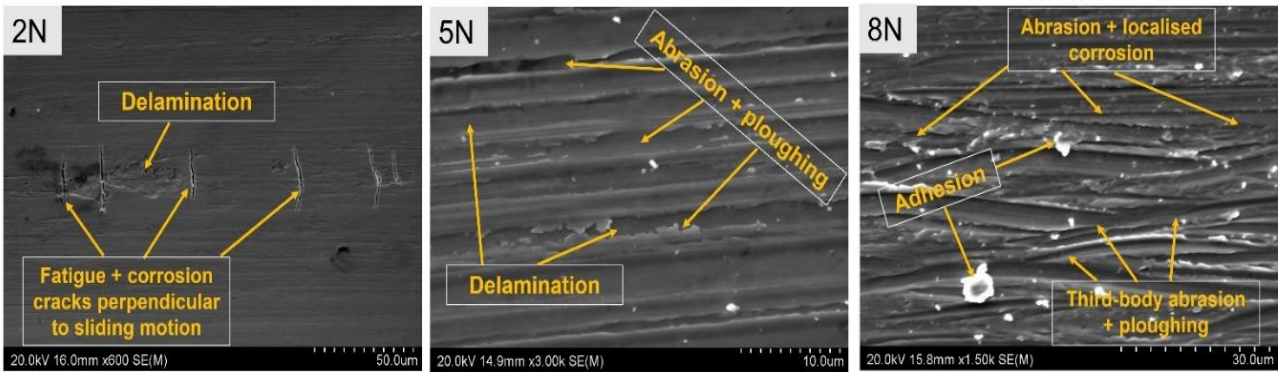

Fig. 8.1: SEM images showing the wear track microstructure of NiTiNOL60 alloy sample under different mechanical loads.

EDS elemental analysis of selected areas revealed the elemental compositions at various point scans as shown in Figure 8.2. From the table, the EDS analysis for some selected areas exhibits increased oxygen content at higher loads, while no oxygen element was detected for a 2N load. According to Yan, et al. [166], this indicated that the exfoliation or delamination of the oxide layer during the reciprocating sliding exposes the surface of the alloy to the corrosive medium and, thus, accelerates the corrosion of the material. At 2N and 5N, the formation of the Ti-Ti phase indicates the likely occurrence of TiO_2 following the oxide layer, whereas Ti-Ni occurred at 8N. From the tables in Fig. 8.2, it is clear that more oxide layer was formed at the applied load of 8N, and this could be attributed to the larger surface area created during the sliding action.

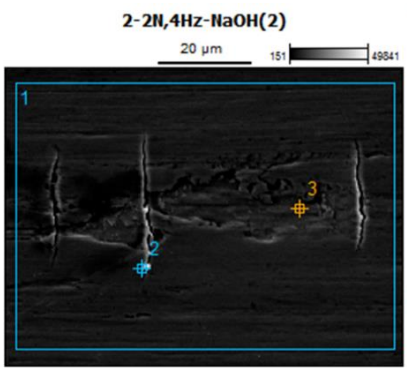

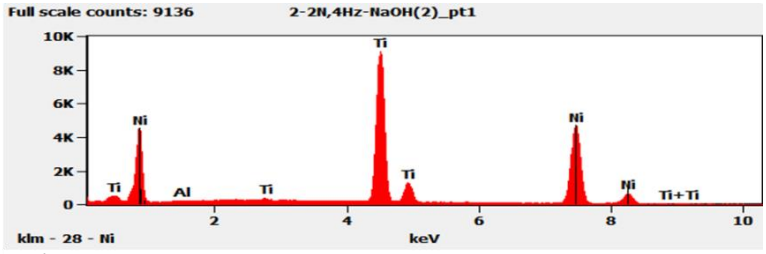

Weight %

	Al	Ti	Ni
2-2N,4Hz-NaOH(2)_pt1	0.32	40.19	59.49
2-2N,4Hz-NaOH(2)_pt2	0.26	39.41	60.33
2-2N,4Hz-NaOH(2)_pt3	0.24	40.89	58.87

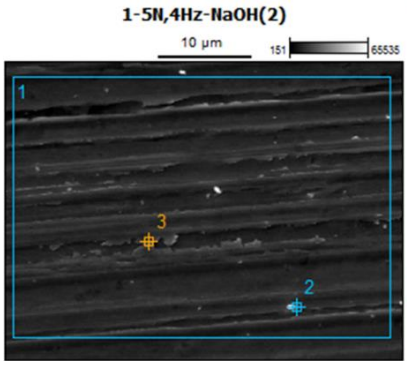

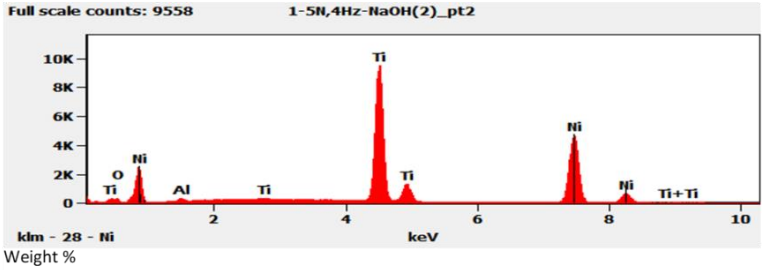

Weight %

	O	Al	Ti	Ni
1-5N,4Hz-NaOH(2)_pt1			41.57	58.43
1-5N,4Hz-NaOH(2)_pt2	2.04	0.65	40.16	57.15
1-5N,4Hz-NaOH(2)_pt3			41.32	58.68

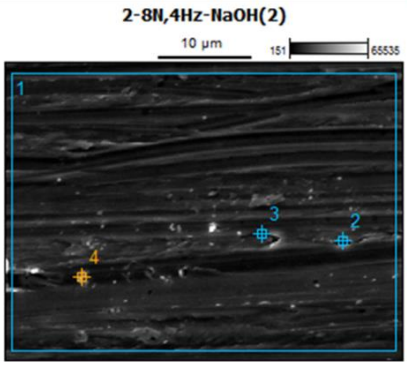

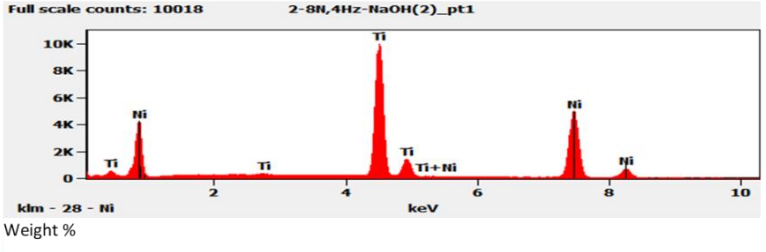

Weight %

	O	Al	Ti	Ni
2-8N,4Hz-NaOH(2)_pt1			41.50	58.50
2-8N,4Hz-NaOH(2)_pt2	3.36	1.22	40.31	55.11
2-8N,4Hz-NaOH(2)_pt3			41.39	58.61
2-8N,4Hz-NaOH(2)_pt4			41.21	58.79

Fig. 8.2: EDS analysis for the wear track of NiTiNOL60 at different applied loads.

This is due to the larger wear track width and wear volumes for sliding wear tests conducted at higher applied loads. Also, the counter material (Al_2O_3) deposits on the wear track increase at higher loads. Figure 8.3 shows the SEM images for the different Al_2O_3 balls used for sliding tests.

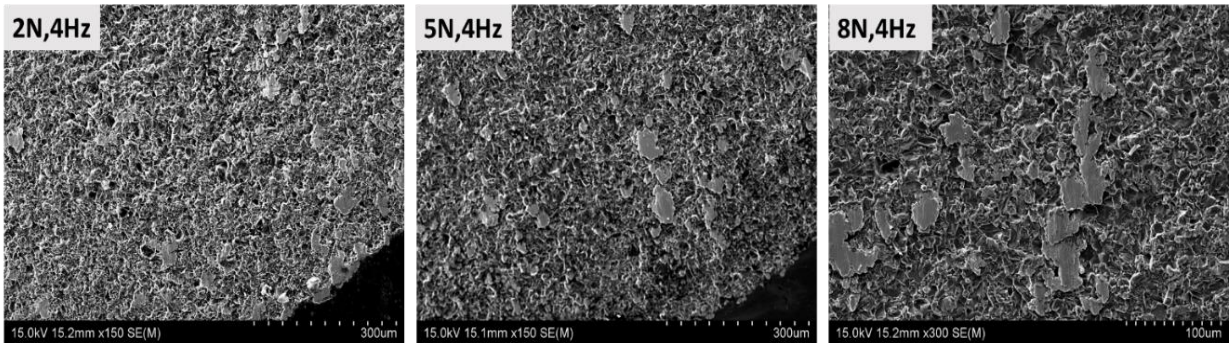

Fig. 8.3: SEM images of Al_2O_3 balls after reciprocating sliding actions.

Further EDS analyses were conducted to determine the elemental composition of the debris adhered to the alumina ball. Figure 8.4 presents the spectral imaging and elemental composition in wt.%. of the alumina ball after a tribocorrosion test conducted under 4Hz sliding frequency and 8N load.

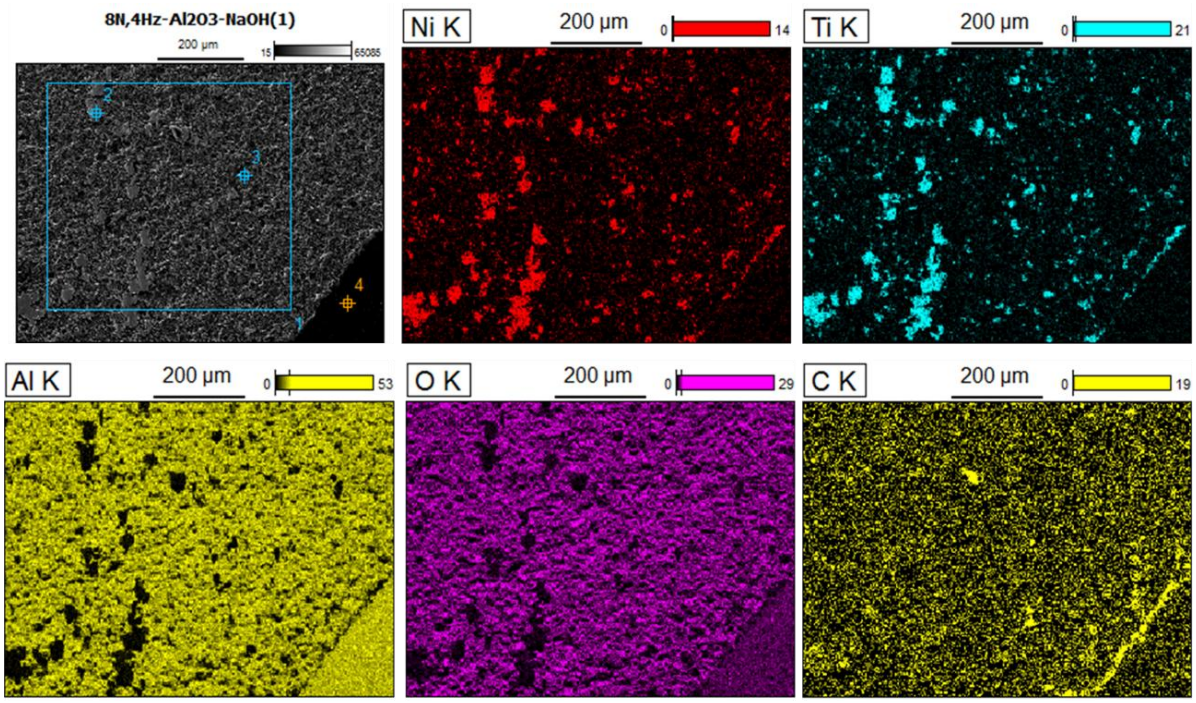

	C	O	Al	Ti	Ni
8N,4Hz-Al2O3-NaOH(1)_pt1	6.84	41.77	40.39	4.17	6.82
8N,4Hz-Al2O3-NaOH(1)_pt2	2.11		1.39	38.98	57.52
8N,4Hz-Al2O3-NaOH(1)_pt3	3.84	51.22	44.94		
8N,4Hz-Al2O3-NaOH(1)_pt4	3.69	38.73	57.58		

Fig. 8.4: Spectral imaging and EDS composition of Al_2O_3 ball after tribocorrosion test conducted at 8N load and 4Hz frequency.

The detected carbon at different points examined could be a result of some carbonaceous materials within the EDS chamber. Point 1 gives the overall scan of the surface examined, and the identified elements are listed in the accompanying table. While the high percentage composition of Ni and Ti at point 2 confirms the adhesion of NiTiNOL60 debris, points 3 and 4 show the composition of the counter material (Al_2O_3) without the adhesion of the NiTiNOL60 debris.

Similarly, an EDS analysis of the wear tracks of the sample tested at a higher load of 8N was carried out, and the results are presented in Figure 8.5. It is noted that more oxide layers occur during repassivation, whereas in lower loads where the contact pressure is insignificant, the formation of passive film on the anode surface hinders the reaction between the anode surface and the solution. As the passive film gradually dissolves, the reaction tends to balance, and the potential tends to be stable [101].

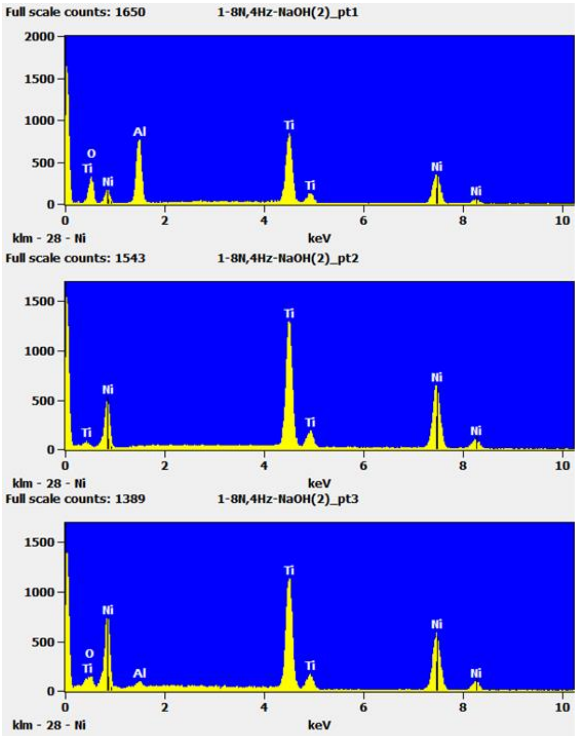

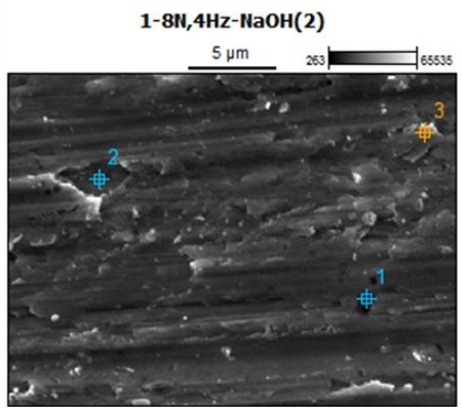

Weight %

	O	Al	Ti	Ni
1-8N,4Hz-NaOH(2)_pt1	30.16	15.90	24.34	29.61
1-8N,4Hz-NaOH(2)_pt2			41.77	58.23
1-8N,4Hz-NaOH(2)_pt3	9.93	1.36	36.60	52.10

Fig. 8.5: EDS examination of the wear track of the NiTiNOL60 sample tested at 8N load and 4Hz sliding frequency.

8.2.3.2. Frictional behaviour and the effect of sliding contact on electrochemical potential

The variations of the coefficient of friction (CoF) with time for samples tested under different loads were recorded from the tribometer via WINDUCOM software, and the results are presented in Figure 8.6. From the plot, it could be seen that the CoF increases as the applied load increases, thereby resulting in more wear and different wear

mechanisms along the wear track. The graphical trend for the 2N load shows a running-in time within the sliding time of 500 s, which shows there was no adequate contact pressure from the applied load. After the barrier, the counter material was able to wear off the passive oxide layer and penetrate the NiTiNOL60 sample, thus maintaining a relatively stable CoF. Whereas at higher loads, almost no running-in was recorded until the curves attained a steady state. According to Yan, et al. [166], the recorded trend can be attributed to partial rebuilding of passivation film under sliding contact, but the partial rebuilding becomes difficult at larger normal loads. Irrespective of the higher wear rate, the samples displayed more stable friction coefficients at higher loads. The relatively stable CoF trend could be a result of the dynamic equilibrium between electrochemical passivation and mechanical passivation during tribocorrosion. This also indicates that the passive film is gradually destroyed during the sliding contact, as reported previously by Yan, et al. [166]. The results presented in Figures 8.3 and 8.4 showed the adherence of the NiTiNOL60 material onto the ball surface, which impacts the surface roughness in the contact interface. The introduction of this roughness, due to the micro-scale material transfer during the wear process, resulted in fluctuating frictional behaviour presented in Figure 8.6.

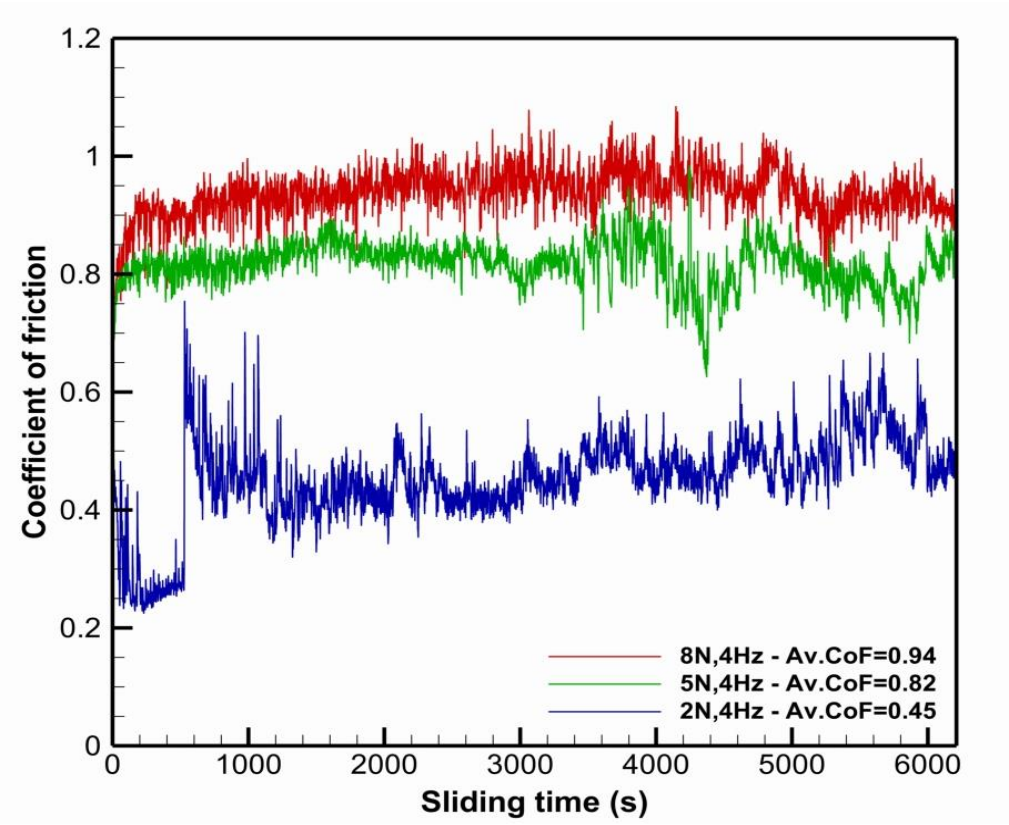

Fig. 8.6: Evolution of the coefficient of friction with sliding time for NiTiNOL60 alloy sliding against Al_2O_3 ball at different applied loads in NaOH.

The Tafel curves obtained after the OCP and during potentiodynamic polarisation measurements are represented in Figure 8.7. In an electrochemical system, the corrosion potential indicates the corrosion tendency of an alloy and is determined by its constituent elements with different electrode potentials [101]. This implies that the higher the electrode corrosion potential, the weaker the corrosion tendency. As shown in Figure 8.7, the curves depict a clear passivation platform area, indicating that a stable passivation film is formed on the surface of the material within the corresponding self-corrosion potential range in order to protect the surface from localised corrosion [164, 274]. According to Alkan and Gök [262], the OCP or corrosion potential (E_{corr}), which promotes passivation, is the potential created by the electrochemical processes at a metal surface immersed in a solution.

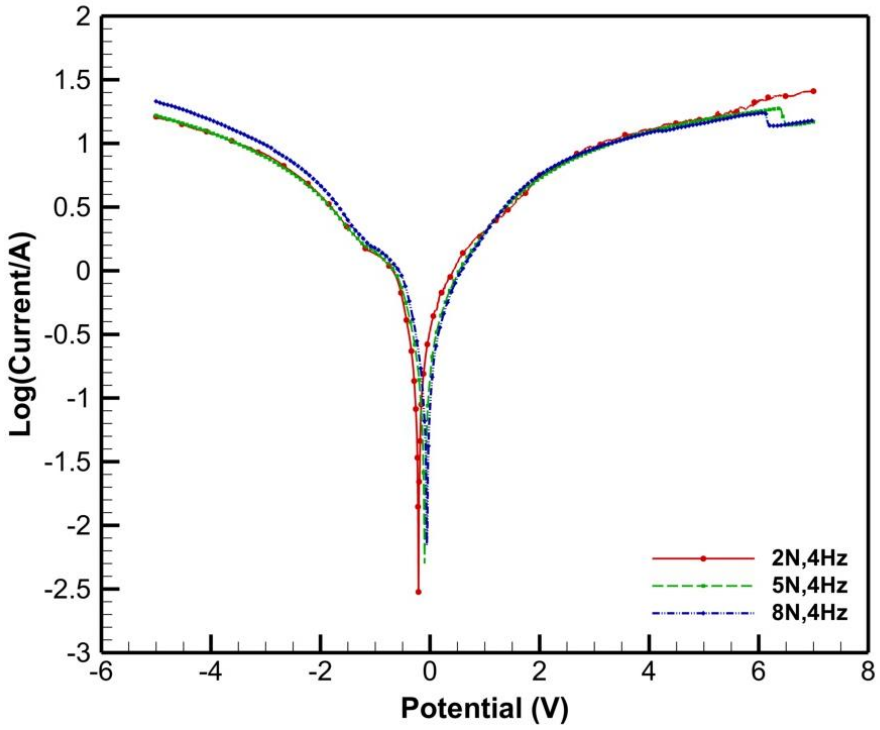

Fig. 8.7: Potentiodynamic polarisation curves of NiTiNOL60 at different load conditions.

From the plots, it is evident that E_{corr} for the 2N load is more negative when compared to the 8N load, while the I_{corr} increased with load increase. As a result, a higher corrosion rate was recorded at a higher load, and this clearly indicates the promoting effect of sliding contact on corrosion.

The corrosion potential, corrosion current density and the corrosion rate, summarised in Table 3, were obtained through the standard Tafel measurements using Ivium software. The open circuit potential represents the electrochemical activity of the material at the various conditions investigated. It shows that the potential of the sample is more negative

at lower loads, which indicates that higher loads accelerate the electrochemical activity. This shows that open circuit stabilisation occurred at the cathodic region, whereas the wear recorded in the anodic regime contributed to the significant corrosion current density. From the results in Table 8.1, the corrosion potential at different loads investigated is lower, which means they corrode faster, though the corrosion rate and corrosion currents are lower. This implies that the repassivation layer significantly enhanced the corrosion resistance under the exposed conditions of the metal-solution interface, thereby causing the surface of the metal to corrode.

Table 8.1: Tafel fitting parameters of NiTiNOL60 at different normal loads.

Sample	E_{corr} (V)	I_{corr} (A) $\times 10^{-3}$	R_p (Ω)	Corrosion Rate (mmpy)
NiTiNOL60 - 2N, 4Hz	-1.7364	1.104	812.5	0.868
NiTiNOL60 - 5N, 4Hz	-1.4401	2.277	487.1	1.790
NiTiNOL60 - 8N, 4Hz	-0.2730	2.810	294.9	2.209

The surface conditions of NiTi-based alloys are known to strongly influence the corrosion behaviour, particularly passivity [176, 230, 254]. Moreover, the corrosion resistance of NiTi-based alloy is related to the formation of the titanium oxide film. The parameters outlined in Table 8.1 reveal that the corrosion resistance decreased with load increase yet possessed a stronger ability to form an oxide film. Du, et al. [101] reported that the corrosion tendency is weaker at higher corrosion potentials. However, Table 3 shows that a higher corrosion rate is established in this investigation following a higher shear deformation, which allows more wear and creates a larger surface area for corrosion to occur, thus reducing the protective effect of the passive film. Overall, it is evident that the corrosion rate increased with load increase. While corrosion potential and corrosion current density are seen to increase with load increase, the resistance is reversed, thus leading to an increased corrosion rate. According to Du, et al. [101], the electrode potential difference could equally be affected by the different phases in NiTi-based alloys. As a result, the dominance of Ni_4Ti_3 phase bequeaths corrosion resistance to the NiTiNOL60 alloy.

8.2.3.3. Wear mechanisms

Following the analysis above, it is evident that wear due to sliding contact would result in accelerated corrosion. It is, therefore, imperative that the possible mechanisms occurring during the tribocorrosion be determined. From the SEM images of the samples

under the tribocorrosion test at different load conditions, various wear mechanisms were recorded. Figure 8.8 shows a summarised plot for the mechanical wear and chemical corrosion, respectively. The specific wear rate, as well as the corrosion rate, increased with load increase, and this follows the existing literature information [101, 166].

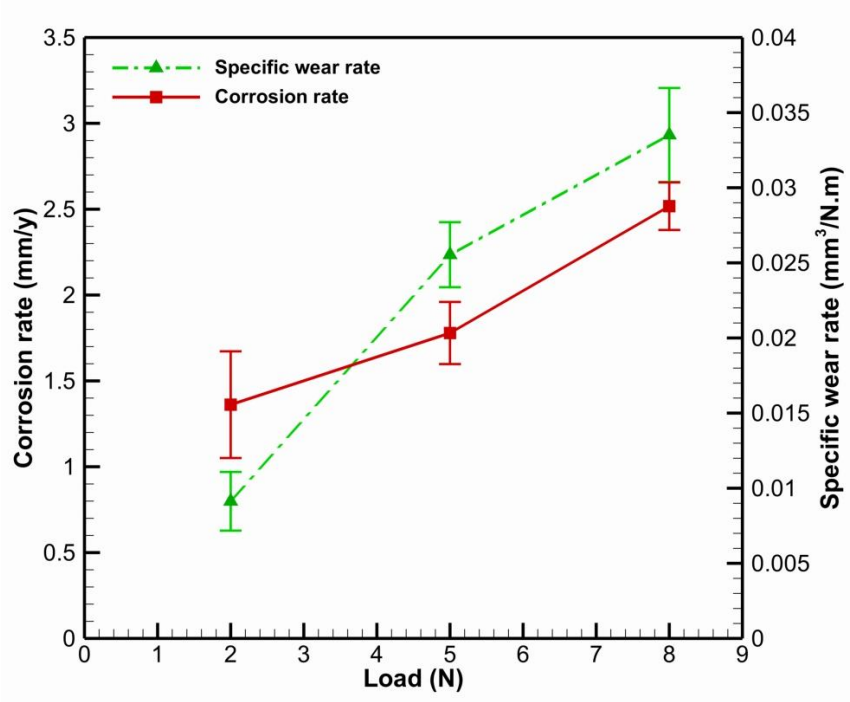

Fig. 8.8: Specific wear rates and corrosion rates at different normal loads.

Figure 8.8 shows that the corrosion rate increases with load. This is attributed to the amount of contact pressure made on the surface during the reciprocal sliding wear. Hence, at higher loads, continuous sliding results in enhanced shear deformation, thereby destroying the passive films/ layers and exposing fresh layers which are easily attacked in the electrolyte. In line with the findings of Yan, et al. [166] it is clearly indicated that delamination wear was caused by the exfoliation of oxide during sliding contact, which ultimately leads to the aggravation of corrosion.

The high volume of material loss due to sliding contact is supported by the SEM images in Figure 8.9 where a significant contribution from a third-body wear is recorded following the patterns of the abrasion grooves, micro striation, delamination and debris adhesion. These impacts result in less significant material loss due to the electrochemical corrosion. Therefore, the presence of TiO_2 film formation coupled with the excellent self-healing ability of Ni-Ti alloys [101, 165] helped to promote a better corrosion resistance of the sample. Further, Du, et al. [101] highlighted that appropriate passivation results in the build-up of TiO_2 (a very stable protective layer), which hinders ion exchange.

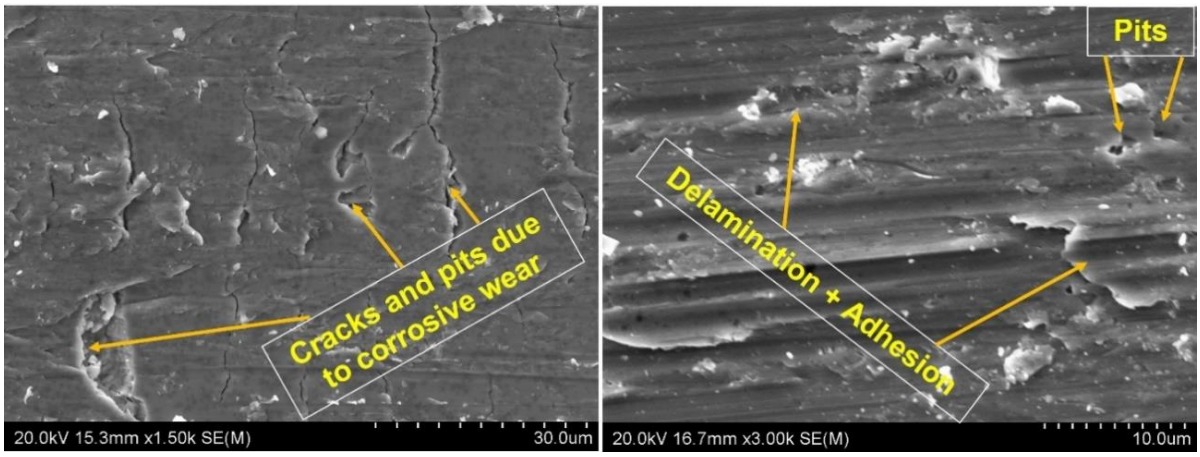

Fig. 8.9: SEM images showing third-body effect and microcracks at 8N load on NiTiNOL60 alloy.

To ascertain the level of deformation and the likely impact on the sample's microstructure, the cross-section of the tested samples was cut under the wear track, etched, and observed under SEM. Figure 8.10 shows the surface examination and the microstructure of the cross-sectional parts of the wear track. From the images, the sample is noted to have more eutectic network structure within 100 μm into the sample cross-section as a result of sliding shear deformation, while the dendritic clusters dominate the lower surfaces of the cross-section.

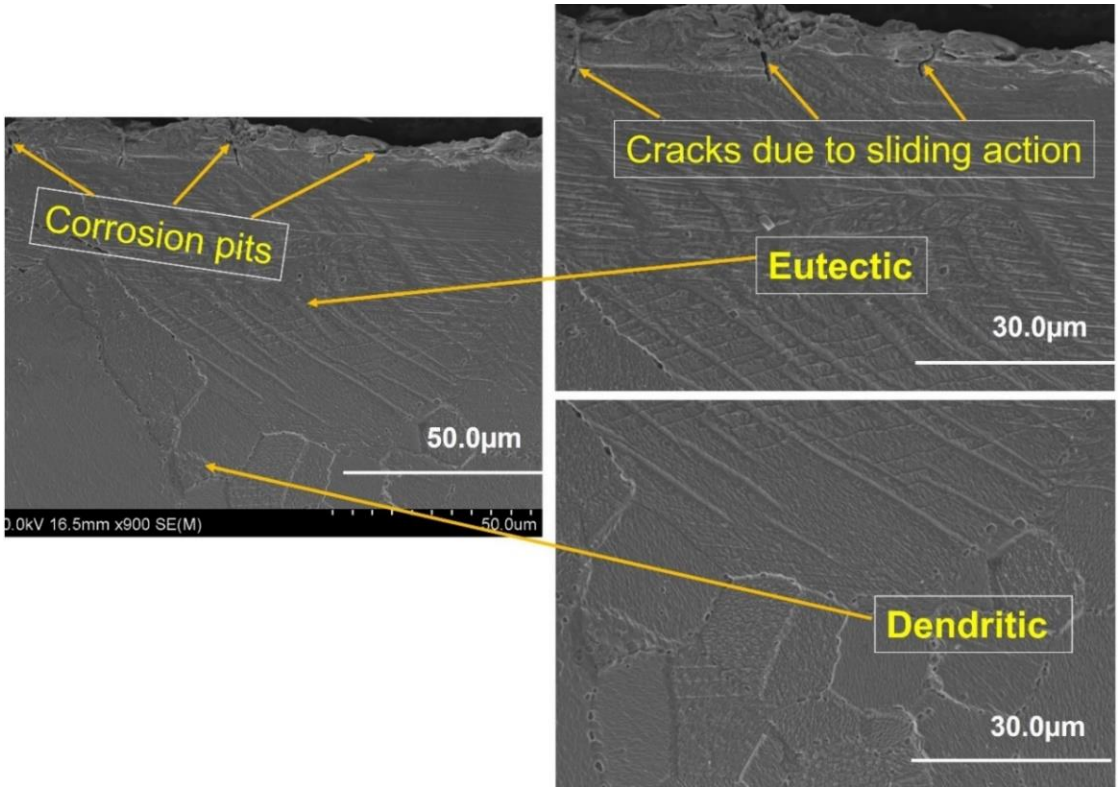

Fig. 8.10: SEM microstructure of the cross-sectional view of etched NiTiNOL60 sample.

Following the distortion of the grain boundaries, it is evident that the microcracks and pits exist around the edges of the cross-sectional surface due to the corrosion attack [172]. As shown in the image, the microcracks initiated from the corrosion pits penetrated beyond the surface of the sample, but its propagation fell within 120 µm of the sample surface. Corrosion pits and cracks occurred due to the electrochemical reactions, while the tribological impact as a result of the reciprocating sliding and the increased temperature due to continuous sliding clearly shows the grain elongation in the direction of sliding actions, as shown in Figure 8.11. Thus, the sliding contact has been deduced to accelerate corrosion.

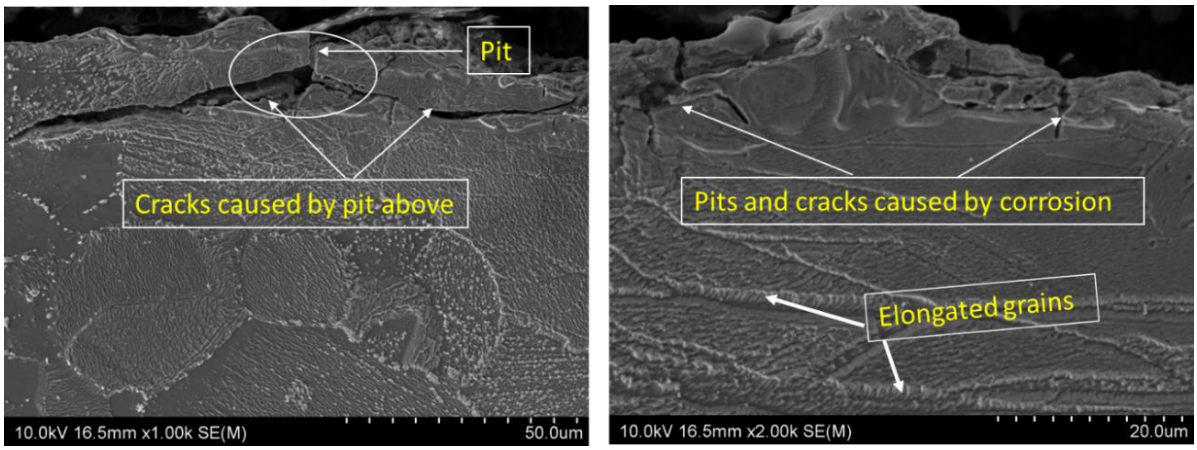

Fig. 8. 11: SEM microstructure of the cross-sectional view of NiTiNOL60 wear track.

As the passive films are easily destroyed because of sliding action, the interfaces of the phase NiTi matrix show more susceptibility to pitting. However, the formation of dense oxide film at lower loads could be attributed to the uniform microstructure and fine dendritic microstructure of the sample since the applied load has less contact pressure to wear off a significant amount of the sample during sliding. Consequently, a report by Vandenkerhove in Du, et al. [101] highlighted that nickel-titanium alloys containing mainly NiTi phase showed a lower corrosion intensity.

Figure 8.12 shows the EDS result obtained from line-scan and point-scan x-rays carried out to determine the level of damage or penetration caused by the oxide layer. While the line scan identified elements such as oxygen, sodium, titanium and nickel, the point-and-shoot scan presents elements like oxygen, aluminium, titanium and nickel. The different coloured lines denote the concentration of the elements; thus, the yellow and blue lines highlight the higher concentration of the parent elements Ni and Ti. The green, red, and orange lines show traces of O_2, Na and Al within the region scanned, i.e., the oxidised location. The point scan further confirmed the identified elements by line scan and their corresponding wt.%, shown in the accompanying table in Figure 8.12.

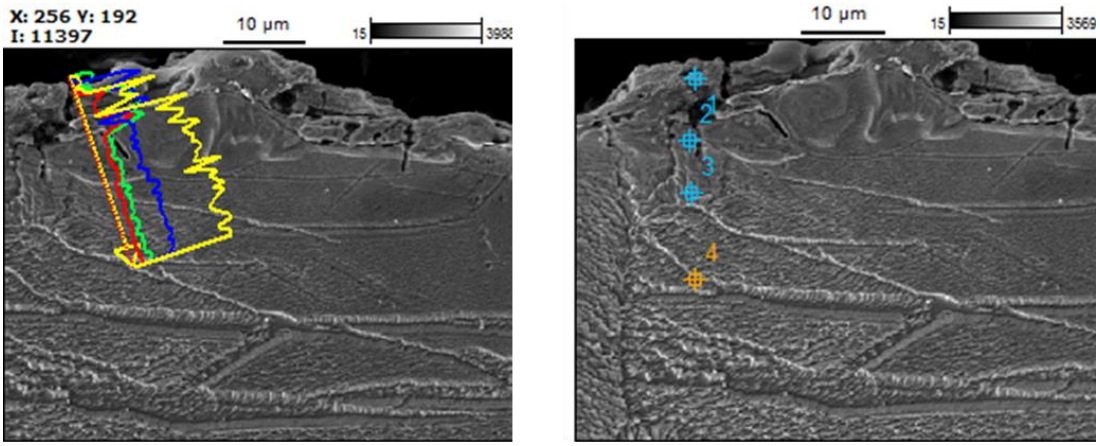

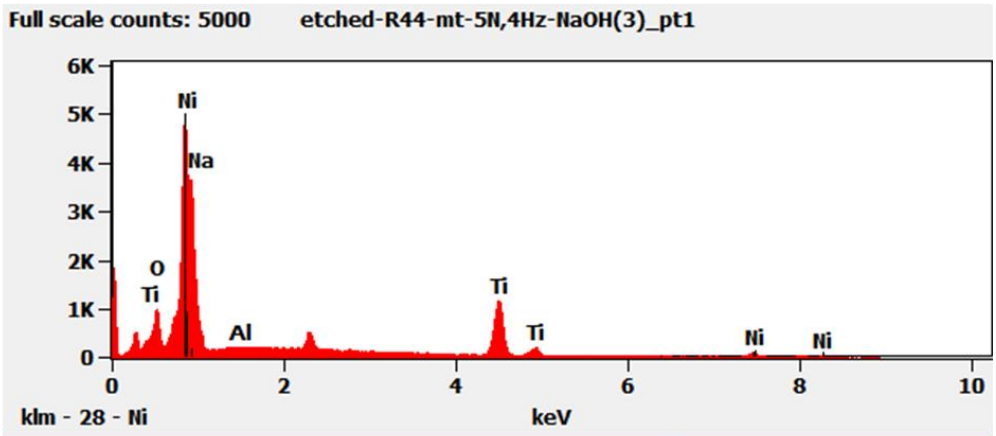

	O	Na	Al	Ti	Ni
etched-R44-mt-5N,4Hz-NaOH(3)_pt1	7.99	0.00	0.06	33.21	58.74
etched-R44-mt-5N,4Hz-NaOH(3)_pt2	3.97			40.00	56.03
etched-R44-mt-5N,4Hz-NaOH(3)_pt3				40.61	59.39
etched-R44-mt-5N,4Hz-NaOH(3)_pt4				46.56	53.44

Fig. 8.12: SEM-EDS analyses using line and point scans x-ray for etched sample.

From the table, the percentage of Al debris only appeared on the top surface and within the oxide layer region. The oxide film exits only at points 1 and 2, as shown by the point-and-shoot scan, whereas the parent material Ni and Ti are recorded at the 4 different points investigated. This supports the explanation in Figure 8.10 that the propagation of cracks and crevices does not penetrate beyond 120 µm of the material surface (particularly the oxide layer region). The change in Ni-Ti wt.% composition recorded at point 4 could be attributed to the grain elongation around the spot.

8.2.4. Summary

This study investigated the behaviour and the effects of sliding wear and electrochemical potential of NiTiNOL60 alloy in an alkaline environment (0.05M NaOH (aq)) under varied normal loads sliding against Al_2O_3 counter-body on a ball-on-plate tribometer configuration. In the sample characterisation, SEM imaging and EDS analysis authenticated the composition of the NiTiNOL60 sample, confirming it as a non-

equiatomic material with a weight percentage composition of 60% Ni and 40% Ti. The material exhibited a cubic crystal structure matrix, with consolidated and unconsolidated regions in its microstructural grains, suggesting the possibility of Ni-rich or Ti-rich zones. From the study, it is evident that an increase in load results in accelerated corrosion. The results reveal a distortion of the microstructure grains due to sliding action and the wear mechanisms on the tribological wear track. Further, an increase in applied load leads to the deterioration of oxide film formed along the wear track due to the higher relative motion between the contact surfaces, and this significantly increases the wear rate of the material under higher loading conditions. This results in a cathodic shift in the potentiodynamic measurements and a higher resistance, leading to a lower corrosion rate. The results from surface examinations presented various wear mechanisms, including abrasion, adhesion, fatigue and oxidative wear, as seen along the wear track. However, the mechanisms of abrasive wear, which involves cutting, fracture, fatigue and grain pull-out, were predominant, especially at higher normal loads.

CHAPTER 9: TRIBOCORROSION TESTING IN THE THREE CORROSIVE MEDIUMS

9.1. Preface

With the goal of better understand the underlying mechanisms of NiTiNOL60 alloy, the electrochemical contribution to tribocorrosion, and/or wear-accelerated corrosion, this chapter compares the performance of the material explored in the three corrosive mediums. The findings have been published in the Journal of Materials Engineering and Performance https://doi.org/10.1007/s11665-024-09646-6 with the following highlights.

Highlights:

- Wear-accelerated corrosion & sliding wear interactions influence 60NiTi degradation.
- pH plays a pivotal role in tribocorrosion processes, shaping material wear patterns.
- Alkaline environments lead to oxide layer depassivation-triggered oxidational wear.
- Acidic medium accelerated mild wear involving abrasion and delamination.
- Increased applied load causes more corrosive wear, especially in saline conditions.

Graphical abstract

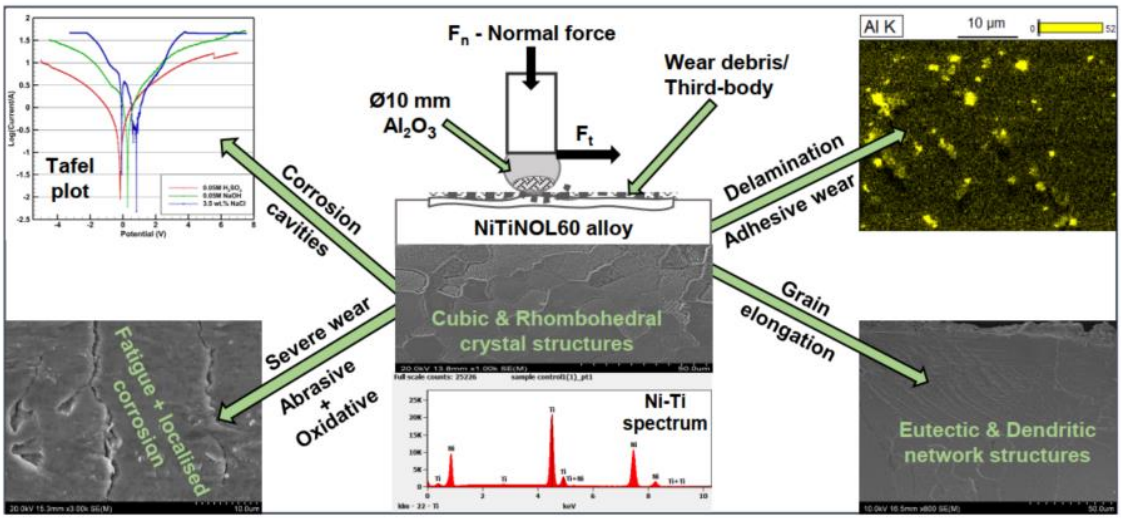

Graphical abstract showing the tribocorrosion interface for NiTiNOL60 alloy.

9.2. Comparative study of the tribocorrosion performance of NiTiNOL60 in acidic, alkaline and saline environments

9.2.1. Overview

Nickel-titanium (Ni-Ti) based alloys are being increasingly explored for use in a range of industries [39] and have, thus, garnered considerable scientific attention due to their unique shape memory and mechanical properties. This study concentrates on NiTiNOL60, also referred to as 60NiTi, which is composed of 60 wt.% Ni and 40 wt.% Ti. NiTiNOL60 possesses unique properties such as high specific strength, low density, biocompatibility, superelasticity, machinability, and good corrosion resistance, which make it suitable for a wide range of applications in marine, aerospace, biomedical, and food processing industries [101, 173]. It is an ordered intermetallic material compound consisting of a B2, cubic crystal structure matrix with one or more secondary phases, which includes the metastable NiTi and Ni_3Ti_2 phases and the equilibrium Ni_3Ti phase, also referred to as the globular Ni_3Ti precipitates. The binary NiTiNOL60 alloy has been shown to achieve the highest hardness among the binary compounds after heat treatment at 1050 ^oC [40]. According to Xu, et al. [204], the high hardness is caused by precipitation hardening through the rapid formation of nanoscale Ni_4Ti_3 precipitates upon cooling from a solution-annealed condition. As shown in Figure 1, the Ni_4Ti_3 precipitates form inside narrow B2 NiTi channels and cause an Orowan strengthening mechanism [39, 40]. These properties are due to the intrinsic thermoelastic martensite transformation under thermal and mechanical loading conditions at different temperatures [275]. At relatively low temperatures and under external force, the initial parent phase (austenite) transforms into a martensite phase accompanied by macroscopic deformation [87].

Several researchers have investigated the properties of this alloy to better understand the desired approach to enhancing the durability and efficiency of the systems in which it is employed. While Yan, et al. [166] studied the microstructure and tribocorrosion performance of NiTiNOL60 alloy in artificial seawater, Kosec, et al. [45] investigated the effects of different microstructures on tribocorrosion behaviour of NiTi alloy in simulated saliva. In their findings, B2 TiNi and stable $TiNi_3$ phases were identified for the as-cast NiTiNOL60 sample, but solution treatment could lead to the precipitation of metastable Ti_3Ni_4 phase in the matrix without dissolving the $TiNi_3$ phase completely. This confirms the Orowan strengthening mechanism [36] as described in Figure 2.1.

For space bearing applications, DellaCorte [138] and Pepper, et al. [24] investigated the superelastic behaviour of NiTiNOL60 alloy. According to DellaCorte [25], 60NiTi is highly elastic, unaffected by rust, combines high hardness, reduced stiffness and

superelasticity, and has a higher load-carrying capacity than steel. However, NiTiNOL60 and many other metals under certain mechanical loading and harsh corrosive conditions deteriorate, which warrants the evaluation of their wear performance [80]. Accordingly, special attention has been paid to remedy the tribological contact using thick barrier coatings and other surface treatments, yet metal/alloy failures prevail. NiTiNOL60 alloy is tribochemically benign in the presence of liquid lubricants, compared to conventional alloys with large concentrations of titanium that proved to be chemically aggressive and cause degradation of many lubricants [138, 276]. Khanlari, et al. [253] investigated the unlubricated sliding wear performance of 60NiTi compared to 440C steel. Their study revealed that 440C steel exhibits more microscopic plasticity than 60NiTi, which hindered the propagation of generated tensile microcracks. Furthermore, Zeng and Dong [181] studied the surface roughness behaviours of the alloy under oil lubrication, and their findings showed a remarkable lubrication performance with an ultra-low coefficient of friction of about 0.008 maintained under castor oil lubrication [171, 182].

Pertaining to reports in the literature that mechanical loading and extreme corrosive conditions increase surface deterioration, this study focuses on a thorough investigation of the tribocorrosion performance of NiTiNOL60 at different corrosive mediums. While Kosec, et al. [45] have categorised the NiTi research conducted so far into the following fields: basic corrosion and electrochemical studies, mechanical and material property studies, and surface treatment studies, the comparative study of the tribocorrosion behaviour of NiTiNOL60 in different chemical environments has remained unexplored.

It is known that corrosion is accelerated when combined with mechanical wear [45]. Tribocorrosion is an irreversible material transformation (surface damage) occurring from the simultaneous action of wear and corrosion due to relatively moving mechanical contact and electrochemical reactions [7, 9, 42]. Wang, et al. [256] studied the tribocorrosion behaviour of titanium alloys in simulated body fluids, and their findings demonstrated that the applied load and concentration of wear particles had important effects on tribocorrosion behaviour. Despite the reported high resistance to wear exhibited by NiTi alloy, an investigation by Guadalupe, et al. [42] compared the tribological behaviour of NiTi alloy to conventional engineering materials such as steels [170], Ni-based [58], and stellite [259, 277] alloys and reported that the wear resistance of conventional tribo-materials strongly depends on their mechanical properties such as hardness, toughness, and work-hardening. In addition, a study by Muñoz and Espallargas [165] highlighted that mechanical parameters strongly influence the electrochemical material removal rate, and, on the other hand, the mechanical material removal rate depends on the prevailing electrochemical conditions. For electrochemical

investigation, it is established that the techniques employed in tribocorrosion rely on the contact geometries of the samples [155]. In the case of a linear reciprocating ball-on-plate configuration, suitable methods include open circuit potential (OCP), potentiodynamic polarisation (PD), potentiostatic polarisation (PS), and electrochemical impedance spectroscopy (EIS) [189]. During an electrochemical reaction, the metal undergoes oxidation by the oxidising agent. Several factors influence the corrosion process, such as the metal's position in the electrochemical series, pH, presence of electrolytes, impurities in the metal, concentration of oxygen, and temperature differences [6]. The material exhibits different electrochemical responses depending on its state: immune state (no corrosion), active state (corrosion resulting in metal loss or dissolution of one of the constituents of the corrosive environment into the metal), and passive state (the metal forms a protective oxide passive film on its surface, reducing the corrosion rate). Metals with low corrosion potentials experience anodic polarisation, leading to an increasing anodic dissolution rate. On the other hand, metals with high corrosion potentials undergo cathodic polarisation, which slows down the dissolution rate [150].

Given the varied behaviours of the material under different environments, it is crucial to thoroughly examine and compare the tribocorrosion phenomena and electrochemical interactions of NiTiNOL60 alloy in different corrosive mediums across a wide pH range. By exploring these aspects, this study aims to provide valuable insights into the tribocorrosion behaviour of NiTiNOL60, facilitating the development of effective strategies to enhance durability and efficiency in applications where this alloy is employed.

9.2.2. Materials and Methods

The experimental procedures presented in Chapter 3 of this thesis were employed for the material preparation, characterisation and tribocorrosion investigations in the three aqueous solutions where NiTiNOL60 alloy samples were fully immersed.

9.2.3. Results and Discussions

Following the synergistic approach and the induced transformations caused by reciprocating sliding, it was necessary to investigate the subsurface of the specimen. After the sliding wear test in a corrosive medium, the specimen was cut through the wear track using wire cutting to obtain a cross sectional part of the specimen that was mounted using phenolic hot mounting resin. The schematic representation of the mounted sample and the sample geometries before and after tribocorrosion are shown in Figure 9.1.

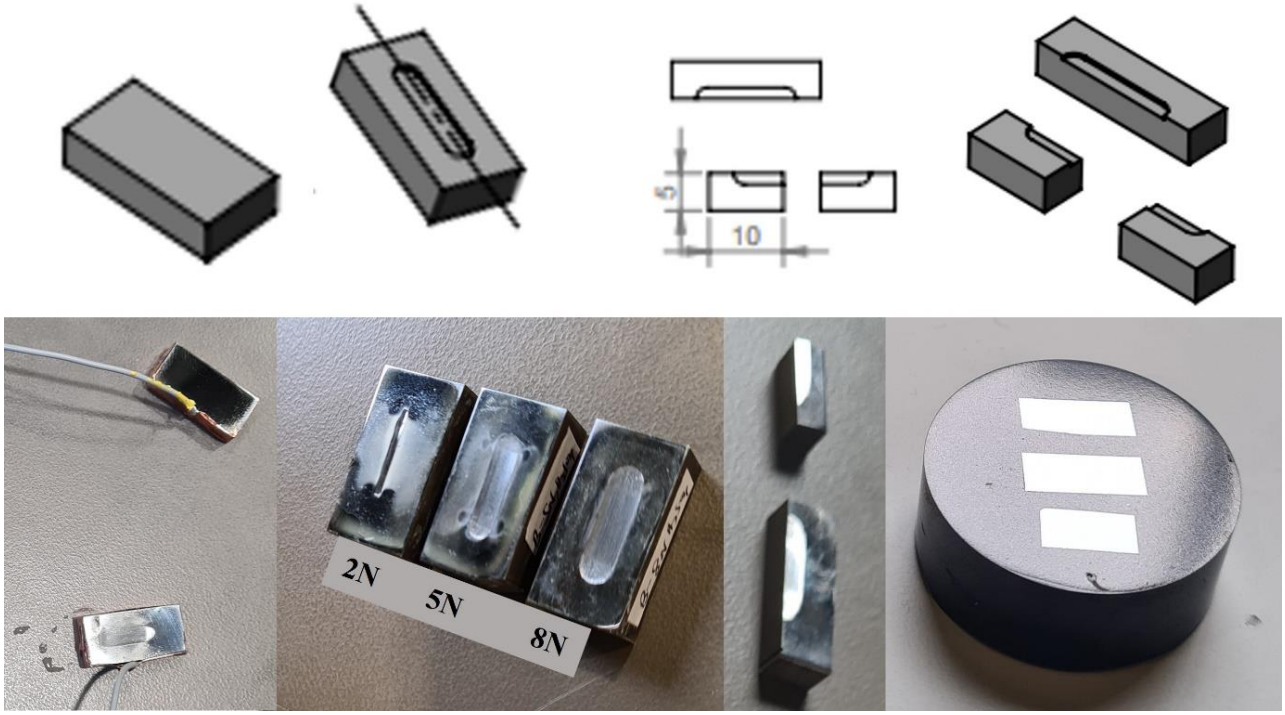

Fig. 9.1: Schematic representation of the sample's geometry and cross-section along the wear track.

Since the tribological contacts involve the simultaneous wear and corrosion processes, leading to irreversible material transformations [167, 262]. Various factors influence the rate of wear and corrosion, and their synergistic interactions need to be analysed to understand the contribution of each process to material removal [1]. Therefore, it is essential to critically examine the wear track using techniques such as optical microscopy, scanning electron microscopy (SEM), and energy dispersive X-ray spectroscopy (EDS) to assess surface topography and subsurface microstructures. Thus, the polished samples with mirror surface finishes were examined using scanning electron microscopy (SEM) and energy dispersive spectroscopy (EDS) for a full scan at 20 KV penetrating voltage. This ensures that the X-rays comprehensively analyse the sample's surface and subsurface. Figure 9.2 shows the NiTiNOL60 alloy's micrograph and the elemental quantitative compositions obtained from SEM/ EDS examination. From the results, it is evident that the alloy investigated has a quantitative elemental distribution of 60 wt.% Ni and 40 wt.% Ti, which is consistent with the observations in the literature [40, 210].

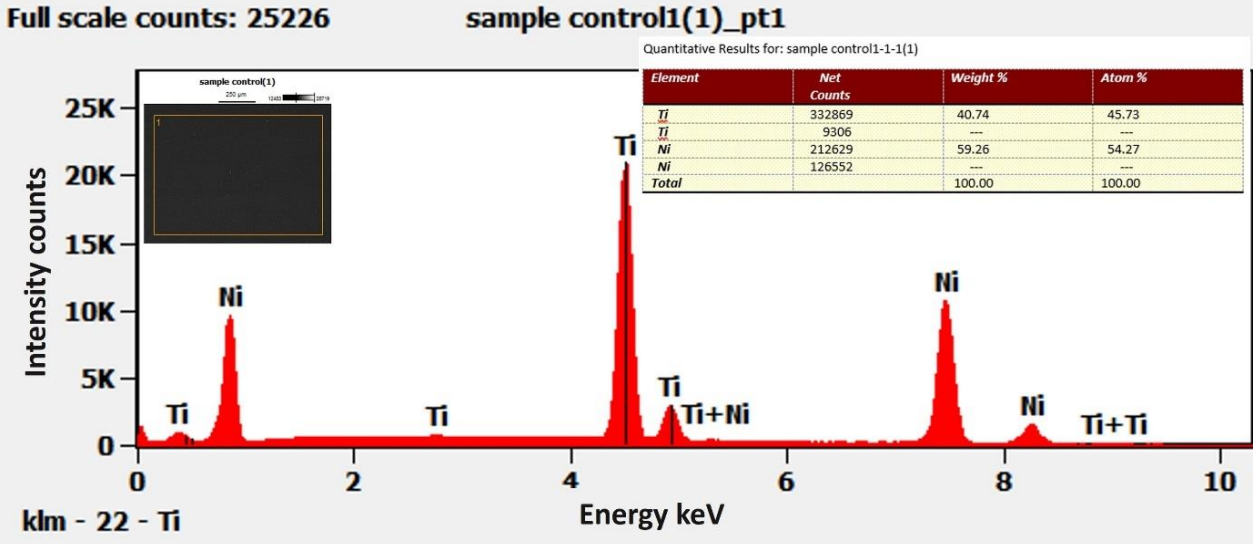

Fig. 9.2: Surface characterisation of polished NiTiNOL60 sample.

Further examination with the optical microscope presents the micrographs in Figure 9.3. The images reveal that the sample is an ordered intermetallic compound of a cubic crystal matrix structure. This confirms the observations in the literature by previous researchers [47, 252]. The micrographs show clear grain boundaries with cluster particles of the microstructural grains in the consolidated and unconsolidated regions. The regions confirm the composition of the sample, indicating a dominance of the B2 NiTi matrix and Ni_4Ti_3 phases, which could be referred to as cubic and rhombohedral crystal structures [249, 252].

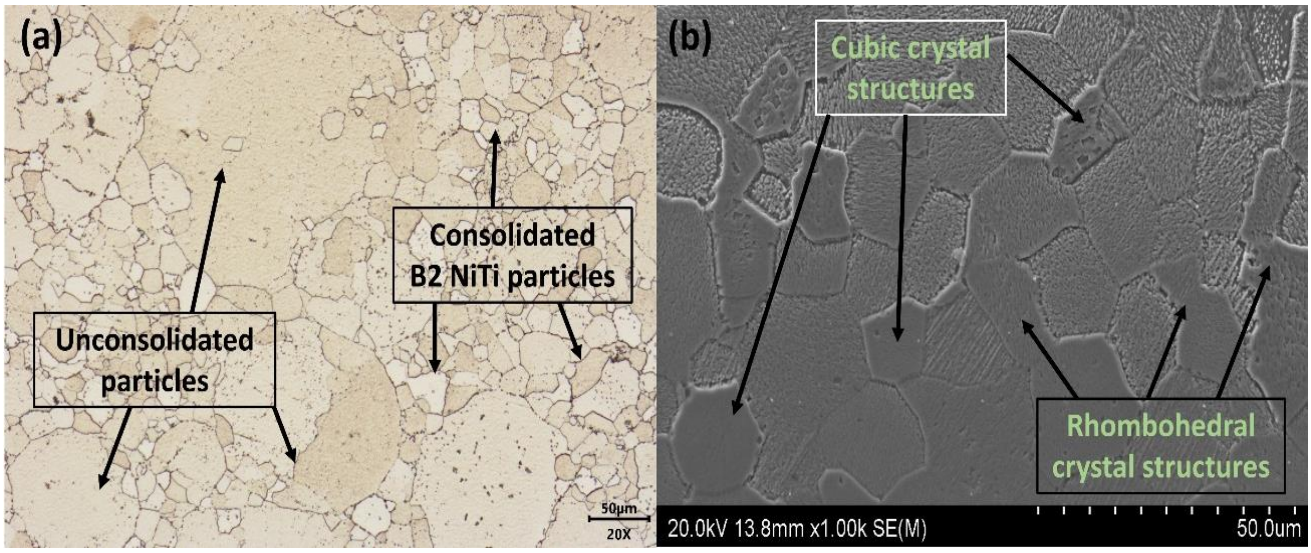

Fig. 9. 3: Microstructure of NiTiNOL60 (a) polished and (b) etched surfaces before tribocorrosion test.

The hardness of the NiTiNOL60 sample was measured before and after tribocorrosion tests in different electrolytes. From the measurements, an average value of the Rockwell

hardness of 62.5 HRC was recorded for the plain/ unused sample, which agrees with existing literature information [170]. Whereas the microhardness measurements of the same sample recorded an average value of Hv 537.77/1.0kgf/10s. Microhardness tests were carried out along the wear tracks of the samples subjected to tribocorrosion tests, while the Rockwell hardness tester was used to measure the macro indentation hardness as specified in Section 9.2.2. For each specimen, the average hardness was obtained by performing five tests on different parts of the surface and the resulting values are shown in Table 9.1. The results show that the overall hardness of the sample increased after tribocorrosion and this is an indication that the continuous sliding actions led to damages on both the surface and crystal structures. Strain hardening of solid crystals involves a modification of the structure due to plastic deformation, which creates dislocation and increases strength at the induced surface. Our analysis confirmed that the sample immersed in the saline solution gained the highest hardness with a value of 67 HRC, which showed that salt has the chemical effect of decomposing the elements. In contrast, the sample in the acidic environment has the least value 63.3 HRC, which is slightly higher than the original value of the plain sample. The increased hardness recorded for the specimens exposed to the three corrosive environments could be attributed to different factors, including work-hardening during the reciprocating sliding, oxide layer formation and debris adhesion along the wear tracks. The strain hardening resulting from compression during the reciprocating sliding significantly altered the microstructure of the specimen. This is evident in SEM micrographs revealing the surface and subsurface damages due to plastic deformation. This aligns with the literature information that presents that plastic deformation increases the dislocation density in the crystal structures [46, 278]. In another study, Bounezour, et al. [46] highlighted that work hardening promotes surface hardness (Hv) and high tendencies of increased brittleness, as cracks on the SEM images show.

Table 9.1: Micro- and macro-hardness of NiTiNOL60 samples after tribocorrosion tests.

Test condition	**Electrolyte**		
	NaCl	NaOH	H_2SO_4
2N,4Hz	Hv 549.63	Hv 538.30	Hv 537.93
5N,4Hz	Hv 575.23	Hv 556.68	Hv 547.77
8N,4Hz	Hv 597.45	Hv 593.53	Hv 578.95
Average Vicker's hardness (Hv) outside the wear track	Hv 538.44	Hv 537.71	Hv 537.83
Average Rockwell hardness (HRC) on the wear track	HRC 67.00	HRC 64.38	HRC 63.30

Figure 9.4 presents the evolution of the friction coefficient during sliding. The initial sliding stage is characterised by frictional interactions that result in localised heating and oxidation of asperities, leading to oxidational wear [148]. It is well-established that surface roughness plays a crucial role in frictional behaviour, manifesting in various forms during the sliding contact. The plotted data clearly indicate that the coefficient of friction (CoF) increases with higher applied loads across the three different mediums investigated. Consequently, the increased load induces more significant wear and activates distinct wear mechanisms along the wear track, as will be confirmed by the subsequent SEM images. Notably, the CoF values at higher loads of 5N and 8N demonstrate that elevated contact pressures intensify wear surface roughness and broaden the wear track compared to the lower applied load of 2N (Figure 9.12d). The CoF plot for the 2N load exhibits a running-in period of approximately 500 s for the sample tested in the saline and alkaline environments. In contrast, the sample tested in the acidic environments recorded a longer running-in time, following consistent wear of the material's surface. This suggests that the applied load of 2N was insufficient to penetrate and remove the passive layer through wear. The plots for the 2N load show less noise during sliding, confirming little or no adhesion and less interference from the wear debris. However, as the counter material continuously slides against the NiTiNOL60 surface, the passive oxide layer gradually wears off, allowing penetration into the sample surface. After the running-in period, the CoF increases and reaches a relatively stable friction coefficient, primarily attributed to the general oxidation of the sliding surfaces. Conversely, at higher loads, the running-in period is negligible, indicating that the contact pressure from the applied load is adequate to break down the passive layer through the reciprocating sliding action of the alumina ball [181]. This process induces surface roughness and triggers various wear mechanisms until the system reaches a relatively steady state characterised by a high CoF. Unlike in the other environments, the CoF trend recorded for higher loads in the H_2SO_4 environment shows a continual decline. This suggests less adhesion and relatively little or no impact from the third-body abrasion as sliding progressed.

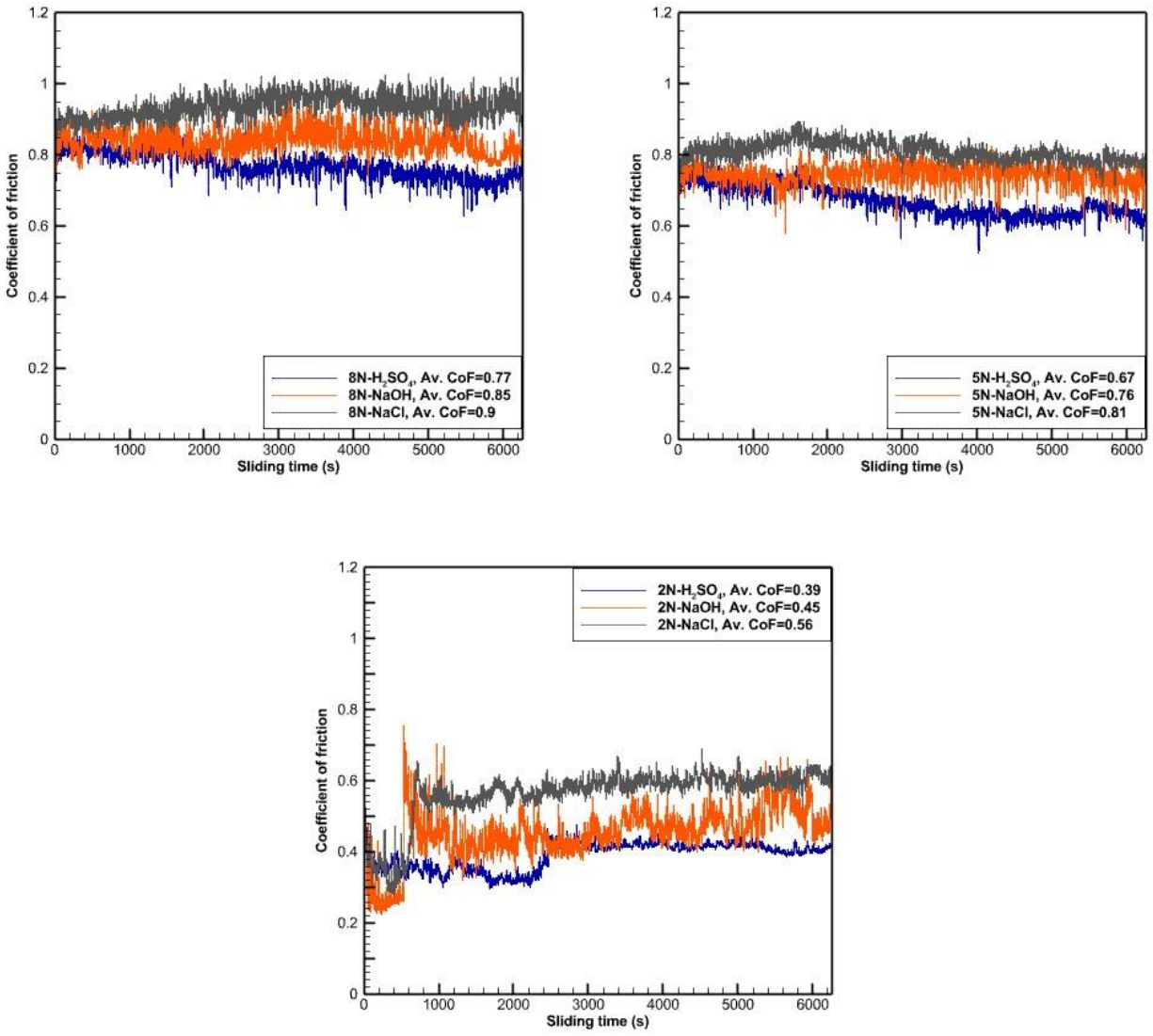

Fig. 9.4: Friction coefficient plots at 2N, 5N and 8N in H_2SO_4, NaOH and NaCl mediums.

To better understand the tribocorrosion behaviour of NiTiNOL60 under different applied loads and electrochemical conditions, a detailed examination of the wear track was performed. The SEM analysis revealed the occurrence of various wear mechanisms on the NiTiNOL60 surface, including abrasion, adhesion, delamination, ploughing, pitting (nucleation and metastable), crevices, and cracks perpendicular to the sliding direction, as depicted in Figure 9.5. During sliding, adhesive wear was observed due to micro-joint formation between the Al_2O_3 ball and the polished NiTiNOL60 surface [147]. Furthermore, surface fatigue was evident at the 8N load, particularly in the saline environment, which could be attributed to cyclic loading induced by reciprocating sliding. Abrasive wear occurred as ploughing or cracking at the interface between the counter material and the NiTiNOL60 surface, with severity varying based on the applied load and

corresponding contact pressure. The wear behaviour exhibited under different regimes suggests that corrosion-induced wear is typically accelerated by oxidation in a corrosive environment, with the extent influenced by the pH of the system. While pitting corrosion may seem less significant, its depth and propagation rate can lead to rapid metal dissolution if the active state persists for an extended duration [151]. The synergistic effects of tribocorrosion revealed that material deformation occurs in various forms depending on the environmental conditions. In alkaline and saline environments with higher pH ranges, oxidational wear leads to mild to severe surface damage, potentially resulting in plastic deformation. In contrast, acidic environments promote abrasion, delamination, and adhesion, resulting in milder wear. The SEM images, particularly under the 8N load, demonstrate that the applied load or contact pressure generates a larger wear track and increased surface roughness, consequently influencing deformation and friction by enhancing asperity deformation. In contrast, lower surface roughness favours adhesive friction. Comparatively, non-unidirectional abrasive wear grooves resulting from third-body wear are more prevalent in the NaOH environment, while the NaCl environment exhibits the highest wear volume among the three investigated environments due to the combined effects of mechanical and chemical wear. This finding confirms the significant role of solution anions, including halide and non-halide ions, in the growth and breakdown of the passive film in aqueous solutions [151]. The NiTiNOL60 samples exposed to the H_2SO_4 environment exhibited the least wear volume from mechanical wear. The wear debris from the alumina ball was observed to be relatively soluble in the electrolyte solution. The elemental quantification using energy-dispersive X-ray spectroscopy (EDS) further supported the dissolution of alumina particles, with fewer traces of Al debris detected along the wear track in the acidic medium compared to the debris accumulation and adhesion observed in the NaOH and NaCl environments. Additionally, as shown in Figure 9.4, the CoF curves for H_2SO_4 at 5N and 8N loads gradually decreased as the sliding progressed. This drop could be attributed to the dissolution of alumina wear debris and general oxidation of the interfacial surfaces.

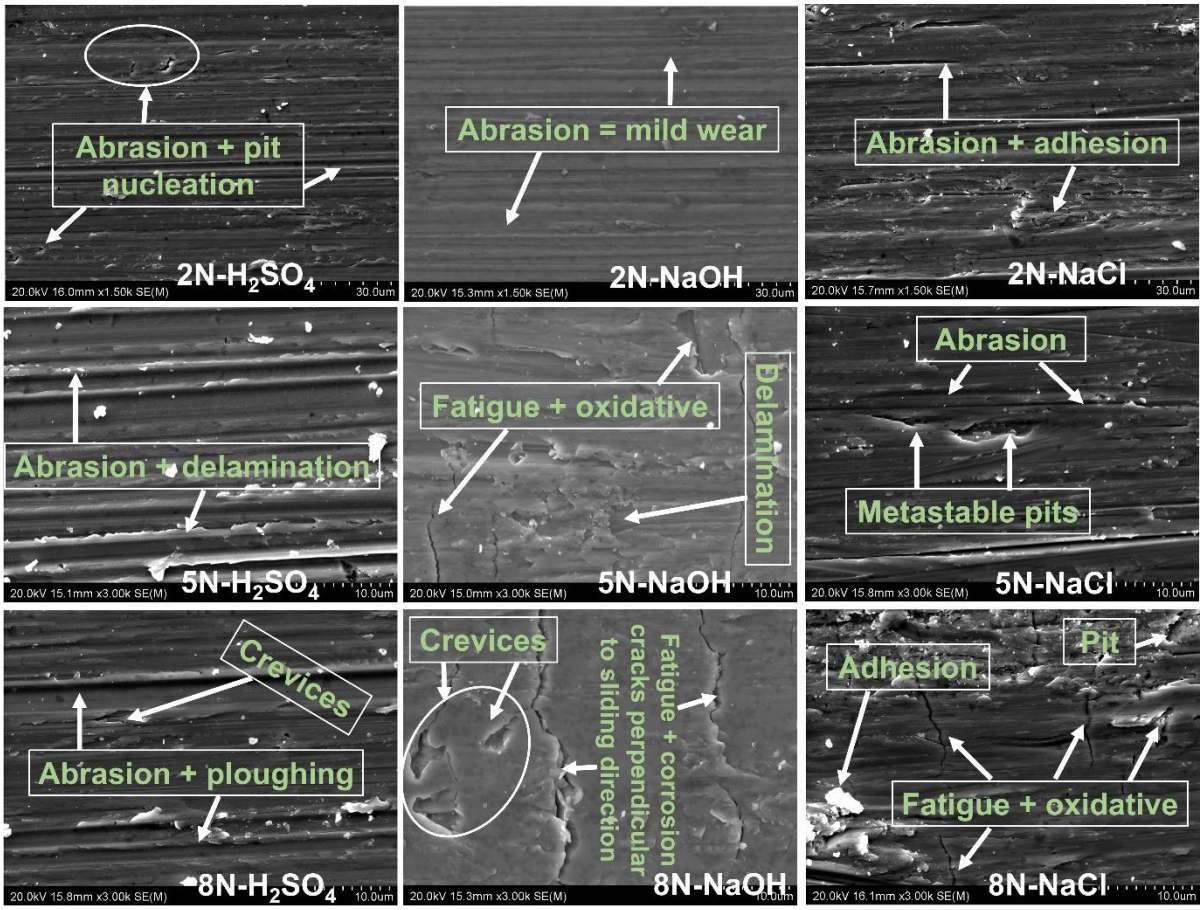

Fig. 9.5: SEM micrographs showing sliding wear effect and worn surfaces after tribocorrosion in three electrolyte environments.

As stated above, further sliding produces more fragments, which promotes adhesion [257]; on that note, our EDS examination of the wear tracks revealed the elemental compositions of the examined surfaces. The results presented in Figure 9.6 confirmed that the wear track surfaces were oxidised during tribocorrosion. The spectrum highlights the level of concentrations of each identified element. The higher the peak in a spectrum, the more concentrated the element in the specimen. The results show a high concentration of the NiTiNOL60 base material (Ni and Ti) followed by aluminium and oxygen concentrations resulting from the adhesion of the counter material debris and surface oxidation. While an area scan shows that the sample exposed to NaOH recorded a distributed oxidised composition and the highest amount of Al debris, which contributed to the third-body wear abrasion [214], as seen in the SEM images. The sample exposed to the acidic medium recorded the least distribution of Al_2O_3 debris when compared with the samples exposed to other corrosive environments. This supports the unidirectional wear groves shown in the SEM images in Figure 9.5, with less impact from the third body effect [214], which eventually resulted in the lowest wear volumes recorded at different test conditions except for the 2N load. In support of the quantitative elemental

distribution, the EDS spectrum shows that Al has the lowest peak, thereby confirming a lower concentration of alumina debris in the acidic environment. According to the data for elemental distribution, the sample tested in a NaOH environment had the maximum oxygen concentration at 8N load with 23.93 %, followed by the saline environment at 13.66 % and the acidic environment at 9.02 %. This finding for the NaOH medium could also be supported by the high oxidation level in Figure 9.5, showing different corrosion attacks for the SEM image of 8N NaOH. In the saline environment, the 13.66 % oxygen concentration is believed to significantly support the halide ions (Cl^-) in contributing to the overall corrosion rate for the NaCl environment.

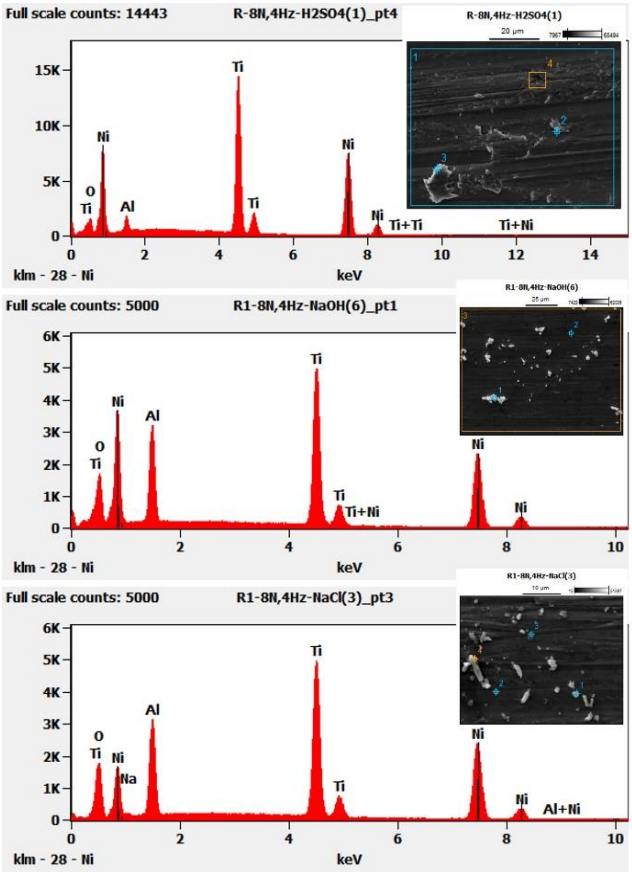

Weight %

	O	Al	Ti	Ni
R-8N,4Hz-H2SO4(1)_pt1	9.02	0.99	34.81	55.18
R-8N,4Hz-H2SO4(1)_pt2		0.10	40.31	59.60
R-8N,4Hz-H2SO4(1)_pt3		0.63	40.09	59.27
R-8N,4Hz-H2SO4(1)_pt4	8.27	2.82	36.81	52.10

Weight %

	O	Al	Ti	Ni
R1-8N,4Hz-NaOH(6)_pt1	23.93	12.54	27.81	35.73
R1-8N,4Hz-NaOH(6)_pt2			41.40	58.60
R1-8N,4Hz-NaOH(6)_pt3	0.85	0.80	40.48	57.87

Weight %

	O	Na	Al	Ti	Ni
R1-8N,4Hz-NaCl(3)_pt1	13.66	2.84	5.11	32.02	46.37
R1-8N,4Hz-NaCl(3)_pt2				41.47	58.53
R1-8N,4Hz-NaCl(3)_pt3	28.55	1.12	12.43	24.74	33.16
R1-8N,4Hz-NaCl(3)_pt4	14.02	3.92	4.72	31.98	45.36

Fig. 9.6: EDS analysis of the wear tracks of the NiTiNOL60 samples tested in three electrolytes under 8N load.

Following the wear mechanisms at the sliding interfaces and the high level of Al debris adhesion observed on the sample surfaces in Figure 9.6, we further examined the surfaces of the counter body (alumina ball) sliding against the NiTiNOL60 specimens after tribocorrosion. Figure 9.7 presents the EDS analysis of the examined Al_2O_3 ball surfaces used for reciprocating sliding in the three different environments. The results confirm an adhesion mechanism on the counter body surface having NiTiNOL60 debris distributed at different compositions. From the results, point 1 gives the quantitative

elemental distribution of an area/ overall scan showing the base material of the ball (Al and O) as well as the composition of the specimen (Ni and Ti). Analyses of the results show that the sample exposed to an acidic medium recorded the least percentage of Ni-Ti adhesion; however, the sample immersed in the saline environment has the highest amount of Ni-Ti debris adhesion onto the ball surface which conforms to the highest wear volume and CoF recorded for the different applied loads in NaCl environment. It also supports the adhesion mechanism highlighted in Figure 9.5 for the NaCl environment. Additionally, the similar concentrations of oxygen presented in the quantitative results for the examined surfaces in the three corrosive environments also confirm the oxidative wear mechanism at both contact surfaces.

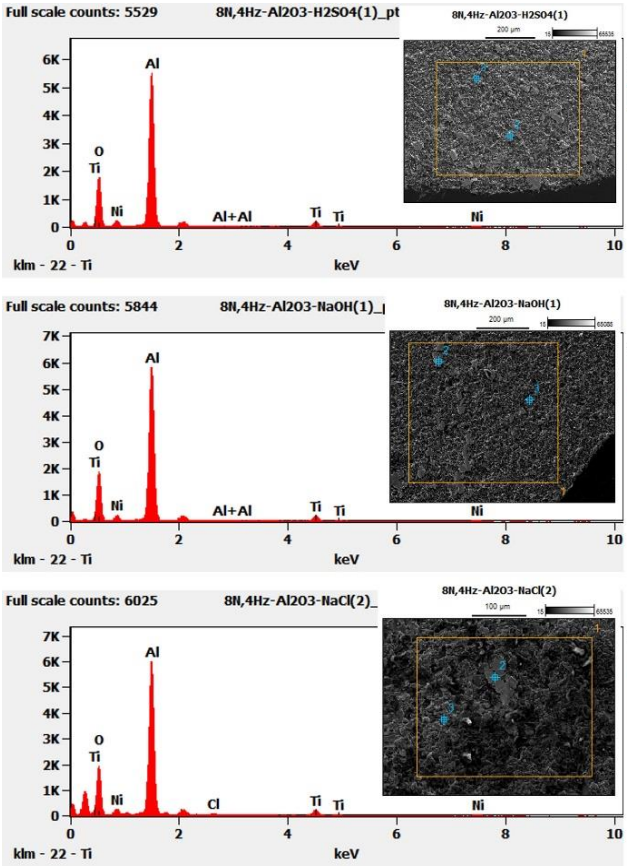

Weight %

	O	Al	Ti	Ni
8N,4Hz-Al2O3-H2SO4(1)_pt1	43.47	43.96	4.79	7.78
8N,4Hz-Al2O3-H2SO4(1)_pt2	17.90	7.24	31.05	43.81
8N,4Hz-Al2O3-H2SO4(1)_pt3	54.19	45.81		

Weight %

	O	Al	Ti	Ni
8N,4Hz-Al2O3-NaOH(1)_pt1	43.22	43.01	4.93	8.84
8N,4Hz-Al2O3-NaOH(1)_pt2	1.71	1.40	39.14	57.74
8N,4Hz-Al2O3-NaOH(1)_pt3	51.71	48.29		

Weight %

	O	Al	Cl	Ti	Ni
8N,4Hz-Al2O3-NaCl(1)_pt1	42.08	42.76	0.88	5.08	9.20
8N,4Hz-Al2O3-NaCl(1)_pt2	4.74			38.40	56.86
8N,4Hz-Al2O3-NaCl(1)_pt3	35.90	57.19		2.54	4.37

Fig. 9.7: EDS analysis of the contact surface of the Al_2O_3 balls tested against NiTiNOL60 in three electrolytes under 8N load.

Considering the electrochemical reactions occurring on the material's surface during tribocorrosion, the activities involve anodic oxidation (removal of electrons from metal atoms) and cathodic reduction (consumption of electrons by the oxidising agent). These reactions are elucidated by analysing the cathodic and anodic regions of the Tafel plots in Figure 9.8 and used to estimate the potentiodynamic polarisation parameters presented in Table 9.2. The Tafel plot illustrates the occurrence of corrosion in both the

anodic and cathodic regions, revealing the sample's susceptibility to pitting within the saline environment. In contrast, corrosion was primarily observed in the cathodic region in the acidic and alkaline environments. It reveals that localised corrosion initiated and progressed in both anodic and cathodic regions after reaching equilibrium for lower loads (2N), where the contact pressure is insufficient to wear away the passive layer. This indicates that the sample surfaces experience anodic polarisation at lower loads with an increased dissolution rate in that region due to their low corrosion potential. Conversely, for higher applied loads (8N), the material surfaces undergo cathodic polarisation at a higher corrosion potential, which slows down the dissolution rate. Accordingly, this leads to an increased corrosion rate, higher wear volume due to corrosion and severe pitting corrosion in saline medium, as presented in Figure 9.8.

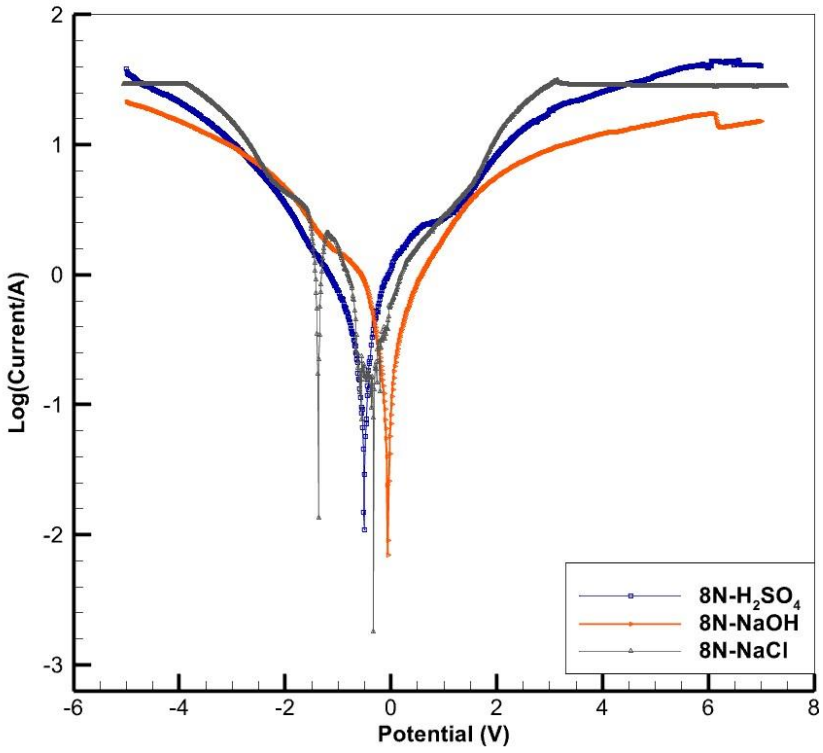

Fig. 9.8: Potentiodynamic polarisation curves showing corrosion behaviour of NiTiNOL60 alloy.

The summarised potentiodynamic polarisation parameters estimated from the Tafel plots are provided in Table 9.2, offering an overview of the electrochemical behaviour during the tribocorrosion testing. From the tabulated results, it is evident that an increase in the applied load decreases the polarisation resistance (R_p). This increases the corrosion current (I_{corr}) and shifts the corrosion potential (E_{corr}) towards the passive direction (i.e., towards zero or to more positive values). The parameters deduced for the sample investigated in the saline environment recorded the highest corrosion rate, the highest

corrosion current density, and the lowest polarisation resistance when compared with the samples tested in the acid and alkaline environments. Equally, the parameters obtained for the sample tested in the acidic medium presented the highest values of polarisation resistance; this invariably results in the lowest corrosion rates for the different applied loads. Whereas the alkaline environment depicted the least values for the corrosion current density and corrosion potential at different loads, the polarisation resistance was higher compared to the values obtained in the 3.5 wt. % NaCl environment. Overall, the results agree with the previous reports stating that the I_{corr} value denotes a lower corrosion rate [279].

Table 9.2: Tafel fitting parameters of NiTiNOL60 at different normal loads and 4 Hz sliding frequency.

Electrolyte	Applied Load (N)	E_{corr} (V)	$I_{corr} \times 10^{-3}$ (A)	R_p (Ω)	Corrosion Rate (mmpy)
H_2SO_4	2	-1.814	1.225	985.30	1.183
	5	-1.257	2.301	570.50	1.651
	8	-0.507	2.565	352.40	2.077
NaOH	2	-1.736	1.104	812.50	0.868
	5	-1.440	2.277	487.10	1.786
	8	-0.273	2.810	294.90	2.208
NaCl	2	-2.105	4.784	744.70	1.346
	5	-1.594	5.473	357.40	2.194
	8	-1.356	6.588	146.90	2.851

Notably, halide ions, such as chlorine (Cl^-), contribute to severe localised corrosion, including pitting and cracks observed in the saline environment. The different stages of localised corrosion reported can be seen in the SEM images shown in Figures 9.9 and 9.10. While Figure 9.9 shows pit nucleation and its propagation, as well as the advancement of corrosion crevices. Figure 9.10 (a, b) shows the pit formation and microcrack propagation in a sliding direction in the NaOH environment before and after etching. Etching of the sample clearly highlights a stable pitting, where the pit and crack propagated beyond the surface of the sample down to about 120 µm, unlike in the other environments where the localised corrosion (pitting) only maintained the nucleation and metastable stages. The continuous reciprocating sliding along the wear track and in the localised corrosion regime induced fatigue wear and promoted stress corrosion. The stress corrosion, which was aggravated by the combined influence of compressive

stresses, increased the dislocation density in the crystal structures. Hence, the increased pitting and crevices as well as the elongated at both minimum and maximum contact pressures. Conversely, the severe corrosion leading to stress corrosion results from the relative motion of a corrosive fluid on the material surface. Pitting, the conventional corrosion form, exists in different stages even though pitting is self-initiating and self-propagating, making it difficult to determine the borders for every stage, including the nucleation, metastable pit formation and stable pitting [151]. Corrosion is typically initiated at defects in the protective oxide film or at the break of the passive film and progresses by forming a dense tubercle of hard rust or scale, with pits present in the underlying metal [151]. According to Ghali [151], the propagation emanating from the pits could result in fatigue corrosion and stress-corrosion cracking. For the environments investigated, there exist similarities in the corrosion mechanism since the localised corrosion failures could be attributed to mechanically assisted corrosion despite the variations in the initiation of pitting and crevice [240]. According to Ghali [151], pitting corrosion is commonly observed in the presence of chlorides and halides, and this is evident in the results obtained where pitting corrosion occurred more in the NaCl environment compared to the other environments. As observed in this investigation, continuous sliding actions at higher loads easily destroy the protective properties of the passive film, thereby exposing more layers of the material surface and resulting in a high corrosion rate before the surface repassivates [6, 163].

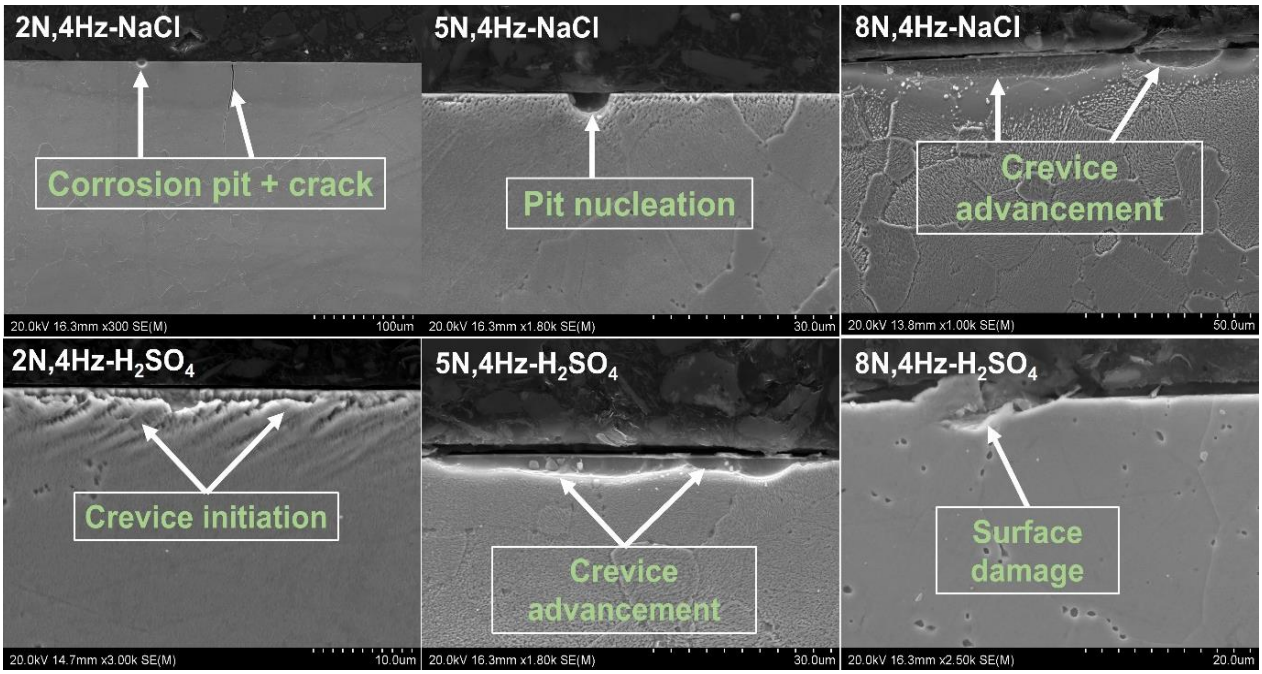

Fig. 9.9: SEM images showing the advancement of localised corrosion in NiTiNOL60 samples tested under different loads in NaCl and H_2SO_4 environments.

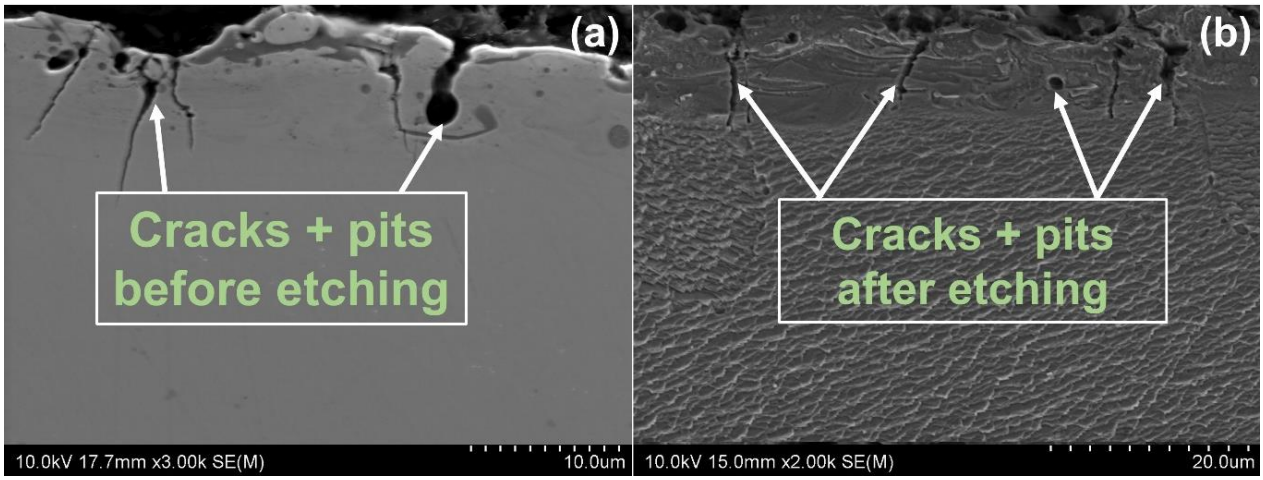

Fig. 9.10: SEM showing crack propagation after tribocorrosion test in NaOH environment before etching and (b) after etching.

Continuous sliding at an 8N load in the NaOH environment resulted in grain elongation and stress-corrosion cracking due to the wear-accelerated corrosion resulting from the tribocorrosion synergy. Accordingly, Figure 9.11 presents the cross-section of the sample, revealing surface damages and distortion in the microstructural arrangement. From the images, it could be deduced that sliding action caused mild to severe surface damages, and the third-body effect from the resulting debris led to a nonuniform direction in the wear track abrasion grooves, thereby causing wear roughening and wear anisotropy [11, 214]. The shear force possibly caused the grain structures to be flattened and elongated longitudinally in the sliding direction, with irregularly shaped eutectic and dendritic growth [101]. This impact could further lead to plastic deformation because of further compression and shear due to sliding and altering the martensite phase comparable to the eutectic and dendritic network structures. Further sliding results in the formation of additional fragments, which then adhere to the original fragment and finally delaminate to produce a much larger conglomerate wear particle. Therefore, the wear mechanisms and/or patterns are significantly influenced by the equilibrium between the depassivation and repassivation rates. This is reinforced by the findings of Ferreira, et al. [128], who reported that the depassivation rate depends on the contact pressure, the sliding velocity, the counter body and mechanical properties of the passive film, such as scratch resistance [170]. Additionally, we have deduced that under tribocorrosion conditions, the synergistic interactions of wear accelerated corrosive and material loss due to sliding contact commonly affect the depassivation mechanisms during the contact surface damage.

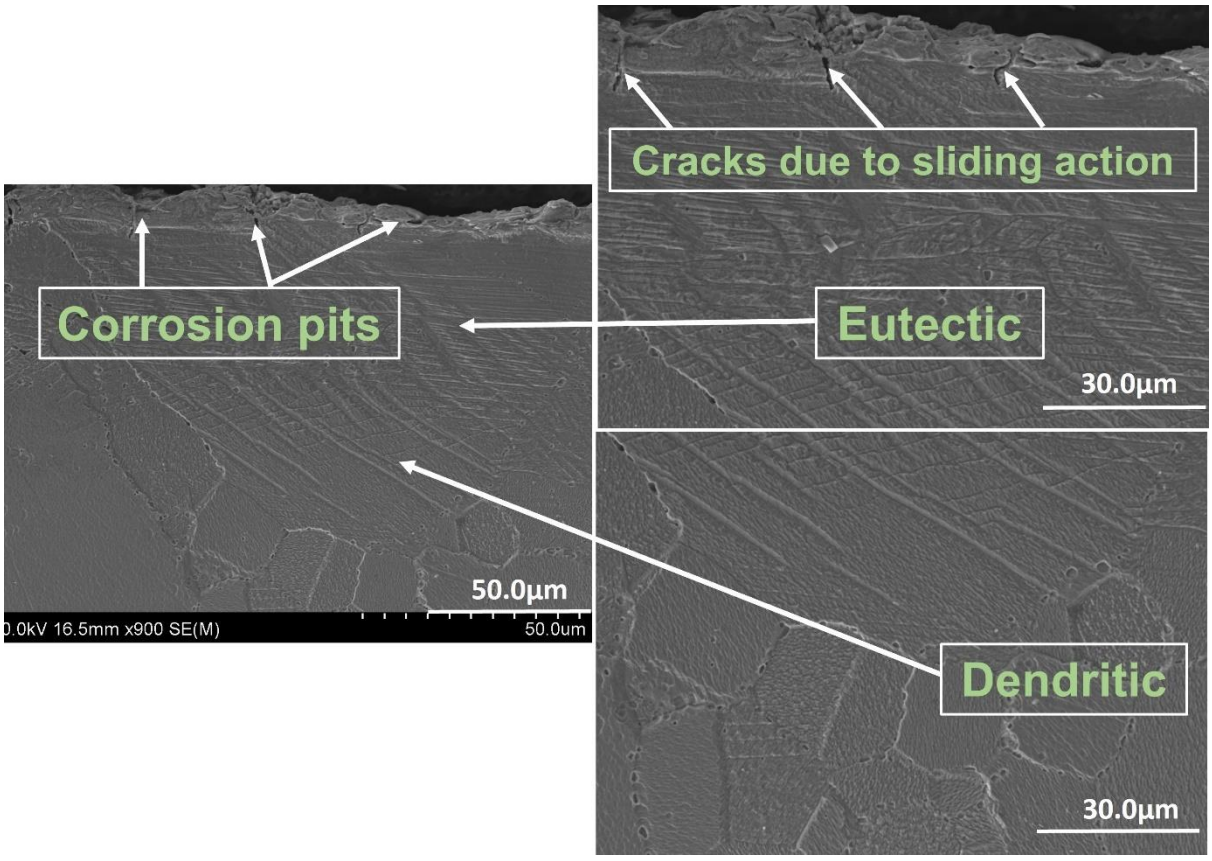

Fig. 9.11: SEM microstructure of an etched cross-sectional part of NiTiNOL60 sample tested at 8N load in NaOH environment.

Figure 9.12 (a-d) presents the summarised relationships between the applied normal loads and corrosion rate (Figure 9.12a), wear volume (Figure 9.12b), specific wear rate (Figure 9.12c) and the wear track profile (Figure 9.12d). Figure 9.12d shows the profiles for samples tested in the acidic medium where the minimum wear was recorded. From the profiles, wear volumes at different loads were estimated using a stylus profilometer and ImageJ software as outlined in section 9.2.2, and the specific wear rate was calculated using Eq. 1. It demonstrates that as the applied load increases, the wear track indentation increases, leading to a higher wear volume. From the results, it is clear that mechanical and chemically induced wear was highest for the sample investigated in the NaCl environment when compared to the samples tested in the acid and alkali environments. Thus, an indication of the significant role played by halides in passive film growth and breakdown. This demonstrates that metals or ions are reduced cathodically during the electrochemical breakdown of various metal oxides [151]. The results highlighted the prevalence of corrosion in all the investigated environments, indicating that fretting corrosion involves both chemical and mechanical factors, with observed damage arising from a combination of these factors [146, 165, 178]. The mechanical

abrasion of the passive film often leads to wear-accelerated corrosion due to the high chemical reactivity of the bare metal surface exposed to the corrosive environment [164]. Additionally, passive films significantly influence the surface mechanical response of metals and the behaviour of the third body in the tribological system [6, 61, 214]. The progressive increase in the pattern of wear rate shown in Figure 9.12 confirms wear acceleration due to the simultaneous electrochemical-mechanical interactions during tribocorrosion. Accordingly, the findings from previous researchers stated that under tribocorrosion conditions, two main mechanisms contribute to material removal from the surface: wear-accelerated corrosion and mechanical removal through sliding contact [165, 257, 280]. According to Yan, et al. [166], the mechanistic approach distinguishes two primary contributions: anodic dissolution (wear-accelerated corrosion) and mechanical removal of metal particles (mechanical wear) [166, 178].

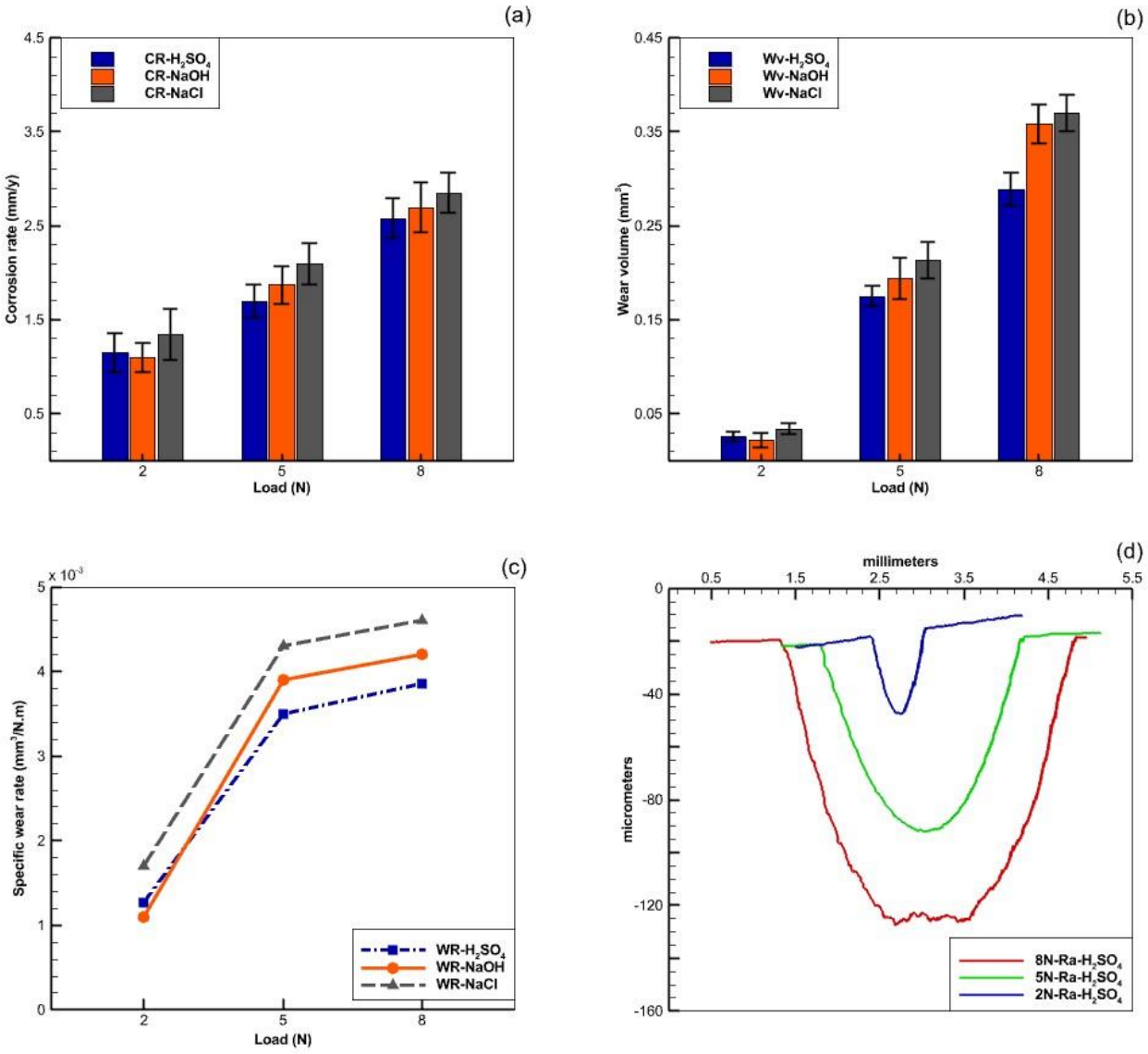

Fig. 9.12: Corrosion and wear rates at different loads after tribocorrosion experiments.

From the plots in Figure 9.12, it is evident that as the applied load increased, the wear rate significantly increased. The sample tested in the H_2SO_4 environment maintained the least wear volume, except for the test condition of 2N load, where the sample yielded more than the sample tested in a NaOH environment. This could be attributed to the prolonged running-in period shown in Figure 9.4, which impacted the material loss through mechanical removal due to inadequate contact pressure from the applied load. Also, the sample tested in the NaOH environment markedly showed the lowest corrosion rate following the running-in time, which delayed the breakdown of the oxide film and reduced the exposure of the sample subsurface. Following the wear pattern at a lower load due to the less contact pressure, a low wear volume was recorded, and this basically occurred as a result of corrosive wear with little contribution of mechanical wear due to sliding [254]. As the load increases, the contact pressure and wear volume increase.

Overall, the graphical trend in Figure 9.12 shows that the highest wear volume was recorded in the NaCl environment, followed by the NaOH and then the H_2SO_4 environment (H_2SO_4 < NaOH < NaCl). The drop in the wear rate observed for the sample exposed to the H_2SO_4 environment could be attributed to the solubility of the alumina debris, unlike in the other environments where the particles/ debris contributed to the third-body wear abrasion.

9.2.4. Summary

This study focused on investigating and analysing the tribo-electrochemical interactions of NiTiNOL60 alloy in various corrosive environments under different test conditions. The experimental results clearly demonstrated the synergistic effect of wear and corrosion, leading to an accelerated degradation of the material surface. The investigation revealed that the material deterioration was attributed to the combined influence of wear-accelerated corrosion and mechanical wear resulting from the reciprocating sliding action. While the synergistic approach revealed that mechanical wear is the predominant factor in material loss, it was observed that corrosive wear was more pronounced at higher loads, particularly in the saline environment. Considering the influences of anodic dissolution (wear-accelerated corrosion) and mechanical removal of metal particles (mechanical wear), the mechanistic approach to wear was evident in all three investigated environments, with a greater prevalence in the hydroxyl medium (NaOH) which had the highest pH value. Moreover, severe and mild wear mechanisms were observed more in the NaCl and NaOH environments unlike in the least pH medium (H_2SO_4), indicating the impact of corrosion on the wear behaviour. The mechanical abrasion of the passive film led to wear-accelerated corrosion due to the high chemical

reactivity in corrosive mediums. The analysis highlighted the significant role of hydrogen ion (H^+) and hydroxyl ion (OH^-) concentrations in the electrolytes, particularly in the acidic environment, where the alumina debris dissolved in the medium during tribocorrosion. In conclusion, this investigation provided insights into the tribo-electrochemical behaviour of NiTiNOL60 alloy. The findings emphasised the importance of considering both wear-accelerated corrosion and mechanical wear when studying material degradation in different corrosive environments. The knowledge gained from this study can contribute to developing improved materials and strategies for mitigating tribocorrosion-related issues in practical applications.

CHAPTER 10: CONCLUSIONS, CONTRIBUTIONS TO KNOWLEDGE AND RECOMMENDATIONS FOR FUTURE RESEARCH

10.1. Conclusions

It is established that the performance of metallic components is usually impacted by the synergistic effects between sliding wear and corrosion, particularly in tribological systems. Accordingly, the tribocorrosion synergistic interaction under sliding contact and corrosive environment formed the basis of this study. To understand the relationship between corrosion and wear rates, assess surface damage (gradual deterioration) of NiTiNOL60 alloy under different conditions in corrosive mediums and reveal the wear mechanisms. The investigation has demonstrated the interactions of various test parameters and their influence on the surface deterioration of NiTiNOL60 alloy. The findings provide insights into wear mechanisms and localised corrosion, highlighting the influence of ions (H^+ and OH^-) on corrosive wear and crack propagation. This study underscores the significant influence of mechanical properties on the rate of material degradation due to corrosion, while also highlighting the substantial impact of prevailing electrochemical conditions on the rate of mechanical material removal.

In the sliding wear tests, the samples tested in dry conditions (no lubrication) revealed more abrasive and adhesive wear, unlike the specimens investigated at high-temperature conditions, where the shearing of asperities promoted more significant deformations, leading to plastic deformation.

According to the electrochemistry investigation, it was established that the corrosion behaviour of Ni-Ti-based alloys, especially the passivity, strongly depends on the surface conditions. Significant changes in corrosion current density and electrochemical impedance were recorded for alloys subjected to cathodic and anodic potentials. The oxidised surfaces exhibited Ni and Ti species present as oxides and hydroxides in the form of Ni^{2+}, Ni^{3+}, TiO_2, etc., and there was a noticeable increase in the hydrophilicity of the sample surfaces. Hence, the study has shown that the corrosion effects of uniform or localised pit growth and arrest of NiTiNOL60 alloy can be attributed to electrochemical charge transfer and ohmic effects.

The tribocorrosion synergistic interactions in different corrosive environments revealed that while abrasive and oxidative wear mechanisms exist concurrently, the pH of the electrolyte plays a significant role in the tribocorrosion process. Thereby leading to electromechanically induced transformations and various wear patterns ranging from mild to severe wear regimes. For instance, the wear volume was highest in saline

environments, with contributions from mechanical wear, corrosion, and third-body abrasion. In the alkaline environment, depassivation of the oxide layer triggered oxidational wear, with the depassivation rate dependent on factors like contact pressure, sliding velocity, and passive film properties. This results in grain deformations observed in the alkaline environment due to shear forces. While in the acidic medium, it was evident that corrosion accelerates mild wear involving abrasion and delamination.

In summary, it is established that the findings from this study have practical implications for optimising the performance and durability of NiTiNOL60 alloy under the tested conditions and offer valuable insights for designers working on load-bearing engineering applications. The key findings and conclusions from our investigation have been enumerated as follows:

- It is evident that the mechanistic interaction promotes the shearing of the asperities at a high strain rate during sliding and the frictional heating at the interface of the contact bodies.
- The surface degradation during tribocorrosion occurs from the combined effects of sliding wear and electrochemical reactions; thus, an increased applied load reduces the corrosion potential, leading to a higher wear volume and increased corrosion rate.
- The friction coefficient and wear volume of NiTiNOL60 alloy increased with the applied load and decreased under elevated temperature conditions
- The synergistic interactions exposed the material surface to various wear mechanisms, including abrasive, adhesive, oxidative, corrosive, fatigue, and crack propagation.
- The water-based electrolytes contributed to the increased hardness (hardened zones) on the wear tracks following the water hydrolysis and titanium oxide and/or hydride formation.
- The wear track analysis illuminated the various wear mechanisms at play, including abrasion, debris adhesion, pitting, delamination, ploughing, and cracking. These mechanisms were influenced by both mechanical and chemical wear, the latter notably due to corrosive attacks.
- Among the various wear mechanisms influenced by tribochemical wear, delamination and micro-cracks are notably prominent under higher applied loads due to surface tensile stress and contact pressure, leading to crack propagation perpendicular to the sliding direction.

- It is established that delamination wear primarily caused by exfoliation of the oxide films during sliding contact ultimately promotes localised corrosion.
- The sliding action promoted a sharp cathodic shift of the potential towards the negative. So, while corrosion potential decreased with increased applied load, corrosion current density increased significantly.
- The electrochemical findings indicate the occurrence of localised corrosion in both cathodic and anodic regimes, with corrosion pit nucleation, cavities, and cracks being accelerated by reciprocating sliding and corrosion potential.
- Anodic reactivity and the passive state of the alloy significantly influence the behaviour at OCP, thereby revealing the need for enhanced hydrophilicity, especially in highly chemically active environments.
- The reciprocating sliding wear test at elevated temperatures and the XRD examination revealed the phase stability of the alloy, thus validating the shape memory effect of Ni-Ti-based alloy.
- The microscopic analysis confirms the alloy's Ni-rich composition, featuring a dense network of B2 NiTi + Ni_4Ti_3 cubic and rhombohedral crystal matrix structures.

10.2. Research limitations

Although the scope of this study was covered, certain factors hindered the expansion of this research focus for further investigation thus:

a. The lack of an adequate setup that heats and maintains the electrolyte temperature prevented tribocorrosion investigation at high temperatures.
b. The ethical conditions around using simulated body fluids affected the investigation of NiTNOL60 performance in a mimicked biomedical environment.
c. The lack of some thermo-analytical instruments, such as thermogravimetric (TGA) and differential scanning calorimeter (DSC), prevented the measurements and insight into the material’s behaviour and mass losses at elevated temperatures.

10.3. Recommendations and future research directions (perspectives)

Following the limitations and timeline that hindered the expansion of this research focus, the areas that need to be investigated further are enumerated as follows:

i. The bio-tribocorrosion investigation following microbial attacks, especially in food processing and marine structures, should be considered. This is based on a high reproduction process of microorganisms and bacteria in seawater and the discharge of atmospheric sulphide in coastal areas.

ii. In the orthopedic application of NiTiNOL60 alloy, it is also necessary to investigate bio-tribocorrosion using a phosphate buffer solution (PBS), which depicts human body fluids.
iii. There is a need to provide insight into the kinetics and thermodynamics analysis of electrochemical reactions and the tribo-electrochemical activities of NiTiNOL60 alloy in corrosive environments.
iv. Investigate the film-electrolyte interface on the exposed surface of the alloy during and after the reciprocating sliding wear and employ software tool(s) to analyse the stress distribution on the contact surfaces (wear track) during the reciprocating sliding.
v. Incorporate environmentally friendly corrosion inhibitors for tribocorrosion study.

10.4. Contribution to knowledge

This study has addressed the knowledge gap presented in Chapter 1 of this thesis and contributed to the existing literature in the field of tribocorrosion. Accordingly, this study's findings and scientific output have presented a comparative study on NiTiNOL60 alloy tribocorrosion performance in corrosive media, which was lacking in the literature before this research. It further presented a comprehensive literature review on the tribocorrosion of Ni-Ti alloys in engineering and biomedical applications since its last review in 2018. It highlighted the significant discoveries, research approaches, and future directions for tribological and tribocorrosion areas. In addition, the investigation on the tribocorrosion, sliding wear, and electrochemistry of NiTiNOL60 alloy and its wear mechanisms have revealed the need for an appropriate choice in the selection of corrosion and wear-resistant materials, especially in food processing due to the varying process conditions (pH, concentration, temperature, etc.).

The findings from this study highlight the practical implications for maximising the performance and durability of NiTiNOL60 alloy in corrosive environments following the tribo-electrochemical synergistic interactions on the degradation of materials in tribological systems. The identified wear mechanisms provide insight into developing different approaches for surface treatments to reduce tribocorrosion and wear on material surfaces. Hence, this study would offer valuable information in designing advanced protective technology to minimise wear on materials in similar conditions.

REFERENCES

[1] A. I. Munoz, N. Espallargas, and S. Mischler, "Tribocorrosion phenomena and concepts," in *Tribocorrosion*, A. Igual Munoz, N. Espallargas, and S. Mischler Eds. Switzerland: Springer Briefs in Applied Sciences and Technology. Springer, Cham, 2020, ch. 4, pp. 35-42.

[2] M. T. Mathew and M. A. Wimmer, "Tribocorrosion in artificial joints: In vitro testing and clinical implications," in *Bio-Tribocorrosion in Biomaterials and Medical Implants*. Sawaton, UK: Woodhead Publishing Series in Biomaterials, 2013, pp. 341-371.

[3] R. R. Boyer, J. D. Cotton, M. Mohaghegh, and R. E. Schafrik, "Materials considerations for aerospace applications," *MRS Bull.,* vol. 40, no. 12, pp. 1055-1066, 2015, doi: 10.1557/mrs.2015.278.

[4] C. DellaCorte, "Novel super-elastic materials for advanced bearing applications," *Advances in science and technology,* vol. 89, pp. 1-9, 2014. [Online]. Available: https://ntrs.nasa.gov/api/citations/20140010477/downloads/20140010477.pdf.

[5] C. DellaCorte and W. A. Wozniak, "Design and manufacturing considerations for shockproof and corrosion-immune superelastic nickel-titanium bearings for a space station application," presented at the NASA/TM-2012-216015. 41st Aerospace Mechanisms Symposium, Pasadena, CA, May 16-18, 2012. [Online]. Available: https://ntrs.nasa.gov/citations/20130001675.

[6] A. López-Ortega, J. L. Arana, and R. Bayón, "Tribocorrosion of passive materials: A review on test procedures and standards," *International Journal of Corrosion,* vol. 2018, pp. 1-24, 2018, Art no. 7345346, doi: 10.1155/2018/7345346.

[7] S. Mischler and A. I. Munoz, "Tribocorrosion," in *Encyclopedia of Interfacial Chemistry*, K. Wandelt Ed. Oxford: Elsevier, 2018, pp. 504-514.

[8] A. I. Munoz, N. Espallargas, and S. Mischler, "Tribocorrosion: Definitions and relevance," in *Tribocorrosion*, A. Igual Munoz, N. Espallargas, and S. Mischler Eds. Switzerland: Springer Briefs in Applied Sciences and Technology. Springer, Cham, 2020, ch. 1, pp. 1-6.

[9] A. Siddaiah, A. Kasar, R. Ramachandran, and P. L. Menezes, "Introduction to tribocorrosion," in *Tribocorrosion: Fundamentals, methods, and materials*, A. Siddaiah, R. Ramachandran, and P. L. Menezes Eds. Cambridge, MA, USA: Academic Press, 2021, ch. 1, pp. 1-16.

[10] P. J. Blau *et al.*, "Future needs and challenges in tribo-corrosion research and testing," in *Proceedings of the 3rd International Symposium on Tribocorrosion*, Atlanta, Georgia, 2013, April 19–20, vol. STP 1563: ASTM Special Technical Publication; STP 1563, pp. 214-226, doi: 10.1520/STP156320120051. [Online]. Available: https://www.astm.org/stp156320120051.html

[11] A. Dalmau, C. Richard, and A. Igual – Muñoz, "Degradation mechanisms in martensitic stainless steels: Wear, corrosion and tribocorrosion appraisal," *Tribology International,* vol. 121, pp. 167-179, 2018, doi: 10.1016/j.triboint.2018.01.036.

[12] J. Du, S. Cao, A. Igual Munoz, and S. Mischler, "Tribological and tribocorrosion behavior of nickel sliding against oxide ceramics," *Wear,* vol. 426-427, pp. 1496-1506, 2019, doi: 10.1016/j.wear.2019.01.007.

[13] G. Koch, J. Varney, N. Thompson, O. Moghissi, M. Gould, and J. Payer, "International measures of prevention, application, and economics of corrosion technologies study," NACE international, Houston TX, NACE international, Houston TX, NACE international, Houston TX 2016, vol. 216. [Online]. Available: http://impact.nace.org/documents/Nace-International-Report.pdf

[14] E. Shekari, F. Khan, and S. Ahmed, "Economic risk analysis of pitting corrosion in process facilities," *Int. J. Pressure Vessels Piping,* vol. 157, pp. 51-62, 2017, doi: 10.1016/j.ijpvp.2017.08.005.

[15] R. J. K. Wood, *Developments in Electrochemistry: Science Inspired by Martin Fleischmann* (Developments in Electrochemistry: Science Inspired by Martin Fleischmann). 2014.

[16] M. H. Shahini, H. E. Mohammadloo, and B. Ramezanzadeh, "Recent approaches to limit the tribocorrosion of biomaterials: A review," *Biomass Conversion and Biorefinery,* vol. 14, no. 4, pp. 4369-4389, 2024, doi: 10.1007/s13399-022-02719-3.

[17] S. Mischler, S. Debaud, and D. Landolt, "Wear-accelerated corrosion of passive metals in tribocorrosion systems," *J. Electrochem. Soc.,* vol. 145, no. 3, pp. 750-758, 1998, doi: 10.1149/1.1838341.

[18] D. Landolt and S. Mischler, *Tribocorrosion of passive metals and coatings*. Amsterdam, The Netherlands: Elsevier, 2011.

[19] T. Zirari and V. Trabadelo, "A review on wear, corrosion, and wear-corrosion synergy of high entropy alloys," *Heliyon,* vol. 10, no. 4, pp. 1-30, 2024, Art no. e25867, doi: 10.1016/j.heliyon.2024.e25867.

[20] E. Gracia-Escosa, I. García, J. J. d. Damborenea, and A. Conde, "Friction and wear behaviour of tool steels sliding against 22MnB5 steel," *Journal of Materials*

Research and Technology, vol. 6, no. 3, pp. 241-250, 2017/07/01/ 2017, doi: 10.1016/j.jmrt.2017.04.002.

[21] K. Khanlari, M. Ramezani, and P. Kelly, "60NiTi: A review of recent research findings, potential for structural and mechanical applications, and areas of continued investigations," *Transactions of the Indian Institute of Metals,* vol. 71, no. 4, pp. 781-799, 2018, doi: 10.1007/s12666-017-1224-5.

[22] S. Cao and S. Mischler, "Tribocorrosion of a CoCrMo alloy in sulfuric acid – Glycerol mixtures," *Wear,* vol. 458-459, 2020, Art no. 203443, doi: 10.1016/j.wear.2020.203443.

[23] A. Delgado-Brito *et al.*, "Bio-tribocorrosion resistance of CoB–Co2B and Co2B layers on CoCrMo alloy," *Journal of Vacuum Science & Technology A,* vol. 42, no. 2, 2024, Art no. 023106, doi: 10.1116/6.0003342.

[24] S. V. Pepper, C. DellaCorte, R. D. Noebe, D. R. Hull, and G. Glennon, "Nitinol 60 as a material for spacecraft triboelements," in *Proceedings of the 13th European Space Mechanisms and Tribology Symposium - ESMATS 13 Conference*, Vienna, Austria, 23–25 September 2009, September 23–25, vol. 670 SP. [Online]. Available: https://ntrs.nasa.gov/api/citations/20090034488/downloads/20090034488.pdf. [Online]. Available: https://ntrs.nasa.gov/api/citations/20090034488/downloads/20090034488.pdf

[25] C. DellaCorte, "NiTi alloys for tribological applications: The effects of serendipity on research and development.," presented at the Annual Postdoctoral Research and Career Symposium, October 6th. NASA/ GRC-E-DAA-TN34568, Argonne IL., 2016. [Online]. Available: https://ntrs.nasa.gov/api/citations/20170003993/downloads/20170003993.pdf.

[26] M. K. Stanford, "Thermophysical properties of 60-nitinol for mechanical component applications," *NASA Technical Report. NASA/TM—2012-216056,* Technical Memorandum, GRC-E-DAA-TN-6187 2012. [Online]. Available: https://ntrs.nasa.gov/citations/20130001731.

[27] C. DellaCorte, R. D. Noebe, M. K. Stanford, and S. A. Padula, "Resilient and corrosion-proof rolling element bearings made from superelastic Ni-Ti alloys for aerospace mechanism applications," *ASTM Special Technical Publication. NASA/TM-2011-217105,* 1542 STP pp. 143-166, 2011, doi: 10.1520/STP103887.

[28] Y. Li, Z. Zhou, and Y. He, "Tribocorrosion and surface protection technology of titanium alloys: A review," *Materials (Basel),* vol. 17 (1): 65, pp. 1-41, 2023, doi: 10.3390/ma17010065.

[29] A. L. Martinez, M. Saugo, D. O. Flamini, and S. B. Saidman, "Enhancing the corrosion behavior of Ti–6Al–4V and Nitinol alloys by simple chemical oxidation in H_2O_2," *Materials Chemistry and Physics,* vol. 295, pp. 1-14, 2023, Art no. 127069, doi: /10.1016/j.matchemphys.2022.127069.

[30] S. Hanke, M. Beyer, A. Silvonen, J. F. dos Santos, and A. Fischer, "Cavitation erosion of Cr60Ni40 coatings generated by friction surfacing," *Wear,* vol. 301, no. 1-2, pp. 415-423, 2013, doi: 10.1016/j.wear.2012.11.016.

[31] N. Mazinanian, G. Herting, I. O. Wallinder, and Y. S. Hedberg, "Metal release and corrosion resistance of different stainless steel grades in simulated food contact," *Corrosion,* vol. 72, no. 6, pp. 775-790, 2016, doi: 10.5006/2057.

[32] J. Pješčić-Šćepanović, G. Vastag, Š. Ivošević, N. Kovač, and R. Rudolf, "Corrosion of NiTiDiscs in Different Seawater Environments," *Materials,* vol. 15, pp. 1-18, 2022, Art no. 2841, doi: 10.3390/ma15082841.

[33] B. C. Hornbuckle, X. X. Yu, R. D. Noebe, R. Martens, M. L. Weaver, and G. B. Thompson, "Hardening behavior and phase decomposition in very Ni-rich Nitinol alloys," *Materials Science and Engineering: A,* vol. 639, pp. 336-344, 2015, doi: 10.1016/j.msea.2015.04.079.

[34] C. Dellacorte, S. V. Pepper, R. Noebe, and D. R. Hull, "Nickel-titanium: A new candidate material for oil-lubricated bearing and mechanical component applications," in *Proceedings of the World Tribology Congress*, Kyoto, Japan, 6–11 September 2009, September 6–11.

[35] W. J. Buehler and F. E. Wang, "A summary of recent research on the nitinol alloys and their potential application in ocean engineering," *Ocean Eng.,* vol. 1, no. 1, pp. 105-120, 1968, doi: 10.1016/0029-8018(68)90019-x.

[36] S. K. Patel and A. Behera, "Evolution of Phases and their Influence on Shape Memory Effect by Varying Sintering Parameters of NiTi Alloys," *Metals and Materials International,* vol. 28, no. 11, pp. 2691-2705, 2022/11/01 2022, doi: 10.1007/s12540-021-01166-5.

[37] J. W. Mwangi, H. Zeidler, R. Kühn, and A. Schubert, "Suitability assessment of micro-EDM in machining Nitinol for medical applications," presented at the euspen's 16th International Conference & Exhibition, Nottingham, UK, May 2016. [Online]. Available: https://www.euspen.eu/knowledge-base/ICE16-P1.72.pdf.

[38] N. Agarwal *et al.*, "Effect of Heat Treatment Time and Temperature on the Microstructure and Shape Memory Properties of Nitinol Wires," *Materials,* vol. 16, no. 19, 2023, Art no. 6480, doi: 10.3390/ma16196480.

[39] S. H. Mills, R. D. Noebe, C. Dellacorte, B. Amin-Ahmadi, and A. P. Stebner, "Development of Nickel-Rich Nickel–Titanium–Hafnium Alloys for Tribological Applications," *Shape Memory and Superelasticity,* vol. 6, no. 3, pp. 311-322, 2020/09/01 2020, doi: 10.1007/s40830-020-00296-w.

[40] C. Miller, C. DellaCorte, and M. Zou, "Nanomechanical properties of hardened 60NiTi," *Mater. Sci. Eng., A,* vol. 800, pp. 1-7, 2021, Art no. 14028, doi: 10.1016/j.msea.2020.140284.

[41] K. Khanlari, M. Ramezani, P. Kelly, P. Cao, and T. Neitzert, "Comparison of the reciprocating sliding wear of 58Ni39Ti-3Hf alloy and baseline 60NiTi," *Wear,* vol. 408-409, pp. 120-130, 2018/08/15/ 2018, doi: 10.1016/j.wear.2018.05.011.

[42] M. S. Guadalupe, S. Mischler, M. Cantoni, W. J. Chitty, C. Falcand, and D. Hertz, "Mechanical and chemical mechanisms in the tribocorrosion of a Stellite type alloy," *Wear,* vol. 308, no. 1-2, pp. 213-221, 2013, doi: 10.1016/j.wear.2013.04.007.

[43] Y. Tang *et al.*, "Tribology, corrosion, and tribocorrosion performance of aged lightweight steels: Effects of oxide film and carbide," *Corros. Sci.,* vol. 231, pp. 1-16, 2024, Art no. 111999, doi: 10.1016/j.corsci.2024.111999.

[44] S. Hellberg, S. Böhm, J. Hummel, P. Krooß, and T. Niendorf, "Microstructural and mechanical properties of dissimilar nitinol and stainless steel wire joints produced by micro electron beam welding without filler material," (in English), *Welding in the World,* Article vol. 64, no. 12, pp. 2159-2168, 12/01/ 2020, doi: 10.1007/s40194-020-00991-3.

[45] T. Kosec, P. Močnik, and A. Legat, "The tribocorrosion behaviour of NiTi alloy," *Appl. Surf. Sci.,* vol. 288, pp. 727-735, 2014, doi: 10.1016/j.apsusc.2013.10.116.

[46] H. Bounezour, L. Laouar, M. Bourbia, and B. Ouzine, "Effects of work hardening on mechanical metal properties—experimental analysis and simulation by experiments," *The International Journal of Advanced Manufacturing Technology,* vol. 101, no. 9, pp. 2475-2485, 2019/04/01 2019, doi: 10.1007/s00170-018-3071-x.

[47] O. Benafan, A. Garg, R. D. Noebe, H. D. Skorpenske, K. An, and N. Schell, "Deformation characteristics of the intermetallic alloy 60NiTi," *Intermetallics,* vol. 82, pp. 40-52, 2017, doi: 10.1016/j.intermet.2016.11.003.

[48] V. Totolin, V. Pejaković, T. Csanyi, O. Hekele, M. Huber, and M. Rodríguez Ripoll, "Surface engineering of Ti6Al4V surfaces for enhanced tribocorrosion performance in artificial seawater," *Materials & Design,* vol. 104, pp. 10-18, 2016, doi: 10.1016/j.matdes.2016.04.080.

[49] R. J. K. Wood and P. Lu, "Coatings and Surface Modification of Alloys for Tribo-Corrosion Applications," *Coatings,* vol. 14, no. 1, pp. 1-43, 2024, Art no. 99, doi: 10.3390/coatings14010099.

[50] R. J. K. Wood, "Tribo-corrosion of coatings: a review," *J. Phys. D: Appl. Phys.,* vol. 40, no. 18, pp. 5502-5521, 2007, doi: 10.1088/0022-3727/40/18/s10.

[51] M. De Stefano, S. M. Aliberti, and A. Ruggiero, "(Bio)Tribocorrosion in dental implants: Principles and techniques of investigation," *Applied Sciences,* vol. 12, no. 15, pp. 1-16, 2022, Art no. 7421, doi: 10.3390/app12157421.

[52] A. O. Okoani, A. Nand, and M. Ramezani, "Comparative Study of the Tribocorrosion Performance of NiTiNOL60 in Acidic, Alkaline, and Saline Environments," *J. Mater. Eng. Perform.,* 2024, doi: 10.1007/s11665-024-09646-6.

[53] A. I. Munoz, N. Espallargas, and S. Mischler, *Tribocorrosion*. Switzerland: Springer Briefs in Applied Sciences and Technology. Springer, Cham, 2020.

[54] K.-Y. Cheng, D. Bijukumar, M. Runa, M. McNallan, and M. Mathew, "Tribocorrosion aspects of implant coatings: Hip replacements," in *Tribocorrosion: Fundamentals, methods, and materials*, A. Siddaiah, R. Ramachandran, and P. L. Menezes Eds. Cambridge, MA, USA: Academic Press, 2021, ch. 5, pp. 93-126.

[55] J. Zou, Z. Wang, Y. Ma, and L. Tan, "Tribocorrosion Behavior and Degradation Mechanism of 316L Stainless Steel in Alkaline Solution: Effect of Tribo-Film," *Acta Metallurgica Sinica (English Letters),* vol. 35, no. 8, pp. 1365-1375, 2022, doi: 10.1007/s40195-022-01374-x.

[56] L. Tan, Z. Wang, and Y. Ma, "Tribocorrosion Behavior and Degradation Mechanism of 316L Stainless Steel in Typical Corrosive Media," *Acta Metallurgica Sinica (English Letters),* vol. 34, no. 6, pp. 813-824, 2021, doi: 10.1007/s40195-020-01182-1.

[57] Y. Sun and V. Rana, "Tribocorrosion behaviour of AISI 304 stainless steel in 0.5M NaCl solution," *Materials Chemistry and Physics,* vol. 129, no. 1, pp. 138-147, 2011, doi: 10.1016/j.matchemphys.2011.03.063.

[58] M. Perrut, P. Caron, M. Thomas, and A. Couret, "High temperature materials for aerospace applications: Ni-based superalloys and γ-TiAl alloys," *Comptes Rendus Physique,* vol. 19, no. 8, pp. 657-671, 2018, doi: 10.1016/j.crhy.2018.10.002.

[59] X. Chen, A. Guo, J. Wang, S. Lu, and T. Fu, "Temperature dependence of tribological properties in NiTi shape memory alloy: A nanoscratching study,"

Tribology International, vol. 197, 2024, Art no. 109812, doi: 10.1016/j.triboint.2024.109812.

[60] H. Choi and S. Roy, "Investigating the effect of operating temperature on the tribo-mechanical behavior of cold rolled superelastic nickel titanium alloy," *Wear,* vol. 523, 2023, Art no. 204729, doi: 10.1016/j.wear.2023.204729.

[61] P. Ponthiaux, F. Wenger, and J.-P. Celis, "Tribocorrosion: material behavior under combined conditions of corrosion and mechanical loading," in *Corrosion resistance*, vol. 1. Hong Kong, China: InTech, 2012, pp. 81-106.

[62] R. Johnsen and C. B. Von Der Ohe, "Tribocorrosion in marine environments," in *Tribocorrosion of Passive Metals and Coatings*, D. Landolt and S. Mischler Eds. Sawston, UK: Woodhead Publishing, 2011, ch. 16, pp. 441-474.

[63] R. J. K. Wood, "Marine wear and tribocorrosion," *Wear,* vol. 376-377, pp. 893-910, 2017, doi: 10.1016/j.wear.2017.01.076.

[64] Q. Chen and G. A. Thouas, "Metallic implant biomaterials," *Materials Science and Engineering: R: Reports,* vol. 87, pp. 1-57, 2015, doi: 10.1016/j.mser.2014.10.001.

[65] J. Primozic, M. Hren, U. Mezeg, and A. Legat, "Tribocorrosion Susceptibility and Mechanical Characteristics of As-Received and Long-Term In-Vivo Aged Nickel-Titanium and Stainless-Steel Archwires," *Materials,* vol. 15, no. 4, 2022, Art no. 1427, doi: 10.3390/ma15041427.

[66] J. Takadoum, "Review on Corrosion, Tribocorrosion and Osseointegration of Titanium Alloys as Biomaterials," *Corrosion and Materials Degradation,* vol. 4, no. 4, pp. 644-658, 2023, doi: 10.3390/cmd4040033.

[67] R. C. C. Silva, R. P. Nogueira, and I. N. Bastos, "Tribocorrosion of UNS S32750 in chloride medium: Effect of the load level," *Electrochimica Acta,* vol. 56, no. 24, pp. 8839-8845, 2011, doi: 10.1016/j.electacta.2011.07.077.

[68] N. Attarzadeh, M. Molaei, K. Babaei, and A. Fattah-alhosseini, "New promising ceramic coatings for corrosion and wear protection of steels: A review," *Surfaces and Interfaces,* vol. 23, pp. 1-23, 2021, Art no. 100997, doi: 10.1016/j.surfin.2021.100997.

[69] A. López-Ortega, R. Bayón, J. L. Arana, A. Arredondo, and A. Igartua, "Influence of temperature on the corrosion and tribocorrosion behaviour of high-strength low-alloy steels used in offshore applications," *Tribology International,* vol. 121, pp. 341-352, 2018, doi: 10.1016/j.triboint.2018.01.049.

[70] S. Shabalovskaya, J. Anderegg, and J. Van Humbeeck, "Critical overview of Nitinol surfaces and their modifications for medical applications," *Acta Biomater.,* vol. 4, no. 3, pp. 447-467, 2008, doi: 10.1016/j.actbio.2008.01.013.

[71] R. Bayón, A. Igartua, J. J. González, and U. Ruiz de Gopegui, "Influence of the carbon content on the corrosion and tribocorrosion performance of Ti-DLC coatings for biomedical alloys," *Tribology International,* vol. 88, pp. 115-125, 2015, doi: 10.1016/j.triboint.2015.03.007.

[72] Y. Chenglong and K. Dejun, "Microstructure, Tribocorrosion and Corrosion Performances of Laser Cladded Ni625-xTiC Coatings in 3.5% NaCl Solution," *J. Therm. Spray Technol.,* vol. 33, no. 1, pp. 260-274, 2024/02/01 2024, doi: 10.1007/s11666-024-01717-3.

[73] C. Skjöldebrand, J. L. Tipper, P. Hatto, M. Bryant, R. M. Hall, and C. Persson, "Current status and future potential of wear-resistant coatings and articulating surfaces for hip and knee implants," *Materials Today Bio,* vol. 15, 2022, Art no. 100270, doi: 10.1016/j.mtbio.2022.100270.

[74] C. Yan, Y. Zhang, Q. Zeng, X. Zhu, Z. Tong, and X. Feng, "Comparative investigation on the tribocorrosion resistance of Ti6Al4V and 60NiTi alloys inimulated seawater environment," *Wear,* vol. 550-551, 2024, Art no. 205423, doi: 10.1016/j.wear.2024.205423.

[75] M. Alhamad, V. A. R. Barão, C. Sukotjo, L. F. Cooper, and M. T. Mathew, "Ti-Ions and/or Particles in Saliva Potentially Aggravate Dental Implant Corrosion," *Materials,* vol. 14, no. 19, 2021, Art no. 5733, doi: 10.3390/ma14195733.

[76] A. Chouhan, H. P. Mungse, and O. P. Khatri, "Surface chemistry of graphene and graphene oxide: A versatile route for their dispersion and tribological applications," *Advances in Colloid and Interface Science,* vol. 283, 2020, Art no. 102215, doi: 10.1016/j.cis.2020.102215.

[77] S. S. A. Kumar, S. Bashir, K. Ramesh, and S. Ramesh, "New perspectives on Graphene/Graphene oxide based polymer nanocomposites for corrosion applications: The relevance of the Graphene/Polymer barrier coatings," *Prog. Org. Coat.,* vol. 154, 2021, Art no. 106215, doi: 10.1016/j.porgcoat.2021.106215.

[78] Y. Zuo *et al.*, "Effect of graphene oxide additive on tribocorrosion behavior of MAO coatings prepared on Ti6Al4V alloy," *Appl. Surf. Sci.,* vol. 480, pp. 26-34, 2019, doi: 10.1016/j.apsusc.2019.02.065.

[79] M. T. Acar, H. Kovacı, and A. Çelik, "Investigation of corrosion and tribocorrosion behavior of boron doped and graphene oxide doped TiO2 nanotubes produced on Cp-Ti," *Materials Today Communications,* vol. 32, 2022, Art no. 104182, doi: 10.1016/j.mtcomm.2022.104182.

[80] W. Xu *et al.*, "Synergistic interactions between wear and corrosion of Ti-16Mo orthopedic alloy," *Journal of Materials Research and Technology,* vol. 9, no. 5, pp. 9996-10003, 2020, doi: 10.1016/j.jmrt.2020.06.095.

[81] L. Vilhena, G. Oppong, and A. Ramalho, "Tribocorrosion of different biomaterials under reciprocating sliding conditions in artificial saliva," *Lubr. Sci.,* Article vol. 31, no. 8, pp. 364-380, 12/01/ 2019, doi: 10.1002/ls.1478.

[82] Z. Zhang, R. S. B. Dandu, E. E. Klu, and W. Cai, "A Review on Tribocorrosion Behavior of Aluminum Alloys: From Fundamental Mechanisms to Alloy Design Strategies," *Corrosion and Materials Degradation,* vol. 4, no. 4, pp. 594-622, 2023, doi: 10.3390/cmd4040031.

[83] U. Puthillam and R. E. Selvam, "Tribocorrosion in biomaterials and control techniques: A review," *Corros. Rev.,* vol. 42, no. 1, pp. 37-56, 2023, doi: 10.1515/corrrev-2023-0008.

[84] X. Huang, N. Kang, P. Coddet, and M. El Mansori, "Effects of test temperature on the ball-on-slab wear behavior of nickel-titanium shape memory alloys fabricated by laser powder bed fusion," *Tribology International,* vol. 196, 2024, Art no. 109666, doi: 10.1016/j.triboint.2024.109666.

[85] G. Li, J. Bao, T. Yu, and M. Chen, "An atomistic study of effects of temperature and Ni element on the phase transition and wear behavior of NiTi shape memory alloy," *Tribology International,* vol. 192, 2024, Art no. 109309, doi: 10.1016/j.triboint.2024.109309.

[86] M. Shahirnia, Z. Farhat, and G. Jarjoura, "Effects of temperature and loading rate on the deformation characteristics of superelastic TiNi shape memory alloys under localized compressive loads," *Mater. Sci. Eng., A,* vol. 530, no. 1, pp. 628-632, 2011, doi: 10.1016/j.msea.2011.10.034.

[87] S. Bao, L. Zhang, H. Peng, Q. Fan, and Y. Wen, "Effects of heat treatment on martensitic transformation and wear resistance of as-cast 60NiTi alloy," *Materials Research Express,* vol. 6, pp. 1-14, 2019, Art no. 086573, doi: 10.1088/2053-1591/ab1b7a.

[88] C. Yan, Q. Zeng, K. Khanlari, X. Zhu, and Z. Wang, "Characterization of microstructure, grain distribution, and tribocorrosion properties of NiTi-based alloy," *Journal of Materials Science,* vol. 57, no. 45, pp. 21237-21250, 2022/12/01 2022, doi: 10.1007/s10853-022-07927-w.

[89] D. Kapoor, "Nitinol for medical applications: A brief introduction to the properties and processing of nickel titanium shape memory alloys and their use in stents," *Johnson Matthey Technology Review,* vol. 61, no. 1, pp. 66-76, 2017, doi: 10.1595/205651317x694524.

[90] A. Ayyagari, B. Gwalani, R. Banerjee, T. W. Scharf, S. Mukherjee, and C. Barthelemy, "Reciprocating sliding wear behavior of high entropy alloys in dry and marine environments," *Materials Chemistry and Physics,* vol. 210, pp. 162-169, 2018, doi: 10.1016/j.matchemphys.2017.07.031.

[91] M. T. Mathew, P. Srinivasa Pai, R. Pourzal, A. Fischer, and M. A. Wimmer, "Significance of tribocorrosion in biomedical applications: Overview and current status," *Advances in Tribology,* vol. 2009, pp. 1-12, 2009, Art no. 250986, doi: 10.1155/2009/250986.

[92] J. Shittu *et al.*, "Tribo-corrosion response of additively manufactured high-entropy alloy," *npj Materials Degradation,* vol. 5, pp. 1-8, 2021, Art no. 31, doi: 10.1038/s41529-021-00177-2.

[93] M. Liu, J.-N. Zhu, V. A. Popovich, E. Borisov, J. M. C. Mol, and Y. Gonzalez-Garcia, "Corrosion and passive film characteristics of 3D-printed NiTi shape memory alloys in artificial saliva," *Rare Metals,* vol. 42, no. 9, pp. 3114-3129, 2023, doi: 10.1007/s12598-023-02329-6.

[94] M. Buciumeanu, A. Bagheri, F. S. Silva, B. Henriques, A. F. Lasagni, and N. Shamsaei, "Tribocorrosion behavior of NiTi biomedical alloy processed by an additive manufacturing laser beam directed energy deposition technique," *Materials,* vol. 15, no. 2, 2022, Art no. 691, doi: 10.3390/ma15020691.

[95] J. Grabarczyk, J. Gaj, B. Pazik, W. Kaczorowski, and B. Januszewicz, "Tribocorrosion behavior of Ti6Al4V alloy after thermo-chemical treatment and DLC deposition for biomedical applications," *Tribology International,* vol. 153, 2021, Art no. 106560, doi: 10.1016/j.triboint.2020.106560.

[96] M. Buciumeanu, A. Bagheri, N. Shamsaei, S. M. Thompson, F. S. Silva, and B. Henriques, "Tribocorrosion behavior of additive manufactured Ti-6Al-4V biomedical alloy," *Tribology International,* vol. 119, pp. 381-388, 2018/03/01/ 2018, doi: 10.1016/j.triboint.2017.11.032.

[97] I. Kaya, H. E. Karaca, M. Souri, Y. Chumlyakov, and H. Kurkcu, "Effects of orientation on the shape memory behavior of Ni 51 Ti 49 single crystals," *Materials Science and Engineering: A,* vol. 686, pp. 73-81, 2017, doi: 10.1016/j.msea.2017.01.026.

[98] P. R. Halani, I. Kaya, Y. C. Shin, and H. E. Karaca, "Phase transformation characteristics and mechanical characterization of nitinol synthesized by laser direct deposition," *Materials Science and Engineering: A,* vol. 559, pp. 836-843, 2013, doi: 10.1016/j.msea.2012.09.031.

[99] L. A. Dobrzański, L. B. Dobrzański, A. D. Dobrzańska-Danikiewicz, and J. Dobrzańska, "Nitinol type alloys general characteristics and applications in

endodontics," *Processes,* vol. 10, pp. 1-59, 2022, Art no. 101, doi: 10.3390/pr10010101.

[100] W. Chen, R. Xi, H. Jiang, X. Li, G. Dong, and X. Wang, "Superelasticity of Geometrically Graded NiTi Shape Memory Alloys," *Metals,* vol. 13, no. 9, p. 1518, 2023. [Online]. Available: https://www.mdpi.com/2075-4701/13/9/1518.

[101] Z. Du, Z. Hu, Y. Feng, and F. Mo, "The effect of powder composition on the microstructure and corrosion resistance of laser cladding 60NiTi alloy coatings on SS 316L," *Metals,* vol. 11, no. 7, pp. 1-16, 2021, Art no. 1104, doi: 10.3390/met11071104.

[102] M. K. Stanford, "Hot isostatic pressing of 60-Nitinol," *NASA Technical Report. NASA/TM-2015-218884,* 2015. [Online]. Available: https://www.techbriefs.com/component/content/article/tb/pub/briefs/manufacturing-prototyping/26497.

[103] M.-L. Li, W.-J. Gao, and Y.-H. Zhou, "Hot deformation behavior of 60NiTi shape-memory alloy fabricated by hot isostatic pressing," *Materials Research Express,* vol. 9, no. 1, pp. 1-10, 2022, Art no. 016511, doi: 10.1088/2053-1591/ac487e.

[104] K. Khanlari *et al.*, "Fabrication of ni-rich 58NiTi and 60NiTi from elementally blended Ni and Ti powders by a laser powder bed fusion technique: Their printing, homogenization and densification," (in eng), *Int. J. Mol. Sci.,* vol. 23, no. 16, pp. 1-23, 2022, Art no. 9495, doi: 10.3390/ijms23169495.

[105] E. Moskvichev, N. Shamarin, and N. Savchenko, "High temperature tribological properties of additively manufactured WC reinforced CuAl7-W composites," *Wear,* vol. 556, 2024, Art no. 205535, doi: 10.1016/j.wear.2024.205535.

[106] C. H. Ortiz, A. Esguerra-Arce, J. Esguerra-Arce, A. Bermúdez Castañeda, J. C. Caicedo, and Y. Aguilar, "The high temperature tribological behavior of an iron oxide strengthened iron compound obtained from an industrial byproduct," *Tribology International,* vol. 175, 2022, Art no. 107834, doi: 10.1016/j.triboint.2022.107834.

[107] A. O. Okoani, A. Nand, and M. Ramezani, "Corrosion and wear interplay: Tribo-electrochemical evaluation of NiTiNOL60 alloy in sulfuric acid," *Results in Materials,* vol. 21, pp. 1-11, 2024, Art no. 100523, doi: 10.1016/j.rinma.2023.100523.

[108] M. Atapour, I. Odnevall Wallinder, and Y. S. Hedberg, "Stainless steel in simulated milk and whey protein solutions - Influence of grade on corrosion and metal release," *Electrochimica Acta,* vol. 331, 2020, Art no. 135428, doi: 10.1016/j.electacta.2019.135428.

[109] S. Varmaziar, M. Atapour, and Y. S. Hedberg, "Corrosion and metal release characterization of stainless steel 316L weld zones in whey protein solution," *npj Materials Degradation,* vol. 6, 2022, Art no. 19, doi: 10.1038/s41529-022-00231-7.

[110] M. S. Jellesen, M. Ø. Hansen, L. R. Hilbert, and P. Møller, "Corrosion and wear properties of materials used for minced meat production," *J. Food Process Eng.,* vol. 32, no. 4, pp. 463-477, 2009, doi: 10.1111/j.1745-4530.2007.00223.x.

[111] A. Zaffora, F. D. Franco, and M. Santamaría, "Corrosion of stainless steel in food and pharmaceutical industry," *Current Opinion in Electrochemistry,* vol. 29, pp. 1-7, 2021, Art no. 100760, doi: 10.1016/J.COELEC.2021.100760.

[112] A. Wadood, "Brief overview on NiTinol as biomaterial," *Advances in Materials Science and Engineering,* vol. 2016, 2016, Art no. 4173138, doi: 10.1155/2016/4173138.

[113] L. A. Khan, E. McCarthy, C. Muilwijk, I. U. Ahad, and D. Brabazon, "Analysis of NiTinol actuator response under controlled conductive heating regimes," *Results in Engineering,* vol. 18, pp. 1-11, 2023/06/01/ 2023, Art no. 101047, doi: 10.1016/j.rineng.2023.101047.

[114] Y. Xue, Y. Hu, and Z. Wang, "Tribocorrosion behavior of NiTi alloy as orthopedic implants in Ringer's simulated body fluid," *Biomedical Physics and Engineering Express,* vol. 5, no. 4, pp. 1-9, 2019, Art no. 045002, doi: 10.1088/2057-1976/ab1db0.

[115] X. Zhu, B. Dang, F. Li, D. Wei, P. Zhang, and S. Li, "Tribocorrosion behavior of Nb coating deposited by double-glow plasma alloying," *Materials Research Express,* vol. 8, no. 1, pp. 1-10, 2021, Art no. 016411, doi: 10.1088/2053-1591/abdc39.

[116] S. Cao, S. Guadalupe Maldonado, and S. Mischler, "Tribocorrosion of passive metals in the mixed lubrication regime: theoretical model and application to metal-on-metal artificial hip joints," *Wear,* vol. 324-325, pp. 55-63, 2015, doi: 10.1016/j.wear.2014.12.003.

[117] M. A. Minnath, "Metals and alloys for biomedical applications," in *Fundamental Biomaterials: Metals*. Duxford, UK: Woodhead Publishing, 2018, pp. 167-174.

[118] M. Geetha, A. K. Singh, R. Asokamani, and A. K. Gogia, "Ti based biomaterials, the ultimate choice for orthopaedic implants – A review," *Prog. Mater Sci.,* vol. 54, no. 3, pp. 397-425, 2009/05/01/ 2009, doi: 10.1016/j.pmatsci.2008.06.004.

[119] W. Brantley, D. Berzins, M. Iijima, E. Tufekçi, and Z. Cai, "Structure/property relationships in orthodontic alloys," in *Orthodontic Applications of Biomaterials*,

T. Eliades and W. A. Brantley Eds. Sawston, UK: Woodhead Publishing, 2017, ch. 1, pp. 3-38.

[120] A. Revathi, A. D. Borrás, A. I. Muñoz, C. Richard, and G. Manivasagam, "Degradation mechanisms and future challenges of titanium and its alloys for dental implant applications in oral environment," *Materials Science and Engineering: C,* vol. 76, pp. 1354-1368, 2017, doi: 10.1016/j.msec.2017.02.159.

[121] H. Dong *et al.*, "Surface Modified Techniques and Emerging Functional Coating of Dental Implants," *Coatings,* vol. 10, no. 11, 2020, Art no. 1012, doi: 10.3390/coatings10111012.

[122] J. Geringer, K. Kim, and B. Boyer, "Fretting corrosion in biomedical implants," in *Tribocorrosion of Passive Metals and Coatings*, D. Landolt and S. Mischler Eds. Sawston, UK: Woodhead Publishing, 2011, ch. 14, pp. 401-423.

[123] S. Waqar, A. Wadood, A. Mateen, and M. A. U. Rehman, "Effects of Ni and Cr addition on the wear performance of NiTi alloy," *International Journal of Advanced Manufacturing Technology,* vol. 108, no. 3, pp. 625-634, 2020, doi: 10.1007/s00170-020-05380-0.

[124] L. Salas *et al.*, "Tribocorrosion and corrosion behavior of quaternary Ti-24Nb-xZr-ySn alloys in SBF," *Mater. Lett.,* vol. 283, 2021, Art no. 128903, doi: 10.1016/j.matlet.2020.128903.

[125] N. S. Manam *et al.*, "Study of corrosion in biocompatible metals for implants: A review," *J. Alloys Compd.,* vol. 701, pp. 698-715, 2017, doi: 10.1016/j.jallcom.2017.01.196.

[126] T. Kosec *et al.*, "Tribocorrosive study of new and in vivo exposed nickel titanium and stainless steel orthodontic archwires," *Coatings,* vol. 10, pp. 1-11, 2020, Art no. 230, doi: 10.3390/coatings10030230.

[127] J. Zupanc, N. Vahdat-Pajouh, and E. Schäfer, "New thermomechanically treated NiTi alloys – A review," *Int. Endod. J.,* Review vol. 51, no. 10, pp. 1088-1103, 2018, doi: 10.1111/iej.12924.

[128] D. F. Ferreira *et al.*, "Synergism between mechanical wear and corrosion on tribocorrosion of a titanium alloy in a Ringer solution," *Journal of Materials Research and Technology,* vol. 8, no. 2, pp. 1593-1600, 2019, doi: 10.1016/j.jmrt.2018.11.004.

[129] A. Berradja, F. Bratu, L. Benea, G. Willems, and J. P. Celis, "Effect of sliding wear on tribocorrosion behaviour of stainless steels in a Ringer's solution," *Wear,* vol. 261, pp. 987-993, 2006/11/20/ 2006, doi: 10.1016/j.wear.2006.03.003.

[130] C. Yan, Q. Zeng, W. He, and J. Zhu, "Enhanced surface hardness and tribocorrosion performance of 60NiTi by boron ion implantation and post-annealing," *Tribology International,* vol. 155, pp. 1-11, 2021, Art no. 106816, doi: 10.1016/j.triboint.2020.106816.

[131] E. Kassab and J. Gomes, "Corrosion induced fracture of NiTi wires in simulated oral environments," *J. Mech. Behav. Biomed. Mater.,* vol. 116, pp. 1-6, 2021/04/01/ 2021, Art no. 104323, doi: 10.1016/j.jmbbm.2021.104323.

[132] P. Močnik, T. Kosec, J. Kovac, and M. Bizjak, "The effect of pH, fluoride and tribocorrosion on the surface properties of dental archwires," *Mater. Sci. Eng. C Mater. Biol. Appl.,* vol. 78, pp. 682-689, 2017, doi: 10.1016/j.msec.2017.04.050.

[133] P. Močnik and T. Kosec, "A critical appraisal of the use and properties of nickel-titanium dental alloys," *Materials,* vol. 14, no. 24, pp. 1-18, 2021, Art no. 7859, doi: 10.3390/ma14247859.

[134] T. D. Costa *et al.*, "Corrosion resistance assessment of nickel-titanium endodontic files with and without heat treatment," *Restorative Dentistry & Endodontics,* vol. 46, no. 1, pp. 1-10, 2021, Art no. 6, doi: 10.5395/rde.2021.46.e6.

[135] I. Sifakakis and C. Bourauel, "Nickel–Titanium products in daily orthodontic practice," in *Orthodontic Applications of Biomaterials*, T. Eliades and W. A. Brantley Eds. Sawston, UK: Woodhead Publishing, 2017, pp. 107-127.

[136] G. E. Romanos, G. A. Fischer, and R. Delgado-Ruiz, "Titanium wear of dental implants from placement, under loading and maintenance protocols," *Int. J. Mol. Sci.,* vol. 22, no. 3, 2021, Art no. 1067, doi: 10.3390/ijms22031067.

[137] M. K. Stanford, "Preliminary investigation of surface treatments to enhance the wear resistance of 60-nitinol," in "NASA Technical Report," NASA, Washington, DC, USA, N0. E-19245, 2016, issue NASA/TM-2016-219121. [Online]. Available: https://ntrs.nasa.gov/citations/20160009222

[138] C. DellaCorte, "Nickel-Titanium alloys: Corrosion “proof” alloys for space bearing, components and mechanism applications," in *Proceedings of the 40th Aerospace Mechanisms Symposium*, Cocoa Beach, FL. USA, May 12–14 2010, May 12–14, pp. 1-7. [Online]. Available: https://ntrs.nasa.gov/citations/20100021919. [Online]. Available: https://ntrs.nasa.gov/citations/20100021919

[139] C. Garcia-Cabezón *et al.*, "Improvements in tribological and anticorrosion performance of porous Ti-6Al-4V via PEO coating," *Friction,* vol. 9, no. 5, pp. 1303-1318, 2021/10/01 2021, doi: 10.1007/s40544-020-0480-2.

[140] B. Fotovvati, N. Namdari, and A. Dehghanghadikolaei, "On Coating Techniques for Surface Protection: A Review," *Journal of Manufacturing and Materials Processing,* vol. 3, no. 1, pp. 1-22, 2019, Art no. 28, doi: 10.3390/jmmp3010028.

[141] S. M. Ramteke, M. Walczak, M. De Stefano, A. Ruggiero, A. Rosenkranz, and M. Marian, "2D materials for Tribo-corrosion and -oxidation protection: A review," *Advances in Colloid and Interface Science,* vol. 331, 2024, Art no. 103243, doi: 10.1016/j.cis.2024.103243.

[142] B. Rahmatian, H. M. Ghasemi, M. H. Sohi, and P. De Baets, "Insight into tribocorrosion resistance and tribofilm formation on titanium boride coatings in a phosphate buffer saline solution," *Journal of Materials Research and Technology,* vol. 27, pp. 6847-6862, 2023, doi: 10.1016/j.jmrt.2023.11.105.

[143] J. Dong, Z. Zhang, D. Wang, Y. Liu, Y. Wu, and Y. Guo, "Research on erosion wear behavior of NiTi alloy coating fabricated via high-frequency induction heating technology," *Wear,* vol. 556-557, 2024, Art no. 205506, doi: 10.1016/j.wear.2024.205506.

[144] Y. Shen *et al.*, "Enhanced Anti-Tribocorrosion Performance of Ti-DLC Coatings Deposited by Filtered Cathodic Vacuum Arc with the Optimization of Bias Voltage," *Coatings,* vol. 12, no. 5, 2022, Art no. 697, doi: 10.3390/coatings12050697.

[145] A. López-Ortega, J. L. Arana, E. Rodríguez, and R. Bayón, "Corrosion, wear and tribocorrosion performance of a thermally sprayed aluminum coating modified by plasma electrolytic oxidation technique for offshore submerged components protection," *Corros. Sci.,* vol. 143, pp. 258-280, 2018/10/01/ 2018, doi: 10.1016/j.corsci.2018.08.001.

[146] Z. Yi *et al.*, "Interfacial friction at action: Interactions, regulation, and applications," *Friction,* vol. 11, pp. 1-28, 2023/03/13 2023, Art no. 2153–2180, doi: 10.1007/s40544-022-0702-x.

[147] I. M. Hutchings, *Tribology: friction and wear of engineering materials*. FL, USA: Boca Raton: Edward Arnold - A division of Hoddr & Stoughton London. CRC Press, 1992.

[148] I. Hutchings and P. Shipway, "Sliding wear," in *Tribology (2nd Edition)*, I. Hutchings and P. Shipway Eds. Oxford, UK: Butterworth-Heinemann, 2017, ch. 5, pp. 107-164.

[149] H. Krawiec and V. Vignal, "Stress/strain effects on electrochemical activity: Metallurgical/mechanical/interactions and surface reactivity," in *Mechanical and*

Electro-Chemical Interactions Under Tribocorrosion, P. Ponthiaux and J.-P. Celis Eds. Sawston, UK: Woodhead Publishing, 2021, pp. 7-27.

[150] J. Yang, Y. Song, K. Dong, and E.-H. Han, "Research progress on the corrosion behavior of titanium alloys," *Corros. Rev.,* vol. 41, no. 1, pp. 5-20, 2023, doi: 10.1515/correv-2022-0031.

[151] E. Ghali, *Corrosion resistance of aluminum and magnesium alloys: understanding, performance, and testing* (Wiley series in corrosion). Hoboken, New Jersey: John Wiley & Sons Inc., Hoboken, New Jersey. ISBN: 978-0-471-71576-4, 2010.

[152] S. Guadalupe, C. Falcand, W. Chitty, and S. Mischler, "Tribocorrosion in pressurized high-temperature water: A mass flow model based on the third-body approach," *Tribology Letters,* vol. 62, no. 1, pp. 1-13, 2016, Art no. 10, doi: 10.1007/s11249-016-0653-3.

[153] N. Perez, *Electrochemistry and corrosion science*. New York, NY, USA: Kluwer Academic Publishers, 2004.

[154] R. G. Wellman, "Methods for studying erosion–corrosion," in *Tribocorrosion of Passive Metals and Coatings*, D. Landolt and S. Mischler Eds. Sawaton, UK: Woodhead Publishing, 2011, ch. 9, pp. 239-264.

[155] M. Azzi and J. E. Klemberg-Sapieha, "Tribocorrosion test protocols for sliding contacts," in *Tribocorrosion of Passive Metals and Coatings*, D. Landolt and S. Mischler Eds. Sawaton, UK: Woodhead Publishing, 2011, ch. 8, pp. 222-238.

[156] P. Ponthiaux, F. Wenger, D. Drees, and J. P. Celis, "Electrochemical techniques for studying tribocorrosion processes," *Wear,* vol. 256, no. 5, pp. 459-468, 2004, doi: 10.1016/s0043-1648(03)00556-8.

[157] M. S. Jellesen, M. Ø. Hansen, L. R. Hilbert, and P. Møller, "A block-on-ring tribocorrosion setup for combined electrochemical and friction testing," *Tribo Test,* vol. 13, no. 3, pp. 115-127, 2007, doi: 10.1002/tt.37.

[158] S. Mischler, "Triboelectrochemical techniques and interpretation methods in tribocorrosion: A comparative evaluation," *Tribology International,* vol. 41, no. 7, pp. 573-583, 2008, doi: 10.1016/j.triboint.2007.11.003.

[159] A. I. Munoz, N. Espallargas, and S. Mischler, "Experimental techniques for tribocorrosion," in *Tribocorrosion*, A. Igual Munoz, N. Espallargas, and S. Mischler Eds. Switzerland: Springer Briefs in Applied Sciences and Technology. Springer, Cham, 2020, ch. 6, pp. 53-64.

[160] X. Z. Wang, Y. Jiang, Y. Wang, C. Ye, and C. F. Du, "Probing the tribocorrosion behaviors of three nickel-based superalloys in sodium chloride solution,"

Tribology International, Article vol. 172, 2022, Art no. 107581, doi: 10.1016/j.triboint.2022.107581.

[161] P. Močnik and T. Kosec, "Tribo-corrosion properties of a NiTi dental wire," (in English), *Materiali in Tehnologije,* Article vol. 48, no. 4, pp. 467-472, 01 / 01 / 2014. [Online]. Available: http://mit.imt.si/Revija/izvodi/mit144/mocnik.pdf.

[162] L. Zhou *et al.*, "Electrochemical Behavior of Laser Powder Bed Fusion (L-PBF) Ti–6Al–4V Alloy: Influence of Phase and Grain Boundaries on Surface Passive Film Formation," *Metals and Materials International,* vol. 30, pp. 1864-1877, 2024, doi: 10.1007/s12540-023-01607-3.

[163] J. Chen and F.-y. Yan, "Tribocorrosion behaviors of Ti–6Al–4V and Monel K500 alloys sliding against 316 stainless steel in artificial seawater," *Transactions of Nonferrous Metals Society of China,* vol. 22, no. 6, pp. 1356-1365, 2012, doi: 10.1016/s1003-6326(11)61326-5.

[164] J. P. Celis, P. Ponthiaux, and F. Wenger, "Tribo-corrosion of materials: Interplay between chemical, electrochemical, and mechanical reactivity of surfaces," *Wear,* vol. 261, pp. 939-946, 2006, doi: 10.1016/j.wear.2006.03.027.

[165] A. I. Muñoz and N. Espallargas, "Tribocorrosion mechanisms in sliding contacts," in *Tribocorrosion of passive metals and coatings*, D. Landolt and S. Mischler Eds. Sawston, UK: Woodhead Publishing, 2011, ch. 5, pp. 118-152.

[166] C. Yan, Q. Zeng, Y. Xu, and W. He, "Microstructure, phase and tribocorrosion behavior of 60NiTi alloy," *Appl. Surf. Sci.,* vol. 498, pp. 1-10, 2019, Art no. 143838, doi: 10.1016/j.apsusc.2019.143838.

[167] A. López *et al.*, "Tribocorrosion behaviour of mooring high strength low alloy steels in synthetic seawater," *Wear,* vol. 338-339, pp. 1-10, 2015, doi: 10.1016/j.wear.2015.05.004.

[168] P. Qin, L. Y. Chen, Y. J. Liu, S. X. Liang, H. Sun, and L. C. Zhang, "Corrosion and passivation behavior of laser powder bed fusion produced Ti-6Al-4V under various prior plastic deformation strains," *Corros. Sci.,* vol. 230, pp. 1-12, 2024, Art no. 111919, doi: 10.1016/j.corsci.2024.111919.

[169] I. Uysal, B. Yilmaz, A. O. Atilla, and Z. Evis, "Nickel titanium alloys as orthodontic archwires: A narrative review," *Engineering Science and Technology, an International Journal,* vol. 36, p. 101277, 2022, doi: 10.1016/j.jestch.2022.101277.

[170] K. Khanlari, M. Ramezani, P. Kelly, P. Cao, and T. Neitzert, "Reciprocating sliding wear behavior of 60NiTi as compared to 440C steel under lubricated and unlubricated conditions," *Tribology Transactions,* vol. 61, no. 6, pp. 991-1002, 2018, doi: 10.1080/10402004.2018.1460434.

[171] Q. Zeng and G. Dong, "Superlubricity behaviors of Nitinol 60 alloy under oil lubrication," *Transactions of Nonferrous Metals Society of China,* vol. 24, no. 2, pp. 354-359, 2014, doi: 10.1016/s1003-6326(14)63068-5.

[172] A. López-Ortega, R. Bayón, and J. L. Arana, "Evaluation of protective coatings for offshore applications. Corrosion and tribocorrosion behavior in synthetic seawater," *Surf. Coat. Technol.,* vol. 349, pp. 1083-1097, 2018, doi: 10.1016/j.surfcoat.2018.06.089.

[173] A. O. Okoani, A. Nand, and M. Ramezani, "Tribocorrosion behaviour of NiTiNOL60 alloy in an alkaline environment," *Results in Engineering,* vol. 19, pp. 1-11, 2023, Art no. 101305, doi: 10.1016/j.rineng.2023.101305.

[174] L. Zhang *et al.*, "Study on the corrosion behavior of NiTi shape memory alloys fabricated by electron beam melting," *npj Materials Degradation,* vol. 6, no. 1, 2022, Art no. 79, doi: 10.1038/s41529-022-00289-3.

[175] A. O. Okoani, A. Nand, and M. Ramezani, "Tribo-electrochemical investigation of 60NiTi alloy in saline solution," *Journal of Alloys and Metallurgical Systems,* vol. 6, p. 100074, 2024/06/01/ 2024, doi: 10.1016/j.jalmes.2024.100074.

[176] H. Chen, Z. Zhang, X. H. Hao, B. X. Huang, X. C. Zhao, and C. C. Hu, "Microstructure and tribocorrosion properties of NiTi/AlNi2Ti ternary intermetallic alloy," *Vacuum,* vol. 184, pp. 1-12, 2021, Art no. 109928, doi: 10.1016/j.vacuum.2020.109928.

[177] Z. Yu *et al.*, "Analysis of microstructure, mechanical properties, wear characteristics and corrosion behavior of SLM-NiTi under different process parameters," *Journal of Manufacturing Processes,* vol. 75, pp. 637-650, 2022, doi: 10.1016/j.jmapro.2022.01.010.

[178] A. C. Vieira, L. A. Rocha, N. Papageorgiou, and S. Mischler, "Mechanical and electrochemical deterioration mechanisms in the tribocorrosion of Al alloys in NaCl and in NaNO3 solutions," *Corros. Sci.,* vol. 54, pp. 26-35, 2012, doi: 10.1016/j.corsci.2011.08.041.

[179] L. O. Paula *et al.*, "Tribo-corrosion and corrosion behaviour of titanium alloys with and without DLC films immersed in synthetic urine," *Journal of Bio- and Tribo-Corrosion,* vol. 4, pp. 1-12, 2018, Art no. 51, doi: 10.1007/s40735-018-0166-8.

[180] Q. Zeng, "Superlubricity of NiTi alloys," in *Superlubricity (2nd Edition)*, A. Erdemir, J. M. Martin, and J. Luo Eds. Amsterdam, The Netherlands: Elsevier, 2020, ch. 26, pp. 517-533.

[181] Q. Zeng and G. Dong, "Influence of load and sliding speed on super-low friction of NiTiNOL 60 alloy under castor oil lubrication," *Tribology Letters,* vol. 52, no. 1, pp. 47-55, 2013, doi: 10.1007/s11249-013-0191-1.

[182] Q. Zeng, G. Dong, and J. M. Martin, "Green superlubricity of Nitinol 60 alloy against steel in presence of castor oil," *Sci. Rep.,* vol. 6, no. 1, pp. 1-9, 2016/07/21 2016, Art no. 29992, doi: 10.1038/srep29992.

[183] J. Jiang, M. M. Stack, and A. Neville, "Modelling the tribo-corrosion interaction in aqueous sliding conditions," *Tribology International,* vol. 35, no. 10, pp. 669-679, 2002, doi: 10.1016/S0301-679X(02)00058-0.

[184] C.-O. A. Olsson, A. N. I. Munoz, S. Cao, and S. Mischler, "Modeling current transients in a reciprocal motion tribocorrosion experiment," *J. Electrochem. Soc.,* vol. 168, no. 3, 2021/03/02 2021, Art no. 031503, doi: 10.1149/1945-7111/abe6ed.

[185] M. M. Stack, "Mapping tribo-corrosion processes in dry and in aqueous conditions: Some new directions for the new millennium," *Tribology International,* vol. 35, no. 10, pp. 681-689, 2002, doi: 10.1016/S0301-679X(02)00059-2.

[186] N. Kovač, Š. Ivošević, G. Vastag, G. Vukelić, and R. Rudolf, "Statistical approach to the analysis of the corrosive behaviour of NiTi alloys under the influence of different seawater environments," *Applied Sciences,* vol. 11, no. 19, pp. 1-41, 2021, Art no. 8825, doi: 10.3390/app11198825.

[187] K. Fallahnezhad, M. Feyzi, K. Ghadirinejad, R. Hashemi, and M. Taylor, "Finite element based simulation of tribocorrosion at the head-neck junction of hip implants," *Tribology International,* vol. 165, 2022, Art no. 107284, doi: 10.1016/j.triboint.2021.107284.

[188] C. B. von der Ohe, R. Johnsen, and N. Espallargas, "Modeling the multi-degradation mechanisms of combined tribocorrosion interacting with static and cyclic loaded surfaces of passive metals exposed to seawater," *Wear,* vol. 269, no. 7-8, pp. 607-616, 2010, doi: 10.1016/j.wear.2010.06.010.

[189] D. Landolt, S. Mischler, and M. Stemp, "Electrochemical methods in tribocorrosion: A critical appraisal," *Electrochimica Acta,* vol. 46, no. 24-25, pp. 3913-3929, 2001, doi: 10.1016/S0013-4686(01)00679-X.

[190] A. A. LotfiNeyestanak and S. Daneshmand, "The effect of operational cutting parameters on Nitinol-60 in wire electrodischarge machining," *Advances in Materials Science and Engineering,* vol. 2013, pp. 1-6, 2013, Art no. 457186, doi: 10.1155/2013/457186.

[191] M. Stemp, S. Mischler, and D. Landolt, "Electrochemical aspects of tribocorrosion," *Tribology Series,* vol. 39, pp. 539-547, 2001, doi: 10.1016/s0167-8922(01)80137-1.

[192] ASTM G119-09, "Standard guide for determining synergism between wear and corrosion," *American Society for Testing and Materials. Book of standards, vol. 03.02. Developed by subcommittee G02.40,* pp. 1-6, 2021, doi: 10.1520/G0119-09R22.

[193] ASTM G133-22, "Standard test method for linearly reciprocating ball-on-flat sliding wear," *American Society for Testing and Materials. Book of standards, vol. 03.02. Developed by subcommittee G02.40,* pp. 1-10, 2022, doi: 10.1520/G0133-22.

[194] ASTM G3-14, "Standard practice for conventions applicable to electrochemical measurements in corrosion testing," *American Society for Testing and Materials. Book of standards, vol. 03.02. Developed by subcommittee G01.11,* pp. 1-9, 2019, doi: 10.1520/G0003-14R19.

[195] S. B. Arya and F. J. Joseph, "Electrochemical methods in tribocorrosion," in *Tribocorrosion: Fundamentals, methods, and materials*, A. Siddaiah, R. Ramachandran, and P. L. Menezes Eds. Cambridge, MA, USA: Academic Press, 2021, ch. 3, pp. 43-77.

[196] A. O. Okoani, A. Nand, C.-P. Jiang, and M. Ramezani, "Investigating the Tribocorrosion Behaviour of NiTiNOL60 Alloy in Engineering and Biomedical Applications—An Overview," *Metals,* vol. 14, no. 12, pp. 1-32, 2024, Art no. 1334, doi: 10.3390/met14121334.

[197] P. Kapsa, "Environmental effects in fretting," in *Tribocorrosion of Passive Metals and Coatings*, D. Landolt and S. Mischler Eds.: Woodhead Publishing, 2011, ch. 4, pp. 100-117.

[198] C. Miller and M. Zou, "Microscale friction and deformation behavior of polydopamine/ polytetrafluoroethylene-coated 60NiTi from nanoscratch tests," *Thin Solid Films,* vol. 743, pp. 1-10, 2022/02/01/ 2022, Art no. 139079, doi: 10.1016/j.tsf.2021.139079.

[199] A. Vahidi, F. Ferreira, and J. Oliveira, "Comparative study of dry high-temperature tribological performance of hydrogen-free and hydrogenated DLC films deposited by HiPIMS in DOMS mode," *Tribology International,* vol. 195, 2024, Art no. 109639, doi: 10.1016/j.triboint.2024.109639.

[200] K. J. Yuan, Y. Wang, L. J. Zheng, and H. Zhang, "Microstructural evolution, mechanical properties, and oxidation performance of highly Ni-rich NiTi alloys

with added V using vacuum arc melting," *J. Alloys Compd.,* vol. 877, pp. 1-10, 2021/10/05/ 2021, Art no. 160263, doi: 10.1016/j.jallcom.2021.160263.

[201] H. Shen *et al.*, "Enhancing thermal stability of laser powder bed fusion fabricated 60NiTi alloy via Nb alloying," *Materials Science and Engineering: A,* vol. 922, 2025, Art no. 147606, doi: 10.1016/j.msea.2024.147606.

[202] H. Vashishtha and D. M. Collins, "The influence of dislocations on B19' and R-phase transformations in a NiTi shape memory alloy," *Scripta Mater.,* vol. 255, 2025, Art no. 116365, doi: 10.1016/j.scriptamat.2024.116365.

[203] Y. Zhou *et al.*, "Heat treatment of hot-isostatic-pressed 60NiTi shape memory alloy: Microstructure, phase transformation and mechanical properties," *Journal of Materials Science & Technology,* vol. 107, pp. 124-135, 2022, doi: 10.1016/j.jmst.2021.10.005.

[204] G. X. Xu, L. J. Zheng, F. X. Zhang, and H. Zhang, "Influence of solution heat treatment on the microstructural evolution and mechanical behavior of 60NiTi," *J. Alloys Compd.,* vol. 775, pp. 698-706, 2019, doi: 10.1016/j.jallcom.2018.10.015.

[205] S. Ingole, "60NiTi alloy for tribological and biomedical surface engineering applications," *JOM,* vol. 65, no. 6, pp. 792-798, 2013, doi: 10.1007/s11837-013-0610-7.

[206] G. Plummer, M. I. Mendelev, O. Benafan, and J. W. Lawson, "Interactions of austenite-martensite interfaces with Ni4Ti3 precipitates in NiTi shape memory alloy: A molecular dynamics investigation," *Int. J. Plast.,* vol. 184, 2025, Art no. 104203, doi: 10.1016/j.ijplas.2024.104203.

[207] A. W. Hansen *et al.*, "Oxide formation on NiTi surface: influence of the heat treatment time to achieve the shape memory," *Materials Research,* vol. 18, no. 5, pp. 1053-1061, 2015, doi: 10.1590/1516-1439.022415.

[208] K. Yan, P. Wei, W. He, and Q. Sun, "Effects of residual stress on the isothermal tensile behavior of nanocrystalline superelastic NiTi shape memory alloy," *Journal of Materials Research and Technology,* vol. 33, pp. 8025-8039, 2024, doi: 10.1016/j.jmrt.2024.11.086.

[209] J. Nasehi, H. M. Ghasemi, and M. Abedini, "Effects of aging treatments on the high-temperature wear behavior of 60NiTinol alloy," *Tribology Transactions,* vol. 59, no. 2, pp. 286-291, 2016, doi: 10.1080/10402004.2015.1073821.

[210] M. K. Stanford, "Hardness and microstructure of binary and ternary nitinol compounds," in "NASA Technical Report," National Aeronautics and Space Administration, Glenn Research Center, No. GRC-E-DAA-TN73728, 2016,

issue NASA/TM-2016-218946. [Online]. Available: https://ntrs.nasa.gov/citations/20160001689

[211] G. Tang, D. Zhang, J. Zhang, P. Lin, and G. Dong, "Self-recovery of worn surface of TiNi shape memory alloy," *Appl. Surf. Sci.,* vol. 321, pp. 371-377, 2014, doi: 10.1016/j.apsusc.2014.09.151.

[212] G. S. Firstov, R. G. Vitchev, H. Kumar, B. Blanpain, and J. Van Humbeeck, "Surface oxidation of NiTi shape memory alloy," *Biomaterials,* vol. 23, no. 24, pp. 4863-4871, 2002, doi: 10.1016/S0142-9612(02)00244-2.

[213] X. Yan, H. Yan, P. Zhang, Q. Lu, and H. Shi, "Fabrication and tribological properties of bionic surface texture self-lubricating 60NiTi alloy via selective laser melting and infiltration," *Tribology International,* vol. 202, 2025, Art no. 110364, doi: 10.1016/j.triboint.2024.110364.

[214] D. Landolt, S. Mischler, M. Stemp, and S. Barril, "Third body effects and material fluxes in tribocorrosion systems involving a sliding contact," *Wear,* vol. 256, no. 5, pp. 517-524, 2004/03/01/ 2003, doi: 10.1016/S0043-1648(03)00561-1.

[215] G. List, G. Sutter, and J. J. Arnoux, "Analysis of the high speed sliding interaction between titanium alloy and tantalum," *Wear,* vol. 301, no. 1-2, pp. 663-670, 2013, doi: 10.1016/j.wear.2012.11.070.

[216] Z. Pang *et al.*, "Ultralow friction and low wear behavior of in-situ formed NiTiO3 from 60NiTi alloy at 350 °C," *Intermetallics,* vol. 168, 2024, Art no. 108271, doi: 10.1016/j.intermet.2024.108271.

[217] I. Milošev and B. Kapun, "The corrosion resistance of Nitinol alloy in simulated physiological solutions Part 2: The effect of surface treatment," *Materials Science and Engineering: C,* vol. 32, no. 5, pp. 1068-1077, 2012/07/01/ 2012, doi: 10.1016/j.msec.2011.08.022.

[218] D. Chen *et al.*, "Hot compressive deformation and microstructural evolution of 60NiTi alloy," *Transactions of Nonferrous Metals Society of China,* vol. 33, no. 1, pp. 189-200, 2023, doi: 10.1016/S1003-6326(22)66099-0.

[219] S. Kossman *et al.*, "Impact of industrially applied surface finishing processes on tribocorrosion performance of 316L stainless steel," *Wear,* vol. 456-457, 2020, Art no. 203341, doi: 10.1016/j.wear.2020.203341.

[220] S. Soltanahmadi, A. Morina, M. C. P. van Eijk, I. Nedelcu, and A. Neville, "Tribochemical study of micropitting in tribocorrosive lubricated contacts: The influence of water and relative humidity," *Tribology International,* vol. 107, pp. 184-198, 2017, doi: 10.1016/j.triboint.2016.11.031.

[221] Y. Zhou, Z. Zhao, S. Jiang, and D. Duan, "Effect of heat treatment on the tribocorrosion behavior of 20Cr13 martensitic stainless steel," *Tribology International,* vol. 197, 2024/09/01/ 2024, Art no. 109768, doi: 10.1016/j.triboint.2024.109768.

[222] X. Huang, N. Kang, P. Coddet, and M. El Mansori, "Analyses of the sliding wear behavior of NiTi shape memory alloys fabricated by laser powder bed fusion based on orthogonal experiments," *Wear,* vol. 534-535, 2023/12/15/ 2023, Art no. 205130, doi: 10.1016/j.wear.2023.205130.

[223] S. Zehra, M. Mobin, and J. Aslam, "1 - An overview of the corrosion chemistry," in *Environmentally Sustainable Corrosion Inhibitors*, C. M. Hussain, C. Verma, and J. Aslam Eds.: Elsevier, 2022, pp. 3-23.

[224] R. E. Melchers, "Predicting long-term corrosion of metal alloys in physical infrastructure," *npj Materials Degradation,* vol. 3, no. 1, pp. 1-7, 2019, doi: 10.1038/s41529-018-0066-x.

[225] M. M. Stack, B. D. Jana, and S. M. Abdelrahman, "6 - Models and mechanisms of erosion–corrosion in metals," in *Tribocorrosion of Passive Metals and Coatings*, D. Landolt and S. Mischler Eds.: Woodhead Publishing, 2011, ch. 6, pp. 153-187e.

[226] F. O. Pessu, E. Saleem, C. Espejo, and A. Neville, "Understanding the local pitting corrosion characteristics of carbon steel in CO2 corrosion environment using artificially machined pits," *Results in Engineering,* vol. 16, pp. 1-14, 2022/12/01/ 2022, Art no. 100700, doi: 10.1016/j.rineng.2022.100700.

[227] F. Ropital, *Corrosion and degradation of metallic materials: understanding of the phenomena and applications in petroleum and process industries* (Institut français du pétrole publications.). Paris: Paris: Editions Technip. ISBN: 978-2-7108-0944-9, 2010.

[228] F. Y. Cheng, "Erosion-accelerated corrosion in flow systems: the behavior of aluminum alloys in automotive cooling systems," in *Tribocorrosion of Passive Metals and Coatings*, D. Landolt and S. Mischler Eds.: Woodhead Publishing, 2011, ch. 17, pp. 475-500.

[229] Y. Yan and A. Neville, "Bio-tribocorrosion: Surface interactions in total joint replacement (TJR)," in *Bio-tribocorrosion in biomaterials and medical implants*, Y. Yan Ed.: Elsevier, 2013, pp. 309-340.

[230] I. García, D. Drees, and J. P. Celis, "Corrosion-wear of passivating materials in sliding contacts based on a concept of active wear track area," *Wear,* Article vol. 249, no. 5-6, pp. 452-460, 2001, doi: 10.1016/S0043-1648(01)00577-4.

[231] X. Gao and M. Liu, "Corrosion behavior of high-strength c71500 copper-nickel alloy in simulated seawater with high concentration of sulfide," *Materials,* vol. 15, no. 23, pp. 1-22, 2022, Art no. 8513, doi: 10.3390/ma15238513.

[232] M. S. Jellesen, A. A. Rasmussen, and L. R. Hilbert, "A review of metal release in the food industry," *Mater. Corros.,* vol. 57, no. 5, pp. 387-393, 2006, doi: 10.1002/MACO.200503953.

[233] B. V. Salas, M. S. Wiener, M. Stoytcheva, R. Zlatev, and M. C. Beltrán, "Corrosion in the food industry and its control," in *Food Industrial Processes - Methods and Equipment*, B. Valdez Ed.: InTechOpen, 2012, ch. 19, pp. 363-378.

[234] J. L. Jeronimo *et al.*, "Microstrutural, mechanical characterizations and corrosion behaviour of borides layers on Inconel 718 superalloy," *Results in Engineering,* vol. 16, pp. 1-11, 2022/12/01/ 2022, Art no. 100783, doi: 10.1016/j.rineng.2022.100783.

[235] P. K. Whitcraft and R. Alloys, "Material issues in the Pharmaceutical Industry," *ASM Handbook, Corrosion: Environments and Industries,* vol. 13C, pp. 810-812, 2006, doi: 10.31399/asm.hb.v13c.a0004203.

[236] S. Gudić, L. Vrsalović, A. Matošin, J. Krolo, E. E. Oguzie, and A. Nagode, "Corrosion behavior of stainless steel in seawater in the presence of sulfide," *Applied Sciences,* vol. 13, no. 7, pp. 1-24, 2023, Art no. 4366, doi: 10.3390/app13074366.

[237] G. A. Rodríguez-Bravo, M. Vite-Torres, and J. G. Godínez-Salcedo, "Corrosion rate and wear mechanisms comparison for AISI 410 stainles steel exposed to pure corrosion and abrasion-corrosion in a simulated marine environment," *Tribology in Industry,* vol. 41, no. 3, pp. 394-400, 2019, doi: 10.24874/ti.2019.41.03.09.

[238] H. Tian, Z. Cui, X. Zhang, and X. Zhang, "Effect of cathodic potential and corrosion product on tribocorrosion behavior of S420 steel in the marine environment," *Materials Today Communications,* vol. 38, pp. 1-15, 2024, Art no. 108372, doi: 10.1016/j.mtcomm.2024.108372.

[239] N. Figueira, T. M. Silva, M. J. Carmezim, and J. C. S. Fernandes, "Corrosion behaviour of NiTi alloy," *Electrochimica Acta,* vol. 54, no. 3, pp. 921-926, 2009/01/01/ 2009, doi: 10.1016/j.electacta.2008.08.001.

[240] A. W. Hansen, L. T. Führ, L. M. Antonini, D. J. Villarinho, C. E. B. Marino, and C. d. F. Malfatti, "The electrochemical behavior of the NiTi alloy in different simulated body fluids," *Materials research,* vol. 18, no. 1, pp. 184-190, 2015, doi: 10.1590/1516-1439.305614.

[241] ASTM G1-03, "Standard practice for preparing, cleaning, and evaluating corrosion test specimens," *American Society for Testing and Materials. Book of standards, vol. 03.02. Developed by subcommittee G01.05,* pp. 1-9, 2017, doi: 10.1520/G0001-03R17E01.

[242] R. G. Kelly, J. R. Scully, D. Shoesmith, and R. G. Buchheit, *Electrochemical techniques in corrosion science and engineering* (Corrosion technology (New York, N.Y.)). New York: Marcel Dekker, Incor., 2003.

[243] K. Shahzad *et al.*, "Electrochemical and thermodynamic study on the corrosion performance of API X120 steel in 3.5% NaCl solution," *Sci. Rep.,* vol. 10, no. 1, pp. 1-15, 2020/03/09 2020, Art no. 4314, doi: 10.1038/s41598-020-61139-3.

[244] M. Keddam and F. Wenger, "Electrochemical methods in tribocorrosion," in *Tribocorrosion of Passive Metals and Coatings*, D. Landolt and S. Mischler Eds.: Woodhead Publishing, 2011, ch. 7, pp. 187-221.

[245] H. Amegroud *et al.*, "A comprehensive investigation of the electrochemical behavior of nickel-aluminum bronze alloy in alkaline solution: The effect of film formation potential," *Colloids Surf. Physicochem. Eng. Aspects,* vol. 614, pp. 1-11, 2021, Art no. 126126, doi: 10.1016/j.colsurfa.2020.126126.

[246] A. O. Mace, M. A. Kurtz, and J. L. Gilbert, "Fretting and fretting corrosion behavior of additively manufactured Ti-6Al-4V and Ti-Nb-Zr alloys in air and physiological solutions," *Journal of Functional Biomaterials,* vol. 15, no. 2, pp. 1-23, 2024, doi: 10.3390/jfb15020038.

[247] M. Sowa and W. Simka, "Electrochemical impedance and polarization corrosion studies of tantalum surface modified by DC Plasma electrolytic oxidation," *Materials,* vol. 11, no. 4, pp. 2-17, 2018, Art no. 545, doi: 10.3390/ma11040545.

[248] S. Virtanen, "1 - Corrosion and passivity of metals and coatings," in *Tribocorrosion of Passive Metals and Coatings*, D. Landolt and S. Mischler Eds.: Woodhead Publishing, 2011, ch. 1, pp. 3-28.

[249] K. Khanlari, M. Ramezani, P. Kelly, P. Cao, and T. Neitzert, "Mechanical and microstructural characteristics of as-sintered and solutionized porous 60NiTi," *Intermetallics,* vol. 100, pp. 32-43, 2018, doi: 10.1016/j.intermet.2018.06.001.

[250] J. Aguirre, M. Walczak, and M. Rohwerder, "The mechanism of erosion-corrosion of API X65 steel under turbulent slurry flow: Effect of nominal flow velocity and oxygen content," *Wear,* pp. 438-439, 2019/11/15/ 2019, Art no. 203053, doi: 10.1016/j.wear.2019.203053.

[251] R. Neupane and Z. Farhat, "Wear and dent resistance of superelastic TiNi alloy," *Wear,* vol. 301, no. 1-2, pp. 682-687, 2013, doi: 10.1016/j.wear.2012.11.017.

[252] K. Khanlari, M. Ramezani, P. Kelly, M. Hayat, P. Cao, and T. Neitzert, "An investigation on microstructural and mechanical properties of porous 60NiTi parts solutionized by different cost-effective methods," *Metallography, Microstructure & Analysis,* vol. 7, no. 3, pp. 334-346, 2018, doi: 10.1007/s13632-018-0443-4.

[253] K. Khanlari, M. Ramezani, P. Kelly, P. Cao, and T. Neitzert, "An investigation on reasons causing inferiority in unlubricated sliding wear performance of 60NiTi as compared to 440c steel," *Tribology Transactions,* vol. 62, no. 1, pp. 96-109, 2019, doi: 10.1080/10402004.2018.1516326.

[254] R. Neupane and Z. Farhat, "Wear mechanisms of NiTinol under reciprocating sliding contact," *Wear,* vol. 315, no. 1-2, pp. 25-30, 2014, doi: 10.1016/j.wear.2014.02.018.

[255] P. Renner, Y. Chen, Z. Huang, A. Raut, and H. Liang, "Tribocorrosion influenced pitting of a duplex stainless steel," *Lubricants,* vol. 9, no. 5, pp. 1-11, 2021, doi: 10.3390/lubricants9050052.

[256] H. Wang *et al.*, "Corrosion behavior of NiTi alloy subjected to femtosecond laser shock peening without protective coating in air environment," *Appl. Surf. Sci.,* vol. 501, 2020, Art no. 144338, doi: 10.1016/j.apsusc.2019.144338.

[257] A. Ghanbarzadeh, F. M. Salehi, M. Bryant, and A. Neville, "A new asperity-scale mechanistic model of tribocorrosive wear: Synergistic effects of mechanical wear and corrosion," *Journal of Tribology,* vol. 141, no. 2, pp. 1-12, 2019, doi: 10.1115/1.4041246.

[258] M. Venkatesh, R. Salloom, A. V. M. Rao, and A. V. Aditya, "Tribocorrosion mechanisms in sliding contacts," in *Tribocorrosion: Fundamentals, methods, and materials*, A. Siddaiah, R. Ramachandran, and P. L. Menezes Eds. Cambridge, MA, USA: Academic Press, 2021, ch. 4, pp. 79-91.

[259] M. J. Carrington *et al.*, "Microstructural characterisation of subsurface deformation and the degradation of Stellite 6 induced by self-mated sliding contact in a simulated PWR environment," *Tribology International,* vol. 158, pp. 1-16, 2021, Art no. 106899, doi: 10.1016/j.triboint.2021.106899.

[260] S. Meddah *et al.*, "Dry sliding wear performance of an annealed TiNi alloy with different nickel contents," *Materials Research Express,* vol. 7, no. 3, pp. 1-10, 2020, Art no. 036508, doi: 10.1088/2053-1591/ab5dea.

[261] C. DellaCorte, "Nickel-titanium alloys for oil-lubricated bearing and mechanical component applications," in *Proceedings of the ASME/STLE 2009 International Joint Tribology Conference*, Memphis, TN, 2009, October 19–21: ASME, pp.

225-227, doi: 10.1115/ijtc2009-15055. [Online]. Available: https://doi.org/10.1115/IJTC2009-15055

[262] S. Alkan and M. S. Gök, "Effect of sliding wear and electrochemical potential on tribocorrosion behaviour of AISI 316 stainless steel in seawater," *Engineering Science and Technology, an International Journal,* vol. 24, no. 2, pp. 524-532, 2021, doi: 10.1016/j.jestch.2020.07.004.

[263] Z. Gao, G. Ji, Z. Shi, and X. Wang, "The tribocorrosion behaviour of YSZ coating deposited on stainless steel substrate in 3.5 wt% NaCl solution," *Ceram. Int.,* vol. 47, no. 15, pp. 21051-21060, 2021, doi: 10.1016/j.ceramint.2021.04.107.

[264] V. Pejaković, V. Totolin, and M. Rodríguez Ripoll, "Tribocorrosion behaviour of Ti6Al4V in artificial seawater at low contact pressures," *Tribology International,* vol. 119, pp. 55-65, 2018, doi: 10.1016/j.triboint.2017.10.025.

[265] P. Jemmely, S. Mischler, and D. Landolt, "Electrochemical modeling of passivation phenomena in tribocorrosion," *Wear,* vol. 237, no. 1, pp. 63-76, 2000, doi: 10.1016/S0043-1648(99)00314-2.

[266] C. Yan, Q. Zeng, Y. Hao, Y. Xu, and M. Zhou, "Friction-induced hardening behaviors and tribological properties of 60NiTi alloy lubricated by lithium grease containing nano-BN and MoS2," *Tribology Transactions,* vol. 62, no. 5, pp. 812-820, 2019, doi: 10.1080/10402004.2019.1619889.

[267] H. Duan *et al.*, "Tribological properties of AlCoCrFeNiCu high-entropy alloy in hydrogen peroxide solution and in oil lubricant," *Wear,* vol. 297, no. 1-2, pp. 1045-1051, 2013, doi: 10.1016/j.wear.2012.11.014.

[268] J. Chen, H. Mraied, and W. Cai, "Determining tribocorrosion rate and wear-corrosion synergy of bulk and thin film aluminum alloys," *Journal of Visualized Experiments,* vol. 2018, no. 139, 2018, doi: 10.3791/58235.

[269] M. V. Rahul, V. Balaji, and S. Narendranath, "Optimization of wire-EDM process parameters for Ni–Ti-Hf shape memory alloy through particle swarm optimization and CNN-based SEM-image classification," *Results in Engineering,* vol. 18, pp. 1-11, 2023/06/01/ 2023, Art no. 101141, doi: 10.1016/j.rineng.2023.101141.

[270] M. Elahinia, N. Shayesteh Moghaddam, M. Taheri Andani, A. Amerinatanzi, B. A. Bimber, and R. F. Hamilton, "Fabrication of NiTi through additive manufacturing: A review," *Prog. Mater Sci.,* vol. 83, pp. 630-663, 2016, doi: 10.1016/j.pmatsci.2016.08.001.

[271] E. O. Ezugwu, Z. M. Wang, and A. R. Machado, "The machinability of nickel-based alloys: A review," *J. Mater. Process. Technol.,* vol. 86, no. 1-3, pp. 1-16, 1998, doi: 10.1016/S0924-0136(98)00314-8.

[272] L. Zhang, H. Peng, Q. Qin, Q. Fan, S. Bao, and Y. Wen, "Effects of annealing on hardness and corrosion resistance of 60NiTi film deposited by magnetron sputtering," *J. Alloys Compd.,* vol. 746, pp. 45-53, 2018, doi: 10.1016/j.jallcom.2018.02.227.

[273] J. Z. He, J. N. Lu, X. Y. Deng, X. Q. Xing, and Z. C. Luo, "Premature fracture of high-strength suspension springs caused by corrosion fatigue cracking," *Results in Engineering,* vol. 16, pp. 1-9, 2022/12/01/ 2022, Art no. 100749, doi: 10.1016/j.rineng.2022.100749.

[274] J. P. Celis and P. Ponthiaux, *Testing tribocorrosion of passivating materials supporting research and industrial innovation: A handbook* (Testing Tribocorrosion of Passivating Materials Supporting Research and Industrial Innovation: A Handbook). Maney Publishing, UK, 2012, pp. 1-203.

[275] S. H. Mills, C. Dellacorte, R. D. Noebe, M. J. Mills, A. P. Stebner, and B. Amin-Ahmadi, "Heat treatment – microstructure – hardness relationships of new nickel-rich nickel-titanium-hafnium alloys developed for tribological applications," *Materialia,* vol. 16, pp. 1-13, 2021/05/01/ 2021, Art no. 101064, doi: 10.1016/j.mtla.2021.101064.

[276] C. Dellacorte, S. V. Pepper, R. Noebe, D. R. Hull, and G. Glennon, "Intermetallic Nickel-Titanium alloys for oil-lubricated bearing applications.," *NASA Technical Report. NASA/TM-2009-215646,* pp. 1-26, 2009. [Online]. Available: https://ntrs.nasa.gov/api/citations/20090019112/downloads/20090019112.pdf.

[277] V. L. Ratia *et al.*, "Comparison of the sliding wear behaviour of self-mated HIPed Stellite 3 and Stellite 6 in a simulated PWR water environment," *Wear,* vol. 426-427, pp. 1222-1232, 2019, doi: 10.1016/j.wear.2019.01.116.

[278] J. H. Weber, Y. Khalfalla, and K. Y. Benyounis, "Nickel alloys: Thermal treatment and thermomechanical processing," in *Reference Module in Materials Science and Materials Engineering*: Elsevier, 2016.

[279] E. B. Caldona, A. C. C. de Leon, J. D. Mangadlao, K. J. A. Lim, B. B. Pajarito, and R. C. Advincula, "On the enhanced corrosion resistance of elastomer-modified polybenzoxazine/graphene oxide nanocomposite coatings," *React. Funct. Polym.,* vol. 123, pp. 10-19, 2018/02/01/ 2018, doi: 10.1016/j.reactfunctpolym.2017.12.004.

[280] A. I. Munoz, N. Espallargas, and S. Mischler, "Characterization of worn surfaces," in *Tribocorrosion*, A. Igual Munoz, N. Espallargas, and S. Mischler Eds. Switzerland: Springer Briefs in Applied Sciences and Technology. Springer, Cham, 2020, ch. 7, pp. 65-70.

APPENDICES

Appendix A: Experimental test conditions and other supplementary materials

The following table shows the parameters considered for the experimental design to select optimal parameters during the preliminary investigations. Table A.1 shows the different corrosive environments, such as sulphuric acid, saline solution and aqueous sodium hydroxide, covering a wide pH range. These solutions mimic the environments where NiTiNOL60 alloy has vast applications.

Table A.1: Experimental parameters and the design of the experiment.

Electrolytes covering a wide pH range		
Electrolyte	**Concentration**	**pH**
H_2SO_4	0.05 M and 0.1 M	1.5 – 4
NaCl	3.5 wt.%	6.8 – 7.2
NaOH	0.05 M and 0.1 M	11 – 13

Test parameters for reciprocating sliding wear	
Parameters	**Values**
Load (N)	2, 5, 8, 10
Frequency (Hz)	2, 4, 6
Temperature (℃)	22 ± 2 (RT), 200, 400, 600
Stroke length (mm)	10
Sliding distance (m)	500

Effect of load at room temperature (RT)			
Experimental run	**Variables**		
	Load (N)	**Frequency (Hz)**	**Temperature (℃)**
1	2	4	RT
2	5	4	RT
3	8	4	RT
4	10	4	RT

Effect of frequency at room temperature (RT) using 8 N load			
	Variables		
	Load (N)	**Frequency (Hz)**	**Temperature (℃)**
5	8	2	RT
(same as 3)	~~8~~	~~4~~	~~RT~~
6	8	6	RT

Effect of temperature at an applied load of 8 N			
	Variables		
	Load (N)	Frequency (Hz)	Temperature (℃)
(same as 3)	~~8~~	~~4~~	~~RT~~
7	8	4	200
8	8	4	400
9	8	4	600

From the Table, 9 experimental runs x 3 repeats = **27 experiments** required for each environment. Thus, a total of 81 experiments will be carried out for the tribocorrosion tests using the three (3) different corrosive solutions.

The considerations for an alumina ball as a counter body in a sliding wear test

Alumina ball (Al_2O_3) possesses anti-wear, heat-resistant, anti-oxidant and corrosion-resistant properties, making it the ideal material for tribocorrosion investigation in corrosive solutions. Its advantages over steel balls include

- weight (59 % lighter than steel balls), which implies less centrifugal force and less wear on the groove at high frequency during reciprocating sliding.
- 44 % larger elastic modulus, indicating less deformation under applied load.
- Suitable for high temperatures up to 1050 ℃ while only ¼ coefficient of thermal expansion of steel can endure sharp temperature variation.
- Excellent surface finish (R_a ~4 – 6 nm), non-magnetic, non-conductive and can roll without lubrication.

Images of some instrument/equipment used, material preparation and results obtained during the experimental investigation

Fig. A.1: An ultrasonic cleaning equipment.

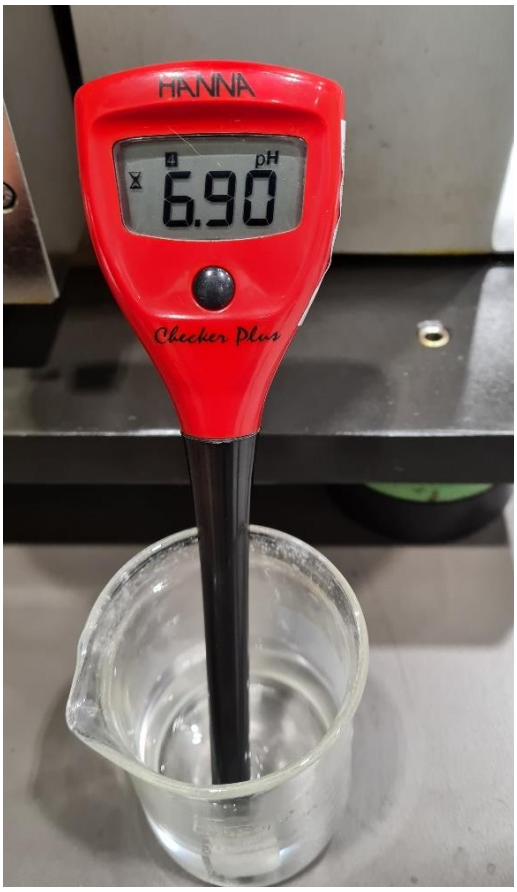

Fig. A.2: A pH meter while measuring an electrolyte medium.

Fig. A.3: Struers wet polishing equipment.

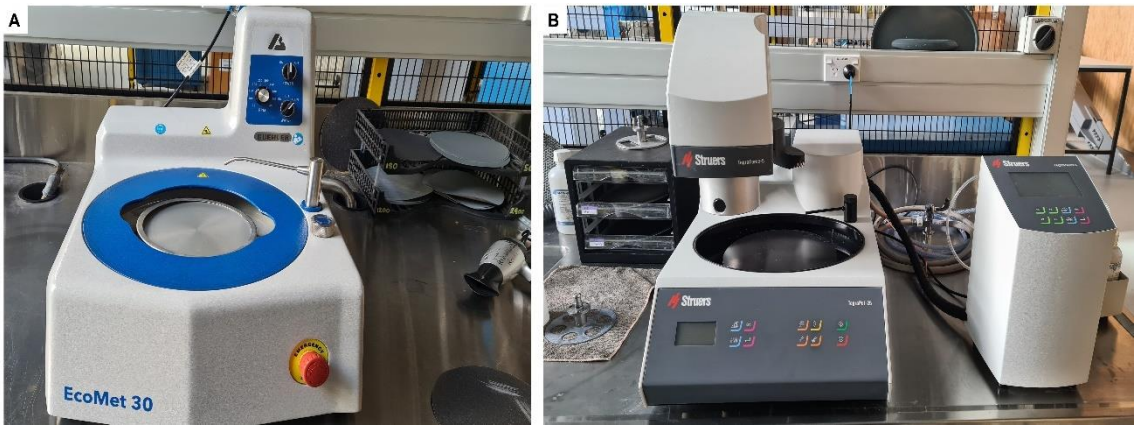

Fig. A.4: (a) wet grinding and (b) polishing machines.

Fig. A.5: Optical microscope.

Fig. A.6: Struers hot press mount and the cross-sectional parts of NiTiNOL60 alloy mounted using phenolic resin.

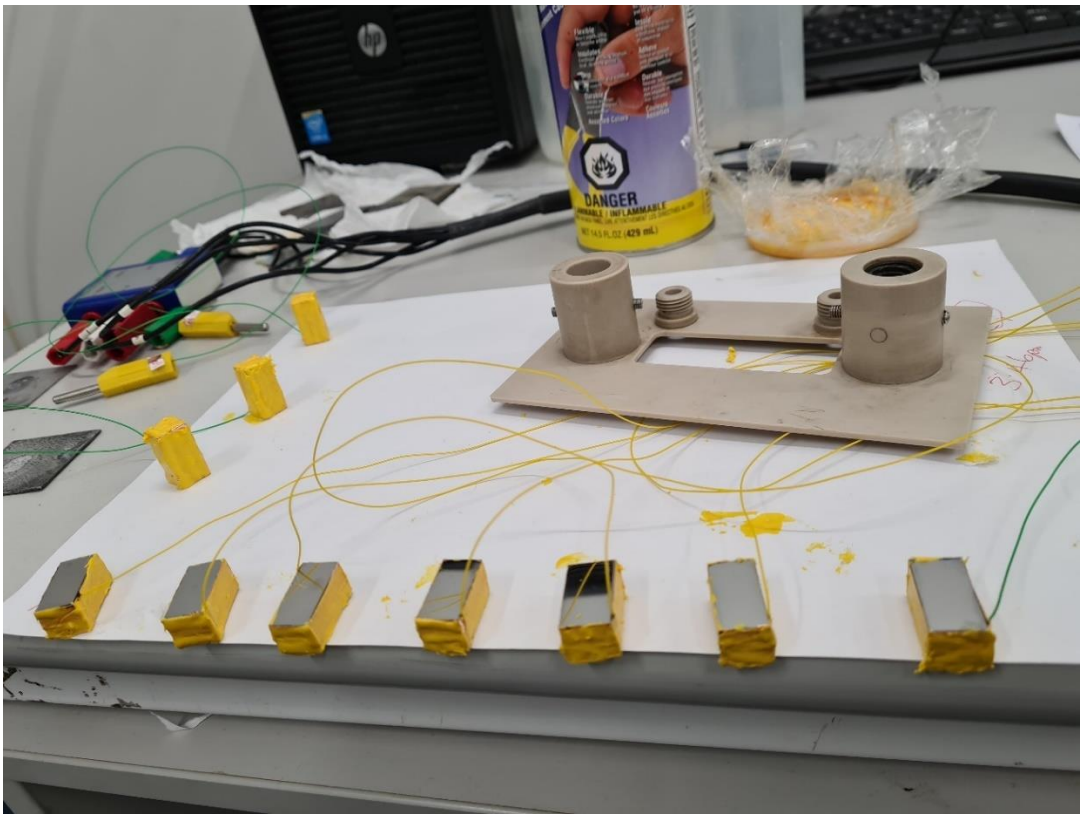

Fig. A.7: Polished surfaces and plasti-dip adhesive coating of test specimens.

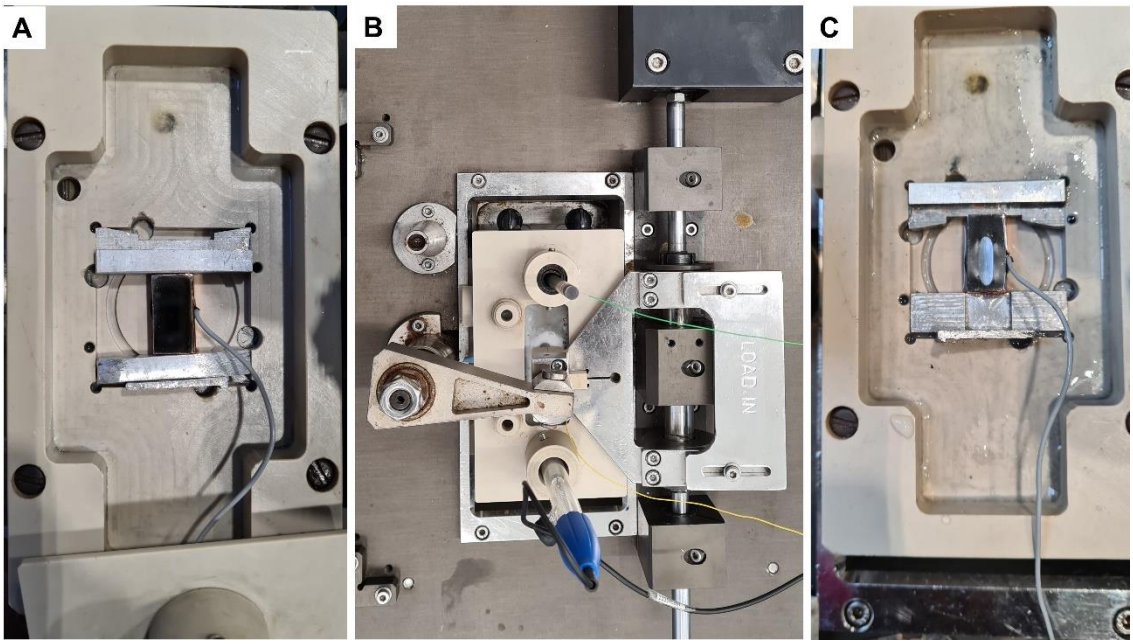

Fig. A.8: NiTiNOL60 specimen showing (a) polished surface before tribocorrosion (b) tribocorrosion measurement, and (c) wear track after tribocorrosion test.

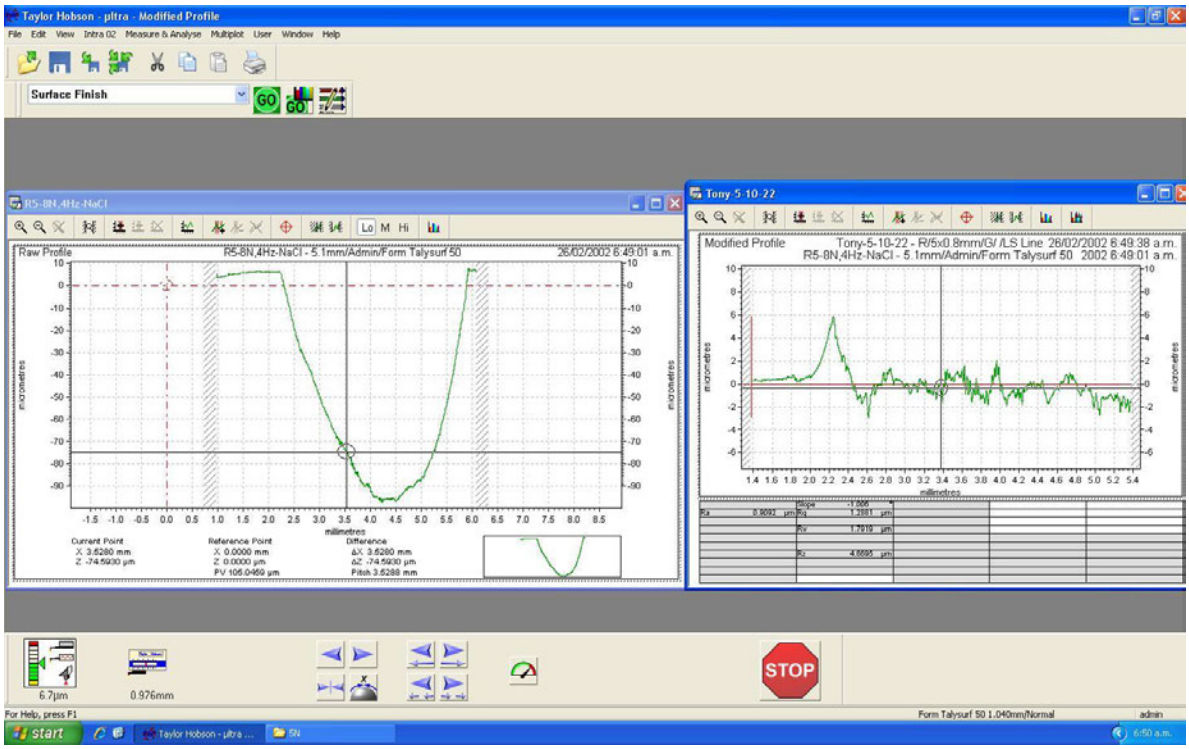

Fig. A.9: Wear scar profile for the roughness measurement using stylus profilometry.

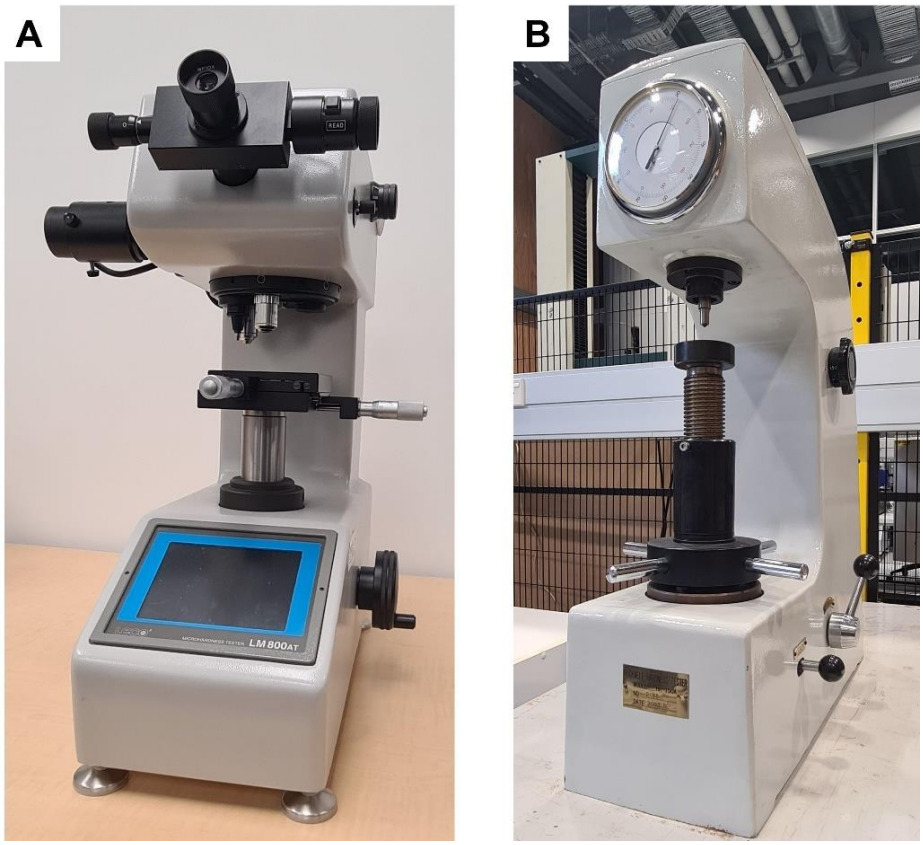

Fig. A.10: (a) Vicker's and (b) Rockwell hardness testers.

Appendix B: Cover pages for the research outputs in journal publications

Results in Engineering 19 (2023) 101305

Contents lists available at ScienceDirect

Results in Engineering

journal homepage: www.sciencedirect.com/journal/results-in-engineering

Tribocorrosion behaviour of NiTiNOL60 alloy in an alkaline environment

Anthony Okoani [a,c,**], Ashveen Nand [b], Maziar Ramezani [a,*]

[a] Department of Mechanical Engineering, Auckland University of Technology, Auckland, New Zealand
[b] Faculty of Engineering, University of Auckland, Auckland, New Zealand
[c] Department of Mechanical Engineering, University of Nigeria, Nsukka, Nigeria

ARTICLE INFO

Keywords:
NaOH electrolyte
NiTiNOL60 alloy
Sliding wear
Tribocorrosion

ABSTRACT

NiTi-based alloys subjected to aggressive tribocorrosion working conditions can deteriorate by the combined action of mechanical and chemical wear. The synergistic interaction under sliding contact and corrosive environment formed the basis of the current study. This study employed a linear reciprocating tribometer coupled with an electrochemical cell of a three-electrode configuration to investigate the behaviour of NiTiNOL60 alloy sliding against an alumina ball (Al_2O_3) in a NaOH environment. The resulting wear track surfaces were examined using a scanning electron microscope, optical microscope, energy dispersive spectroscopy (EDS), and stylus profilometry. While the synergistic interactions reveal that abrasive and oxidative wear mechanisms exist concurrently, an increase in applied load reduces the corrosion potential, thereby leading to a higher wear volume and increased corrosion rate. The experimental results showed that a higher corrosion rate and wear volume occurred at a higher load. The wear track analysis illuminated the various wear mechanisms at play, including abrasion, debris adhesion, pitting, delamination, ploughing, and cracking. These mechanisms were influenced by both mechanical and chemical wear, the latter notably due to corrosive attacks. EDS elemental analysis showed an increase in oxygen content at higher loads, which suggests increased corrosion due to the delamination of the oxide layer during the reciprocating sliding.

Results in Materials 21 (2024) 100523

Contents lists available at ScienceDirect

Results in Materials

journal homepage: www.sciencedirect.com/journal/results-in-materials

Corrosion and wear interplay: Tribo-electrochemical evaluation of NiTiNOL60 alloy in sulfuric acid

Anthony Onyebuchi Okoani [a,c,**], Ashveen Nand [b], Maziar Ramezani [a,*]

[a] Department of Mechanical Engineering, Auckland University of Technology, Auckland, New Zealand
[b] Faculty of Engineering, University of Auckland, Auckland, New Zealand
[c] Department of Mechanical Engineering, University of Nigeria, Nsukka, Nigeria

ARTICLE INFO

Keywords:
NiTiNOL60 alloy
H_2SO_4 electrolyte
Tribocorrosion
Wear mechanisms

ABSTRACT

The combined corrosion and wear behaviour of NiTiNOL60 alloy is important in various engineering applications. While previous studies have explored its performance in artificial seawater environments, limited information exists regarding its tribocorrosion characteristics in acidic conditions. This paper investigates the synergistic interaction between sliding wear and electrochemical processes for NiTiNOL60 alloy in a sulfuric acid environment, employing experimental procedures compliant with ASTM standards. Microscopic analysis confirms the alloy's Ni-rich composition, featuring a dense network of B2 NiTi + Ni_4Ti_3 cubic and rhombohedral crystal matrix structures. Our research and results reveal that material degradation during tribocorrosion arises from the combined effects of sliding wear and electrochemical reactions. Consequently, multiple wear mechanisms influenced by tribochemical wear are observed, with delamination and micro-cracks being notably prominent under higher applied loads due to surface tensile stress and contact pressure, leading to crack propagation perpendicular to the sliding direction. These findings have practical implications for optimising the performance and durability of NiTiNOL60 alloy in acidic environments, offering valuable insights for load-bearing engineering applications.

Journal of Alloys and Metallurgical Systems 6 (2024) 100074

Contents lists available at ScienceDirect

Journal of Alloys and Metallurgical Systems

journal homepage: www.journals.elsevier.com/journal-of-alloys-and-metallurgical-systems

Tribo-electrochemical investigation of 60NiTi alloy in saline solution

Anthony Onyebuchi Okoani [a,c,*], Ashveen Nand [b], Maziar Ramezani [a,**]

[a] Department of Mechanical Engineering, Auckland University of Technology, Auckland, New Zealand
[b] Faculty of Engineering, University of Auckland, New Zealand
[c] Department of Mechanical Engineering, University of Nigeria, Nsukka, Nigeria

ARTICLE INFO

Keywords:
3.5 wt% NaCl electrolyte
NiTiNOL60 alloy
Three-body abrasion
Corrosion-wear
Oxidation
Wear mechanisms

ABSTRACT

This research explores the tribocorrosion behaviour of 60NiTi alloy, also known as NiTiNOL60, when exposed to a saline environment. Our investigation focuses on understanding the relationship between corrosion and wear rates and assessing surface damage and material degradation. To conduct our experiments, we employed a linear reciprocating ball-on-plate tribometer coupled with electrochemical polarisation using a three-electrode cell configuration to assess the combined effects of corrosion and sliding wear. Surface characterisation was carried out through scanning electron microscopy and energy dispersion spectroscopy, revealing the material to be a Ni-rich 60NiTi alloy, with surface oxidation evident in the electrolyte medium. Our electrochemical findings indicate the occurrence of localised corrosion in both cathodic and anodic regimes, with corrosion pit nucleation, cavities, and cracks being accelerated by reciprocating sliding and corrosion potential. These interactions exposed the material surface to various wear mechanisms, including abrasive, adhesive, oxidative, corrosive, and fatigue processes. This study underscores the significant influence of mechanical properties on the rate of material degradation due to corrosion, while also highlighting the substantial impact of prevailing electrochemical conditions on the rate of mechanical material removal. This paper offers valuable insights for designers working on load-bearing structures in saline environments.

JMEPEG
https://doi.org/10.1007/s11665-024-09646-6

©The Author(s)
1059-9495/$19.00

ORIGINAL RESEARCH ARTICLE

Comparative Study of the Tribocorrosion Performance of NiTiNOL60 in Acidic, Alkaline, and Saline Environments

Anthony Onyebuchi Okoani, Ashveen Nand, and Maziar Ramezani

Submitted: 6 November 2023 / Accepted: 2 May 2024

In order to enhance the durability of tribological interfaces, an investigation into the synergistic effects of sliding wear, corrosion, and their interactions is crucial. This study focuses on understanding the deformation mechanisms of NiTiNOL60, a nickel-rich nickel-titanium alloy, during sliding against Al_2O_3 in different corrosive environments, including acidic, alkaline, and saline mediums. The pH of the environments is found to play a significant role in the tribocorrosion process, leading to electromechanically induced transformations and various wear patterns. Plastic deformations are observed on the wear track surfaces, particularly in the severe and mild wear regimes. In an alkaline environment, depassivation of the oxide layer triggers oxidational wear, with the depassivation rate dependent on factors like contact pressure, sliding velocity, and passive film properties. The wear volume is highest in saline environments, with contributions from mechanical wear, corrosion, and third-body abrasion. Grain deformations occur in the alkaline environment due to shear forces, while in the acidic medium, corrosion accelerates mild wear involving abrasion and delamination. The findings provide insights into wear mechanisms and localized corrosion, highlighting the influence of H^+ and OH^- groups (pH values) on corrosive wear and crack propagation.

Keywords 3.5 wt.% NaCl, electrochemistry, H_2SO_4, NiTiNOL60 alloy, NaOH, sliding wear, tribocorrosion

metals

MDPI

Review

Investigating the Tribocorrosion Behaviour of NiTiNOL60 Alloy in Engineering and Biomedical Applications—An Overview

Anthony O. Okoani [1,2], Ashveen Nand [3], Cho-Pei Jiang [4] and Maziar Ramezani [1,*]

[1] Department of Mechanical Engineering, Auckland University of Technology, Auckland 1010, New Zealand; anthony.okoani@aut.ac.nz
[2] Department of Mechanical Engineering, University of Nigeria, Nsukka 410001, Nigeria
[3] Faculty of Engineering, University of Auckland, Auckland 1010, New Zealand; ashveen.nand@auckland.ac.nz
[4] Department of Mechanical Engineering, National Taipei University of Technology, Taipei 10608, Taiwan; jcp@mail.ntut.edu.tw
* Correspondence: maziar.ramezani@aut.ac.nz

Abstract: This review covers the literature that is currently accessible, as well as emerging research into the performance of NiTi-based alloys exposed to corrosive environments in both engineering and medical applications. It provides an overview of the state-of-the-art research in the study of tribocorrosion of Ni-rich NiTi alloy by highlighting significant discoveries, research approaches, and future research directions following the limited reviews on tribocorrosion in the past decade. The practical impacts, as well as the economic implications of tribological applications on daily life, coupled with the increasing failures of metals and biomaterials, make it imperative to investigate tribocorrosion and update the subject area on the recent focus. Tribocorrosion is commonly observed on the surface of different metals, including NiTi alloys, such as NiTiNOL60 (60 wt.% Ni and 40 wt.% Ti), which possess unique properties applicable across various engineering and biomedical fields. In its application, the material experiences wear due to the depassivation of tribofilms caused by relative motion (sliding, fretting, or impact) in aggressive environments, including corrosive mediums, high temperatures, and pressures. This study elucidates the synergistic interactions between mechanical wear, corrosion, and their associated tribocorrosion mechanisms in corrosive media.

Keywords: NiTiNOL60 alloy; biocompatibility; electrochemistry; tribocorrosion; wear

check for updates

Citation: Okoani, A.O.; Nand, A.; Jiang, C.-P.; Ramezani, M. Investigating the Tribocorrosion Behaviour of NiTiNOL60 Alloy in Engineering and Biomedical Applications—An Overview. *Metals* **2024**, *14*, 1334. https://doi.org/10.3390/met14121334

Academic Editor: Beatrice N. Grgur

Received: 15 October 2024
Revised: 17 November 2024
Accepted: 18 November 2024
Published: 25 November 2024

Copyright: © 2024 by the authors. Licensee MDPI, Basel, Switzerland. This article is an open access article distributed under the terms and conditions of the Creative Commons Attribution (CC BY) license (https://creativecommons.org/licenses/by/4.0/).

1. Introduction

The demand for a better understanding of surface degradation processes, mainly when tribological components are operating in corrosive environments, has arisen because of the need to choose or design new surfaces for future equipment, minimise operating costs, and extend the life of existing machinery [1,2]. This has led to the current study field of tribocorrosion, which aims to address the aforementioned issues and understand the mechanisms of surface deterioration when mechanical wear and chemical/electrochemical processes combine [3–5]. Tribocorrosion is a multifaceted degradation phenomenon that occurs when metals are subjected to mechanical wear and corrosion simultaneously [6–8].

The interaction between moving surfaces in a tribological loading situation/contact is a concept that exists in many phenomena in nature, be it in the components of spacecraft [9], human joints [10], rolling elements of a jet turbine [11], etc. The literature states that tribological contacts result in a global economic loss of approximately USD 300 billion annually, with friction contributing to 73% of the total loss and wear contributing to 27% [12]. Corrosion is also reported to have a global estimated cost of about USD 2.5 trillion, equivalent to 3.4% of the 2013 Gross Domestic Product of the United States [13]. Tribological applications in a corrosive environment often result in a surface alteration [14–16], and understanding this complex phenomenon and its complexity arises from the interactions involved in moving surfaces, as influenced by several parameters (mechanical, material, electrochemical